Functional characterization of DEEPGENES to enhance deeper rooting in cereal crops

Fusi Riccardo

Thesis Submitted to the University of Nottingham for the degree of Doctor of Philosophy

November 2021

Acknowledgements

I would like to start by saying many thanks to my main supervisors Jonathan Lynch and Malcolm Bennett who gave me the opportunity to join their ARPA-E DEEPER project which funded my PhD studentship. Joining such a large and high motivated multidisciplinary research group gave me the opportunity to interact with amazing scientists from several fields, which resulted in a substantial professional growth in myself as a future researcher. To Malcolm Bennett I would like to say many thanks for being an amazing mentor, not only professionally but also for all your personal support given to me for all the up and downs of this Ph.D. project. No matter what the problem was, personal or professional, you have always been there for me, I will never forget this. Many thanks also to Silvio Salvi and all the University of Bologna crop genetic division group to give me the opportunity to work on their barley projects from my master through all of my PhD. Thanks also to Serena Rosignoli for all the support on the genetic part of the barley TILLMore mutant characterisation, seed bulking and also for being a good friend.

I would say a particular thanks to Rahul Bhosale who Co-supervised me during my entire Ph.D. Thanks for providing me with the initial GWAS predictions in maize and for all your precious computational biology advice. Thanks also for teaching me a lot of bioinformatics, molecular biology, statistics (and more) and for being an amazing friend, always available when needed. I would never say thanks enough for your effort in helping me write the papers arising from this thesis. Thanks also to Anthony Bishopp for supporting me with my PIN1 related work, cloning and providing me with the amazing opportunity to co-organise/teach an online workshop during the pandemic. A special thanks also to my colleague and girlfriend at that time Mia (Haoyu Lou). Thanks for teaching me a lot of molecular biology in the lab and all the amazing times we spent travelling which created very special memories.

It is not possible to name all the amazing colleagues that I've meet during this Ph.D. experience. I would just say thanks to all the DEEPER colleagues from Jonathan Lynch group in PennState (USA) particularly Molly and Hannah for providing the initial GWAS phenotypic data, Shawn Kaeppler group in WCIC (USA) particularly Vai and Ray for your support in generating transgenics, Matthew Tucker group in University of Adelaide (Australia) and last

but not least all my colleagues at the University of Nottingham in the Root Groups. Thanks for always being patient with me and for all the amazing time we spent together. A special mention also to Jacob Pattem and Gleb Yukabov from the NCMH for their support with the AFM work for the EGT1 manuscript.

Thanks to my family for always being supportive in all the choices I made in my career as a researcher. Being far away from home during the COVID-19 pandemic has been a very tough challenge, but you have always been there for me. There is no better thing to know that wherever I will be in the world you'll always be there. A special thanks also to my dear flatmate Emil, who lived with me since the beginning of this experience for being the best flatmate I could ever ask, always listening to me when I was down due to bad days in the lab or for any personal breakdowns. Thanks to all my friends I met in Nottingham, and my closest friends my hometown Como and Bologna.

Finally, I would dedicate all this work to my dearest friend Filippo who lost his life too young. Soo many endless nights spent on studying biology to get our Master degree and the amazing time we spent having fun together. I'm sure you're now somewhere smiling and saying "Well done Ricky!".

--

Grazie alla mia famiglia, per avermi sempre supportato in tutte le scelte per la mia carriera da ricercatore. Essere cosi distanti in aggiunta alla pandemia di COVID-19 e' stata veramente una prova dura ma siete sempre stati al mio fianco. Non c'e' piu bella cosa di sapere che in qualunque parte del mondo io sia, voi sarete sempre li a supportarmi. Un grazie speciale anche a tutti I miei amici piu stretti nell amia citta' natale Como e adottiva, Bologna.

Infine, voglio dedicare tutto questo lavoro al mio caro amico Filippo, che ha perso la vita troppo presto. Grazie per le tante notti infinite a studiare biologia per ottenere il nostro Master ma anche per tutto il divertimento passato insieme. Questo mio traguardo e' anche merito tuo. Sono sicuro ora sarai da qualche parte a dire "Grande Ricky!"

I also acknowledge, Giuseppe Sangiorgi, Riccardo Bovina and Sara G. Milner for performing the cloning of EGT1 and PIN1 and exome capture. Thanks to Aditi Borkar for the help in performing the structural modelling on EGT1 protein variants. Thanks to Jayne Davis, Gwendolyn Kirschner, Bipin Pandey for the support with lab experiments. Thanks to Larry York, Brian Atkinson, Craig Sturrock and Sacha Mooney for providing materials and support for the X-Ray/soil experiments at the Hounsfield Facility. Cristobal Uauy for providing wheat EGT1 single mutants and Cristian Forestan generating EGT1 mutant lines in tetraploid wheat. Thanks to Frank Hochholdinger, Matthew Tucker, Axel Himmelbach, Nils Stein, Martin Mascher, Kerstin Nagel, James Simmonds for the overall experimental supervision.

I also acknowledge the technical support of Simona Corneti, Anne Fiebig, Sandra Stefanelli, Alessandro Tondelli. Thanks to ARPA-E DEEPER (USDOE ARPA-E ROOTS Award Number DE-AR0000821) and the Hounsfield Facility Centre at the University of Nottingham for all the support provided for this work. The Hounsfield Facility received funding from European Research Council (Futureroots Project, Grant agreement ID: 294729), Biotechnology and Biological Sciences Research Council of the United Kingdom and The Wolfson Foundation. Thanks Future Food Beacon Nottingham Research and BBSRC Discovery Fellowship (BB/S011102/1). The rhizotron study received funding from the European Union's Horizon 2020 research and innovation programme under grant agreement No 731013 (EPPN2020). Work described here is supported in part by the project 'Rooty- A root ideotype toolbox to support improved wheat yields' funded by the IWYP Consortium (project IWYP122) via the Biotechnology and Biological Sciences Research Council in the United Kingdom (BB/S012826/1). Thanks also to the support provided by the University of Adelaide - University of Nottingham joint PhD scholarship program. Thanks also to Anne McLaren Fellowship at University of Nottingham and the challenge grant (CHG\R1\170040) and BBSRC Discovery Fellowship (BB/V00557X/1).

Table of contents

Acknowledgements **2**

Table of contents **5**

Summary of figures **8**

Summary of Tables **13**

Abstract **14**

Chapter 1 ..... **15**

Introduction **15**

Importance of maize and barley for global food production 16

The need of deeper rooting crops in a climate change scenario 16

Maize, Barley, Rice and *Brachypodium distachyon* root systems 18

Maize root system 18

Barley root system 20

Rice root system and anatomy 21

Brachypodium distachyon root system 23

Root structural and anatomical differences between monocots and *Arabidopsis thaliana* 24

Controls of root angle in model and crop roots 26

Gravitropic Setpoint Angle (GSA) and Anti-Gravitropic Offset (AGO) angle 28

Genetic resource available to investigate deeper rooting in maize and barley 28

Exploiting mutagenized populations of crops 29

Exploiting natural variation 30

Gene editing using CRISPR-Cas9 31

Constraints of using crops as model for functional genomic studies 32

Aims of this PhD study 34

Chapter 2 ..... **35**

Identification and functional characterisation of genes regulating root anatomical traits in cereal models **35**

Introduction 36
DeepGenes Pipeline 37
Material and methods 39
Results 44
DeepGenes analysis pinpointed candidate cortical regulatory genes in maize and orthologues in *Brachypodium distachyon* and rice. 44
Developing Deepgenes mutant lines using CRISPR-cas9 via tissue culture in *Brachypodium distachyon*, rice and maize. 49
The *BdQKY* candidate regulatory gene controls root growth and nodal root anatomy 52
Evaluation of RCA formation in rice Ethylene Insensitive lines 54
Ethylene effects on maize root anatomy and aerenchyma formation 55
Conclusions 57
Chapter 3 59
Root angle is controlled by *EGT1* in cereal crops employing a novel anti-gravitropic mechanism. 59
Introduction 60
Materials and Methods 61
Results 69
Barley TILLING mutant TM194 exhibits steeper root growth angle in every root class 69
Exome sequencing of TM194 reveals a mutation in *ENHANCED GRAVITROPISM 1* (*HvEGT1*) 71
Mutations in a highly conserved motif in the HvEGT1Tubby domain disrupt gene function 73
The role of *EGT1* in controlling root growth angle is conserved in wheat 77
HvEGT1 controls root growth angle via an anti-gravitropic offset (AGO) mechanism 79
HvEGT1 appears to function in an auxin-independent AGO mechanism 81
HvEGT1 transcriptionally regulates ROS homeostasis and cell wall modifying enzymes 83
HvEGT1 is highly expressed in root stele tissues distinct from gravitropic responsive tissues 86
Discussion 87
Chapter 4 90
The auxin efflux carrier PIN1a regulates vascular patterning in cereal roots 90

Introduction 91
Material and methods 94
Results 99
A novel barley short root mutant exhibits defects in root cell number, size and patterning 99
The short root phenotype is caused by a recessive mutation in the *HvPIN1a* gene 101
HvPIN1a is essential for vascular patterning in barley roots 106
PIN1a plays a conserved role regulating root vascular patterning in other cereals 112
Discussion 117
Chapter 5 120
Discussion & Perspectives 120
Exploiting advanced phenomics and genomics to pinpoint root anatomical regulatory genes 120
Exploiting forward genetics to pinpoint novel root angle regulatory genes in crops 121
References 126
List of abbreviations 144
Papers arising from this thesis 145
Supplementary information 146
Supplementary Datasets 160

Summary of figures

Chapter 1

Fig. 1.1. Phenotypic differences in Root Cortical Aerenchyma (RCA), Cortical Cell File Number (CCFN) and Cortical Cell Size (CCS) and their impact on plant fitness under stress condition. 17

Fig. 1.2. Representation of root architecture and anatomy of maize roots (adapted from Hochholdinger, 2009a). 19

Fig. 1.3. Representation of root architecture and anatomy of barley roots. 21

Fig. 1.4. Representation of root architecture and anatomy of rice roots (adapted from Rebouillat et al., 2009). 22

Fig. 1.5. Representation of root architecture and anatomy of Brachypodium distachyon roots. 24

Fig. 1.6. Representation of architectural and anatomical differences between monocots and the dicot model *Arabidopsis thaliana*. 25

Chapter 2

Fig. 2.1. Schematic overview on DEEPER project. 37

Fig. 2.2. DeepGenes pipeline overview. 38

Fig. 2.3. Schematic representation of gRNA selection and cloning strategy to suit Single and Double gRNA constructs for developing CRISPR edited lines in Brachypodium distachyon and Maize. ..41

Fig. 2.4. Tissue culture pipeline used to generate stable transformed CRISPR edited lines in Brachypodium distachyon. 42

Fig. 2.5. Summary of resulted candidate Deepgenes derived from GWAS analysis on maize CCC, CCFN, TCA and RCA. 48

Fig. 2.6. Organ and tissue specificity expression of BdQKY, BdFERONIA and OsHIF1a. 49

Fig. 2.7. List of events with dendrograms carrying successful edits for QKY89_gRNA (Pos1). 51

Fig. 2.8. Representative images of BdQKY mutant Pos1_8(1). 53

Fig. 2.9. Resulting bar plots of root length and anatomical traits of Brachypodium distachyon wild type Bd21-3 and the QKY edited mutant Pos1_8(1) indicates QKY to affect both root development and anatomy. 54
Fig. 2.10. Preliminary results of RCA formation in rice ethylene mutants. 55
Fig. 2.11. Root length differences in ethylene treated maize seedlings. 56
Fig. 2.12. Root anatomical differences in ethylene treated maize seedlings. 56

S.Fig. 2.1. Phylogenetic analysis of Malectin-like tyrosine kinases sequences in maize, barley, rice, *Brachypodium distachyon* and Arabidopsis. 150
S.Fig. 2.2. Phylogenetic analysis of C2 C-terminus-phosphoribosyltransferases sequences in maize, barley, rice, *Brachypodium distachyon* and Arabidopsis. 151

Chapter 3

Fig. 3.1. TM194 mutant shows steeper angle in every root class in soil conditions. 69
Fig. 3.2. TM194 mutant shows steeper seminal and lateral root angle phenotype in semi-hydroponic conditions. 70
Fig. 3.3. Exome and WGS sequencing of TM194 identifies mutation in EGT1. 72
Fig. 3.4. TM3580 mutation causes a splice acceptor variant, resulting into a premature stop codon. 73
Fig. 3.5. Mapping of mutant alleles and key haplotypes identified from the WHEALBI population onto the HvEGT1 Tubby domain structure. 75
Fig. 3.6. Phylogenetic conservation of HvEGT1 residues. 76
Fig. 3.7. Phylogenetic analysis of Tubby-like F-Box Protein sequences in barley, wheat, rice, maize and Brachypodium distachyon. 78
Fig. 3.8. HvEGT1 controls root growth angle via auxin-independent anti-gravitropic offset (AGO) mechanism. 80

Fig. 3.9. Root bending response assay revealed also TM3580 to respond faster to gravitropic stimulus. 81

Fig. 3.10. HvEGT1 transcriptionally regulates peroxidases and cell wall loosening enzymes and it is specifically expressed in root vasculature tissues. 82

Fig. 3.11. Cell wall gene expression clusters that likely to respond to loss of HvEGT1 expression.... 84

Fig. 3.12. Spatiotemporal expression of selected cell-wall and peroxidases related genes in rice roots. 86

Chapter 4

Fig. 4.1. Phylogenetic analysis of PIN Protein sequences in Arabidopsis barley, wheat, rice, maize and Brachypodium distachyon. 93

Fig. 4.2. Barley TILLING mutant line TM5992 shows short root phenotype with root growth and development defects. 100

Fig. 4.3. Mutation in HvPIN1a causes short root phenotype and developmental defects. 103

Fig. 4.4. HvPIN1a allelic mutant lines TM5141 and TB13081 exhibit similar root growth rate as line TM5992. 104

Fig. 4.5. HvPIN1a allelic mutant lines TM5141 and TB13081 exhibit similar root developmental defects as line TM5992. 105

Fig. 4.6. Hvpin1a mutant alleles shows root vascular defects that can be mimicked by blocking PIN activity in Morex by NPA treatment. 107

Fig. 4.7. Phenotypic anatomical data collected from mid seminal root cross sections of barley seedlings of the genotypes Morex, TM5141, and TM5992. 108

Fig. 4.8. Phenotypic anatomical data collected from mid seminal root cross sections of barley seedlings of the genotypes Barke, Barke_WT, and TB1381 (Barke_PIN1a) exhibits similar root anatomical defects as line TM5992 and TM5141. 109

Fig. 4.9. Short root phenotype in HvPIN1a mutant alleles can be mimicked in barley wild type roots using NPA treatment. 111
Fig. 4.10. The role of PIN1a in root vascular patterning is conserved in cereal model Brachypodium distachyon. 114
Fig. 4.11. Architectural and anatomical data collected from mid primary root cross sections of Brachypodium distachyon seedlings of genotypes Bd21-3(WT), BdPIN1A-1, BdPIN1b-1 and 2153-24. 115
Fig. 4.12. Short root phenotype in HvPIN1a mutant alleles can be mimicked in Brachypodium distachyon wild type roots using NPA treatment. 116

Discussion & Perspectives Chapter

Fig. 5.1. Atomic Force Microscope (AFM) to investigate stiffness properties in root tissues. 124
Fig. 5. 2 AFM nanomechanical force spectroscopy of tissues within the elongation zone of the root meristem in Morex and TM194 125

Supplementary information

S.Tab. 2.1. Summary of genes and corresponding genetic resource we attempted to develop to characterise Deepgenes. 146
S.Tab. 2.2. gRNAs, primers and PCR conditions use to generate and sequence DeepGenes Brachypodium distachyon CRISPR events. 147
S.Tab. 2.3. gRNAs and PCR conditions use to generate and sequence DeepGenes Maize CRISPR events. 147

S.Tab. 2.4. List of primers used for screening by genotyping of the maize Deepgenes CRISPR lines. List of primers used for screening by genotyping of the maize Deepgenes CRISPR lines. 148
S.Tab. 2.5. Summary table of protein domain conservation analysis of main monocots and Arabidopsis orthologues of ZmFERONIA. 149

S.Fig. 2.1. Phylogenetic analysis of Malectin-like tyrosine kinases sequences in maize, barley, rice, Brachypodium distachyon and Arabidopsis. 150
S.Fig. 2.2. Phylogenetic analysis of C2 C-terminus-phosphoribosyltransferases sequences in maize, barley, rice, Brachypodium distachyon and Arabidopsis. 151

S.Fig. 3.1. TdEGT1 loci also control root growth angle in wheat. 152
S.Fig. 3. 2. Methodology to measure root bending angle (Root angle adjusted to time [0]) using FIJI. 153
S.Fig. 3. 3. Additional quantification of root and shoot bending angle and root length from the root bending response assay on Morex, TM194 and TM3580. 154
S.Fig. 3. 4. Auxin root bending sensitivity bioassay. 155
S.Fig. 3.5. Shoot bending response assay revealed no significant differences between Morex and TM194. 156
S.Fig. 3. 6. Schematic of probe design for EGT1 RNA in situ hybridisation experiment. ... 157
S.Fig. 3. 7. In Situ Hybridisation (ISH) on root tips of Morex with HvEgt1 sense probe. 158

S.Fig. 4.1. Measured root growth parameters of TM5992 and Morex. 159
S.Fig. 4.2. Orthogonal Z-stack view of a longitudinal section in Morex. 159

Summary of Tables

Tab. 2.1. Summary of T0 Events genotyping showing positive CRISPR-Cas9 edits in Brachypodium Deepgenes orthologues. 50

Abstract

Global food security and climate change represent major challenges faced by humankind during this century. Developing deeper rooting, more resource efficient crops represents an attractive solution to increase crop production sustainably whilst also enhancing soil carbon (C) sequestration. For example, planting maize varieties with a root system 0.5m deeper than currently sown in USA is predicted to improve foraging for water and nitrogen resources in sub-soil layers whilst burying up to two thirds of carbon related to US transportation emissions. The aim of this PhD project is to identify and characterise key genes that control anatomical and architectural traits contributing to deeper rooting in cereal crops such as maize and barley (as part of the DEEPER project funded by the ARPA-E ROOTS initiative).

A DEEPGENES discovery pipeline was initially developed to pinpoint candidate genes that controlled key traits determining deeper rooting in maize. Root anatomical traits included cortical cell number, cortical cell file number, total cortical area and root cortical aerenchyma plus architectural traits such as crown root angle. Promising DEEPGENE candidates where then shortlisted based on root expression and tissue specificity using maize and cross-species transcriptomic datasets in model plants such as rice and *Arabidopsis thaliana*. Loss of function mutants in candidate DEEPGENES were designed and/or developed in maize and the cereal model *Brachypodium distachyon* using CRISPR-Cas9 based approaches, respectively. Phenotypic analysis revealed a candidate regulator for root cortical cell number encoded by the QKY gene.

In parallel with maize studies, a forward genetics approach was used to pinpoint root angle or root length mutants in the barley TILLMore population. Two mutants were characterised which disrupted either: 1) *HvPIN1A*, encoding an auxin-efflux carrier, which controls root growth and vascular patterning in cereal roots; and 2) A novel Tubby1-like gene called *HvEGT1 (**E**nhancing **G**ravi**t**ropism 1)* which regulates root gravitropic set point angle in cereals. Barley and wheat mutant lines disrupting *EGT1* function exhibited a deeper rooting phenotype, revealing this sequence as a promising DEEPGENE target to create novel cereal varieties.

Chapter 1

Introduction

Importance of maize and barley for global food production

Wheat (*Triticum aestivum*), rice (*Oryza sativa*), maize (*Zea mays*) and barley (*Hordeum vulgare*) represent the top four cereal crops sustaining global food security. Maize, harvested either as a kernel or as silage represent very important sources of calories in human diet and/or for livestock production. Despite its tropical origin, maize is now cultivated world-wide. It is the second most cultivated crop (>200M Ha) after wheat but, with over 1100 million tons harvested annually it is the first in terms of production (FAO, 2019). Barley is also harvested as a kernel and is used in animal and human diets together with brewing. It is the fourth most important cereal crop (>50M Ha) with more than 158 million tons production and, like maize, is widely cultivated across the globe (FAO, 2019). Both are also staple crops in lower-income countries, where they play an essential role in human diet with 200 kcal/capita/day, which is almost equal to the calories supported by wheat in these regions (FAO, 2019).

The need of deeper rooting crops in a climate change scenario

As a result of rising global population, combined with climate change causing elevated temperature and decreasing rainfall (IPCC, 2014), crop breeders need new genetic and phenotypic tools to develop new future-proofed varieties to guarantee global food security. Crops with more sustainable traits will be essential for both low-input and high-input agriculture. Low-input agriculture is typical of developing nations and is characterized by suboptimal availability of Nitrogen (N) and water, whereas an excess of the same resources in high-input agriculture are a cause of environmental pollution in developed countries (Lynch, 2015). N in particular, when in the highly soluble form of nitrate (NO_3^-), is not captured by soil particles, quickly leaching through the soil and leading to groundwater pollution. Maize lines with deeper roots have been demonstrated to be more effective at capturing more nitrate than shallower rooting lines (Schneider *et al.*, 2021*a*) .

A steep, deep and cheap root ideotype for maize has been proposed to optimize soil exploration through exploiting root architectural and anatomical phenes (phene to phenotype as gene to genotype) (Lynch, 2013, 2015). Several architectural phenes regulate

deeper rooting and improve soil exploration (e.g. root angle, root number, root hair density etc.) were shown to improve plant performances under stress conditions (Lynch, 2015,2019). Angle represents the most architectural determinants for rooting depth in maize and resource capture, especially under drought conditions in maize and other cereal crops (Ho et al., 2005; Mace et al., 2012; Trachsel et al., 2013). In rice, a gene called Deeper Rooting 1 (DRO1) promotes faster gravity response and steeper roots, resulting in DRO1 containing rice plants being more resistant to water stress conditions (Uga *et al.*, 2013). Root anatomical phenes, particular in the cortical tissue, have been identified to improve crop performance under stress conditions (Lynch, 2015, 2019). Maize plants with high Root Cortical Aerenchyma (RCA), low Cortical Cell File Number (CCFN) and large Cortical Cell Size (CCS) (Fig 1.1) exhibit decreased root respiration, enabling crops to build a deeper root system, improving resource capture and yield under low N and low water availability (Chimungu *et al.*, 2014; Lynch, 2015).

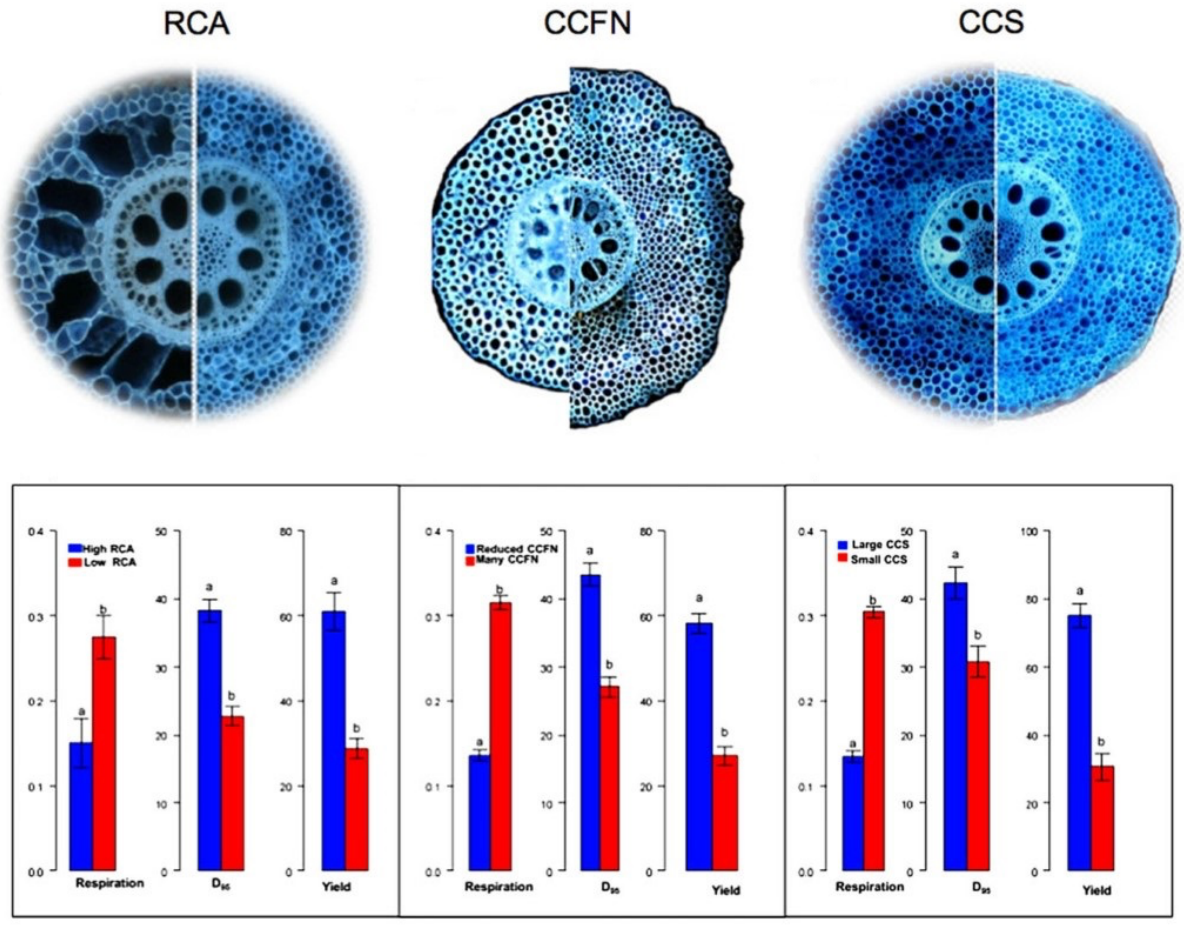


Fig. 1.1. Phenotypic differences in Root Cortical Aerenchyma (RCA), Cortical Cell File Number (CCFN) and Cortical Cell Size (CCS) and their impact on plant fitness under stress condition.

In details, high level of RCA under low N, high CCS and low CCFN under drought condition decrease respiration, increase root depth (D_{95}) and yield. (Adapted from Lynch, 2015).

Despite the clear potential for improvements to the root systems of crops, this organ is still not very well studied in the field environment and generally considered as the "hidden-half" of plants, for several different reasons including: 1) soil is not (generally) an accessible growth environment for high throughput genetic studies, 2) the high degree of phenotypic plasticity exhibited by roots in different soil environments, and 3) the complexity of root system components (Hochholdinger et al., 2018). Given such challenges studying root systems in crops, researchers are developing resources in more tractable model species such as barley and *Brachypodium distachyon* to facilitate more rapid molecular genetics and functional studies (Draper *et al.*, 2001).

Maize, Barley, Rice and *Brachypodium distachyon* root systems

In this section, I briefly summarise similarities and differences between the root systems of the cereal species studied in this thesis. In particular, I will describe the different elements composing Root System Architecture (RSA), together with root anatomy of maize, barley, rice and *Brachypodium distachyon*.

Maize root system

Maize has a complex root architecture composed of embryonic and post-embryonic root systems (Fig. 1.2) (Hochholdinger, 2009). The embryonic root system, originating from the seed, provides support to the plant during the first weeks after germination. It is composed of the primary root originating from the embryo and seminal roots which originate from the scutellar node (Fig 1.2a). The post-embryonic root system, originating from the shoot, is the main root system during later vegetative stages. It is composed of crown roots originating from the hypocotyl which is organized in ~6 whorls (Fig 1.2a), brace roots originated from the epicotyl organized in 2-3 whorls (Fig 1.2b) (Hoppe *et al.*, 1986; Feldman, 1994) and lateral roots (Fig 1.2a) which are important for water and nutrient uptake during all developmental

stages (McCully and Canny, 1988; Lynch, 1995). Regarding the root anatomical structure

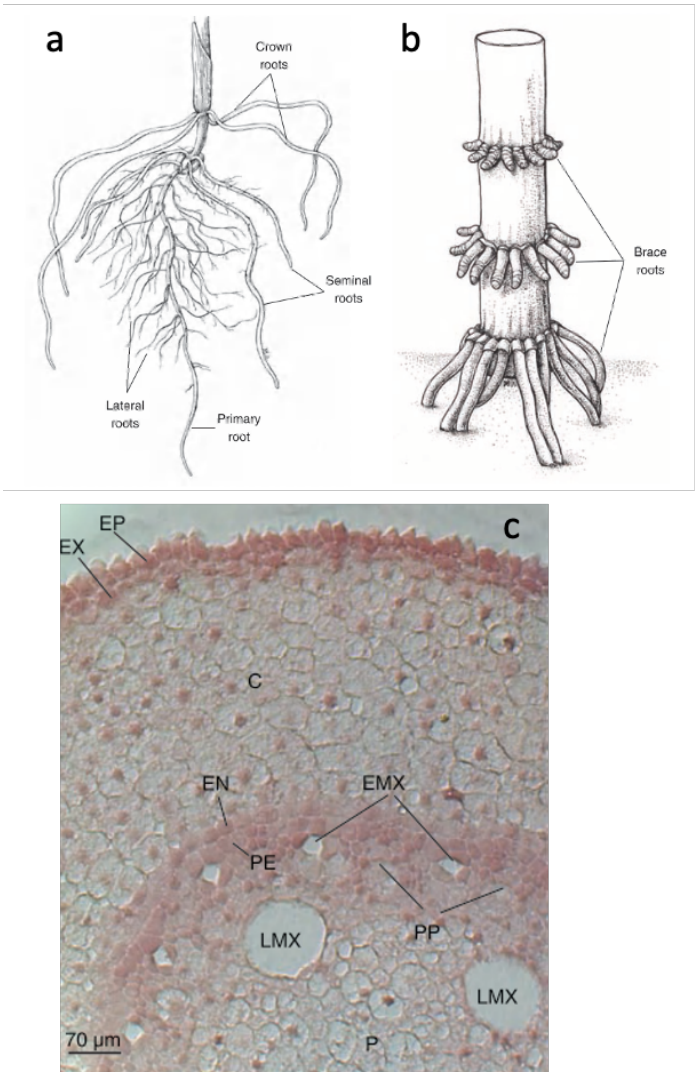


Fig. 1.2. Representation of root architecture and anatomy of maize roots (adapted from Hochholdinger, 2009a).

a) Schematic of maize belowground root architecture. b) Schematic of maize aboveground root architecture. c) Radial cellular organization of seminal and crown root of maize. EP=epidermis, EX=exodermis, C=cortex, EN=endodermis, PE=pericycle, EMX= early metaxylem, LMX= late metaxylem, PP=phloem pole, P=pith.

of maize, the central cylinder (CC) contains the vascular element such as early and late meta-xylem vessels (EMX, LMX) also known as peripheral meta-xylem (PMX) and central meta-xylem (CMX) respectively (Hochholdinger, 2009*a*; Kirschner *et al.*, 2017). Phloem vessels (PP),

between meta-xylem vessels, are functionally important for enhancing water and nutrient uptake and photosynthate redistribution. The central cylinder is enclosed by a layer of pericycle (PE) and endodermal cells (EN). This is surrounded by several layers of cortical cells (C), which collectively form the root cortical layer, which is itself enclosed by exodermis (ES) and epidermis (EP) which are the outermost root tissues and are directly in contact with the rhizosphere and are responsible for producing root hairs. It was recently reported that (from 10 cm behind the root tip) the outermost cortical cell layers can form highly lignified small cells which contribute to mechanical stress resistance and are termed Multiseriate Cortical Sclerechyma (MCS) cells (Schneider *et al.*, 2021*b*). Older root cortical layers can also undergo Program Cell Death (PCD), forming hypoxia induced air-filled spaces called Root Cortical Aerenchyma (RCA), which I describe in detail in the next chapter (Fig. 1.2a-b from Hochholdinger,2009).

Barley root system

The barley root system has been of research interest since the early 20th century (Jackson, 1922). In this report, the existence of two root systems was described: a branched main root system emerging from the seed and a nodal (or crown) root system emerging from below the tillers on the hypocotyl(Ramireddy *et al.*, 2018). Within the main root system, the primary root can be discriminated from seminal roots as the first root to emerge from the seed, but are otherwise identical at anatomical and morphological levels (Kirschner *et al.*, 2017)(Fig. 1.3a-b). Anatomically, the radial section is similar to maize and seminal and nodal roots differ for having single and multiple CC respectively (usually 4 to 5) (Kirschner *et al.*, 2017; Oyiga *et al.*, 2020)(Fig. 1.3c-d). However, in contrast to maize RCA, barley undergoes Root Cortical Senescence RCS (Deacon *et al.*, 1986; Schneider *et al.*, 2017). Like RCA, RCS leads to a reduction in cortical cell area by forming large air-filled empty spaces regulated by ethylene and PCD related genes (Schneider *et al.*, 2018). In contrast to RCA, it is independent from the level of hypoxia in the media and it is driven by cell anucleosis from the outer to the inner root cortical cell layers.

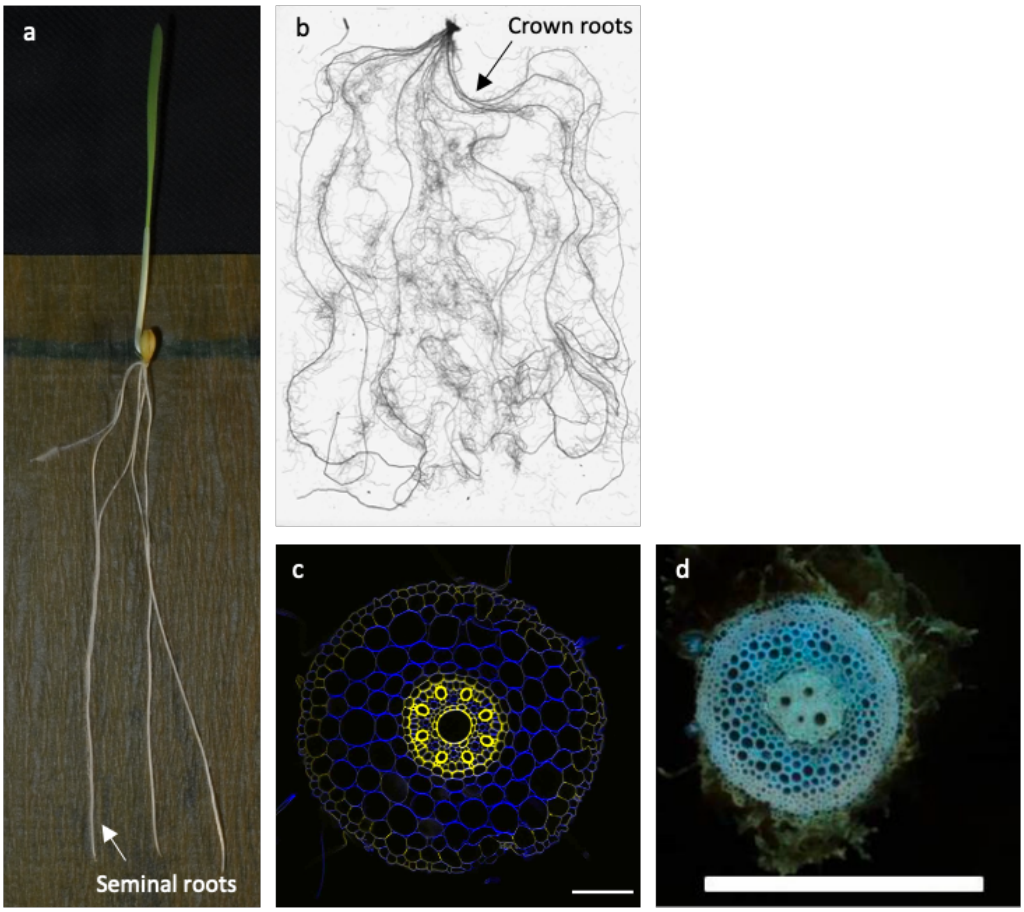


Fig. 1.3. Representation of root architecture and anatomy of barley roots.

a) Representative image of a 4 DAG barley seedlings grown in paper roll with highlights on seminal roots. b) Representative image of a 50 DAG barley seedlings grown in soil column with highlights on crown roots (courtesy of Haoyu Lou). c) Cross section of 4 DAG seminal mid root in barley stained with calcofluor white (general cell wall components) and Basic fuchsin (lignin). d) Cross section of nodal root from mature plant of barley obtained using LAT (adapted from Oyiga et al., 2020)

Rice root system and anatomy

Similarities in the root structure of maize and barley can also be observed rice (Fig. 1.4). The rice root system is composed of a single primary root emerging from the embryo and a crown root system originating from the mesocotyl, where the latter represents the majority of the rice root system of an adult plant (Yoshida and Hasegawa, 1982; Rebouillat *et al.*, 2009). Regarding root anatomy, there are no major differences in the radial organization compared

to other cereal crop species other than the constitutive formation of RCA to facilitate air exchange in hypoxic paddy environments (Rebouillat *et al.*, 2009). However, when cultivated in rain-fed upland (aerobic) conditions, rice roots contain a highly lignified sclerenchymatous cell layer present beneath the exodermis to protect the inner tissues from water stress.

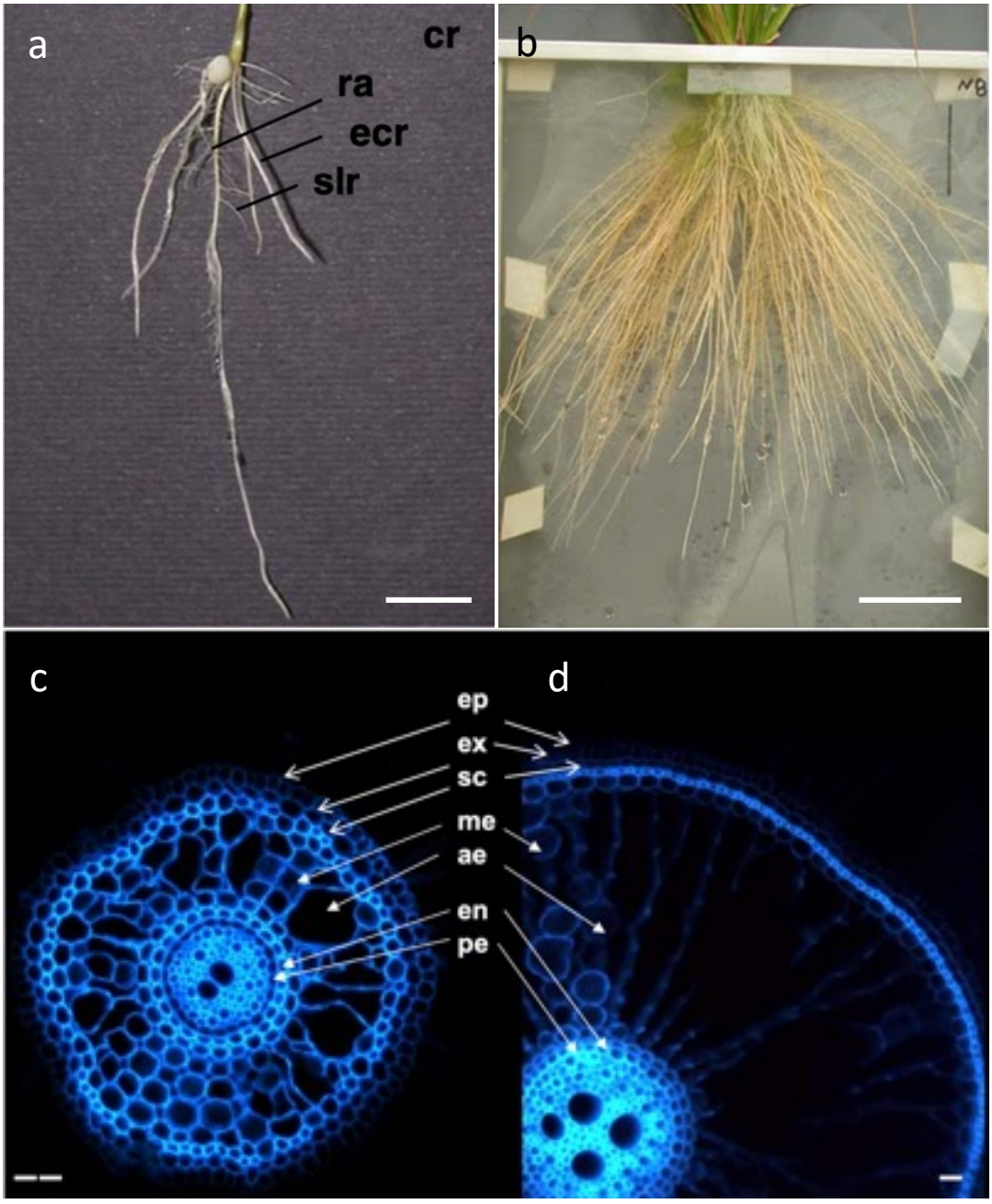


Fig. 1.4. Representation of root architecture and anatomy of rice roots (adapted from Rebouillat et al., 2009).

a) rice embryonic root architecture system. Bar = 1cm; b) rice crown root system at maturation stage. Bar = 5cm; c-d) radial section of the primary root (c) and crown root (d) of

rice. ep= epidermis, ex= exodermis, sc= sclerenchyma, me= mesodermis (cortex), en= endodermis, pe=pericycle.

Brachypodium distachyon root system

Despite a more compact simpler root architecture system *Brachypodium distachyon* shows many similarities with other cereals root systems (Watt *et al.*, 2009; Chochois *et al.*, 2015) (Fig. 1.5).

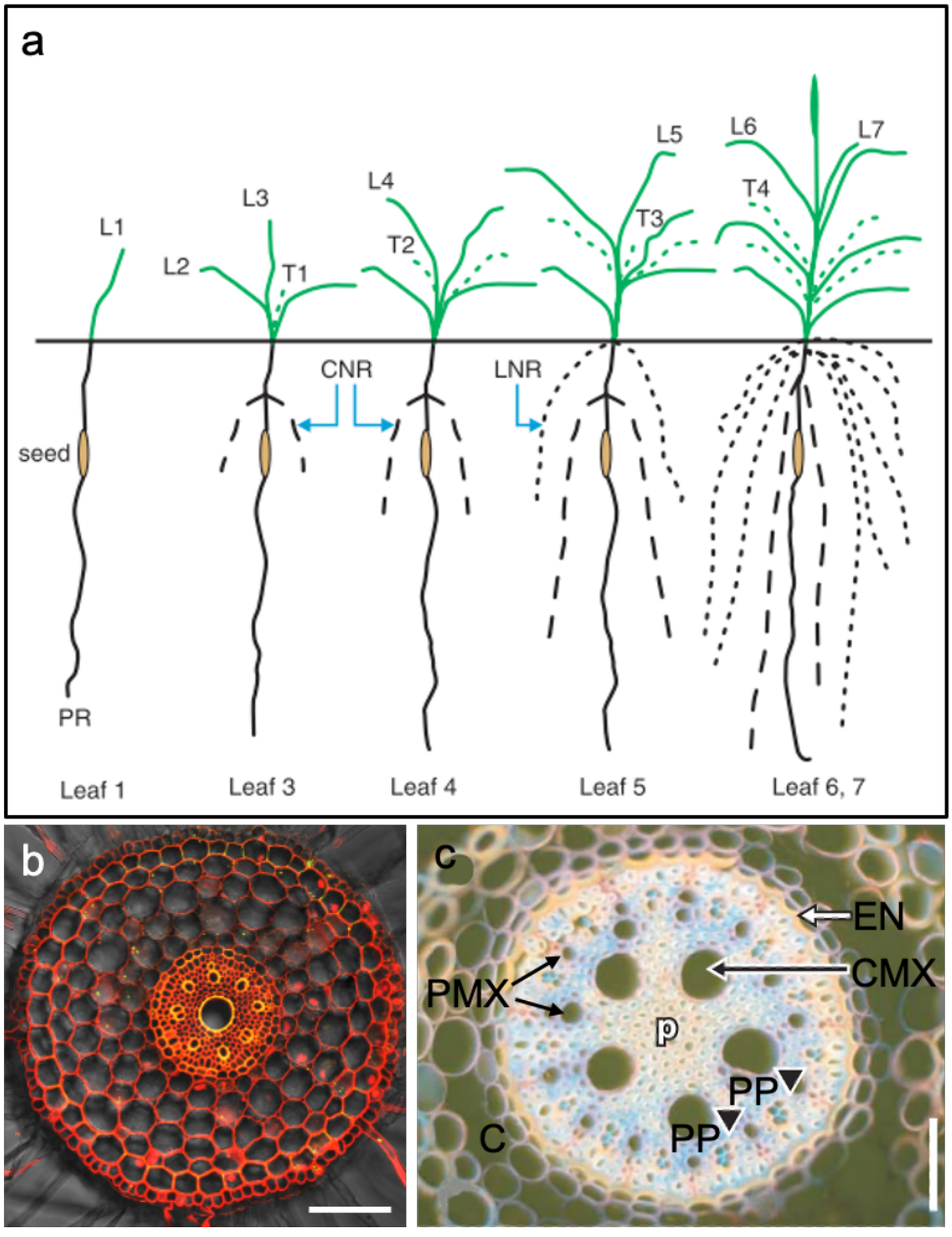


Fig. 1.5. Representation of root architecture and anatomy of *Brachypodium distachyon* roots.

a) Adapted schematic of *Brachypodium distachyon* root system architecture from Watt et al., 2009 . L = leaf , T = Tiller, PR = primary root, CNR = coleoptile nodal root, LNR = leaf nodal root. b) Primary root cross section in *Brachypodium distachyon*. c) Adapted schematic of *Brachypodium distachyon* CNR and LNR cross section highlights anatomical insights, from Watt et al., 2009. C = cortex, p = pith, PP = phloem poles, CMX = central meta-xylem, PMX = peripheral meta-xylem, EN = endodermis.

Brachypodium distachyon is composed by a single primary root emerging from the seed and an adventitious root system termed the Coleoptile Nodal Roots (CNR) emerging at the 3rd leaf stage from the basal part of the mesocotyl and Leaf Nodal Roots (LNR) emerging from the basal part of the coleoptile after the 5th leaf has emerged. From studies conducted in soil, root anatomy was revealed to be very similar to other cereals (Watt *et al.*, 2009). This study shows that the only primary root is in fact characterised by the presence of a single central xylem surrounded by 4-8 peripheral xylem poles, whereas the anatomy of CNR and LNR exhibit up to seven central xylem poles surrounded by 7 to 15 peripheral xylem vessels. Roots are also shorter and reduced in number compared to other cereals presented, allowing this plant to not suffer stresses on the overall growth imposed by small pot size. The similarities between *Brachypodium distachyon* and the other member of the grass family makes this plant a very suitable model to adopt for greenhouse studies with limited space available.

Root structural and anatomical differences between monocots and *Arabidopsis thaliana*

Researchers have noted that differences in architecture and radial anatomical organisation between roots of cereal crops and Arabidopsis make it difficult to the use the latter specie as a model (Hochholdinger and Zimmermann, 2008)(Fig. 1.6a-b). At a root architectural level, *Arabidopsis* is characterised by the presence of a single embryonic root that develops from the seed and remains active through its whole life cycle with lateral roots of different orders emerging from it (Smith and De Smet, 2012). In contrast, the majority of the root system in cereal crops is represented by adventitious roots, whereas the embryonic roots are only

functionally relevant during early stages of their life cycles. In addition, very noticeable differences are also observed at the anatomical level especially concerning the organisation of the central stele and cortical layer (Benfey *et al.*, 2010; De Smet *et al.*, 2015; Di Ruocco *et al.*, 2018) (Fig. 1.6c). Monocots are characterised by a single or multiple enlarged central meta-xylem surrounded by a variable number of peripheral metaxylem and phloem distributed radially around the central stele (Rebouillat *et al.*, 2009; Kirschner *et al.*, 2017) (Fig. 1.6d). The Arabidopsis central stele in contrast contain protoxylem and protophloem poles patterned in a perpendicular direction (Dolan *et al.*, 1993). Monocot roots also exhibit multiple cortical cell layers that vary between species, whereas Arabidopsis has only a single cortical cell layer (Chimungu *et al.*, 2014). Moreover, lysigenous aerenchyma formation was observed only in the central stele of Arabidopsis roots upon hypoxic stress (Mühlenbock *et al.*, 2007) whereas constitutive or induced aerenchyma or RCS are commonly present in root cortical tissues in crops (Fagerstedt, 2010; Schneider *et al.*, 2017).

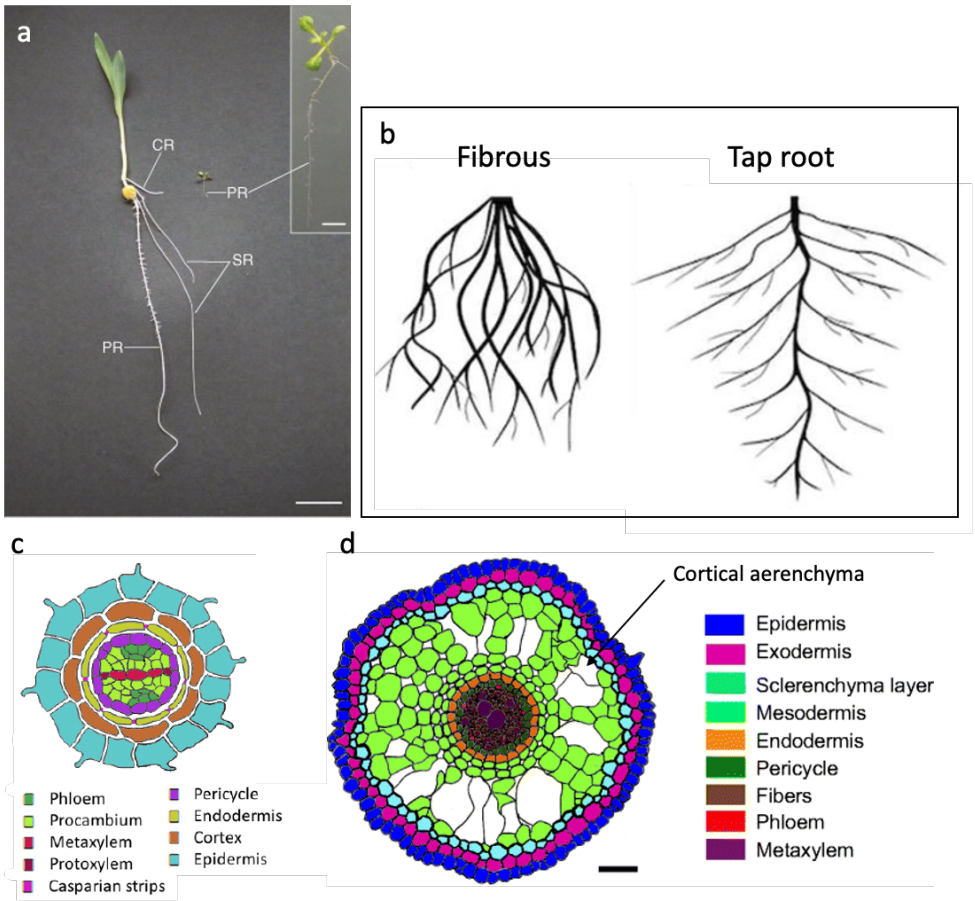


Fig. 1.6. Representation of architectural and anatomical differences between monocots and the dicot model Arabidopsis thaliana.

a) Comparison of root architecture difference between maize and Arabidopsis young seedlings (from Hochholdinger and Zimmermann, 2008) PR=primary root, SR=seminal root, CR= crown root, bar= 2cm (maize) 2mm (*Arabidopsis*). b) schematic representation of fibrous root system (monocots) and tap root system (dicots) at maturation stage. c,d) Comparison of radial cellular organization between Arabidopsis and rice seminal roots (Rebouillat et al., 2009; De Smet et al., 2015)

Controls of root angle in model and crop roots

Gravitropism has been studied by biologists since the 18th century (Duhamel du Monceau, 1758; Knight, 1806; Darwin and Darwin, 1880). Gravitropism involves two distinct phases; a gravity perception phase where a specialised gravity sensing organelle senses changes in plant orientation; then a gravitropic response phase where the growing root or shoots undergo a bending response to re-orient the organ relative to gravity (Went, 1926; Cholodny, 1927; Hart, 1990; Myers *et al.*, 1994).

The molecular events controlling gravitropism has been studied in detail in the eudicot model *Arabidopsis thaliana* over the past several decades. Gravity sensing is mediated by the sedimentation of statoliths, starch filled organelles present in root tip columella cells, which move within these cells after root reorientation (Yoder *et al.*, 2001; Morita and Tasaka, 2004). In rice, the Rice Morphology Determinant (RMD) protein was demonstrated to link statoliths with actin filaments. The *RMD* rice mutant exhibited faster root bending due to faster sedimentation of statoliths within columella cells (Huang *et al.*, 2018). Other proteins, such as ARG1, MAR2 and CHUP1, are reported to also have effects on cytoskeleton-statolith interactions (Boonsirichai *et al.*, 2003; von Braun and Schleiff, 2008; Jouhet and Gray, 2009).

Regarding the transduction of a physical (i.e. statolith movement) to a biochemical/molecular signal, the hormone auxin is widely identified to be the master regulator of this process. Auxin is present as Indole-3-Acetic-Acid (IAA^-), travelling between cells in a polar direction using specialised influx and efflux carriers. AUX1 is the primary auxin influx carrier firstly characterised in roots of *Arabidopsis* where *aux1* mutants exhibit an agravitropic phenotype (Bennett *et al.*, 1996*a*). AUX1 was expressed in root tissues involved in gravity transduction

and response such as columella, lateral root cap (LRC) and epidermis (Swarup *et al.*, 2005). Auxin redistribution among these root tissues it is controlled by the auxin efflux carrier family encoded by PINFORMED (PIN) genes. PIN3 and PIN7 are reported to be relocalised after gravistimulus to the 'new' lower surface of columella cells, redirecting a lateral auxin gradient to the lower side of the root (Friml *et al.*, 2002; Kleine-Vehn *et al.*, 2010). Auxin is then transported shootwards by AUX1 and PIN2 carriers in LRC and epidermal tissues (Abas *et al.*, 2006). The generation of a gravity induced lateral auxin gradient was demonstrated by Brunoud et al, 2012 and Band *et al.*, 2012 employing the DII-VENUS auxin biosensor. Moreover, when the auxin biosensor was imaged in the Arabidopsis starchless mutant *pgm-1*, no lateral auxin gradient between lower and upper root sides was detected 2 hrs after a gravistimulus was applied. This demonstrated that, as consequence of root reorientation, an intracellular physical stimulus generated from statolith sedimentation in the columella cell is converted into an auxin gradient which is then transported shootward in the columella, lateral root cap and epidermis.

Transduction of this auxin gradient results in a differential auxin response in elongation zone epidermal cells where their expansion is repressed on the lower side of the root and promoted on the upper side, resulting in bending towards the gravity vector (Swarup *et al.*, 2005). At a molecular level the auxin AUX/IAA complex is well known to be perceived by the F-box SCF TIR1/AFBs/ASKs complex which leads to AUX/IAA ubiquitination and degradation, resulting in the de-repression of class A Auxin Responsive Factors (ARFs), in particular ARF7, ARF19 and other auxin responsive genes such as IAA1, IAA2, AXR2, AXR3 (Gray *et al.*, 2001; Band *et al.*, 2012; Brunoud *et al.*, 2012). Expression in root epidermal cells of cell-wall related genes involved in the remodelling of the xyloglucan-cellulose network and cell expansion, AtXT18 and AtXT19, are known to be regulated by ARF7 and ARF19 (Vissenberg *et al.*, 2005; Sato *et al.*, 2015). The lateral auxin gradient on the lower (versus upper) root bending sides is speculated to regulate the expression of such cell wall related genes that control the root bending response to gravity.

Gravitropic Setpoint Angle (GSA) and Anti-Gravitropic Offset (AGO) angle

Not all plant organs exhibit positive or negative gravitropic growth angles like primary roots or shoot tissues, but adopt intermediate angles, raising the question of how this is controlled? This led to the concept of Gravitropic Setpoint Angle (GSA) which is defined as the angle at which a specific organ maintain its growth equilibrium with respect to the gravity vector (Digby and Firn, 1995). By this definition, an organ growing parallel to the gravity vector will have a GSA of 0° in the case of a root growing straight downwards, versus 180° in the case of a shoot growing straight upwards. Any organ that doesn't exhibit a vertical growth angle will then have a GSA between 0° to 180°. GSA appears to be an innate property of a plant organ (Roychoudhry and Kepinski, 2015). This means that when an organ's orientation is altered by tilting, it will rapidly reset to its initial GSA value. GSA depends on the interplay between gravitropic and Anti-Gravitropic Offset (AGO) mechanisms (Roychoudhry *et al.*, 2013). Despite its definition, GSA can change during development. For example the regulation of the non-vertical growth and the constant reset of GSA has been observed in lateral roots of *Arabidopsis thaliana* (Guyomarc'h *et al.*, 2012). Non-vertical growth response is regulated by auxin via the SCF TIR1/AFB/Aux-IAA pathway, where mutants with loss of positive regulators (*tir1*, *afb4* and *afb5*) exhibit lateral roots whose GSA is reset more horizontally compared to wild type. Conversely, mutants with loss of negative regulators of auxin signalling (*axr3*, *arf10* and *arf16*) exhibit lateral roots which grow more vertically than wild type. Consistent with this auxin-dependence, when exogenous auxins 2,4D were applied it was observed that lateral roots adopt a more vertical GSA than untreated roots not only in Arabidopsis but also in rice and bean. It was concluded that auxin regulates the AGO mechanism which antagonistically counterbalances gravitropism, where the relative strength between those determines the growth angle adopted by each organ.

Genetic resource available to investigate deeper rooting in maize and barley

Over the past decades, most of the fundamental molecular mechanisms regulating root growth have been described in the simple dicot model *Arabidopsis thaliana* (Benfey et al, 2010). However, recent advances in Next Generation Sequencing (NGS) (which includes NGS genome and transcriptome sequencing) combined with forward and reverse genetic

approaches has revolutionised studies in crops. This led to the possibility of 1) developing genome-mapped mutagenized populations 2) sequencing a large number of crop genotypes in order to map genetic variations in natural population 3) implementation of gene editing protocols using CRISPR-Cas9 to precisely manipulate plant genomes to assist the identification of gene functions in different biological processes.

Exploiting mutagenized populations of crops

Mutagenized populations represent vital genetic resources to discover novel root mechanisms in crops. For example, to support functional genomic studies in maize, a transposon based mutagenized population in the W22 background called UniformMu using *Roberson Mutator* was generated with more than 26000 insertions in 5000 seeds stocks, making this one of the largest mutant population available for maize (McCarty *et al.*, 2005*a*). *Robertson mutator* (*Mu*) is part of a two-module system composed of autonomous elements (*MuDR*) and multiple non-autonomous elements (*Mu*). By turning on and off the *MuDR* elements via backcross, it is possible to generate a high number of stable mutated maize lines as result of a change in the expression in the targeted genes by the *Mu* elements. Genomic location of transposon insertions, together with maize genomic and transcriptomics resources, are available for both B73 and W22 background in the maize web repository www.maizegdb.org (McCarty *et al.*, 2005*a*; McCarty and Meeley, 2009; Portwood II *et al.*, 2019). Once a mutation is found in a target gene it is possible to use the TIR sites of the *Mu* elements as a marker to confirm the mutation using a simple PCR protocol, making this another great advantage for functional biology studies. Several other *Ac/Ds* and *Mu* mutagenized populations with genome mapping information are available in maize (Bensen *et al.*, 1995; May *et al.*, 2003; Raizada, 2003; Kolkman *et al.*, 2005; Li *et al.*, 2013). In *Brachypodium distachyon* it is available as a fully sequenced T-DNA population composed of more than 20.000 mutant lines. In addition, some of the T-DNA inserts are tagged with GFP and GUS modules which has the potential to act as a gene trap when the insert is localised downstream of a gene or a promoter (Bragg *et al.*, 2012; Hsia *et al.*, 2017).

Compared to this wide range of mutant population available in crop models like maize, barley resources for reverse genetics studies remain an underdeveloped field. A transposon based *Ac/Ds* system was developed in barley by *Zhao et al., 2016* although low frequency of transposition doesn't allow a mutation coverage across the genome when compared to TILLING (Brown *et al.*, 2015). TILLING (Targeting Induced Local Lesions IN Genomes) is the favoured reverse and forward genetic approach in barley (see listing by *Huang, 2019)*. In this crop, seeds are commonly chemically mutagenized using Sodium Azide (NaN_3) producing GC >AT mutations in DNA at a very high frequency (i.e. up to 1/154 base pairs) leading to missense - stop gain substitutions at the protein level (Schreiber *et al.*, 2019). A very versatile TILLING resource for root biology studies in barley is the TILLMore population (Talamè *et al.*, 2008; Bovina *et al.*, 2011). A high mutation rate of 1/374 mutated base pairs was reported and a wide range of altered root phenotypes (mainly focussed on root architectural and root hairs) were observed in 70 lines of TILLMore making this one of the best resources to identify genes regulating root processes (Bovina *et al.*, 2011). Locating the positions of such mutations can be achieved by 1) coupling Bulk Segregant Analysis (BSA) with exome capture in a forward genetic fashion 2) DNA pooling followed by PCR amplification of multiple target genes 3) *In-silico* TILLING which exploits NGS approaches to sequence genomes of entire populations (Salvi *et al.*, 2014). In chapters 3 and 4, I will report how coupling BSA analysis using a TILLING resource helped map two genes regulating root architectural traits in barley.

Exploiting natural variation

Breakthroughs in genomic sequencing allowed sequencing of a large number of genotypes to pinpoint mutations in a specific background, whilst exploring allelic variations within natural populations and associate the frequency of this variation with specific phenotypes using Genome Wide Association models (GWAS). In this context the Winsconsin Diversity Panel population (WIDIV) represents a very useful resource for phenotypic screens in maize is (Hansey *et al.*, 2011). This association panel includes more than 500 maize genotypes collected in the upper Midwest region of the USA for which genomic coding sequence information were collected using RNA-seq. Phenotyping of root architectural and anatomical data were collected at field sites on different continents (e.g. USA and South Africa), locations

(e.g. Winsconsin, Pennsylvania and Arizona) and abiotic stress conditions (Nitrogen and Water) over several years of trials. As a result, studies using WIDIV recently provided new insights on root architectural and anatomical adaptive traits (Schneider *et al.*, 2020 *a*,*b*; Klein *et al.*, 2020). In barley, one the biggest natural population available is the WEALBI panel (https://www.whealbi.eu). This panel is composed of more than 500 fully sequenced barley natural accessions collected from Europe, Africa and Asia, providing a wide range of diversity in this crop (Bustos-Korts et al., 2019). Sequence information is also available for another barley panel composed of around 200 natural accessions originating all around the world. Root architecture and anatomy of such accessions was investigated in water-stressed conditions in the field and GWAS studies revealing multiple QTLs containing crucial genes for plant responses to water deficiency (Oyiga *et al.*, 2020).

Gene editing using CRISPR-Cas9

The Clustered Regularly Interspaced Palindromic Repeat (CRISPR-Cas9) system, also called gene editing, was revolutionised genetic studies in plants (Jaganathan *et al.*, 2018). First used in rice (Xie and Yang, 2013) it has proved a versatile tool used to generate gene specific mutated alleles in more than 20 crops (Wang *et al.*, 2019*b*).

CRISPR-Cas9 system is a defence system discovered in Streptococcus pyogenes mediating the response against prophage DNA (Deltcheva *et al.*, 2011; Jinek *et al.*, 2012). Its engineered version requires a specific gRNA located upstream of a Protospacer Adjacent Motif (PAM; usually 5'-NGG) site in a gene of interest, which targets a nuclease enzyme (Cas9) which acts as a molecular scissor to create a double strand cleavage 3-4 bp upstream of the PAM site (Jinek *et al.*, 2012). The natural DNA repair system called Non-Homologous End Joining Recombination (NHEJ) allows insertion or deletion of INDELs, generating a mutation in the complementary DNA target area of the gRNA (Jinek *et al.*, 2012). Several platforms are now available to predict the specificity and efficiency of potential target gRNAs in the selected sequence in order to maximise final editing efficiency (Schoonenberg *et al.*, 2018; Concordet and Haeussler, 2018). Hence, genomic insertion/deletion generates a frameshift which usually leads to gene knock-out (Lawrenson and Harwood, 2019). In maize and barley, this system was effective by multiplexing gRNAs, allowing targeting of multiple genomic loci to

generate multiple gene knockouts (Xing *et al.*, 2014; Cermak *et al.*, 2017; Char *et al.*, 2017; Gasparis *et al.*, 2018). In the same direction, a high-throughput CRISPR-Cas9 pipeline was recently presented where the authors where able to successfully target more than 700 genes in maize using a multiplex gRNAs system (Liu *et al.*, 2020). The presented versatility of CRISPR-Cas9 systems makes it the most promising biotechnological toolkit to overcome some of the constraints which limits functional genomic studies in crops.

Constraints of using crops as model for functional genomic studies

To date, *Arabidopsis thaliana* has been considered the reference for molecular research studies in plants due to its short life cycle (2-3 months), compact plant size, small genome, very easy to transform and high amount of seed production. Compared to Arabidopsis, crops suffer many disadvantages when used as a model species: a) Longer life cycle that takes up to 6 months from sowing to harvest; b) Plants are usually bigger in size (i.e. maize > 3 m in height); c) specialised growth conditions (e.g. rice); d) Large genomes (e.g. wheat); e) Transformation depends on cultivars and requires tissue culture facilities and personnel (Kumlehn, 2016). Moreover, restrictions are present in many countries on growing GMOs in open field which limits the use of this technology on a larger scale. Promising progress has been made to shorten crop life cycle and stature. In particular, speed breeding protocols for crops grown in long day environments were shown to be effective in barley and many other crops where it was able to obtain up to 6 generations per year (Ghosh *et al.*, 2018; Watson *et al.*, 2018). In maize a dwarf fast flowering inbred line (Mini-Maize) completed its life cycle up to 5 times per year (McCaw *et al.*, 2016) and successful transformation via *Agrobacterium* using immature embryo was recently performed in this line (Jones *et al.*, 2019).

Despite the progresses, another option is to use model plants which are evolutionary closer to maize and other crops than *Arabidopsis thaliana*. Is this sense, *Brachypodium distachyon* was recently shown to be a good model for genetic studies in crops, exhibiting high synteny with maize and other crops (Draper *et al.*, 2001; Brutnell *et al.*, 2015). *Brachypodium distachyon*, together with barley maize and rice is a monocotyledon plant member of the grass family of Poaceae. The most important technical advantages of using *Brachypodium distachyon* as a model is the compact plant and genome size, a life cycle of 3-4 months and

efficient transformation (Vogel and Hill, 2008). From a root biology point of view, *Brachypodium distachyon* also displays a similar root architecture and anatomy to maize, rice and barley making this a very suitable model for cross-species functional genetics studies.

Aims of this PhD study

The aims of this study are to identify genes controlling rooting depth in crops and model cereal species. These aims can be summarized as:

1) Identifying and characterizing genes regulating root anatomical traits in maize and model crops such as rice and *Brachypodium distachyon* by implementing a pipeline called DeepGenes. This pipeline is part of bigger project called DEEPER (Refer to Fig 2.1 DEEPER grant summary, courtesy of J.P.Lynch) which employs bioinformatics (GWAS), molecular (CRISPR-Cas9) and novel high-throughput phenotyping tools to identify candidate genes and molecular markers to be implemented in maize genomic selection models to select deeper rooting varieties.
2) Using a TILLING population in barley to identify and characterise gene controlling root angle, leading to the identification of *HvEGT1 (**E**nhancing **G**ravi**t**ropism 1)*.
3) Using a TILLING population in barley to characterise the *HvPIN1A* gene which regulate root growth and anatomical traits such as vascular patterning in barley and other plant species.

Chapter 2

Identification and functional characterisation of genes regulating root anatomical traits in cereal models

Introduction

Root anatomical traits play a key role aiding crop resilience and performance in water and nutrient depleted environments (Lynch, 2015, 2019). For example, several cortical traits have been identified as to reduce root respiration which results in plants with in deeper roots and better carbon reallocation under water and nitrogen stress (Chimungu *et al.*, 2014; Lynch, 2015). These anatomical traits include Total Cortical cell Area (TCA) is defined as a parenchymatic cell layer between endodermis and exodermis that is composed of a Cortical Cell Number (CCN) of different Size (CCS) organized in multiple layers or Files (CCFN) and, in some crop species, non-living cells which by undergoing programmed cell death (PCD) forms gas-filled pore structure called root cortical aerenchyma (RCA). For example, an increase in RCA decreased respiration by 50%, leading to an approximately two-fold increase in root depth and yield in maize. However, despite the physiological advantages of such processes being clear, the genetic basis behind the regulation of root cortical cell developmental traits remains poorly studied in crops like maize. To accelerate understanding, studies in model crops such as *Brachypodium distachyon* and *Oryza Sativa* promise to facilitate molecular studies due to their high genomic synteny with maize (Brutnell *et al.*, 2015). However, *Brachypodium distachyon* does not produce RCA in its roots unlike rice and maize (Shiono and Yamada, 2014). As a result, *Brachypodium distachyon* is the best model for investigating root cortical cell traits (CCS, CCFN, TCA) whilst rice is best to study aerenchyma formation (RCA).

In order to investigate the mechanisms regulating root cortical cell developmental traits, it was implemented a gene discovery pipeline termed DeepGenes (Fig. 2.1) to pinpoint candidate regulatory genes using advanced bioinformatics, molecular and phenotyping tools in maize and close related model crop species *Oryza sativa sp.* and *Brachypodium distachyon* . In parallel with this, we characterised aerenchyma formation in rice ethylene mutants *ein2* and *eil1,* revealing roles for ethylene and ABA effects on RCA formation.

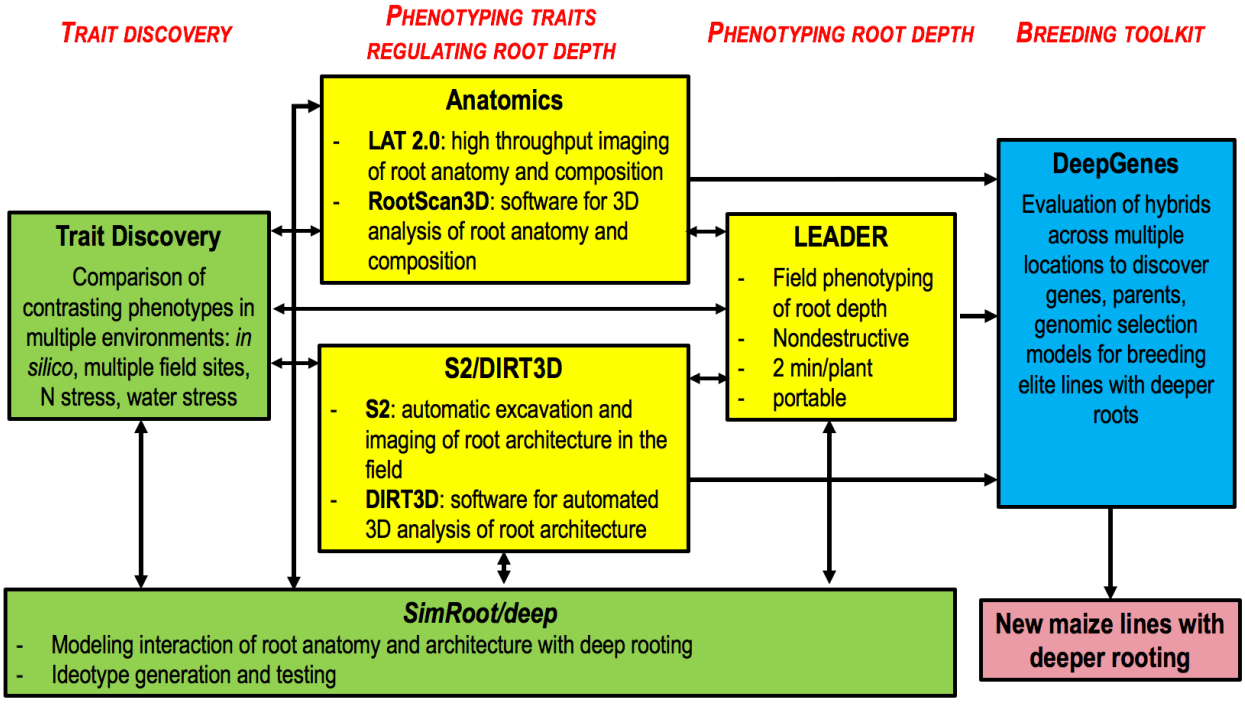


Fig. 2.1. Schematic overview on DEEPER project.

In detail, the focus at the UoN went from Trait Discovery using GWAS models to the evaluation of predicted root anatomical candidates using innovative phenotyping platforms contained in Anatomics (e.g. A new version of laser ablation tomography called LAT 2.0 will be implemented) to DeepGenes by evaluating root soil exploration of different isolines of maize and model crops (courtesy of Jonathan P. Lynch).

DeepGenes Pipeline

A schematic of the Deepgenes pipeline is showed in Fig. 2.2. A subset of 450 maize isolines from the WIDIV diversity collection of US landraces (Hansey *et al.*, 2011) were sequenced using RNA-Seq by University of Winsconsin (Shawn Kaeppler's Lab) to generate 400K (and a more recent 900K) Single Nucleotide Polymorphisms (SNPs) genotyping arrays. WIDIV genotypes were grown in South Africa during the 2015 field season. Field grown samples of maize roots were sampled using shovelomics (Trachsel *et al.*, 2011), then sectioned using Laser Ablation Tomography (L.A.T.) (Strock *et al.*, 2019) to generate root anatomical datasets. CCN, CCS, CCFN, TCA, RCA anatomical traits which were measured using Root Scan 3D and field shovelomics by the Lynch lab at Penn State University (PSU).

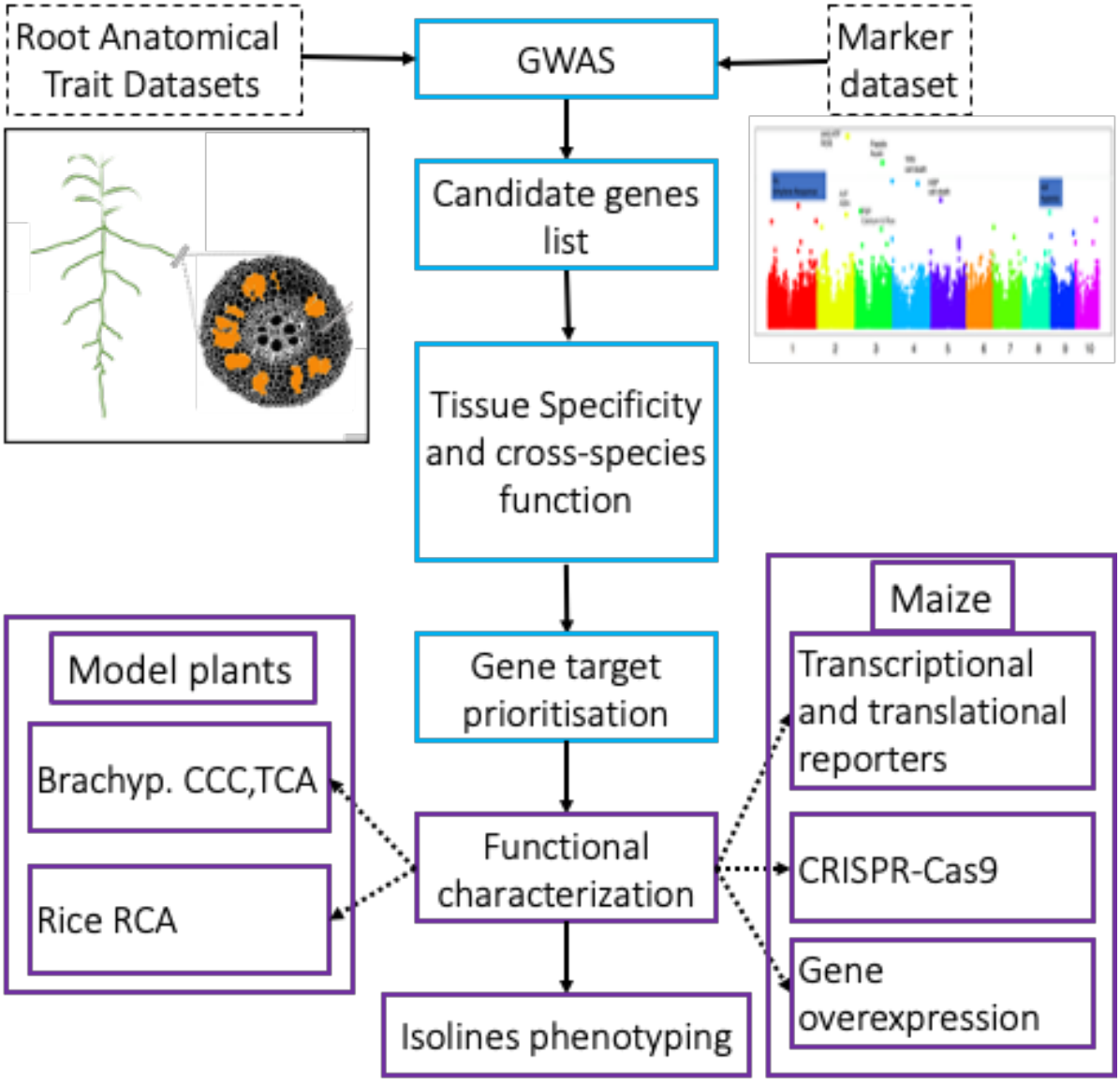


Fig. 2.2. DeepGenes pipeline overview.

Blue boxes represent the computational part of DeepGenes which starts with GWAS analysis for each root anatomical trait in the maize WIDIV panel and ends with a prioritised gene list by checking the tissue specific expression in maize and model plants such as rice. The core of the research reporter in this Chapter is the development of different genetic resources for top candidate genes in maize, *Brachypodium distachyon* and rice.

Phenotypic data and genetic sequences were combined in a Genomic Wide Association model (termed GWAS), a powerful statistical tool to investigate the genetic basis of phenotypic variation (Burghardt *et al.*, 2017). GWAS is based on the association between the Linkage

Disequilibrium (LD) values of SNPs at different locus in the genome with the phenotypic data of the trait of interest. The level of correlation between SNPs and traits were quantified as LOD (Linkage of Odds) values and a threshold set as a limit of significance using FarmCPU as the GWAS model. Results revealed a strong SNPs-Phenotype association for RCA with genes involved in hormone, calcium, PCD and ROS pathways as mentioned in the previous sections, helping us to prioritise candidate genes for experimental validation. The genes carrying SNPs leading to a significantly different phenotype, with a LOD value above the threshold were next analysed for root specific and tissue-specific expression in the root cortical layer of maize (Sekhon *et al.*, 2011; Opitz *et al.*, 2016; Stelpflug *et al.*, 2016; Tai *et al.*, 2016), *Arabidopsis thaliana* (Dinneny *et al.*, 2007) and *O. Sativa* (Sato *et al.*, 2013), leading to a shortlist of candidate genes. Top candidates in maize were subsequently analysed for homology and expression level in model plants *Oryza Sativa* and *Brachypodium distachyon.* In order to validate candidate gene function, different genetic approaches were implemented. Several existing mutagenized populations such as Mu-insertion in maize (McCarty *et al.*, 2005*a*) were screened for mutation in the candidate genes. We also attempted to engineer CRISPR-Cas9 edited genes in maize, *Brachypodium distachyon* and rice in order to generate loss of function genes.

Material and methods

GWAS and candidate Deepgenes identification in maize.

Phenotypic anatomical data from crown roots of more than 450 genotypes were initially. collected from mature maize plants grown in South Africa and Penn State from Jonathan Lynch's group (Hansey *et al.*, 2011; Schneider *et al.*, 2020*a*). Genomic sequences of such genotypes were collected using RNA-seq which generated a 400K and a more recent 900K SNPs array dataset. The phenotypic data for root anatomical of CCC,CCFN,TCA and RCA and the resulting SNPs arrays were then used to run GWAS model using GAPIT and FarmCPU models (Liu *et al.*, 2016). Logarithm of Odds ($-\log_{10}(p)$) values for each SNPs were generated by associating phenotypic data from CCC, CCFN and TCA to the 400K SNPs array and phenotypic data from RCA was associated the 900K SNP array. LOD cut-off values was set at 4-5 and combined with the results from GAPIT algorithm to generate an initial list of candidate genes. These genes were then analysed for tissue specificity expression information in rice

and Arabidopsis as well as their orthologues information when known in order to finalise a more coherent Deepgenes candidates list. (Winter *et al.*, 2007; Sato *et al.*, 2013)

Phylogenetic Genetree and orthologues identification in model crop species.

For *ZmQKY* and *ZmFERONIA*, the full protein sequence was initially used as a seed gene to select orthologous genes (>40 identity percentage, bitscore >500) from key monocot species such as barley (Hordeum Vulgare), rice (Oryza Sativa spp. Japonica), maize (Zea Mays B73) and *Brachypodium distachyon* and Arabidopsis (Arabidopsis thaliana) using interactive phylogenetic module of Monocots Plaza 4.5 (Van Bel et al., 2017). Protein sequences were aligned using MUSCLE and tree was constructed using FastTree algorithm. Generated Newick file was imported into iTOL to create the unrooted trees. The additional protein domain structure analysis on *ZmFERONIA* malectin-like and tyrosine-kinase domains was performed by combining the protein structure information from the Uniprot and PFam database to derive each specific domain location in each orthologue. Each specific protein domain sequences were then aligned using *ZmFERONIA* as query using NCBI blastp algorithm.

Developing CRISPR lines for *Brachypodium distachyon* Deepgenes orthologue *BdQKY* and *BdFERONIA*.

In order to generate CRISPR lines for BdQKY and *BdFERONIA* in *Brachypodium distachyon*, strain Bd21-3 was chosen as wild type, and protocol from O'Connor et al., 2017 was optimized and implemented using single gRNA constructs pOs-sgRNA and pH-Ubi-cas9-7 respectively as entry and destination vectors (Miao et al., 2013) (Fig. 2.3). Guide RNAs (gRNAs) were designed using benchling (reference) based on: 1) position - as close as possible to the starting codon 2) specificity - using cutoff score = 90 (Hsu et al., 2013) and 3) efficiency - using a cutoff score = 50 (Doench et al., 2016). Furthermore, gRNAs were chosen for the ones with the less off-target number in the exonic region to avoid problems associated with non-specific targets.

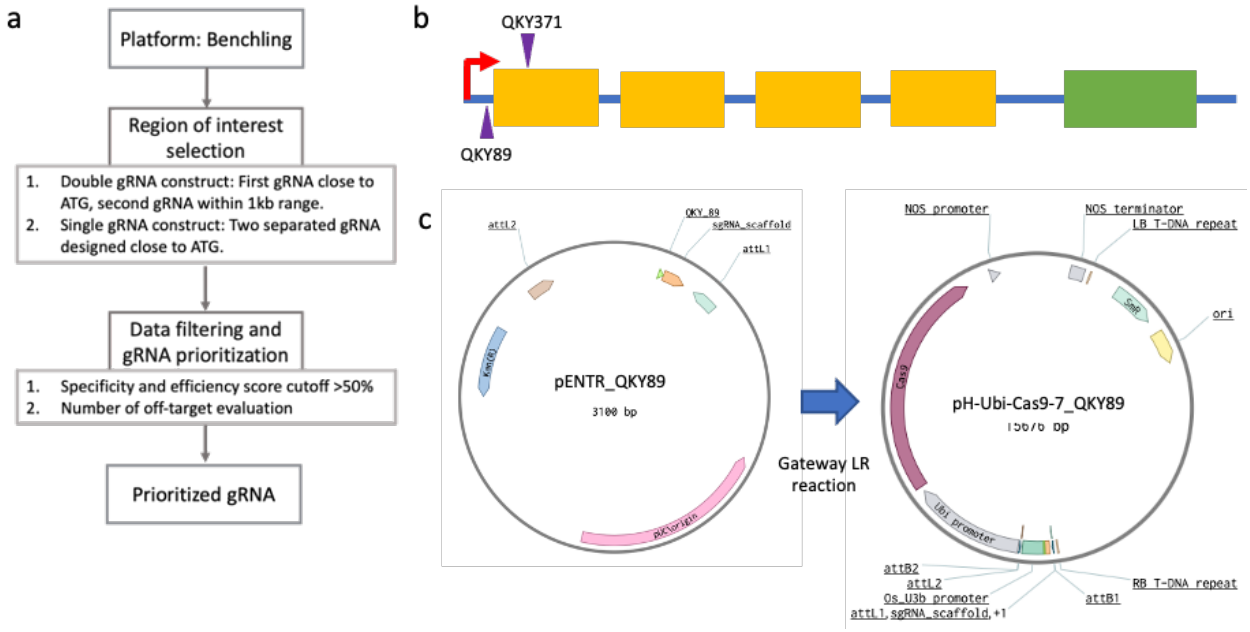


Fig. 2.3. Schematic representation of gRNA selection and cloning strategy to suit Single and Double gRNA constructs for developing CRISPR edited lines in *Brachypodium distachyon* and Maize.

a) Pipeline used for prioritizing gRNAs using benchling platform based on position within specific genes, specificity (off-target numbers and positions) and efficiency (accessibility to DNA). b) CDS structure of BdQKY and an example of the position of where the 2 gRNAs are located (Red arrow: start codon, Yellow: C2 domains, Green: phosphoribosyltransferase-like protein). c) Cloning strategy using entry vector (pENTR_OsU3B_sgRN) and destination vector (pH-Ubi-cas9-7) developed by Miao *et al.*, 2013.

Transformation of embryogenic callus was optimized and performed using the protocol form Vogel and Hill, 2008 (Fig. 2.4). For each construct, 8-10 immature embryos were initially dissected to generate embryogenic calluses, which were then sub-cultured and a final number of about 500-1000 calluses were transformed for each construct using *Agrobacterium*. Each step condition and media was performed according to the initial protocol. Regenerated single events were initially vernalized for 7 days at 6^{o} C and then sequenced using Sanger sequencing. (gRNAs, primers and PCR conditions are listed in S.Tab. 2)

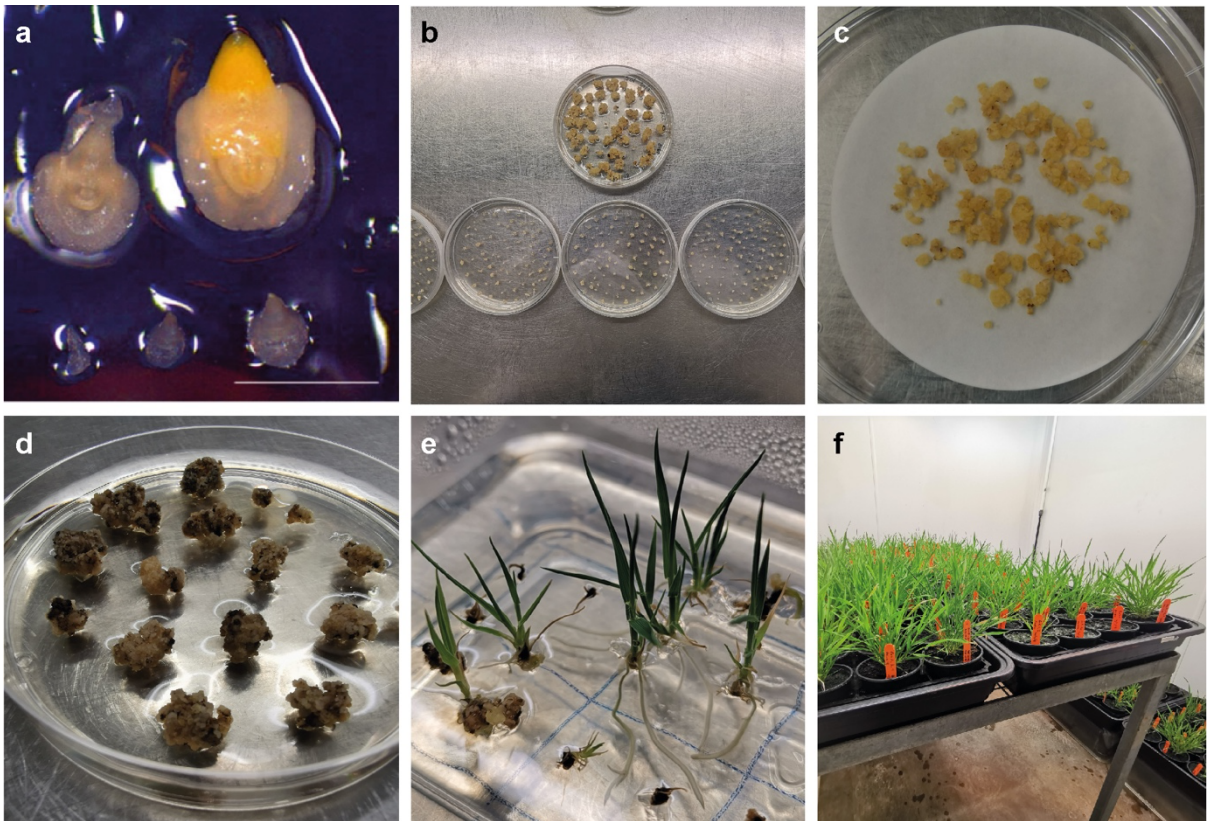


Fig. 2.4. Tissue culture pipeline used to generate stable transformed CRISPR edited lines in *Brachypodium distachyon*.

a) Representative image of immature embryo of *Brachypodium distachyon* used for tissue culture (Bragg N. et al., 2014). b) Sub-culturing stage used to increase the number of calluses which will undergo transformation and maintain calluses active. c) Co-cultivation stage of callus with Agrobacterium after inoculation. d) Callus selection on hygromycin media, dark colours indicated non-transgenic calluses, yellow indicates positive transgenic calluses. e) Regeneration of positive transgenic calluses with well-formed coleoptile and roots ready to be transferred into soil. f) Positive regenerated plants growing in the growthroom. All this protocol was adapted from Bragg N. et al., 2014.

Developing CRISPR edits for Maize Deepgenes

To generate CRISPR edits in maize DeepGenes top candidates *ZmHAL3*, *ZmACCsynthase*, *ZmCLAVATA3*, *ZmEPFL6*, *ZmQKY* and Zm*ZmHIF1a*, we took the advantage of the WCIC transformation facility at Wisconsin University (USA) in order to facilitate the transformation system. In this case, a double gRNA backbone was used to transform maize cv. HII. The addition of a GFP tagged system downstream the Cas9 sequence was used to help in

characterizing calluses that were successfully transformed already at the tissue culture stage. Notice that, this is not an indication of the efficiency on the system but it helps in characterizing the calluses that are expressing the Cas9 protein. gRNAs were designed as above with the difference of designing a second gRNA approximately 1kb downstream the first one to increase the chances of a successful editing by creating a big deletion spanning from the first and the second gRNA (gRNAs are listed in S.Tab. 3). *Agrobacterium* mediated transformation was performed and T_0 plants regenerated were backcrossed with HII and genotyping of T_1 lines was performed using Sanger Sequencing (Primers used for genotyping are listed in S.Tab. 4).

Characterising anatomical traits in *BdQKY*

Seeds from *BdQKY* CRISPR line Pos1_8(1) and wild-type Bd21-3 were dehusked and sterilised with 20% bleach for 5 minutes and rinsed 5 times with RO water. Seeds were then plated in 1%agar 1/2MS 5.7ph, and grown for 20 days. Root cross section were then generated from 1cm of primary and nodal roots fixed in 4.5% agarose blocks using vibratome (100um slice, 1um amplitude 50Hz frequency) (Atkinson and Wells, 2017). Slices were then stained using Calcofluor white (SIGMA 18909-100ML-F) for 30" to 1' and visualised using a confocal microscope Leica SP5 (wavelength excitation using UV laser at 405 nm) Agarose blocks were processed immediately after as the cortical layer of *Brachypodium distachyon* roots coming from such media undergo rapid hyperoxidation which generates sample degradation and staining. Images were then analysed using Fiji(ImageJ) (Schindelin *et al.*, 2012) and statistical differences were determined using RStudio (RStudio Team, 2020).

Using rice OsEIL1 mutant to investigate RCA formation

Rice MHZ6-1 (OsEIL1) map-based cloned mutant previously characterized (Yang et al., 2015b) and MHZ7-1 (OsEIN2) were used to investigate RCA formation rice. Seeds of Nipponbare (WT), MHZ6 (OsEIL1), MHZ7 (OsEIN2) were pre-germinated and then grown in hydroponic condition for 9 days using full strength YOSHIDA solution. Primary root was dissected in the region 2-3cm close to the root fragments were fixed in agarose gel using the protocol from Atkinson and Wells (2017) then stained with calcofluor white and observed under confocal microscope SP5 to observe anatomical changes in root structure. Data were then processed using MIPAR for quantification of root anatomical features.

Maize Ethylene and ABA treatment to underpin RCA formation and root cortex expansion

In order to study the role of ethylene and ABA on aerenchyma formation, we pre-germinated maize cv. Adept for 2 days in dark at 28 C. Plants with equal root length were then moved onto paper-roll system and grew for 2 days at 28 C, 12h daylight. At the end of this point we applied 2 different treatments: 1) 30ppm ethylene in gas chamber; 2) 200µM ABA dissolved in TRIS pH 9.1. Root cross sections were made in two positions in the primary root: 1) P1 = 2-3cm from seed, 2) P2 = 2-3cm from the root tip. These two positions were chosen in order to investigate RCA progression in both mature (P1) and developmental region (P2) (Fig.10). Cross sectioning and imaging was then performed according to Atkinson and Wells, 2017 and RCA was quantified using rootscan2 (Burton et al., 2012). ANOVA and Tukey test were performed using statistical software R, using threshold of confidence alpha=0.05. Root length data were analyzed in FIJI (ImageJ) and Tukey test was performed using RStudio.

Results

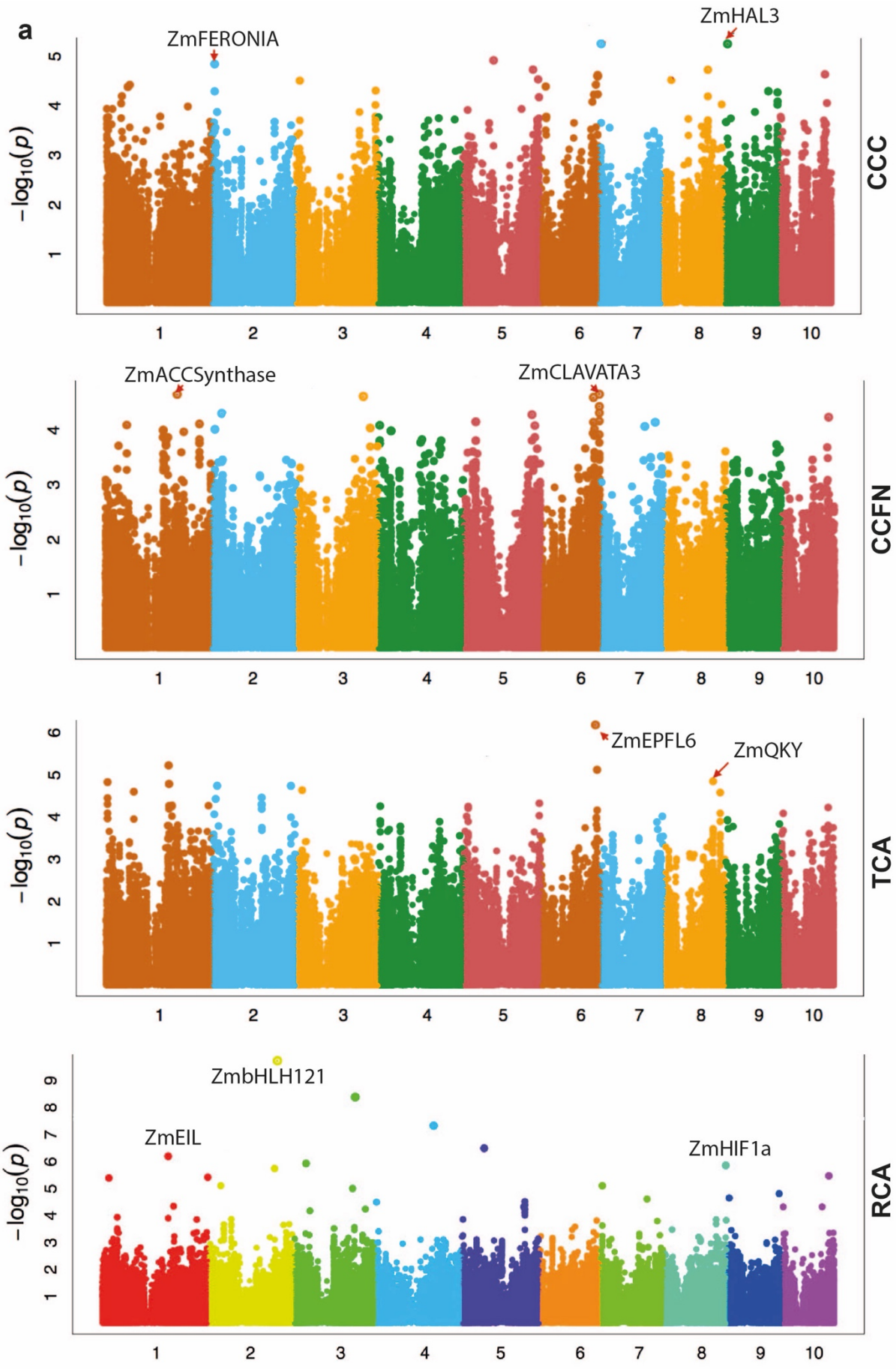
DeepGenes analysis pinpointed candidate cortical regulatory genes in maize and orthologues in *Brachypodium distachyon* and rice.

The Deepgenes pipeline (see Fig. 2.2) was initially used to pinpoint candidate genes regulating several different cortical traits in a maize diversity collection (Hansey *et al.*, 2011) grown at a field site in South Africa in 2015. Field grown samples of maize roots were originally sampled using shovelomics (Trachsel *et al.*, 2011), then sectioned using Laser Ablation Tomography (L.A.T.) (Strock *et al.*, 2019) to generate root anatomical datasets. CCN, CCS, CCFN, TCA, RCA anatomical traits (see introduction for details). Phenotypic and genetic data were combined in a Genome Wide Association model (GWAS) to investigate the genetic basis of phenotypic variation (Burghardt *et al.*, 2017). GWAS results revealed a strong SNPs-Phenotype association for RCA with genes involved in hormone, calcium, PCD and ROS pathways, helping prioritisation of candidate genes for experimental validation (Fig. 2.5a).

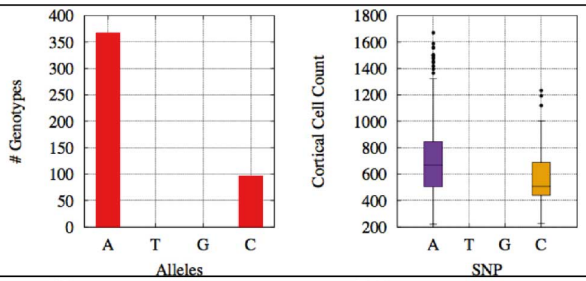
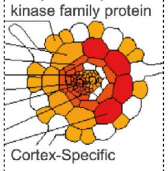
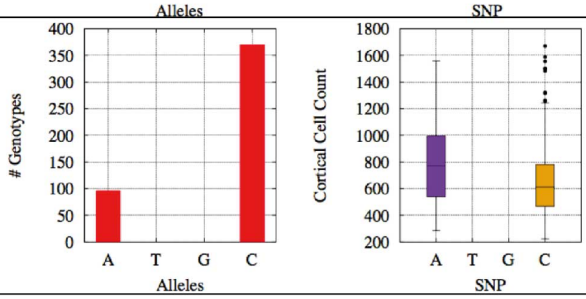
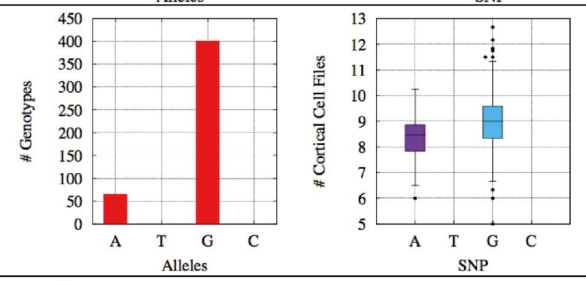
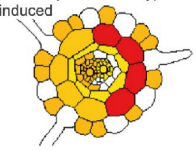
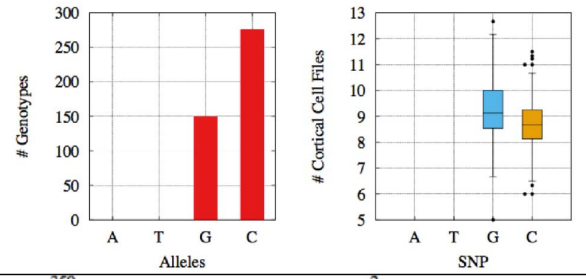
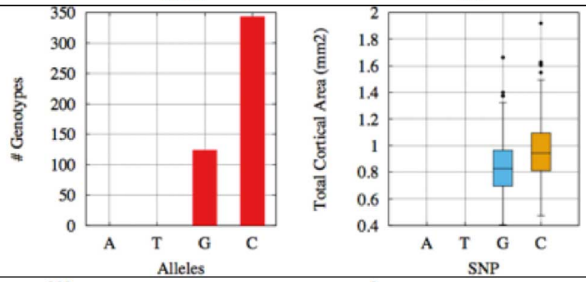
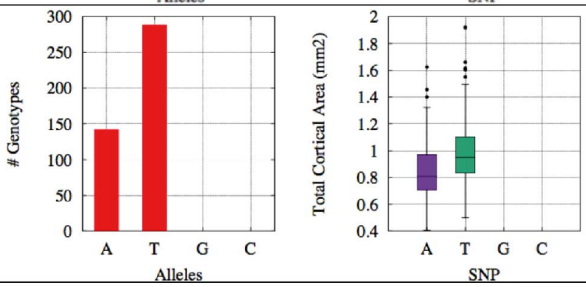
Genes carrying SNPs with a LOD value above the threshold were next analysed for root specific and tissue-specific expression in the root cortical layer of maize (Sekhon *et al.*, 2011; Opitz *et al.*, 2016; Stelpflug *et al.*, 2016; Tai *et al.*, 2016), *Arabidopsis thaliana* (Dinneny *et al.*,

2007) and *O. Sativa* (Sato *et al.*, 2013), leading to a shortlist of candidate genes (Fig. 2.5b). Top gene candidates included ZmHAL3, ZmFERONIA (CCC) ZmQKY, ZmEPFL6 (TCA), ZmCLAVATA3, ZmACCsynt (CCFN), ZmbHLH-121 and ZmHIF-1α (RCA). SNPs within ZmbHLH-121 showed the highest correlation for RCA, and later studies carried out by the Lynch lab in Penn State (USA) confirmed this gene's functional importance for this trait (Schneider et al, 2021), demonstrating the effectiveness of the Deepgenes gene discovery pipeline.

A summary of the prioritised candidate genes is listed in Fig. 2.5b. I then proceeded to find the maize orthologues of candidate regulator genes (for anatomical traits denoted in brackets) in *Brachypodium distachyon* (CCC,CCFN, and TCA) and rice (RCA). Coding regions of *ZmHAL3* (CCC), *ZmFERONIA* (CCC) and *ZmQKY* (TCA) exhibited a high level of similarity with their homologs in *Brachypodium distachyon BdHAL3* (coverage: 63%; identity: 83%), *BdFERONIA* (coverage: 94%; identity: 75%) and *BdQKY* (coverage: 99%; identity: 85%). Phylogenetic gene tree analysis based on protein sequences of ZmFERONIA and ZmQKY (S.Fig. 1-2) revealed that a clear clade is formed between orthologues in monocot species (rice, barley and *Brachypodium distachyon*, whereas in both cases orthologues of Arabidopsis fall into a separate clade, especially for *ZmFERONIA*.


a
ZmFERONIA
ZmHAL3
CCC
ZmACCSynthase
ZmCLAVATA3
CCFN
ZmEPFL6
ZmQKY
TCA
ZmbHLH121
ZmEIL
ZmHIF1a
RCA
−log10(p)
1
2
3
4
5
6
7
8
9
10

b

	MaizeID	ArabOrtho	OrthoBackground	Allele Frequency and SNP effect on the phenotype
CCC	GRMZM2G127911	AT3G18030 HAL3, halotolerance determinant 3 catalyzes a key step in coenzyme A biosynthesis.	Involved in salt and osmotic tolerance, and light-regulated plant growth. Trimerization of HAL3 recruits and activates the E3 ubiquitin-protein ligase HIP1, which leads to the degradation of cell cycle suppressors, resulting in enhancement of cell division and plant growth Overexpression of HAL3 => **increased cell number**	
	GRMZM2G042055 Cortex and Stele specfic	AT3G51550 (FER) Malectin/ receptor-like protein kinase family protein  Cortex-Specific	FER, upon external signal recognition recruits the GEF1–ROP/ARAC network with time and space specificity and **promote or inhibit cell elongation in different cell types** FER positively regulate auxin- induced cell elongation and negatively regulate ABA response **Down regulated in hypoxia as well as ABA treatments**	
CCFN	AC210731.3_FG002 **Root-specific**	No ortholog	Rice Ortho : CLAVATA3/ESR (CLE)-related protein Important in maintaining stem cell population	
	AC234528.1_FG006 **Root specific**	AT2G36690 2-oxoglutarate (2OG) and Fe(II)-dependent oxygenase superfamily protein,	Homolog of ACC synthase, ethylene biosynthesis Cortex specific and Hypoxia induced 	
TCA	GRMZM5G852378	AT1G74720 (QKY) QUIRKY	QKY functions in Ca2+ dependant in the SCM signalling that controls cell shapes and orientations of cell division Fulton et al., 2009	
	GRMZM2G125037	AT2G30370(EPFL6) Epidermal Patterning Factor Like 6	Part of signaling machinery that is important in cell-to-cell and intertissue communications that regulate stomatal development (density/ numbers) in response to environmental signals	

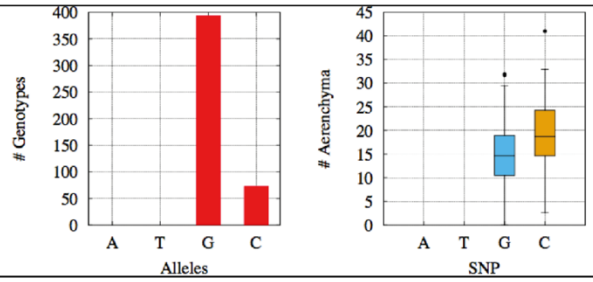
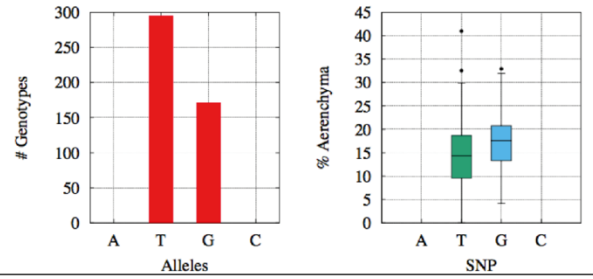
	MaizeID	ArabOrtho	OrthoBackground	Allele Frequency and SNP effect on the phenotype
RCA	GRMZM2G083504 bhlh121 - bHLH-transcription factor 121	AT3G07340, basic helix-loop-helix (bHLH) DNA-binding superfamily protein. CIB3 / CIL2 Cortex and Stele specific	CIBs and CILs are CRY-interacting bHLH transcription factors. In response to blue light, CRYs binds to CIB proteins and triggers nuclear accumulation of ROS, which regulates Programmed Cell Death. Consistently, cry mutants suppresses blue light and **ROS-dependant PCD in arabidopsis**.	
	GRMZM2G079468 Root elongation zone specific	AT5G19840.1, 2-oxoglutarate (2OG) and Fe(II)-dependent oxygenase superfamily protein Panther Family : **HYPOXIA-INDUCIBLE FACTOR 1 ALPHA INHIBITOR-RELATED** (PTHR12461);	The key regulator of the hypoxia response is the hypoxia inducible factor 1 (HIF-1). HIF-1 is a heterodimer composed of the rate limiting factor HIF1α and the constitutively expressed HIF-1β. HIF-1α is induced by hypoxia. The induction of HIF-1 by hypoxia takes place at the protein level, because HIF-1α mRNA expression remains unchanged. During normoxia, HIF-1α protein is expressed but is unstable.	

Fig. 2.5. Summary of resulted candidate Deepgenes derived from GWAS analysis on maize CCC, CCFN, TCA and RCA.

a) Results from GWAS on Maize WIDIV on CCC, CCFN and TCA using a 400K SNP array dataset and for RCA a 900K SNP using FarmCPU algorithm. b) Summary Deepgenes list summary resulted from the GWAS analysis. In the first two columns we show the resulted gene code from the SNP hit with its annotations form maize V3 genome version and Arabidopsis orthologue genes annotation with tissue specificity summary when known. It is also provided a brief summary from literature of the candidate gene orthologues in Arabidopsis. For each gene and its underlying SNP we provide the allele frequency in the WIDIV genotypes population and the effect of the SNP change in the phenotype.

Regarding RCA, the CDS of *ZmHIF1α* showed a high level of similarity with its rice homolog *OsHIF1α* (coverage: 97%; identity: 79%), suggesting a similar function in the two species. Expression level was assessed from *Sibout et al., 2017*, revealing that *BdFERONIA* and *BdQKY* are functionally expressed at different levels in 35 DAG root of *Brachypodium distachyon* as well as aerial tissues (Fig. 2.6). Expression and tissue specificity level of maize orthologue *OsHIF1α* was instead investigated in the database from *Sato et al., 2013* revealing that it is expressed in roots at different growth stages and is highly expressed in the maturation zone (Fig. 2.6), which is the area where RCA starts to form, suggesting it might be involved in triggering RCA formation. From these results, we attempted to develop mutant and reporter

lines in maize, *Brachypodium distachyon* and rice (summarised in S.Tab. 2.1) which will be discussed in the next sections.

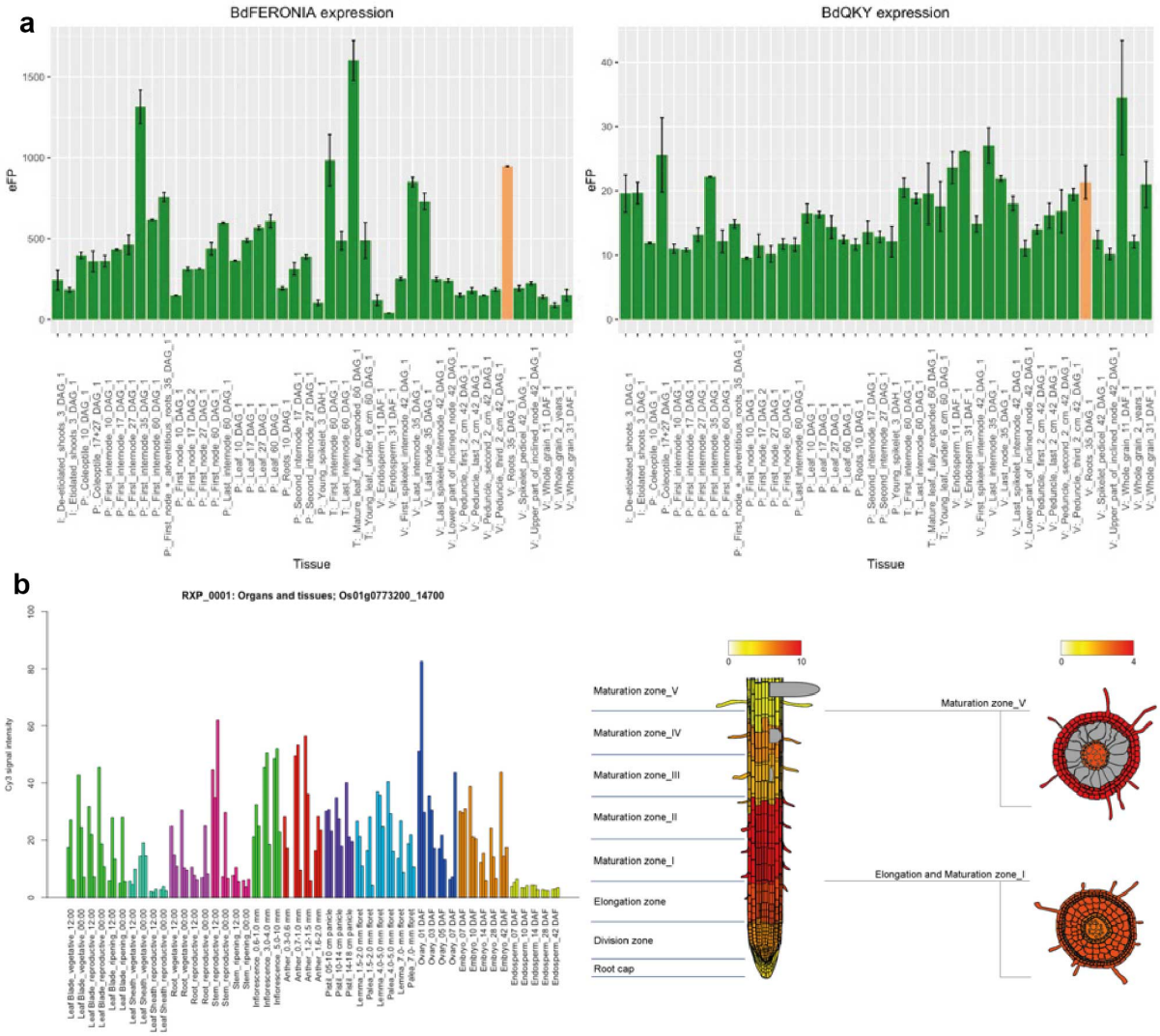


Fig. 2.6. Organ and tissue specificity expression of BdQKY, BdFERONIA and OsHIF1a.

a) Expression of BdFERONIA and BdQKY in *Brachypodium distachyon* in different plant tissues. Shoot tissues (green), 35 DAG root tissue (orange) (adapted from Sibout et al., 2017). b) Expression of OsHIF1a in rice in different plant tissues and in different RAM sections (adapted from Sato et al., 2013)

Developing Deepgenes mutant lines using CRISPR-cas9 via tissue culture in *Brachypodium distachyon*, rice and maize.

The success of CRISPR-Cas9 technique in plant biology has been widely demonstrated over the past several years, particularly to generate frameshift mutations arising from SNPs

insertion/deletion. *Brachypodium distachyon* has been proved to be a very suitable system for CRISPR-Cas9 technique stable transformation studies (Brutnell et al., 2015; O'Connor et al., 2017). In this experiment, I was able to regenerate transgenic callus for all 6 constructs (two independent single gRNA Crispr-Cas9 constructs targeting *BdQKY, BdHAL3* and *BdFERONIA*). Results for T_0 generation of plants are summarized in Tab. 1.

Target gene	gRNA number	Line name	T_0 Hom/Het	Event type
BdQKY	1	POS1_4_2	Het	
		POS1_8_1	Hom	GG deletion
		POS1_10	Het	
		POS1_13_1	Het	
		POS1_14	Hom	GG deletion
	2	POS2_3	Het	
		POS2_5_2	Het	
BdFERONIA	1	POS6_2	Hom	A insertion
		POS6_6	Het	
		POS6_7_1	Hom	T insertion
		POS6_14	Het	
		POS6_17	Het	
		POS6_19	Het	
	2	POS7_1	Het	
		POS7_8_1	Het	
BdHAL3	No positive edits			

Tab. 2.1. Summary of T0 Events genotyping showing positive CRISPR-Cas9 edits in *Brachypodium distachyon* Deepgenes orthologues.

Here we present a brief summary of the CRISPR edited lines resulting from tissue culture transformation in *Brachypodium distachyon*. Based on Sanger sequencing genotyping, we identified a total of 15 events where 4 showed to be homozygous mutation 3-4 base pairs downstream PAM.

CRISPR-cas9 generated a total of 78 transgenic events among the constructs, with a transformation efficiency spanning from 5% to 18% where a positive event was generated. Of the gRNAs tested, both gRNAs sequences in *BdQKY* and *BdFERONIA* showed positive edits, whether events from both *BdHAL3* gRNAs didn't show any edits. Sanger sequencing revealed a wide range of insertion/deletions located ~ 3-4 bp upstream of the PAM site (example in Fig 2.7). As shown, we identify a *BdQKY* mutant named as Pos1_8(1) and Pos1_14 to carry a homozygous GG deletion and then selected for further characterization.

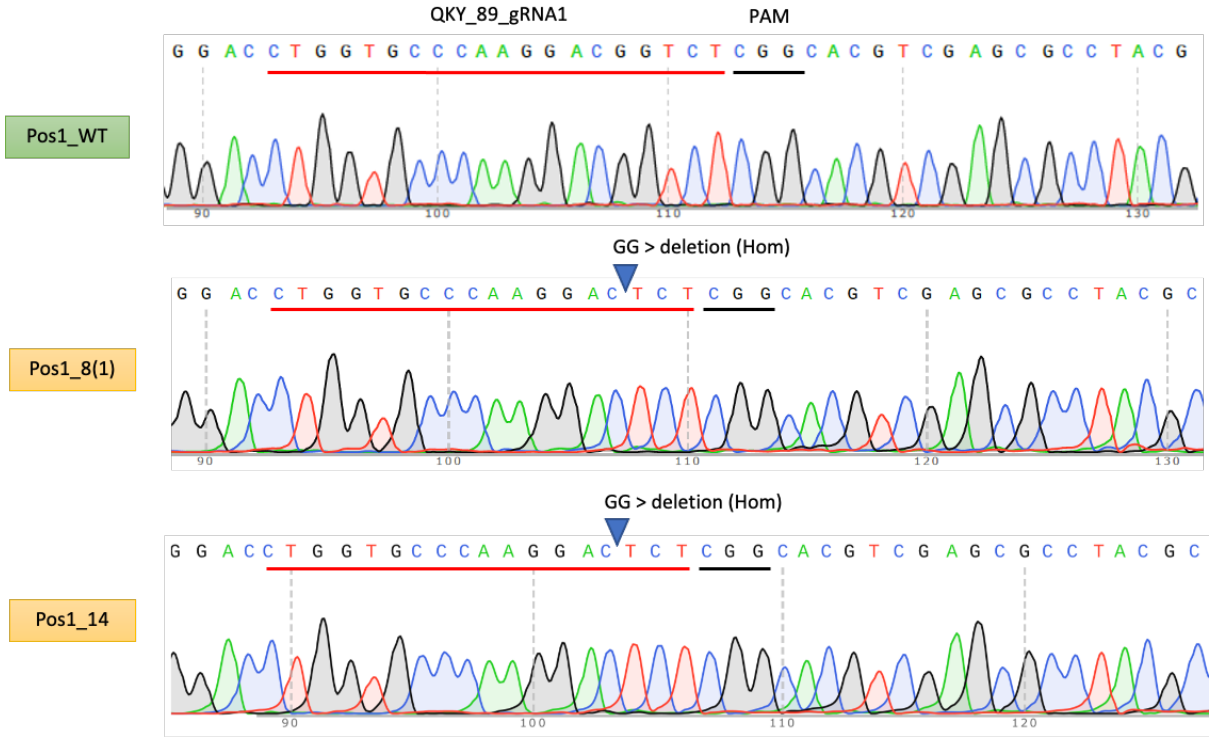


Fig. 2.7. List of events with dendrograms carrying successful edits for QKY89_gRNA (Pos1). The first dendrogram highlights the genomic region surrounding the PAM sequence target of QKY89_gRNA, followed by the two homozygous events carrying a homozygous GG deletion 3-4 base pairs downstream the PAM sequence.

For the gRNAs that worked, we assessed an editing efficiency among the events ranging from 33% to 40%. Due to the efficiency of the CRISPR system, some events generated biallelic/homozygous mutations in QKY_gRNA1 and FER_gRNA1 that were moved on T_1

generation to perform preliminary phenotyping experiments. At this stage, homozygous lines for BdQKY were extremely weak and plants were revealed to not be fertile and unable to produce seeds even when plants were placed on a long day-light cycle.

Note that I also attempted to develop CRISPR-cas9 edited line for all the candidate Deepgenes in maize (in collaboration WCIC, USA) using a double gRNA and GFP tagged vector and OsHIF1-a in rice using the same vector describe for *Brachypodium distachyon*. However, in maize we were not able to detect any positive edits after screening using sequencing. Similarly, in rice we were not able to recover healthy calli after agrobacterium inoculation. In parallel, we also attempted to genotype *Mu-insertion* lines in maize (McCarty *et al.*, 2005*b*), however PCR assays didn't reveal clear bands indicating successful genotyping. As a result of this, further experiments focused on *Brachypodium distachyon* edited lines and existing rice hormone mutants.

The *BdQKY* candidate regulatory gene controls root growth and nodal root anatomy

To investigate the role of the *BdQKY* gene, experiments were performed on root architecture and anatomy using gene edited mutant Pos1_8(1) from T_1 seeds. Representative images of wild type Bd21-3 and gene edited mutant Pos1_8(1) 20 days old seedlings grown vertically on agar plates are shown in Fig. 2.8. Differences in root length and (via confocal imaging) radial anatomy in nodal roots were observed, suggestive of a cortical patterning defect.

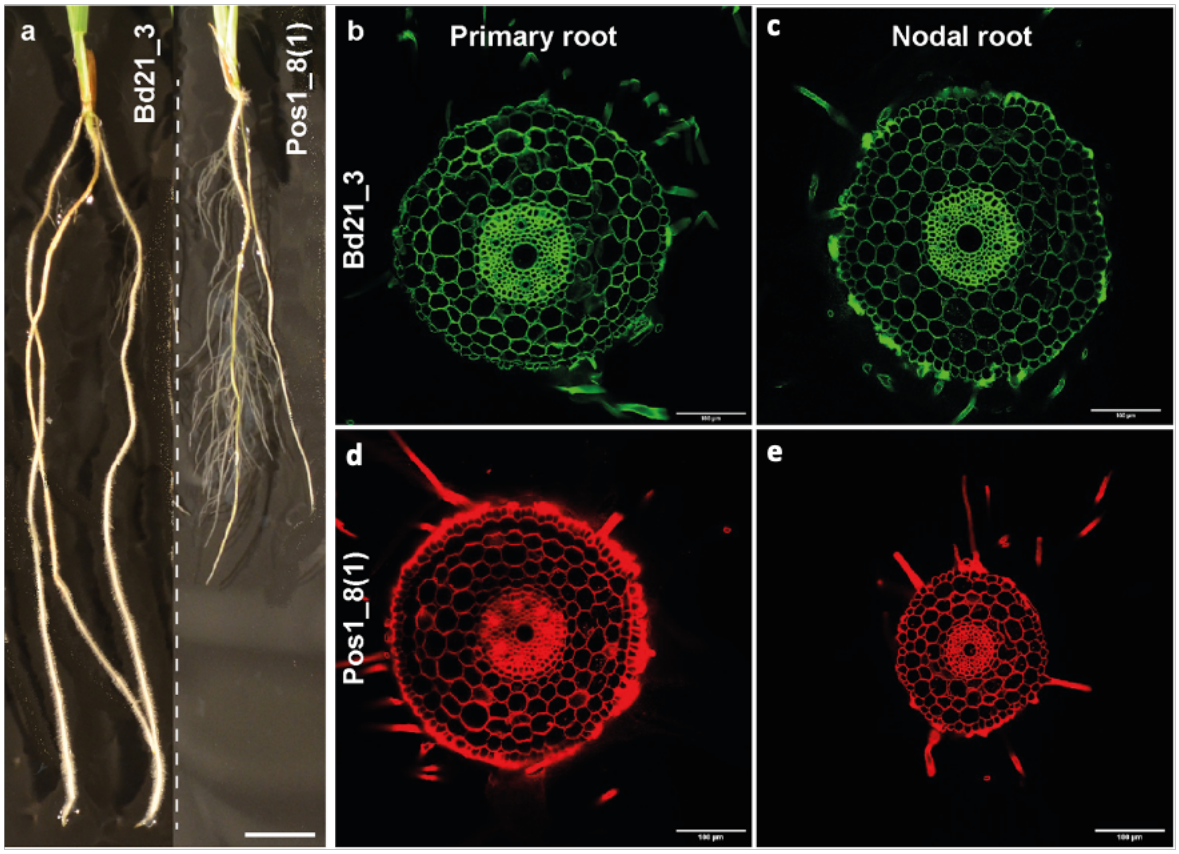


Fig. 2.8. Representative images of BdQKY mutant Pos1_8(1).

Pictures showing differences in *Brachypodium distachyon* root architecture (a) and anatomy (b-e) between wild type Bd21-3 and the QKY mutant Pos1_8(1) grown for 20 days in MS agar media. Scale bar = 1cm (a) 100μm (b-e)

Quantitative results are shown in Fig. 2.9 revealing a significant reduction between 30% to 50% in both primary root and nodal root length between Bd21-3 and Pos1_8(1). At a cellular level, there is a reduction in root diameter and TCA between wild type and Pos1_8(1). A significant reduction in root diameter, TCA and CCFN between wild type and Pos1_8(1) was also observed. In more detail, there was a 40% reduction in root diameter, 60% reduction in TCA and 1-2 less cell files in Pos1_8(1) compared to wild type. These preliminary results indicate BdQKY is important from root cortical patterning as well as the overall root growth of nodal roots in *Brachypodium distachyon*, suggesting this gene might act specifically in nodal root.

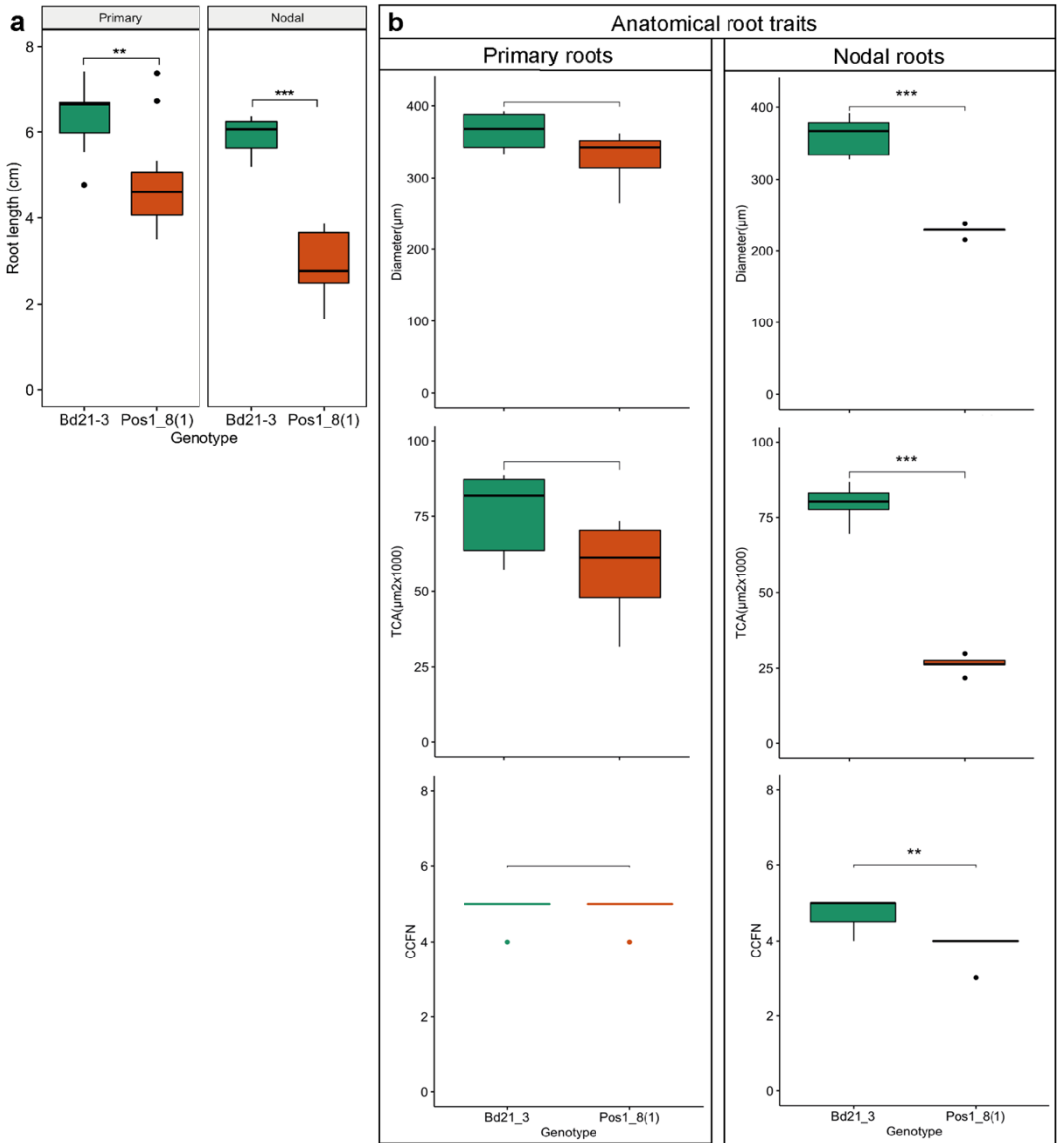


Fig. 2.9. Resulting bar plots of root length and anatomical traits of *Brachypodium distachyon* wild type Bd21-3 and the QKY edited mutant Pos1_8(1) indicates QKY to affect both root development and anatomy.

a) Quantification of root length, b) quantification of root anatomical traits such as diameter (µm), TCA (µm^{2}x1000), and CCFN. *** and ** indicates statistically significant difference using Welch's T-Test at p<0.001 and *p*<0.001 in n=8-11 replicates for root length and n= 5-10 for anatomical traits, respectively using RStudio. TCA (µm^{2}x1000) = Total Cortical Area scaled down 1000 times, CCFN = Cortical cell File Number.

Evaluation of RCA formation in rice Ethylene Insensitive lines

The Deepgenes gene discovery pipeline identified a number of ethylene synthesis (ACC synthase) and response (EIL1) pathway encoding candidate genes (Fig. 2.5a). To investigate

the role of this hormone signal during root cortical cell developmental, we analysed 2 rice ethylene response mutants (disrupting EIN2 and EIL1 genes; (Yang *et al.*, 2015)). In hydroponically grown roots I observed a reduction in % RCA in primary roots of both ethylene response mutants (Fig. 2.10) and this difference was more evident by comparing MHZ7-1 (OsEIN2) (16.52±3.9) and Nipponbare (29.35±3.4) then MHZ6-1 (OsEIL1) respectively. This trend suggests that maize orthologs of OsEIN2 or OsEIl1 represent interesting candidates to investigate RCA formation in maize.

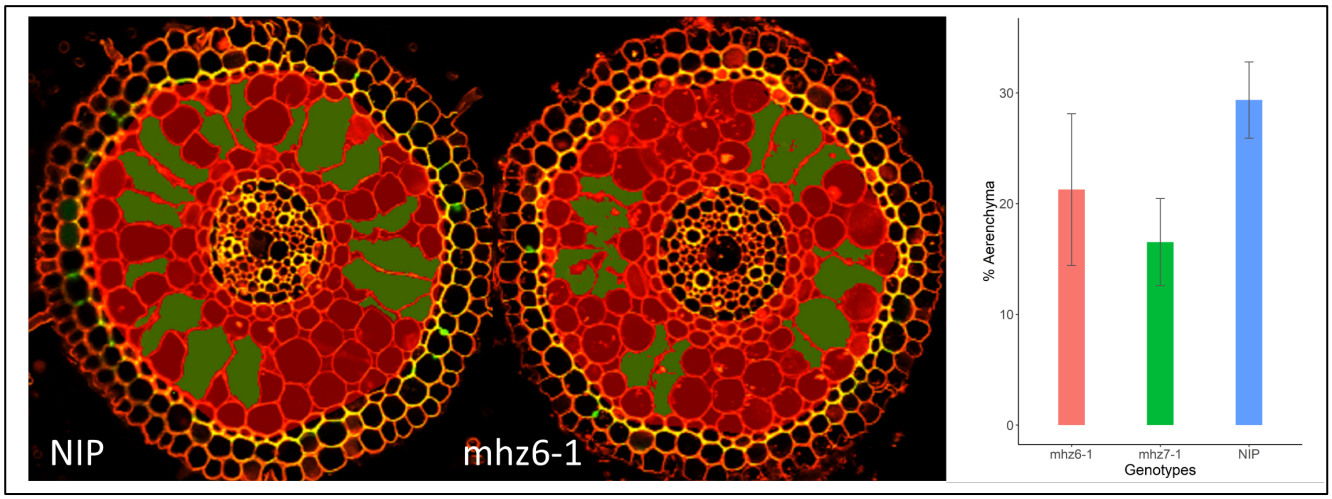


Fig. 2.10. Preliminary results of RCA formation in rice ethylene mutants.
Left: Comparison between cross-sections of NIP and MHZ6-1(*OsEIL1*) as output from MIPAR. Right: barplot showing the differences of %Aerenchyma formation between MHZ6-1(*OsEIL1*), MHZ7-1(*OsEIN2*) and Nipponbare(WT). n>3

Ethylene effects on maize root anatomy and aerenchyma formation

Ethylene treatment was performed in maize in order to investigate its role in regulating aerenchyma formation in this species. Consistent with previous reports (Konings & de Wolf, 1984; Hu *et al.*, 2016), primary roots treated with ethylene (30 µM) showed a significant ($p<0.001$) reduction in the growth (mean ± SD) compared with control (Fig. 2.11). Root aerenchyma formation was also analysed in two different root zones, one mature area close to where the seed coat attaches (P1) and the other in the elongation/maturation zone close to the root apex (P2). Regarding root anatomy, we observed a significant increase in Total Cortical Area in ethylene (0.24 ± 0.03) treatments compared to control (0.16 ± 0.02) in the maturation region i.e. 2-3 cm from the root tip (P2) (Fig 2.12).

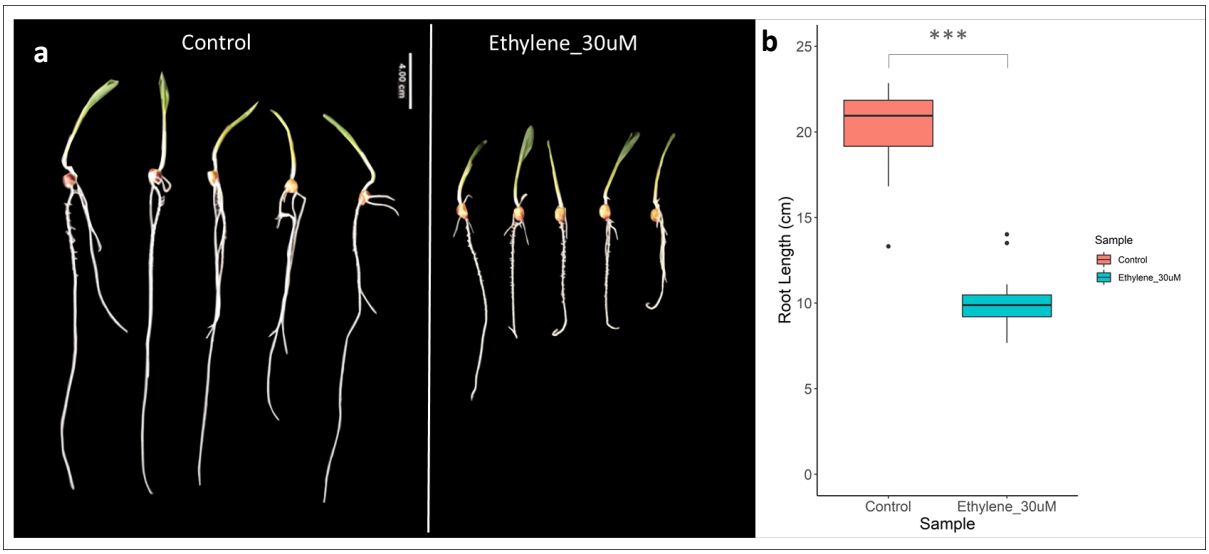


Fig. 2.11. Root length differences in ethylene treated maize seedlings.

a) Representative images of 6-day old maize cv. Adept seedlings grown in control and 30µM ethylene. b) Boxplot showing differences in root growth between control and treatment with 30µM ethylene.n=10-19 *** indicates statistical significance for $p < 0.001$ using Welch's t-test. Scale bar = 4cm

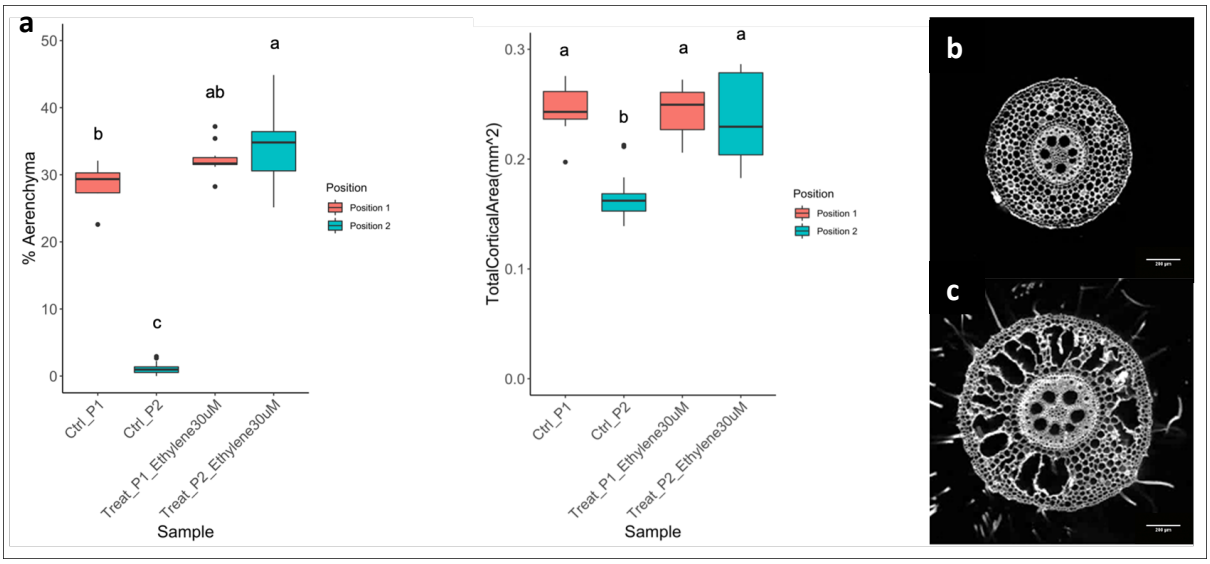


Fig. 2.12. Root anatomical differences in ethylene treated maize seedlings.

a) Differences in %Aerenchyma and Total Cortical Area in control and 30µM ethylene treated 6-day old maize cv. Adept in two different position of primary root, P1-mature area (2-3 cm from seed) and P2-maturation zone (2-3 cm from root tip). Different letters indicates statistically significant differences between samples using ANOVA and Tukey test was

performed using R, a=0.05, n=5-9. b-c) Representative cross section images in the maturation zone close to the root tip (P2). Scale bar = 100µm

I was able to confirm the positive effect of ethylene on regulation of root cortical aerenchyma formation (Fig. 2.12). Collected data on RCA showed a significant increase in % RCA in P2 after a 30µM ethylene treatment (34.05 ± 5.10%) compared to control (1.14 ± 0.95) whereas no significant differences was observed in P1 between ethylene-treated and control roots (Fig. 2.12).

Conclusions

Functional studies described in this chapter characterizing specific genes or hormones identified using the Deepgenes pipeline, validated its effectiveness for pinpointing regulatory genes and signals for root anatomical traits. In particular, genes like *ZmQKY* were selected for their high homology to sequences in model plants such as *Brachypodium distachyon* to develop CRISPR edited lines (UoN), whilst several others were selected in maize (*ZmHAL3, ZmEPFL6, ZmQKY, ZmHIF1, ZmCLAVATA3, ZmACCsynt*) for developing CRISPR knockout lines in collaboration with WCIC (WI, USA). *Brachypodium distachyon* proved a good model to develop CRISPR mutants in *BdQKY* and *BdFERONIA* orthologs at high gene editing efficiency (33-40%; Miao *et al.*, 2013; Bragg N. *et al.*, 2014). The observed low transformation efficiency score is likely due to the lower temperature conditions during the regeneration stage of tissue cultures of our system, compared to the protocol suggested by Vogel and Hill, 2008. However, a good editing efficiency was observed in *Brachypodium distachyon*, as out of six different gRNA event sequenced in *Brachypodium distachyon*, four were able to generate deletion/insertions edits.

The CRISPR-cas9 resources developed in *Brachypodium distachyon* revealed anatomical changes in the root cortical layer in the *BdQKY* mutant Pos1-8(1). QKY is member of the protein family STRUBELLIG/SCRAMBLED (SUB/SCM) encoding for a multiple C2 receptor-like kinase transmembrane protein. In Arabidopsis QKY was shown to impact the floral tissue organization and crucial for cell-cell communication in the STRUBELLIG pathway using Ca_{2+} as a cofactor (Fulton *et al.*, 2009; Trehin *et al.*, 2013). In Arabidopsis roots, QKY defects in the

SCM domain reduced cortical cell division rate and disrupts development of overlying root hair cells (Kwak et al., 2005). In maize and *Brachypodium distachyon* roots, which feature multiple cortical cell files, mutating QKY results in >60% reduction in TCA and 1-2 less cell files compared to wild type. Hence, *BdQKY* appears to negatively regulate TCA, root diameter, CCFN as well as overall growth in nodal roots of *Brachypodium distachyon*. More detailed studies need to be performed on QKY mutant lines in mature plants grown in real soil and on several different root classes to more fully assess the role of QKY during root development in cereals.

The Deepgenes gene discovery pipeline also identified a number of candidate genes encoding either ethylene synthesis (ACC synthase) and response (EIL1) pathway components (Fig. 2.5a). Two rice ethylene response mutants (disrupting EIN2 and EIL1 genes; (Yang *et al.*, 2015)) were used to investigate this hormones role during root cortical cell development. Consistent with earlier reports of ethylene functioning as a positive regulator of RCA, *osein2* and *oseil1* mutants exhibited a reduction in % RCA in primary roots (Fig. 2.10). Considering the complexity of the monocot root system, ethylene's regulation of RCA might be different depending on root class (e.g. primary, seminal, crowns). New phenotyping technologies such as L.A.T. 2.0 will be very useful to address this question in future. In summary, this Chapter has demonstrated how an anatomical phenotyping based GWAS approach combined with bioinformatics and model species can provide a highly effective gene discovery pipeline to identify novel regulatory genes and signals.

Chapter 3

Root angle is controlled by *EGT1* in cereal crops employing a novel anti-gravitropic mechanism.

Introduction

Root architectural traits such as angle plays an important role adapting plant growth to different environmental conditions and aiding capture of soil resources such as water and nutrients. For instance, deeper root growth angle is advantageous for accessing subsoil water and enhancing drought tolerance, while shallow root growth angle improves capture of nutrients like phosphorus (P) that accumulates in topsoil (Uga *et al.*, 2013; Huang *et al.*, 2018). Recent studies also report that modified root angle increases yield under saline conditions (Kitomi *et al.*, 2020). Hence, improved understanding of the genes and mechanisms controlling root growth angle would facilitate breeding of crop varieties better suited for different abiotic stresses arising from future climatic conditions.

The growth angles of different root classes (e.g., primary, seminal, lateral and crown) are often distinct to limit inter-root competition. The distinct angles adopted by each root class are referred to as their gravitropic setpoint angle (GSA). The vertical GSA of primary roots is dominated by the positive gravitropic mechanism, while non-vertical GSA in other root classes is determined by competing gravitropic and anti-gravitropic offset (AGO) mechanisms (Roychoudhry *et al.*, 2017). Root gravitropism has been extensively studied in *Arabidopsis thaliana*, revealing that a change in root orientation is perceived in gravity sensing columella cells at the root tip, triggering the formation of a lateral auxin gradient which the lateral root cap transports to epidermal cells in the elongation zone, leading to differential growth and root bending (Ottenschläger *et al.*, 2003; Swarup *et al.*, 2005; Band *et al.*, 2012). In contrast to the detailed knowledge obtained about the genes, signals and mechanisms involved in the root gravitropic response, the AGO mechanism is only recently beginning to be unravelled. Auxin transport has been linked with the AGO mechanism, implying that the interaction of two opposing gravitropic and AGO regulated auxin fluxes could determine the angle of organ growth (Rosquete *et al.*, 2013; Roychoudhry *et al.*, 2013). However, detailed knowledge about auxin-dependent or auxin-independent components of AGO mechanism(s) still remains unclear. Recently cytokinin was discovered to regulates GSA in lateral root of *Arabidopsis thaliana* by contrasting cell growth in the upper cell side during the early stages of gravity response (Waidmann *et al.*, 2019). Similarly, *LZY* family genes have been showed to regulate

lateral root GSA by reducing the response to gravistimulus by organising auxin redistribution along with PINs during the early stages of gravity response (Kawamoto *et al.*, 2020; Jiao *et al.*, 2021). However, most of the studies on GSA and AGO were performed on adventitious lateral roots in Arabidopsis thaliana, very little is known about this mechanism on the more complex root system of crops.

Here, we report the identification of a putative component of a novel AGO mechanism in cereal roots termed *ENHANCED GRAVITROPISM 1* (*EGT1*). Screening of a barley TILLING mutant collection identified a mutant exhibiting a striking steeper root growth angle phenotype compared to wild type. SNP array-based bulk-segregant analysis of the mutant line outcrossed to barley cv Barke mapped the mutation within a region of c. 130 Mb on chromosome 6. Subsequent exome and WGS sequencing analyses identified mutations in the coding sequence of *HORVU6Hr1G068970* (Tubby-like F-box protein). Genetic characterisation of TM194 and an additional independent mutant allele (TM3580) confirmed that mutations in *HvEGT1* caused steeper root growth angle. Significantly, mutant studies revealed *EGT1* function is also conserved in durum wheat. Intriguingly, *HvEGT1* appears to function as part of a novel auxin independent AGO mechanism. *HvEGT1* is highly expressed in root stele tissues, which is distinct from the known auxin-mediated gravity responsive lateral root cap and epidermal tissues. RNA sequencing analysis further identified that many vascular expressed peroxidases and cell wall softening/stiffening enzymes and cofactors are differentially regulated in *hvegt1* mutant root tips compared to wildtype. We propose that *HvEGT1* controls root growth angle by functioning as an AGO component in a parallel auxin-independent pathway in elongating vascular tissues, via regulation of peroxidases and enzymes involved in cell wall stiffening and loosening, thereby serving to counteract root gravitropic bending via its outermost tissues.

Materials and Methods

Plant Material

Barley *Hvegt1* mutant alleles (TM194, TM3580, from the TILLMore barley mutant population(39)), wheat *Tdegt1* mutant alleles (*Tdegt1_wtA/mutB, Tdegt1_mutA/wtB and*

Tdegt1_mutA/mutB, from a wheat TILLING population described in Talamè *et al.*, 2008) and respective wildtypes (cv. Morex and cv. Kronos) were used for root growth angle imaging and measurement analyses on paper roll using semi-hydroponic systems and in soil using rhizotrons and X-ray micro-computed tomography (microCT) and X-ray computed tomography (CT). An F_2 population obtained by crossing TM194 mutant and another barley wildtype cv. Barke was used for Bulk Segregant Analysis (BSA). TM194 and TM3580 mutant alleles were used for whole genome sequencing (WGS) experiment and mapped to Morex v.1 reference genome. Morex, TM194 and TM3580 mutant alleles were used for gravistimulus induced root bending assays (on mock, NAA and NPA supplemented media), RNAseq and *in-situ* hybridisation analysis. Selected lines from the barley WHEALBI diversity panel (https://www.whealbi.eu/) were used for haplotype network analysis and root growth angle measurements. Methodology and growth conditions for each experiment are described below.

Barley and Wheat 2D root phenotyping

For semi-hydroponic system, seeds were washed in 70% (v/v) ethanol for 1 min, then in 1% sodium hypochlorite (v/v) + 0.02% (v/v) TritonX-100 for 5 min and rinsed with distilled water. Sterilised seeds were pre-germinated for 24 h at 28 °C in wet filter paper. Equally germinated seeds (seedlings with similar radicle length were assessed visually) were placed between two sheets of 50 x 25 cm of filter paper (Carta filtro Labor, Gruppo Cordenons SpA, Milan, Italy) soaked in demineralized water, rolled, positioned vertically in a 5-litres plastic beaker with 1 liter of demineralized water. Barley seedlings were grown for ten days at 24°C and wheat seedlings were grown for seven days at 22°C with a 16/8 hours photoperiod. Root growth from both experiments were imaged using DSLR camera and vertical root angle for seminal and lateral (from the insertion with the seminal root) roots were calculated using ImageJ software. For 2D soil experiment purpose, barley and wheat *egt1* mutants and their respective wildtypes were grown up to 20 days in the GrowScreen-Rhizo rhizotrons automated platform and analysed as previously described (Nagel *et al.*, 2012).

Barley non-destructive 3D root phenotyping

Non-destructive 3D phenotyping was performed on Morex and TM194 using X-ray microCT and X-ray CT (n=6 independent replicates). For X-ray microCT, seeds were pre-germinated in

petri dishes for 1 day at 21°C in dark. Successful seedlings with equally germinated roots were grown in PVC columns (8 cm diameter x 15 cm height) filled with sandy loam soil from UoN experimental farm field sieved at <2mm and maintained at notional field capacity moisture until 9 DAG. Each column was scanned using a Phoenix v|tome|x M ® 240kV X-ray microCT scanner (Waygate Technologies (a Baker Hughes business), Wunstorf, Germany) at the Hounsfield Facility (University of Nottingham, Sutton Bonington Campus, UK). The voltage and current were set at 180 kV and 180 µA, respectively. A voxel resolution of 55 µm was used in all scans. During the scan, the specimen stage rotated through 360° at a rotation step increment of 0.166° collecting a total of 2160 projection images. Each image was the integration of 4 frames with a detector exposure time of 250 ms, resulting in a 75 minutes scan time. A 0.1 mm copper filter was applied to the front of the exit window of the X-ray tube during the scan to reduce beam hardening artefacts. For the X-ray CT, well-watered plants were grown in larger PVC soil columns (20 cm diameter, 100 cm height) until full maturation stage. Each column was then scanned using a Phoenix v|tome|x L Custom ® 320kV X-ray CT system (Waygate Technologies (a Baker Hughes business), Wunstorf, Germany) at the Hounsfield Facility (University of Nottingham, Sutton Bonington Campus, UK). The voltage and current were set at 290 kV and 6200 µA respectively. A voxel resolution of 150 µm was used in all scans. During the scan, the specimen stage rotated through 360° at a rotation step increment of 0.15° collecting a total of 2400 projection images. To reduce image noise, each projection image was an integration of 12 frames with a detector exposure time of 131 ms. Each scan took approximately 240 minutes. A 1mm copper filter was applied to the exit window of the X-ray tube and a further 0.5mm Cu filter applied over the detector panel to reduce beam hardening artefacts.

For all CT images, the scans were reconstructed using DatosRec software (Waygate Technologies (a Baker Hughes business), Baker Hughes Digital Solutions GmbH, Wunstorf, Germany). Radiographs were visually assessed for sample movement before being reconstructed in 16-bit depth volumes with a beam hardening correction of 8. An inline median filter was applied to reduce noise in the image of the CT X-ray data. Reconstructed volumes were then post processed in VG Studio MAX (version 2.2.0; Volume Graphics GmbH, Heidelberg, Germany). Reconstructed image stacks were segmented using the polyline tool within VGStudio Max and root traits where quantified using PAM (Polyline Angle Measurement), an in house developed software tool that measures the angle from polyline

segmented roots. PAM extracts the 3D coordinate points (2-5 XY slices apart) for each polyline and translates these into a 3D model. The angle of each polyline (root) is calculated from the difference of a vertical vector from the position of the uppermost coordinate point of the polyline (e.g. the soil surface). Therefore, steeply growing roots have a low angle value and shallow roots have a large angle value. Measurement of root angle was terminated once the root has touched or interacted with the pot wall to avoid any physical interference on undisturbed root angle.

Bulked segregant analysis (BSA)

BSA was carried out on F_2 plants derived from the cross TM194 $\times$ cv. Barke which were grown in flat rhizotrons, each composed by a rigid 38.5 x 42.5 cm black plastic screen and by two wet filter paper sheets. Seeds were disinfected for 5 minutes in a 1.2% solution of sodium hypochlorite and incubated for 24 hours at 28°C. Five pregerminated seeds per rhizotron were placed between two filter paper sheets. Rhizotrons were vertically positioned inside a plastic tank filled with deionized water to reach a level of 5 cm from the bottom and put in a growth chamber with a 16/8h photoperiod and a temperature of 22°/18°C for 13 days. After that period, root growth angles were measured, and seedlings were divided into wildtype and mutant phenotype groups. 15 plants from each group were selected for single plant DNA extraction. Leaves were lyophilized and foliar samples of approximately 2 cm^2 were homogenized for 3 minutes in a TissueLyser. DNA was extracted with the Macherey-Nagel Nucleospin® Plant II kit and quantified with NanoDrop. Two DNA bulks, steeper and wildtype root angle phenotype were prepared in double, mixing equal amounts of each plant and bringing to a final concentration of 50 ng/ul, in addition to single plant DNA from 10 plants showing steeper angle and all sample were genotyped with the 9k Illumina Infinium iSelect barley SNP array. The results were analysed with GenomeStudio (Illumina, San Diego, Inc.), and delta theta values used as index of allele proportion at each SNP marker. Delta theta values were calculated as the squared difference between the theta value of wildtype and steeper angle phenotype bulk.

Whole genome sequencing (WGS)

Genomic DNA for WGS of the two mutants TM194 and TM3580 was prepared as described above and sequenced with Illumina HiSeq PE150, obtaining 727,190,417 paired-end reads for an average coverage of approximately 23x for TM194 and 792,713,857 paired-end reads for an average coverage of approximately 25× for TM3580. Reads were aligned to Morex v.1 reference sequence (Mascher *et al.*, 2017) with BWA v.7.12 (Li and Durbin, 2009)and variants in the genomic space were called with SAMtools v.1.3 (Li, 2011), filtering for a minimum read depth of 5×, PHRED quality > 40. To discard background mutations due to the differences between the Morex reference sequence and the Morex parental seeds which had previously been used in the mutagenesis, the SNP calling for TM194 considered further eight TILLMore mutants WGS data that was available at that moment, filtering with a custom AWK script for a minimum ratio DV/DP of 0.8 for the *Hvegt1* mutants and a maximum ratio of 0.2 in every other mutant, where DP is the coverage depth at the SNP position and DV is number of non-reference bases at the same position. SNP effects were predicted with SNPEff v.3.0.7 (Cingolani *et al.*, 2012). TM194 mutant was predicted to harbour a mis-sense substitution within 4th exon while TM3580 mutation at the end of first intron was predicted to cause splice-acceptor variant (SI Dataset 1).

Haplotype analysis of *HvEGT1* in WHEALBI barley germplasm collection

A haplotype analysis of SNP data from the barley diversity panel WHEALBI (Bustos-Korts *et al.*, 2019), consisting of 459 barley accessions, of which 199 are cultivars, 202 landraces and 4 wild, was conducted in the coding region of *HvEGT1*. Files were imported into R Studio and package *pegas* (Paradis, 2010) v.0.14 was used to detect haplotypes. Six haplotypes were found. The MUSCLE multi-alignment was produced with Mega X v.10.2.4 (Kumar *et al.*, 2018) and exported to the NEXUS format (Maddison *et al.*, 1997). The haplotype TCS network (Clement *et al.*, 2002) was produced with PopART (http://popart.otago.ac.nz).

HVEGT1 structure modelling and *Hvegt1* mutant allele mapping

The protein sequence obtained by translating Transcript 3 (427 aa) from *HvEGT1* (HORVU6Hr1G068970) entry was used to construct a homology model using the Phyre2 (Kelley *et al.*, 2015) server. A homology modelling approach was chosen over *de novo* structure prediction from first principles as the gene of interest was inferred to have F-box and Tubby-Like domains, which were confirmed by the protein domain analysis using EBI

Interproscan tool. Tubby-Like domain was alone used in the structure prediction algorithm. WGS and haplotype analysis identified mis-sense amino acid substitutions (TM194 and Haplotype II and IV, respectively) were mapped on the predicted structure. Splice acceptor mutation (TM3580) was also visualised with respect to organised F-box and Tubby-like domains. Protein sequence was further studied for its conservation to function prediction across plant species using ConSurf algorithm.

Wheat EGT1 mutant identification

Durum wheat (*Triticum turgidum*) *Tdegt1* mutants were identified from a TILLING population developed in tetraploid *cv* Kronos(40). Two selected lines (Kronos2551 and Kronos3926) carrying premature termination codons in TRITD6Bv1G159700, the *TdEGT1* homoeologous gene on the B genome (*TdEGT1_wtA/mutB*), were both crossed with the line Kronos2708, carrying a splice donor mutation in TRITD6Av1G172130, the *TdEGT1* homoeologous gene on the A genome (*TdEGT1_mutA/wtB*). F1 plants obtained from both crosses were self-pollinated. Progenies of selected wild-type, single and double mutant F2 individuals derived from the two independent initial crosses (*TdEGT1_mutA/mutB*) were grown in semi-hydroponic system and analysed for seminal root angle analysis as mentioned above.

Phylogenetic analysis of Tubby-like F-Box Protein Sequences in selected monocots

HvEGT1 was used as a seed gene to select orthologous genes (>40% identity) from key monocot species such as barley (*Hordeum Vulgare*), wheat (*Triticum turgidum*), rice (*Oryza Sativa spp. Japonica*), maize (Zea Mays B73) and *Brachypodium distachyon* using interactive phylogenetic module of Monocots Plaza 4.5 (Van Bel *et al.*, 2018). Protein sequences were aligned using MUSCLE and tree was constructed using FastTree algorithm. Generated Newick file was imported into iTOL to create an unrooted tree.

Gravity and auxin sensitivity bioassays

Seedlings of Morex, TM194, TM3580 were pre-germinated for 2 days in dark at 21°C. Equally germinated seeds were then transferred on 12cm squared plates containing 1% agar media and grown 1-2 days at 21°C with 12/12 hours photoperiod. For gravity response bending bioassay, plates were then rotated by 30°, 60° and 90° and then images were collected at multiple timepoints using a Nikon D5100 camera. For the auxin sensitivity assay, barley

seedlings were then transferred to mock, 10nM NAA and 1µM NPA media for 2 hours before rotating plates by 90°. Time lapse image stack was then generated by taking images every 30 minutes for 12 hours in dark and then once at 24 hours after gravistimulus using the robotic imaging facility at the University of Nottingham (Band *et al.*, 2012). Root tip bending angle was the quantified using the line tool of FIJI (Schindelin *et al.*, 2012). For consistent measurements, lines were always drawn toward the right-hand side. A schematic of rotation and quantification using the acquired angle data are shown in S.Fig. 3.2 . For consistency, only roots (and shoot) with an angle at t[0] within a range of ± 15° were chosen for the analysis. Root length adjusted to day [0] measurement were acquired using the segmented line tool in FIJI was used using the same formula used to calculate root and shoot bending angles.

RNA-sequencing and data analysis

Seeds of Morex, TM194, TM3580 genotypes were sterilised with 0.5% Sodium hypochlorite solution for 5 mins followed by five washes of sterile water. Sterilised seeds were germinated on sterile Whatman filter paper placed in a petri dish for 2 days at 21°C in dark. Equally germinated seeds were vertically grown on 1% agar plates for 2 days at 22°C, 16/8 hours photoperiod. Root tips from seminal roots growing on media surface were dissected at the first visible root hairs and samples were snap frozen using liquid nitrogen and then stored at -80°C. Root tips from 15 seedlings were pooled together per replicate and RNA extraction was then performed using Trizol and RNeasy mini kit (Qiagen) for RNA seq analysis. For each genotype, 4 biological replicates were prepared.

Library preparation and Illumina sequencing was performed by Novogene (UK) Company Limited. RNAseq was performed on an Illumina Hiseq 2000 platform and 150 bp paired end reads were generated according to Illumina's protocol. Data analysis was performed by standard Novogene bioinformatics pipeline. Raw reads were first processed to remove adapter and poly-N sequences and low-quality reads. High quality paired-end clean reads were mapped to reference genome IBSC_v2 using HISAT2 software (Kim *et al.*, 2019). Cufflinks Reference Annotation Based Transcript (RABT) assembly method (Roberts *et al.*, 2011)was used to assemble the set of transcript isoforms of each bam file obtained din the mapping step. HTSeq (Anders *et al.*, 2015) was used to count the read numbers mapped of

each gene, including known and novel genes. FPKM of each gene was calculated based on the length of the gene and reads counts mapped to this gene. The hierarchical cluster analysis of gene expression among replicates indicated poor correlation for one of the four replicates for sample TM194, which was removed from further analysis. Differential expression analysis between TM194 vs Morex, TM3580 vs Morex and TM3580 vs TM194 was performed using DESeq2 (Anders and Huber, 2010) R package. The resulting *P* values were FDR corrected using the Benjamini and Hochberg's approach and genes with an adjusted *P* value < 0.05, -1.5 < fold change > 1.5 and FPKM >1 were assigned as differentially expressed. GO enrichment was performed using gProfiler (Raudvere *et al.*, 2019) web server with settings (Statistical domain space = All known genes; significance threshold = g:SCS, 0.05). REVIGO (Supek *et al.*, 2011) (http://revigo.irb.hr, default settings) was used to remove semantically redundant GO terms.

Barley RNA *in situ* hybridisation

RNA *in situ* hybridization was performed to target *HvEGT1* expression in Morex. Seeds of barley cultivar Morex were surface sterilized in 20% (v/v) sodium hypochlorite solution for 10 min, then rinsed with MilliQ water five times before pre-germination overnight. Seeds were then placed into germination pouches (Phytotc) for 5 days. Fresh root tips (2 cm) were harvested and fixed in Formalin-Acetic acid-Alcohol (FAA) (50%v/v 100% ethanol, 5%v/v glacial acetic acid, 25%v/v 16% paraformaldehyde (electron microscopy grade), 20%v/v diethyl pyrocarbonate (DEPC)-H_2O, 0.1%v/v Tween 20). Root tips with FAA were placed on ice for 2 hours including 15 min of vacuum infiltration, followed by two 10 min washes in 70% ethanol/DEPC-H_2O, and then stored at 4°C overnight. The samples were dehydrated and cleared with a series of ethanol and Histochoice washes before being embedded in molten paraffin wax. The embedded samples were stored at 4°C under RNase free conditions before sectioning. The paraffin wax blocks with the root samples were sectioned at 7 µm thickness using a Leica microtome and mounted onto poly-L-lysine coated slides prior to in situ hybridization. Digoxigenin-labelled antisense and sense probes were designed and synthesized as shown in S.Fig. 3.6. The probes specific to *HvEGT1* were amplified from Morex root cDNA, using primers fused with the T7 promoter sequence at the 5' end to allow in vitro transcription. The probes were designed to recognize the end of the coding sequence and 3' untranslated region (UTR) of the gene. The barley histone H4 gene was used as a positive

control. The *in-Situ* hybridization and detection were performed using the InsituPro VSi robot (Intavis) (Zeng *et al.*, 2017).

Results

Barley TILLING mutant TM194 exhibits steeper root growth angle in every root class

A barley root mutant line TM194 exhibiting a striking steeper seminal and lateral root phenotype (Fig. 3.1) was initially identified in a chemically mutagenized population of the cv. Morex (Talamè *et al.*, 2008) using a semi-hydroponic rhizotron screening system. 3D root architecture phenotyping of 10-days old TM194 roots using X-ray micro–Computed Tomography (CT) revealed the steeper seminal root angle phenotype directly in soil (Fig. 3.1a). Phenotyping TM194 roots of 10-days using semi-hydroponic system (Fig. 3.2), 20-days after germination using soil-filled rhizotrons and at grain maturation stage using microCT, revealed lateral and crown root angles are also significantly steeper compared to wildtype Morex (Fig. 3.1b-d). Hence, the TM194 mutant exhibited steeper root growth angle in every root class examined, in both semi-hydroponic and soil conditions.

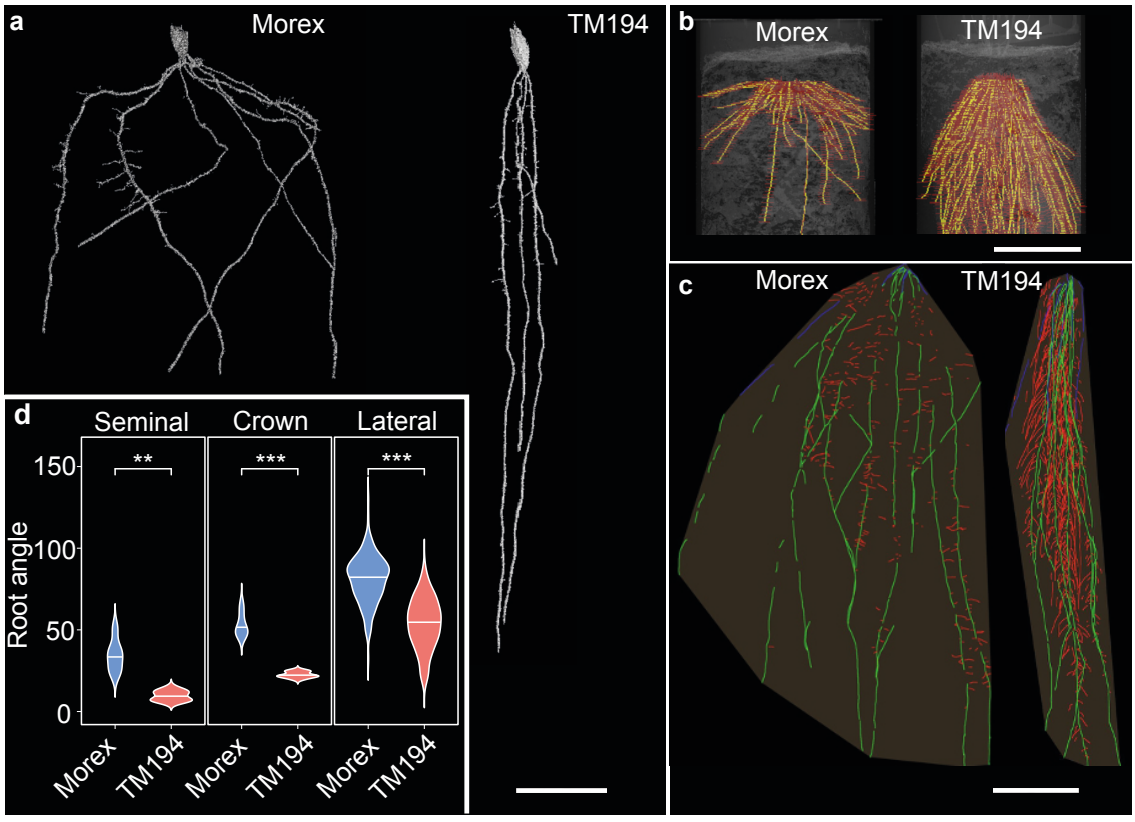
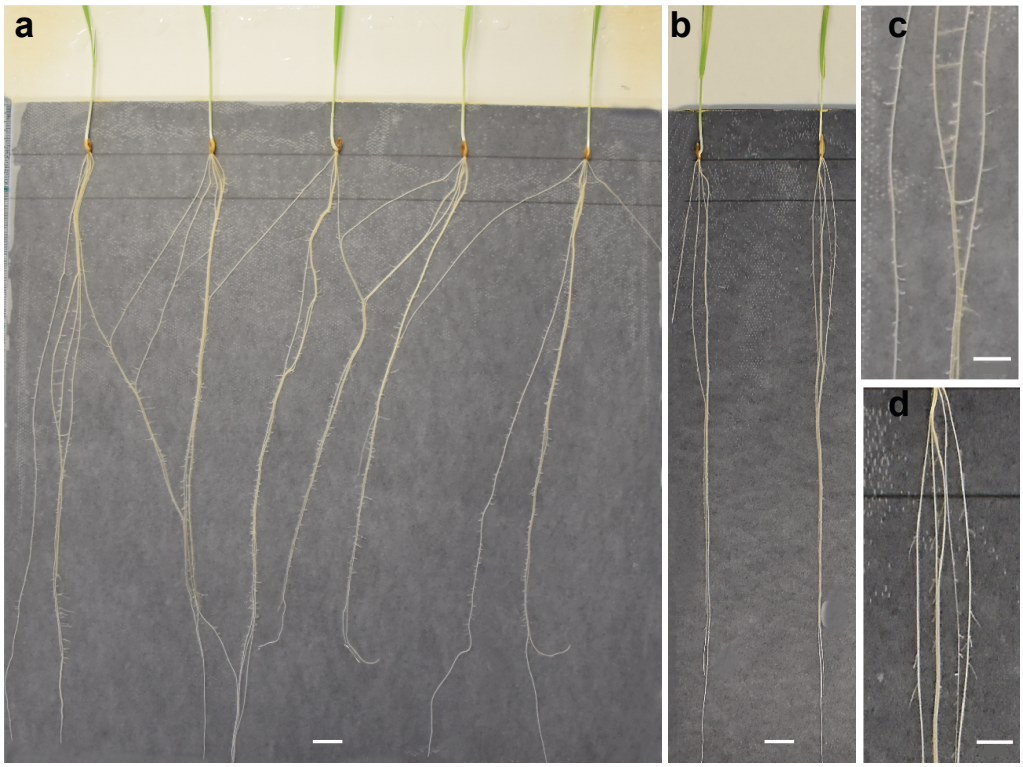


Fig. 3.1. TM194 mutant shows steeper angle in every root class in soil conditions.

a) Representative X-Ray micro-CT scan image of 10 DAG wildtype (Morex) and TM194 roots, showing major differences in seminal root vertical angle. Scale bar = 2 cm. b) Representative X-Ray CT scan image of fully grown plants at grain maturation stage revealing major difference in crown root vertical angle between Morex and TM194. Scale bar = 10 cm. c) Representative image of 20 DAG Morex and TM194 revealing difference in lateral root insertion angles (red coloured). Scale bar = 10 cm d) Quantification of vertical root angle from segmented seminal roots, crown roots and lateral roots. *** and ** indicates statistically



significant difference using Welch's *T*-Test at $p<0.001$ and $p<0.001$ in n>4 independent replicates, respectively. CT = computed tomography, DAG = days after germination.

Fig. 3.2. TM194 mutant shows steeper seminal and lateral root angle phenotype in semi-hydroponic conditions.

a-b) 2D Root architecture phenotype of 10 DAG seedlings of barley a, cv. Morex. and b, TM194 in semi-hydroponic conditions. Scale bar = 1cm. c-d) Magnified image of (c) Morex and (d) TM194 seminal roots highlighting phenotypic difference in lateral root insertion angles. Scale bar = 1 cm.

Exome sequencing of TM194 reveals a mutation in *ENHANCED GRAVITROPISM 1* (*HvEGT1*)

To examine the genetic and molecular basis of the TM194 root growth angle phenotype, the mutant was initially out crossed to Barke, a barley cv., which exhibits a similar root growth angle phenotype to cv. Morex. Whilst F_1 plants exhibited a wildtype phenotype, F_2 plants (n = 75) segregated in a Mendelian pattern for either a steeper or wildtype seminal root phenotype (59:16 plants, wildtype vs steeper, respectively, X^2 3:1, n.s.), consistent with the TM194 root growth angle phenotype segregating as a single recessive allele. Using the same F_2 population, a SNP-based bulk segregant analysis (BSA) revealed that the mutated locus mapped to chromosome 6 (Fig. 3a), in a large pericentromeric region spanning c. 130 Mb between markers *BOPA2_12_30144* and *BOPA1_4109-90*. To pinpoint the mutation, we performed exome sequencing on TM194. This revealed missense mutations in four genes within the chromosome 6H region highlighted by BSA (Fig. 3b-c, SI Dataset 1). To pinpoint the key relevant gene, we exome sequenced a second steeper root angle mutant line TM3580 from the original tilling population. TM3580 was shown to carry total six mutations in the same chromosome region, while only one mutation in *HORVU6Hr1G068970* (encoding Tubby-Like F-box Protein) overlapped with TM194. Specifically, TM3580 contained a mutation in the first intron of *HORVU6Hr1G068970,* predicted to cause a splice acceptor variant (Fig. 4, SI Dataset 1). Bulk RNAseq analysis of TM3580 and Morex root samples confirmed the TM3580 mutation caused a splice acceptor variant, resulting in a premature stop codon (Fig. 4). Taken together, these results provided conclusive evidence that mutations in *HORVU6Hr1G068970* are responsible for the steeper root angle phenotype, leading us to name this gene as barley ***E****NHANCED* ***G****RAVI****T****ROPISM* ***1*** (*Hv****EGT1***).

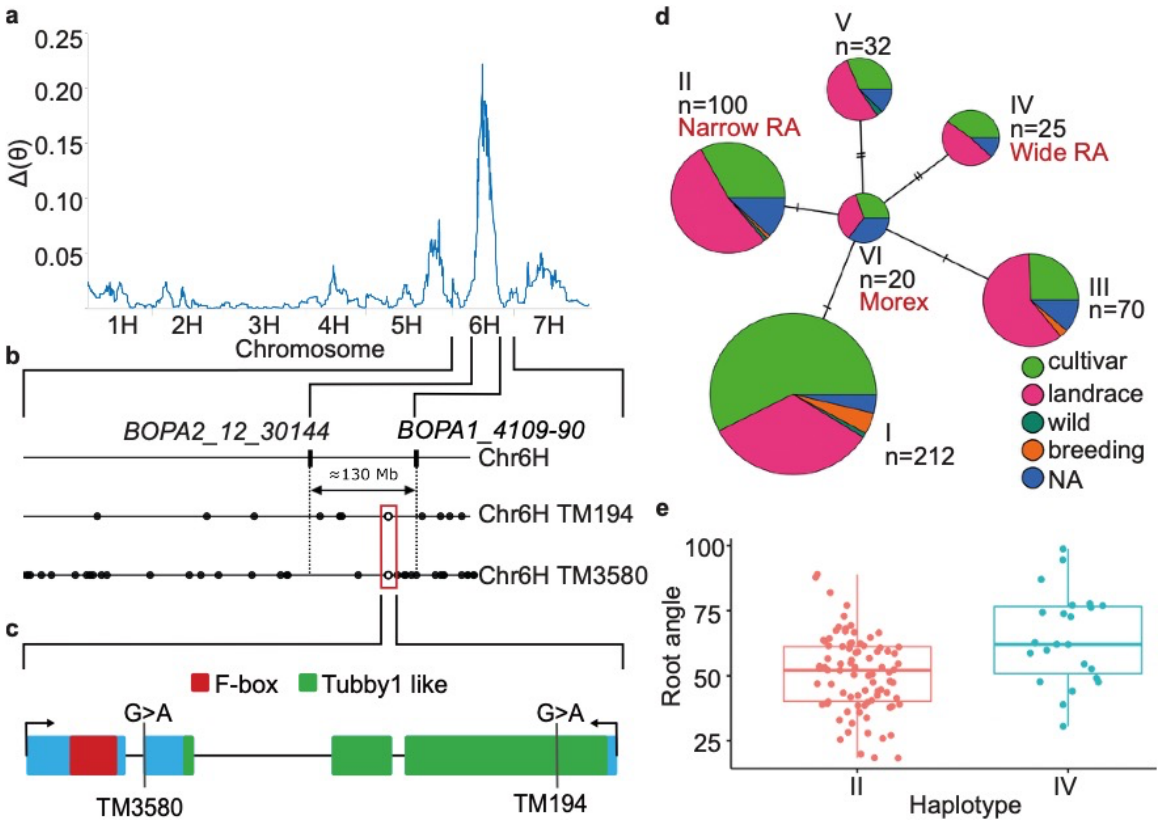


Fig. 3.3. Exome and WGS sequencing of TM194 identifies mutation in EGT1.

a-b) SNP based Bulk Segregant Analysis (BSA) from F2 plants from TM194 X cv. Barke outcross. a) Genome-wide plot of unbalanced allelic frequency from SNP-based BSA. ΔTheta parameter represents the difference in allele frequency for each tested SNP. b) Schematic representing a region spanning ~c.130 Mb on chromosome 6H between markers *BOPA2_12_30144* and *BOPA1_4109-90*. Filled circles indicate all SNPs within genes present in this region while empty circles (in red rectangle) indicate SNPs within pinpointed *HORVU6Hr1G068970* gene. Whole-Genome Shotgun (WGS) sequencing of another mutant allele of *HORVU6Hr1G068970* also showed steeper root growth angle phenotype. This gene is further named as ***E**NHANCED **G**RAVI**T**ROPISM 1* (***EGT1***). c) Schematic representation of *EGT1* and the position of the two mutations in relation to the F-box domain (red) and the Tubby-like protein domains. d-e) Haplotype analysis of *EGT1* nucleotide sequence variation present in WHEALBI barley germplasm collection. d) Haplotype network analysis revealed that haplotype II and IV carry missense substitutions, while remaining four haplotypes carry synonymous substitutions. *n* indicates number of genotypes within each class. e) Root growth angle distribution of WHEALBI barley lines carrying haplotype II (86 lines) and IV (25 lines).

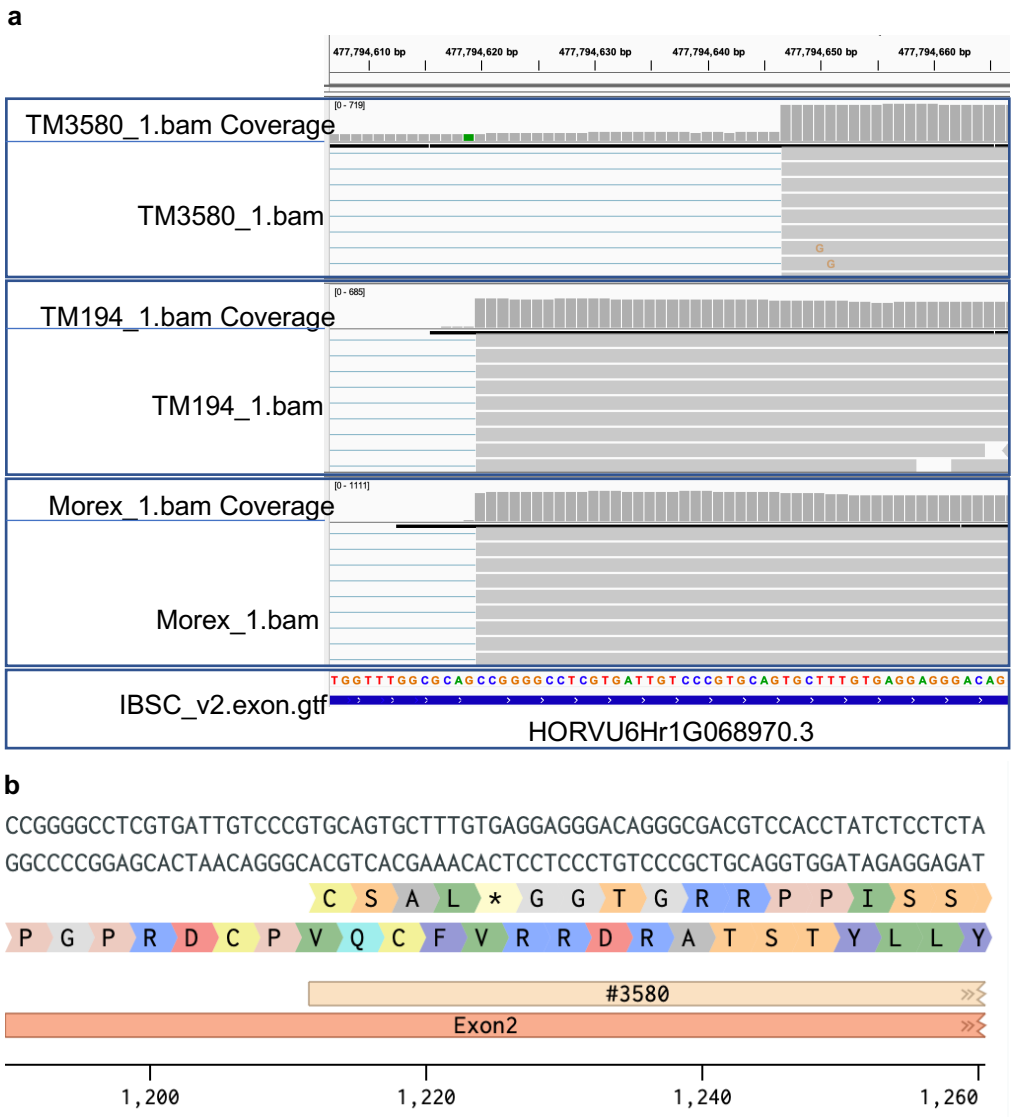


Fig. 3.4. TM3580 mutation causes a splice acceptor variant, resulting into a premature stop codon.

a) Snapshot of Integrative Genomics Viewer (Robinson *et al.*, 2011) showing visualisation of G to A splice acceptor mutation in TM3580 (green base marked by red arrow) causing trimmed version of Exon2 in TM3580 (compared to Morex and TM194) mapped to barley reference genome (IBSC_v2.exon.gtf). b) Schematic showing that the mutation in TM3580 causes 8 amino acid frameshift leading to premature stop codon.

Mutations in a highly conserved motif in the HvEGT1Tubby domain disrupt gene function

Next, we examined whether nucleotide polymorphisms within *HvEGT1* could provide a source of natural variation in root growth angle observed in barley diversity panels. We exploited the

availability of exome sequence of a large barley germplasm collection (WHEALBI collection) (Bustos-Korts *et al.*, 2019). Using haplotype network analysis of nucleotide sequence variation within the *HvEGT1* coding sequence, we identified two haplotypes (II and IV) carrying missense substitutions and four other haplotypes carrying synonymous substitutions (I, III, V and VI) (Fig. 3.3d). Based on this result, we phenotyped barley accessions carrying haplotypes II (n = 86) and IV (n = 25) using a semi-hydroponic system. Accessions carrying haplotype II exhibited significantly steeper seminal root angle distribution than accessions carrying haplotype IV (50.9 ±14.8 *vs*. 64.3 ±17.6, median ± s.d. degree angle, respectively; P <0.001) (Fig. 3.3e). To understand this further, we mapped their substitutions onto the HvEGT1 protein structure and compared them with the TM194 mutation. Interestingly, haplotype II causes a F391L substitution, just four amino acids away from TM194 (G395E) and both these substitutions lie within a highly evolutionary conserved motif (position 391-400) shared by 37 plant species (Fig. 3.5 and 3.6). In contrast, haplotype IV causes a S306C substitution, 89 amino acids upstream of the TM194 mutation (Fig. 3.5c). To investigate the effect of these mutations on EGT1 structure and function we constructed a homology model for Tubby and F-box domains using Phyre2 (Kelley *et al.*, 2015)(Fig. 3.5a-b). For example, G395 sits in a highly positively charged cavity, likely to be stabilized by an adjacent negatively charged C-terminal site. The TM194 G395E substitution causes a small, neutral amino acid to be substituted by a larger, negatively charged residue, which is likely to destabilise this region and impact protein function. Our results suggest haplotype II and TM194 impact a highly conserved motif 391-400 within the Tubby domain, disrupting HvEGT1 function and causing a steeper root angle phenotype.

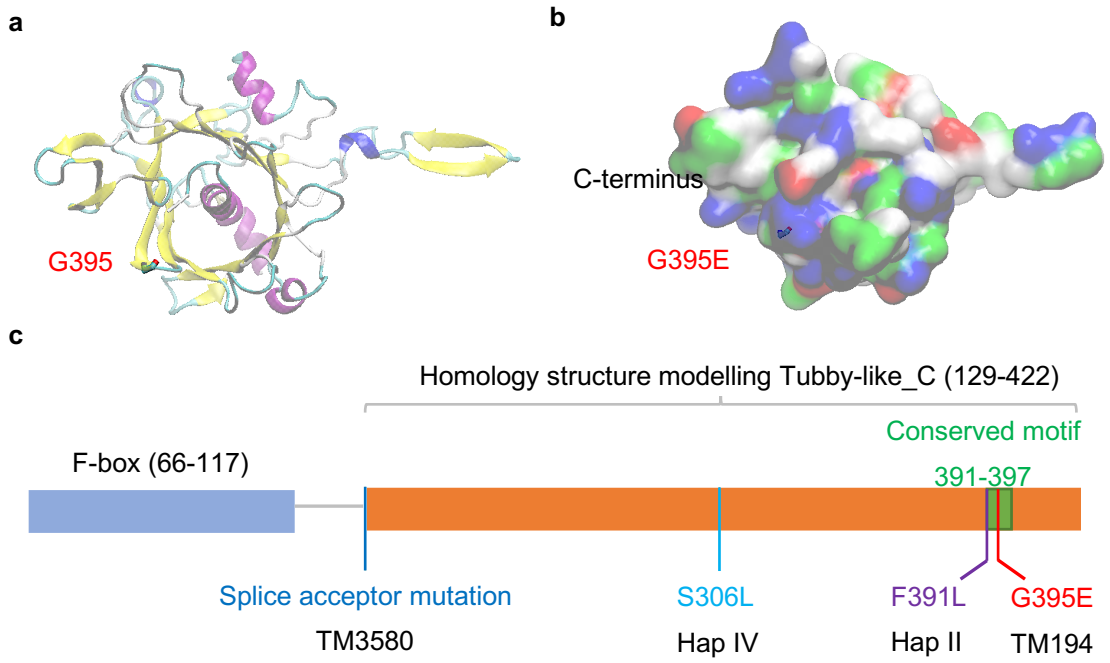


Fig. 3.5. Mapping of mutant alleles and key haplotypes identified from the WHEALBI population onto the HvEGT1 Tubby domain structure.

a) Homology model for the Tubby-like domain of HvEGT1 obtained using Phyre2(Kelley *et al.*, 2015). Magenta, yellow, cyan and white colour indicate alpha helices, beta strands, turns and random coils, respectively. G395 indicates the mis-sense substitution position of TM194 mutant on the predicted domain. b) Amino acid charge distribution in a is colour coded as follows Blue (basic, positively charged), red (acidic, negatively charged), green (polar) and white (non-polar). G395 sits in a highly positively charged cavity, probably stabilized by an adjacent negatively charged C-terminal site. G395E substitution leads to a small, neutral amino acids to a larger, negatively charged residue is highly likely to destabilise this region of the protein, likely affecting its function. c) Domain organisation and mapping of TM3580 and TM194 mutations and haplotypes II and IV identified from the WHEALBI population (Bustos-Korts *et al.*, 2019).

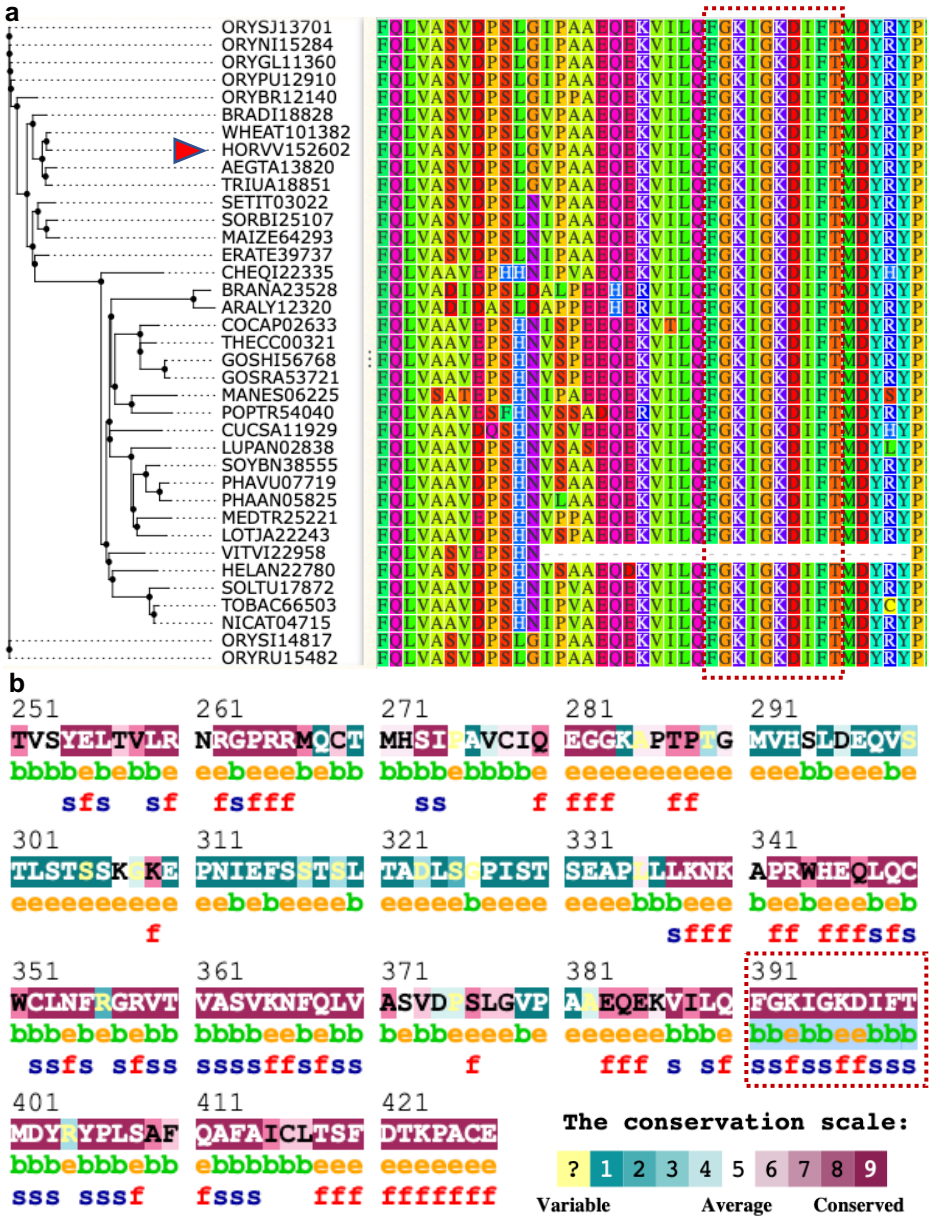


Fig. 3.6. Phylogenetic conservation of HvEGT1 residues.

a) Trimmed multiple sequence alignment and phylogenetic tree using WASABI (http://wasabiapp.org, through ConSurf(4)) showing conserved residues 391 to 400 (red dotted rectangle) in the homologous sequences of HvEGT1 from 37 other plant species (UniProtKB - F2DEK2_HORVV; Phylogenetic database OMA(5) Group 512684). Red filled arrow indicates HvEGT1. b) Conservation to function prediction using ConSurf (Berezin *et al.*, 2004) highlighting residues 391 to 400 (red dotted rectangle). G395E and haplotype II (Fig. 3.5d-e) lie within this highly conserved region. Coloured letters indicate, 'e' = exposed and 'b' = buried residues according to the neural-network algorithm; 'f' = predicted functional

residue (highly conserved and exposed) and s = predicted structural residue (highly conserved and buried).

The role of *EGT1* in controlling root growth angle is conserved in wheat

Phylogenetic analysis of Tubby-like F-Box protein sequences in barley, wheat, rice and *Brachypodium distachyon* identified closely related proteins in all these species (Fig. 3.7). To address EGT1 function in another cereal, we screened (*in-silico*) a TILLING population of tetraploid (AA BB) wheat cv. Kronos (Krasileva *et al.*, 2017). Kronos2551 and Kronos3926 lines encoded premature termination codons in TRITD6Bv1G159700 (*HvEGT1* homoeologous gene on wheat B genome) and the Kronos2708 line carrying a splice donor mutation in TRITD6Av1G172130 (*HvEGT1* homoeologous gene on wheat A genome). Kronos2551 × Kronos2708 and Kronos3926 × Kronos2708 were crossed, then F1 plants were self-pollinated to create F2 plants. Progenies of selected wildtype and homozygous double mutants from two independent crosses were grown for seven days in rhizoboxes for root growth angle analysis. Both the double mutants exhibited steeper seminal and lateral root growth angle compared with the progenies carrying wildtype alleles in both homologs (S.Fig. 3.1). Hence, our results revealed that *TdEGT1* loci also control root growth angle in wheat and possibly other cereal and plant species.



Fig. 3.7. Phylogenetic analysis of Tubby-like F-Box Protein sequences in barley, wheat, rice, maize and *Brachypodium distachyon*.

HvEGT1 was used as a seed gene to select orthologous genes (>40% identity) from key monocot species such as barley (*Hordeum Vulgare*), wheat (*Triticum turgidum*), rice (*Oryza Sativa spp. Japonica*), maize (*Zea Mays B73*) and *Brachypodium distachyon* using interactive phylogenetic module of Monocots Plaza 4.5 (Van Bel *et al.*, 2018). Protein sequences were aligned using MUSCLE (Edgar, 2004) and tree was constructed using FastTree algorithm (Price *et al.*, 2009). Generated Newick file was imported into iTOL (Price *et al.*, 2009) to create an unrooted tree. Green colour highlights the distinct clade formed by EGT1 with 2 orthologs each from wheat and maize and 1 ortholog each from rice and *Brachypodium distachyon*,

Tree scale = 1 indicates 100% of aminoacidic substitution occurred between two aminoacidic sequences. Confidence between clades was calculated using bootstrap method (>100 interactions)

HvEGT1 controls root growth angle via an anti-gravitropic offset (AGO) mechanism

Different root classes adopt specific gravitropic setpoint angles (GSA), which are maintained by competing gravitropic and anti-gravitropic offset (AGO) mechanisms (Ottenschläger *et al.*, 2003; Swarup *et al.*, 2005; Band *et al.*, 2012; Rosquete *et al.*, 2013; Roychoudhry *et al.*, 2013, 2017). In *Hvegt1* mutants, seminal, lateral and crown roots are no longer able to maintain their non-vertical GSA, suggesting *HvEGT1* operates as part of the AGO pathway. To validate this, we compared root bending responses of four-day old seminal roots in *Hvegt1* (TM194) and Morex after either a 30°, 60° or 90° gravistimulus (Fig. 3.8a). Similarly, this was confirmed in the *Hvegt1* variant TM3580 where we observed faster gravitropic response, similarly TM194, when compared to Morex (Fig. 3.9). If the gravitropic mechanism was compromised in *Hvegt1*, its root bending rate would be slower. In contrast, if the AGO mechanism was compromised in *Hvegt1,* the countering gravitropic mechanism would confer a higher bending rate. Our results revealed *Hvegt1* roots exhibited a significantly higher bending angle and faster gravitropic response than Morex even after 0.5 hour at a 30° tilting gravistimulus and this difference became even more exaggerated with increasing tilting angle (Fig. 3.8b). This experiment also revealed that faster root bending is not related to root growth where in fact both *Hvegt1* alleles revealed slower root growth compared to Morex (Fig.3.9c, S.Fig.3.3b). Moreover, we observed no differences in shoot bending angle in the early timepoints of this experiment (S.Fig. 3.3 c-f) as well as in control conditions from the auxin sensitivity assay presented in the next section (S.Fig. 3.5 a-b) suggesting *HvEGT1* controls a root specific mechanism. Hence, the *Hvegt1* mutant appears compromised in its anti-gravitropic response, consistent with *HvEGT1* encoding a putative component of the AGO mechanism.

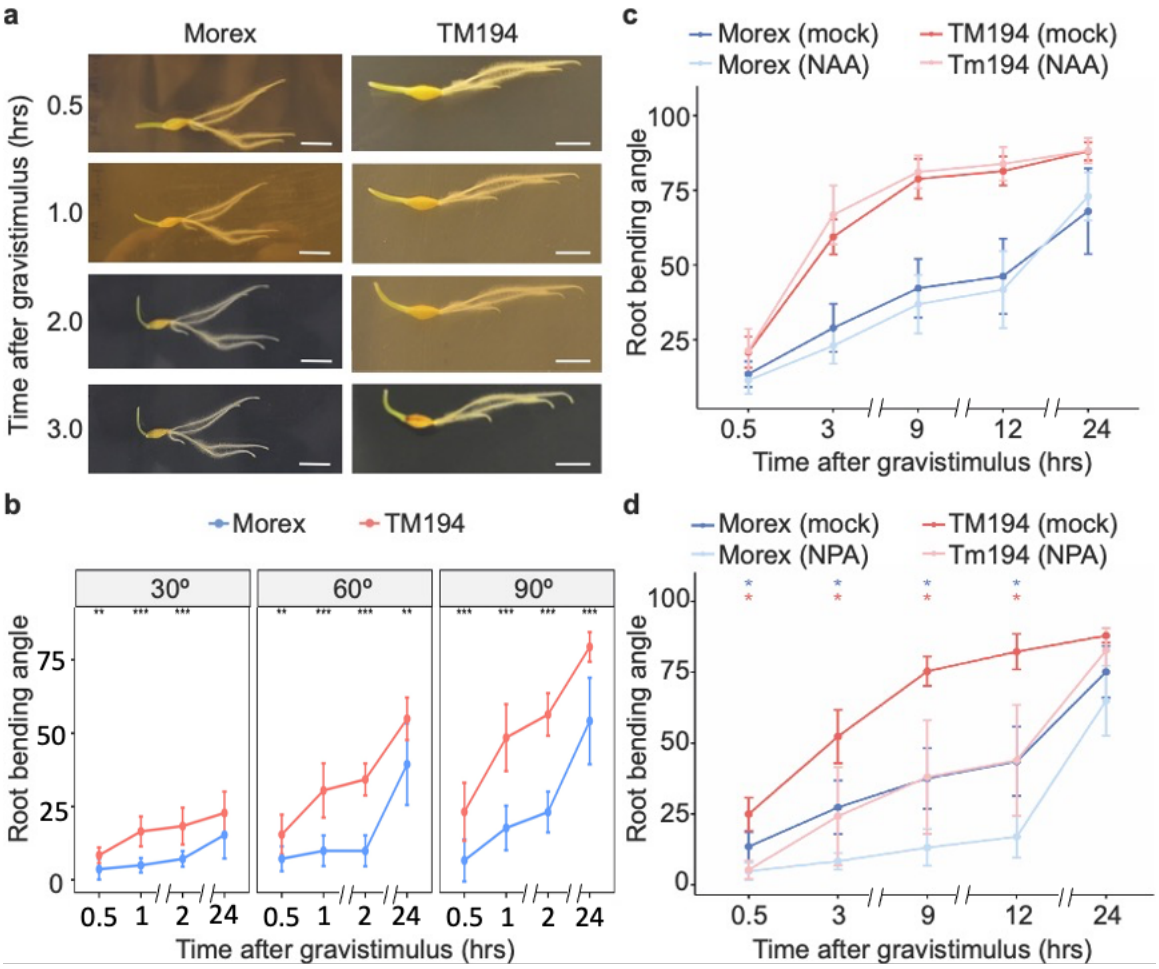


Fig. 3.8. HvEGT1 controls root growth angle via auxin-independent anti-gravitropic offset (AGO) mechanism.

a) Representative images of root bending response of 4-day old seminal roots in Morex and TM194 at 0.5, 1, 2 and 3 hours after 90° tilting gravistimulus. b) Measurement of dynamic change in root tip bending angle with increasing titling angle gravistimulations (from 30° to 60° to 90°) in Morex and TM194. c-d) Auxin root bending sensitivity assay. Quantification of root bending response in Morex and TM194 at 0.5, 3, 9,12 and 24 hours after a 90° gravistimulus during a, exogenous application of 10nM 1-Naphthaleneacetic acid (NAA) and b, 1µM auxin transport inhibitor 1-N-Napthylphthalamic acid (NPA). The final 12 hours were performed in light so gravitropic and phototropic effect were considered during this timepoints. * represents statistically significant difference, between treated and mock samples from respective genotype, assessed using Welch's *T*-Test at $p<0.05$ in n=3-6 independent replicates.

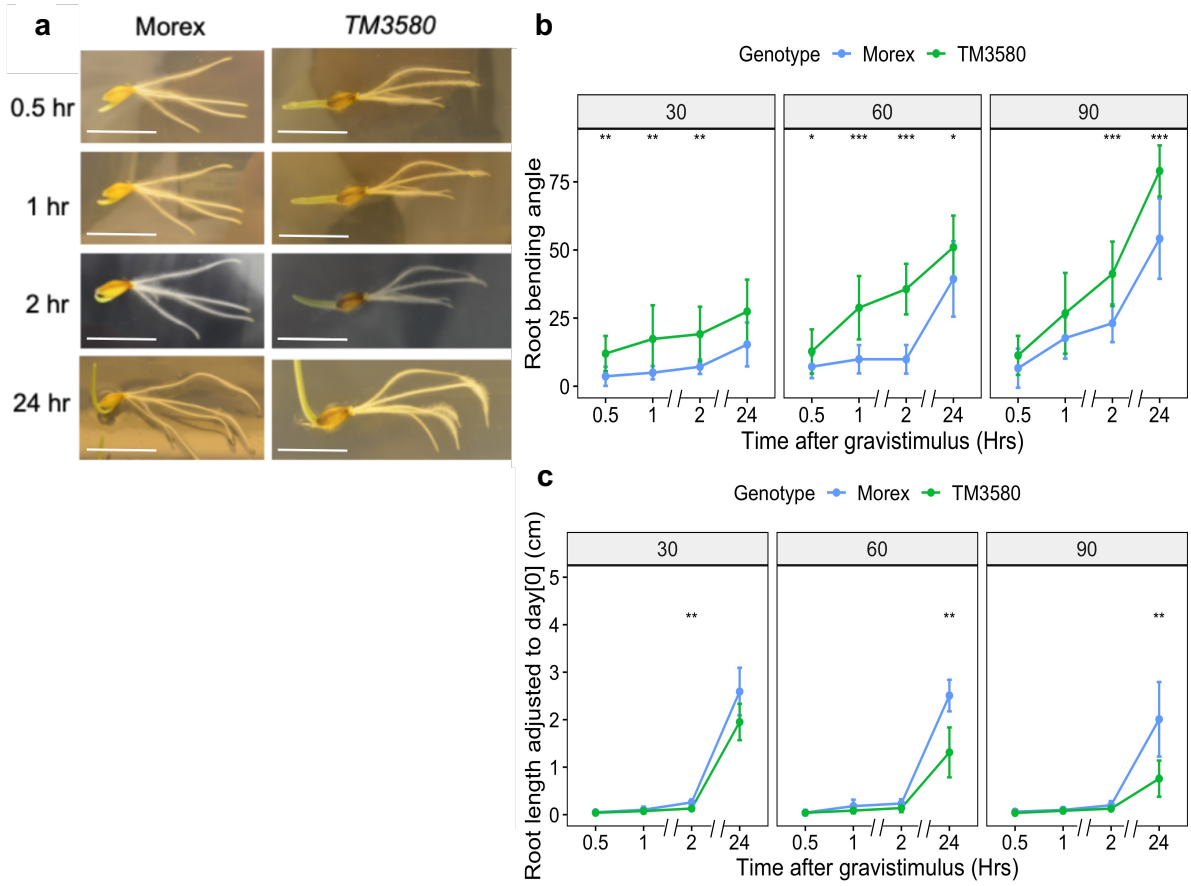


Fig. 3.9. Root bending response assay revealed also TM3580 to respond faster to gravitropic stimulus.

a) Representative images of root bending response of 4-day old seminal roots in Morex and TM3580 at 0.5, 1, 2 and 24 hours after 90° tilting gravistimulus. Scale bar = 2cm b) Measurement of dynamic change in root tip bending angle with increasing titling angle gravistimulations (from 30° to 60° to 90°) in Morex and TM3580. c) Root length measurements of the growth increment adjusted to day [0] for each timepoint considered (0, 0.5,1,2 and 24 hours). The final 12 hours were performed in light so gravitropic and phototropic effect were considered during this timepoints. * represents statistically significant difference, between treated and mock samples from respective genotype, assessed using Welch's T-Test at $p<0.05$ in n=3-6 independent replicates.

HvEGT1 appears to function in an auxin-independent AGO mechanism

Auxin transport and response has been reported to play a role in both gravitropic and AGO mechanisms (Friml *et al.*, 2002; Swarup *et al.*, 2005; Band *et al.*, 2012; Rosquete *et al.*, 2013; Roychoudhry *et al.*, 2013), as exogenous application of auxin transport inhibitor or auxin

influences vertical as well as non-vertical GSA. We tested whether the *Hvegt1* mutant phenotype was influenced by exogenous auxin and auxin inhibitor treatment. NPA treatment significantly reduced root growth angle in both wildtype and *Hvegt1* while NAA treatment did not show any significant change. Similarly, root bending response at 0.5, 3, 9, 12 and 24 hours after a 90° gravistimulus during NPA treatment significantly reduced root bending velocity to similar degrees in both mutant and wildtype, while no significant change was observed for NAA and 2,4D treatment (Fig. 3.9c-d, S.Fig. 3.2). This indicated that auxin-mediated gravitropic and AGO mechanisms remain intact in *Hvegt1*. Consistently, our root RNAseq dataset did not show any overrepresentation of auxin signalling genes in either *Hvegt1* mutants compared to wildtype (Fig. 3.10a). Taken together, our bioassays and RNAseq results suggest that *HvEGT1* functions as part of an auxin independent AGO mechanism.

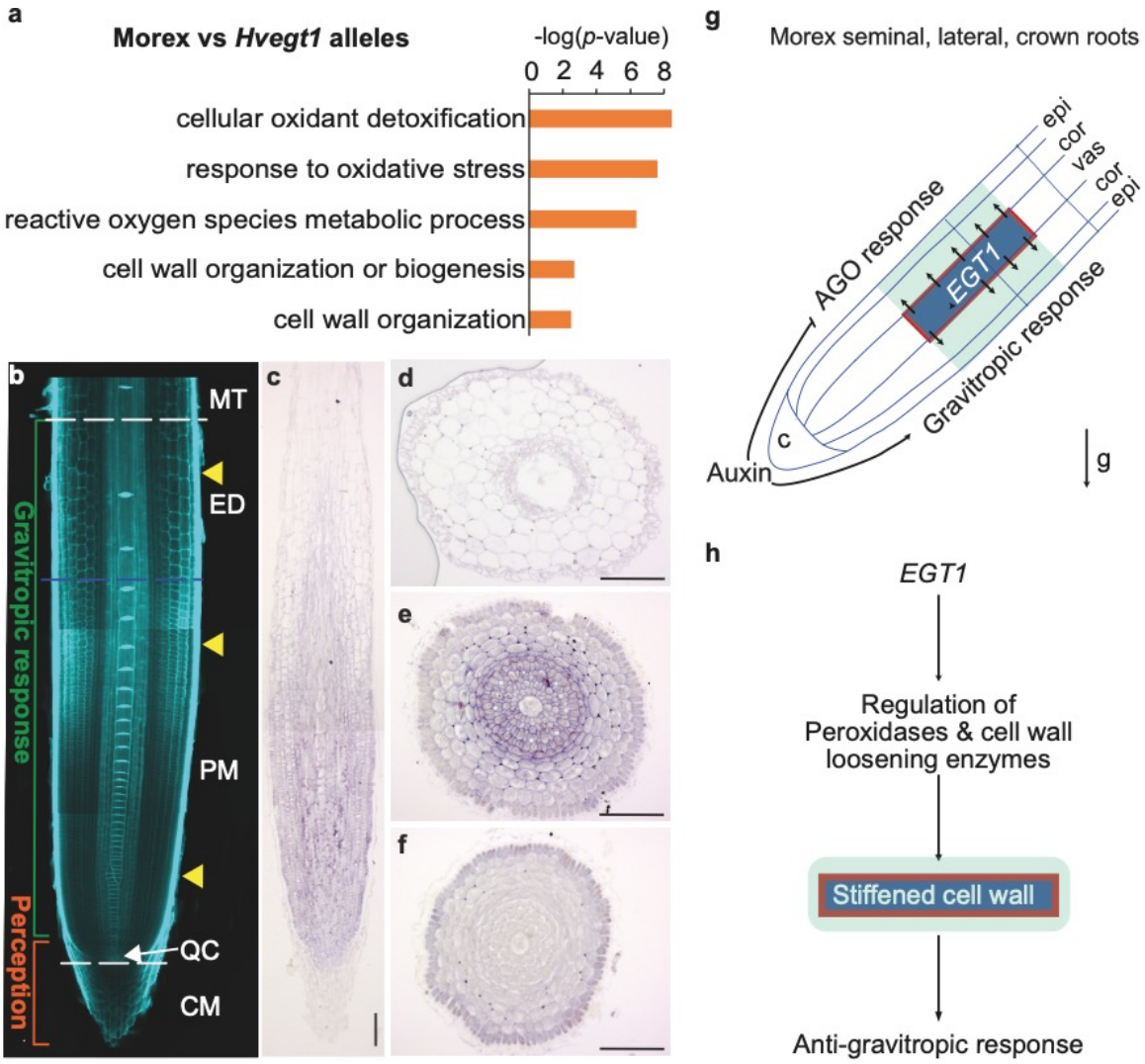


Fig. 3.10. HvEGT1 transcriptionally regulates peroxidases and cell wall loosening enzymes and it is specifically expressed in root vasculature tissues.

a) Pruned version of GO enrichment of genes differentially expressed between Morex and both *hvegt1* mutant alleles (-1.5<FC>1.5; Benjamini Hochberg FDR corrected Pvalue < 0.05; FPKM>=1). gProfiler(61) web server was used to perform GO enrichment analysis (settings: Statistical domain space = All known genes; significance threshold = g:SCS, 0.05) (SI Dataset 3). GO enrichments were pre-filtered using REVIGO(62) (http://revigo.irb.hr, default settings) to remove semantically redundant GO terms. Terms were pruned on REVIGO frequency (>0.25% and <2.5%) and top 5 most significant GO categories visualized. b) Schematic of gravitropic sensing and responding machinery in relation to root meristematic zones in barley cv. *Morex*: Maturation zone (MT), Elongation-Division zone (ED), Proximal Meristem (PM), Quiescent Center (QC), Columella (CM), blue line identifies the transition zone, yellow arrows highlight the approximate region where the cross sections were taken (d,e,f) (scale bar=100µm). c, *In Situ* Hybridisation (ISH) on longitudinal section of root tips of cv. Morex with *HvEgt1* anti-sense probe. (d-f) ISH of root tip cross-sections in cv. Morex with *HvEgt1* anti-sense probe in ED (d), higher PM (e) and lower PM (f) (scale bar=100µm). Reference sense probes images showed no signal (S.Fig 3.4). (g-h) Schematic of the proposed model. Auxin-dependent gravitropic and AGO responses are known to function in outer tissues (epidermis, epi; cortex; cor), whereas auxin-independent AGO component *EGT1* functions in inner root tissues (vasculature, vas) temporally in basal meristem and transition zone. We propose that EGT1 transcriptionally regulates peroxidases and cell wall loosening machinery in inner root tissues to counter gravitropic response to determine the gravitropic set point angle.

***HvEGT1* transcriptionally regulates ROS homeostasis and cell wall modifying enzymes**

To determine why *Hvegt1* roots may bend more rapidly than wildtype, we analysed their root transcript profiles to reveal which classes of genes were differentially expressed. In total, 6079 genes were identified to be differentially expressed (Benjamini-Hochberg FDR corrected p-value < 0.05, -1.5<FC>1.5 and FPKM > 1) between comparisons of TM194 *vs* Morex, TM3580 *vs* Morex and TM194 *vs* TM3580 (SI Dataset 2). We focused on the 988 differentially expressed genes in both *Hvegt1* mutant alleles compared to Morex. GO enrichment identified overrepresentation for mainly hydrogen-peroxide and cell wall related biological processes (Fig. 3.10a, SI Dataset 3). Interestingly, hydrogen peroxide catabolic and metabolic processes were explicitly enriched by 24 cell wall peroxidases (SI Dataset 4). As peroxidases produce

ROS as well as oxidise cell wall aromatic compounds within phenolics and polysaccharides (cellulose, hemicellulose e.g., xyloglucans and pectins), they are associated with cell wall loosening and stiffening processes (Francoz *et al.*, 2015; Raggi *et al.*, 2015) Consistently, we observed that cell wall organisation and biogenesis, xyloglucan metabolic and biosynthetic processes were enriched by 27 genes encoding cell wall-modifying enzymes, expansins, glucosyltransferases, pectin-lyase like superfamily proteins, pectin methylesterase inhibitors, fasciclin-like arabinogalactan proteins and xyloglucan hydrolases (SI Dataset 4). Many of these genes have been previously implicated in the modification or hydrolysis of cell wall components during growth and development (Burton *et al.*, 2010; Tucker *et al.*, 2018) Our co-expression analysis with published barley RNAseq data (Mayer *et al.*, 2012) further indicated that several cell wall gene modules responded to loss of *EGT1* (Fig. 3.11). The spatio-temporal expression enrichment of orthologs of these peroxidases and cell wall in rice roots (Takehisa *et al.*, 2012; Sato *et al.*, 2013) revealed that majority of them are mostly expressed in vascular tissues of proximal meristem and elongation zones (Fig. 3.12).

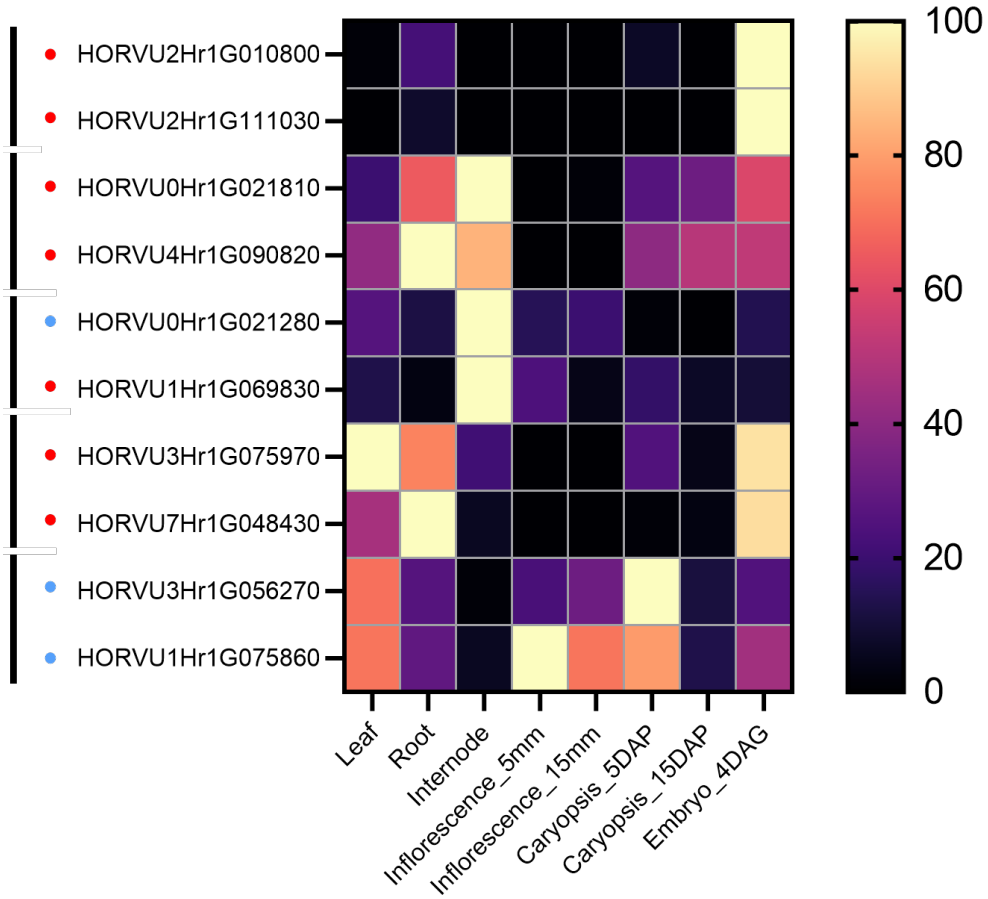


Fig. 3.11. Cell wall gene expression clusters that likely to respond to loss of HvEGT1 expression.

Heat map shows relative transcript abundance of cell wall related genes differentially expressed in *Hvegt1* mutant alleles, in a previously published barley RNAseq dataset (Mayer *et al.*, 2012). Expression values (RPKM) were transformed to proportions of the maximum expression value observed for each gene. Red dots indicate the genes are down-regulated in *Hvegt1* mutant alleles; blue indicates up-regulation. Bars indicate different modules. The changes in expression suggest a complex deregulation of the cell wall machinery in the root of *Hvegt1* mutant alleles. For instance, *HORVU2Hr1G010800* (EXP) and *HORVU2Hr1G111030* (XET) are co-expressed in the root and germinated embryo, and both are downregulated in Hv*egt1*. Another module includes *HORVU3Hr1G056270* (PL) and *HORVU1Hr1G075860* (PME), two putative modifiers of pectin composition that are co-expressed in multiple barley tissues and are similarly upregulated in *Hvegt1* mutants.

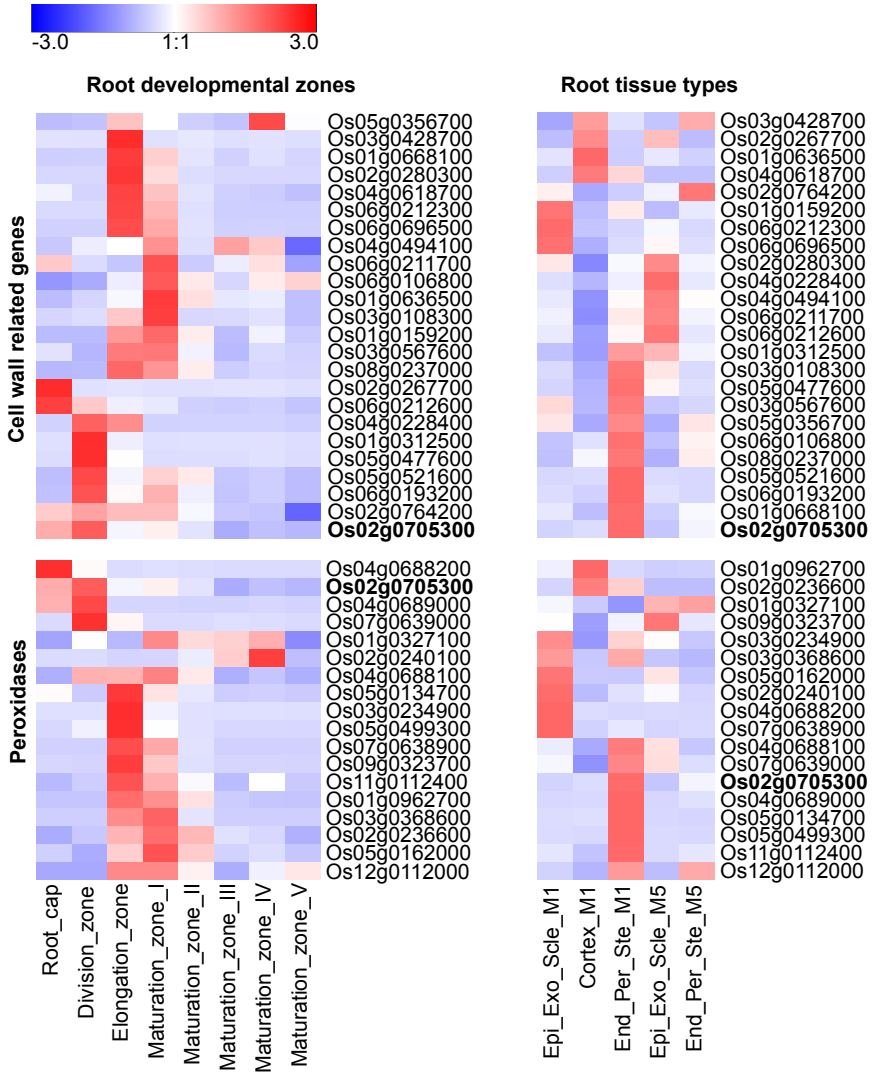


Fig. 3.12. Spatiotemporal expression of selected cell-wall and peroxidases related genes in rice roots.

Heat map shows relative abundance of cell-wall and peroxidases related genes, in rice root developmental stages and tissue types (Takehisa *et al.*, 2012), orthologous to genes that are differentially expressed between Morex and *Hvegt1* alleles. Plaza 4.5 (Van Bel *et al.*, 2018) monocot comparative genomics database was first used to identify best hit family orthologs. Next, Rice Xpro 3.0 (Sato *et al.*, 2013) was used to extract mean raw Cy3 signal intensities for non-overlapping orthologs from RXP_4001 transcriptome experiment. Z-score data was used to generate heatmaps and average linkage WPGMA agglomeration rule was used to create Hierarchical clustering of genes (clustering tree was trimmed to accommodate all images into this figure). Epi.Exo.Scle. = Epidermis/Exodermis/Sclerenchyma; End.Per.Ste. = Endodermis/Pericycle/Stele, M1 = Maturation zone_I, 1-3mm from root tip; M5= Maturation zone_V, 10-20mm from basal side. Gene id in bold indicates rice ortholog of *HvEGT1*.

***HvEGT1* is highly expressed in root stele tissues distinct from gravitropic responsive tissues**

To determine the site of action of *HvEGT1*, we elucidated its spatial expression in root tissues using RNA In-Situ Hybridisation (ISH) (Zeng *et al.*, 2017). A *HvEGT1* specific, non-conserved region (compared to other barley Tubby genes) spanning the end of CDS and the start of 3' UTR was used to design and synthesise digoxigenin-labelled antisense and sense probes (S.Fig. 3.3). *In situ* hybridised longitudinal and radial root sections revealed the *HvEGT1* transcript is most highly abundant in cells in the basal meristem and transition zones (Fig. 3.10b-c, S.Fig. 3.4). The level of *HvEGT1* expression then decreased until it became undetectable in maturation zone cells. The hybridized cross sections revealed highest *HvEGT1* transcript levels in central (vascular) tissues in the proximal meristem and elongation zones. In contrast, sections through the apical meristem showed only a weak signal (Fig. 3.10d-f). Hence, *HvEGT1* expression is primarily associated with inner root tissues as cells start to elongate, consistent with the known spatio-temporal expression of the classes of genes identified to be differentially regulated in our *Hvegt1 vs* wildtype RNAseq analysis (Fig. 3.12).

Discussion

Barley is one of the most important cereal crops worldwide and is commonly used as a genetic model for cereals. Although recent studies have identified major QTLs associated with seminal root angle by genome wide association studies based on phenotyping of different barley genomic populations (Robinson *et al.*, 2016; Jia *et al.*, 2019) knowledge about the underlying genes controlling root angle in barley remains limited. A limited number of root angle regulatory genes have been identified in other cereals including *DRO1* (Uga *et al.*, 2013), *VLN2* (Wu *et al.*, 2015), *PIN2* (Wang *et al.*, 2018) and *RMD* (Huang *et al.*, 2018). To address this knowledge gap, we characterised a chemically mutagenized population of the cv. Morex (Talamè *et al.*, 2008) for a steeper seminal root phenotype, where we identified the TM194 mutant which exhibited steeper growth angle not only for seminal roots but also for lateral and crown roots. Genetic and genomic approaches revealed that a mutation in the *EGT1* (*ENHANCED GRAVTROPISM 1*) gene is responsible for the steeper root angle phenotype.

HvEGT1 encodes Tubby-like protein (TLP) and likewise other plant TLPs, it contains conserved C-terminal tubby and N-terminal F-box domains (Gagne *et al.*, 2002; Lai *et al.*, 2004). Tubby domain containing proteins have been suggested to act as a bipartite transcription regulator (Boggon *et al.*, 1999; Santagata *et al.*, 2001), whereas F-box proteins are shown to be involved in protein ubiquitination by acting as bridges between specific substrates and the components of the SCF-type (Skp1-Cullin-F-box) or ECS-type (ElonginC-Cullin-SOCS-box) E3 ubiquitin ligase complexes (Gagne *et al.*, 2002; Kile *et al.*, 2002) Previous mutant studies in *Arabidopsis thaliana* have identified that Tubby like proteins AtTLP3 and AtTLP2 could play roles in regulation of ROS signalling and of cell wall related genes, respectively (Reitz *et al.*, 2012; Wang *et al.*, 2019*a*). Concurrently, our transcriptome analysis identified that ROS homeostasis and cell wall modifying enzymes are deregulated in mutants compare to wildtypes, suggesting that some of these genes may represent either direct transcriptional or post-translational downstream targets of *HvEGT1*.

Simultaneously, another recent barley TILLING mutant study (Kirschner et al, 2021) demonstrated that mutation in *ENHANCED GRAVITROPISM 2* (EGT2) encoding a STERILE ALPHA MOTIVE containing protein also deregulates cell wall related genes and causes steeper

root growth angle phenotype in barley and wheat. Although both *EGT1* and *EGT2* appear to function in auxin independent AGO mechanisms, each are expressed in distinct tissue types and target different sets of cell wall genes. Additionally, no change in *EGT1* expression was observed in the H*vegt2 mutant* and vice-versa. These observations suggest that these genes function in parallel AGO pathways to control root angle in barley and wheat.

EGT1 appears to play an important role in determining root angle in barley and other cereal crops. Our haplotype analysis revealed that nucleotide polymorphisms within the *HvEGT1* sequence determines natural variation in root growth angle in a barley diversity panel and could underpin a link between *HvEGT1* variation and adaptation of cultivars to specific environmental conditions such as different soil types or variable water table depth. Furthermore, characterization of a mutant line disrupting the orthologous *TdEGT1* genes in durum wheat revealed an identical steeper root angle phenotype. A recent genome wide association study in durum wheat also identified two F-box domain containing proteins on the same chromosome A (Alahmad *et al.*, 2019) suggesting that such F-box proteins (followed by Tubby or other protein-protein interacting domains for recruiting specific targets) could play a major route for controlling root angle in cereals. Further investigation in this direction might open novel avenues to develop crop varieties with optimal root system architecture for efficient resource capture.

How does EGT1 control root angle? *HvEGT1* spatial expression is distinct from known gravitropic perception and response tissues in root columella and epidermis, respectively (Swarup *et al.*, 2005; Band *et al.*, 2012). Instead, we propose that EGT1 controls root angle by regulating cell wall stiffness in expanding inner root tissues (Fig. 3.12g-h), counteracting the gravitropic machinery's known ability to bend roots via the outermost tissues. However, in the absence of EGT1 (based on expression profiling; Fig 3.9a) we reason that cell walls of inner root tissues are less rigid, enabling the gravitropic machinery to bend the *Hvegt1* root much more rapidly. Hence, auxin-dependent bending versus EGT1 dependent stiffening mechanisms operate in spatially distinct sets of outer and inner root tissues, respectively. Such a two-zone mechanical model for regulating root gravitropic bending rate also provides a simple mechanism to explain gravitropic set point angle, where the relative strength of the

gravitropic and anti-gravitropic pathways operating in outer and inner tissues will determine a root set point angle.

Chapter 4

The auxin efflux carrier PIN1a regulates vascular patterning in cereal roots

Introduction

Barley is the fourth most important cereal crop in the world after wheat, maize and rice (Faostat 2018; http://www.fao.org/faostat). It is increasingly utilised in genetic studies due to its diploid nature, low chromosome number, ease of cross breeding and cultivation in different climatic conditions. In recent years, considerable progress has been made in generating novel genetic resources in barley, including high quality genome, genome-wide gene knockout collections for reverse genetics, marker rich genetic diversity panels and synthetic recombinant populations for association genetics (Nice *et al.*, 2016; Mascher *et al.*, 2017; Schreiber *et al.*, 2019). To effectively utilise these resources in crop genetic improvement or breeding approaches, it is necessary to efficiently link genes to important agronomic traits. For instance, root traits play critical role in water and nutrient uptake from the soil. Thus, pinpointing genes underlying root functions would enable the development of crop varieties with improved root system traits. Although a few barley root hair and cytokinin related mutants have been characterized (Gahoonia *et al.*, 2001; Chmielewska *et al.*, 2014; Gasparis *et al.*, 2019), many genes that regulate root traits such as length, angle and density remain to be identified.

The plant hormone auxin plays a crucial role in plant morphogenesis, including root growth and development (Benková and Hejátko, 2009). Auxin is unique amongst plant hormones in having a specialised transport system that mobilises this signal in a polarised manner between cells and tissues (Bennett *et al.*, 1996*b*; Wisniewska, 2006; Swarup and Péret, 2012). AUX1/LAX auxin influx carriers transport auxin into plant cells, while PIN and ABCB classes of auxin efflux carriers pump this hormone out of plant cells. The PIN class of auxin efflux carriers are often asymmetrically localized in plant cells plasma membranes, which contributes to the polarised movement of auxin and formation of hormone gradients that regulate plant growth, positioning of organs and patterning of tissues (Petrášek *et al.*, 2006; Wisniewska, 2006; Adamowski and Friml, 2015). In plant model *Arabidopsis thaliana*, PIN1 is a major auxin transporter with roles described in leaf initiation, leaf margin definition, shoot vascular patterning and embryo development (Leyser, 1999; Benková *et al.*, 2003; Reinhardt *et al.*, 2003; Hay *et al.*, 2006; Scarpella *et al.*, 2006; Bilsborough *et al.*, 2011; Xi *et al.*, 2016). Recent

research has revealed functional diversity in PIN1 and related genes in grasses compared to Arabidopsis and Brassicaceae. *Brachypodium distachyon*
has two duplicate PIN1 clade members PIN1a and PIN1b and a phylogenetic sister to the PIN1 clade SoPIN1, which collectively recapitulate expression domains and polarization behaviours observed for AtPIN1 alone in Arabidopsis in the shoot (Billou *et al.*, 2005; O'Connor *et al.*, 2014, 2017). Similarly, barley has PIN1a, PIN1b and SoPIN1 genes clades mirroring *Brachypodium distachyon* (Fig. 4.1).

During shoot development in Arabidopsis, PIN1 is expressed in the epidermis and vasculature (Guenot *et al.*, 2012). During spikelet development in *Brachypodium distachyon*, SoPIN1 is expressed in the epidermis, PIN1a in inner vasculature and PIN1b in parenchymatic tissues between epidermis and vasculature indicates a potential role in supporting vasculature formation in the new developing organ (O'Connor *et al.*, 2014). In Arabidopsis roots, PIN1 protein is asymmetrically localised rootwards in central stele and cortical cells, whereas it is localised shootwards in epidermal cells (Billou *et al.*, 2005). This pattern of localisation, when combined with other PIN family members (PIN2,3,4, and 7), plays a crucial role maintaining the rootward/shootward auxin polarity which sustain the regular cell division and organ patterning in roots (Gälweiler *et al.*, 1998; Reinhardt *et al.*, 2003; Billou *et al.*, 2005; Zhang *et al.*, 2019). Similarly to Arabidopsis PIN1, HvPIN1a was revealed to be localised in barley root meristem cells in a rootward direction towards the QC in the inner tissues and shootwards in outer cortex-epidermis-lateral root cap cells, suggesting a similar pattern of auxin fluxes in this specie (Kirschner *et al.*, 2017). However, the roles of the individual cereal PIN1 clade members during root growth and development remains unclear.

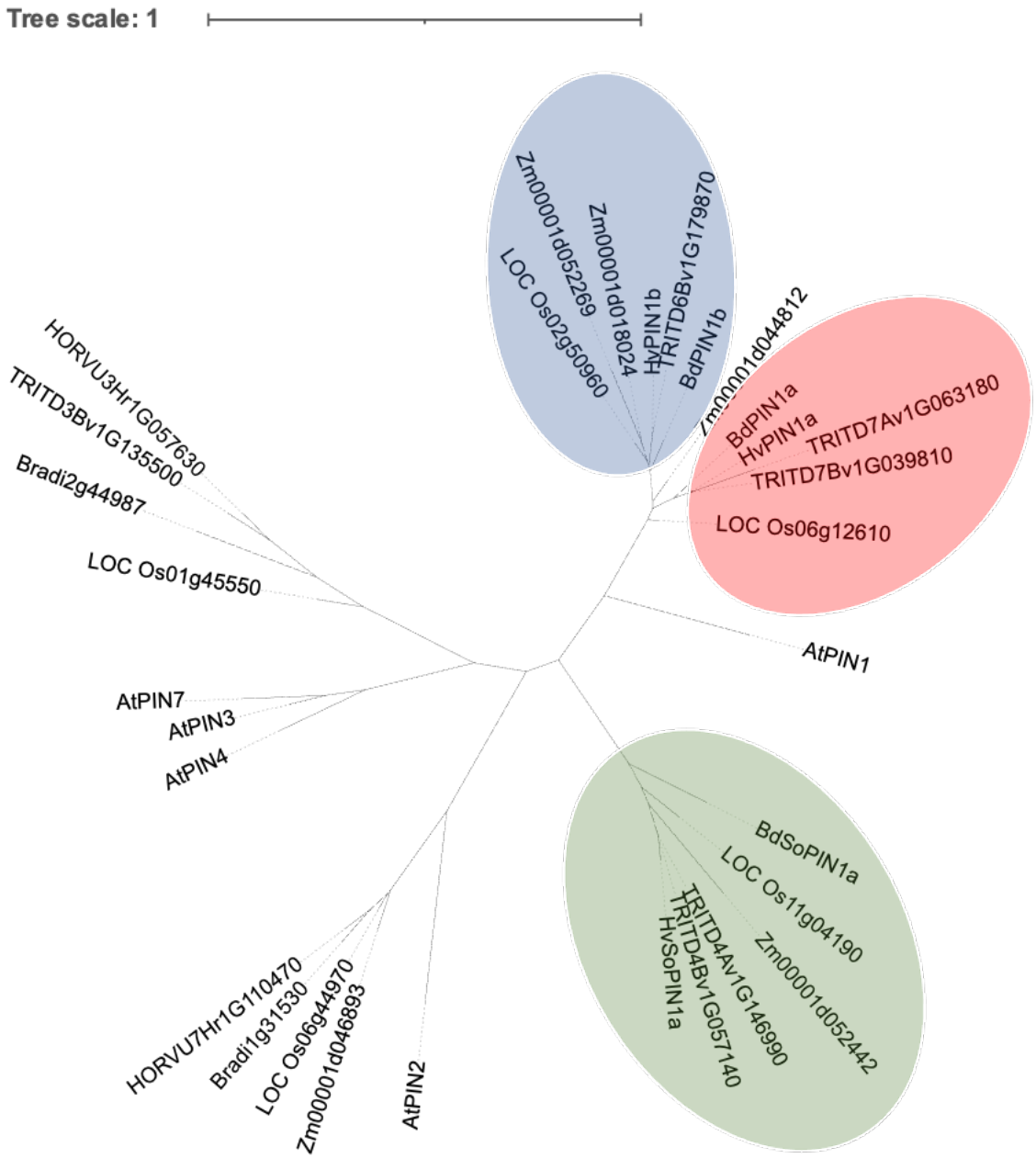


Fig. 4.1. Phylogenetic analysis of PIN Protein sequences in Arabidopsis barley, wheat, rice, maize and *Brachypodium distachyon*.

AtPIN1 was used as a seed gene to select orthologous genes (>50% identity) from plant model Arabidopsis thaliana and key monocot species such as barley (*Hordeum Vulgare*), wheat (*Triticum turgidum*), rice (*Oryza Sativa spp. Japonica*), maize (*Zea Mays B73*) and *Brachypodium distachyon* using interactive phylogenetic module of Monocots Plaza 4.5. Protein sequences were aligned using MUSCLE and tree was constructed using FastTree algorithm. Generated Newick file was imported into iTOL to create an unrooted tree. Red,

blue and green color highlights the distinct clade formed by Pin1a, Pin1b and SoPIN1a members orthologous to AtPIN1. Tree scale = 1 indicates 100% of aminoacidic substitution occurred between two aminoacidic sequences. Confidence between clades was calculated using bootstrap method (>100 interactions)

This Chapter describes the phenotypic and molecular characterisation of a barley root mutant (termed TM5992) from a chemically mutagenized population of barley cv. Morex (termed the TILLMore collection) which exhibited a short root phenotype. SNP array-based bulk-segregant analysis (BSA) of TM5992 outcrossed to barley cultivar cv Proctor mapped the mutation conferring the short root phenotype onto chromosome 7 between 38.8 - 68.4 cM. Subsequent exome and WGS sequencing analyses identified mutations in coding sequences of three genes *HORVU7Hr1G029650* (SEUSS transcriptional corepressor), *HORVU7Hr1G038520* (Nuclear Migration protein) and *HORVU7Hr1G038700* (Auxin efflux carrier family protein, *HvPin1a*) within the cM-range interval. Further genetic characterisation of two independent mutant alleles in cv. Morex and cv. Barke cultivars validated that a mutation in *HvPIN1a* caused the short root phenotype. Imaging root anatomy in *hvpin1a* mutant alleles revealed irregularities in root vascular tissues, which could be mimicked in wild type roots by blocking PIN mediated polar auxin transport using the inhibitor NPA. Further, expression domain and root growth analysis of reporters and mutants of PIN1 members in the cereal model *Brachypodium distachyon* revealed BdPIN1a and BdPIN1b act redundantly during root vascular patterning with BdPIN1a functioning as a central regulator. We conclude by discussing the functional diversity of PIN1 in cereals and conserved role of PIN1a controlling root vascular patterning.

Material and methods

Plant material

Barley *HvPIN1a* mutant alleles (TM5992, TM5141 in cultivar cv. Morex and TB13081 in cultivar cv. Barke background), *Brachypodium distachyon BdPIN1* member mutants (*Bdpin1a* and *Bdpin1b* in Bd21.3 background) (O'Connor *et al.*, 2017) and respective wild-types (Morex, Barke and TB_WT and Bd21.3, respectively) were used for root length and cross-section

imaging analyses. All barley Hvpin1a mutant alleles and their respective wild-type lines were used for root tip staining and confocal imaging. Morex and Bd21.3 were used in NPA treatment assay.

Growth conditions

For all root growth and cross-section phenotyping analyses of barley, seeds were surface sterilized with 0.5% Sodium hypochlorite solution for 5mins followed by five washes with sterile water. Sterilized seeds were germinated on sterile Whatman filter paper placed in a petri dish for 1 day at 21°C in dark. Germinated seedlings were transferred to 1% Agar plates at pH 5.7 in growth room (21°C, 16/8 daylight cycle; 125-150 µmol m^{-2} s^{-1}) and grown vertically for 3-5 days. *Brachypodium distachyon* seeds were surface sterilised using the same method above and then grown in ½ MS, 1% Agar plates at pH 5.7 at the same environmental conditions as above for 7 days.

Identification of barley short root mutant lines TM5992, TM5141 and TB13081

Barley short-root mutants (TM5992 and TM5141) were identified as described in Bovina et al (under preparation) (Bovina *et al.*, 2020). Briefly a chemically (NaN3) mutagenized population (TILLMore population) (Talamè *et al.*, 2008) of approximately 4,000 M6 lines in Morex cv. background was screened for root traits at the seedling (2-week old) stage. TM5992 and TM5141 both showed a short-root phenotype when grown using semi-hydroponics method adapted from (Talamè *et al.*, 2008), when compared to Morex wildtype (Bovina *et al.*, 2020). From the same mutagenized population, a second short-root mutant line (TM5141) was identified. A third HvPIN1a mutant allele (TB13081) was further identified by TILLING (McCallum *et al.*, 2000) by screening an EMS (Ethyl methane sulfonate) treated population of cv. Barke consisting of 10,279 individuals, for which a multidimensional pool of individual DNA samples is available (Gottwald *et al.*, 2009). All mutations found using a capillary electrophoresis system were further validated by re-sequencing using Sanger sequencing and primers listed in Supplementary Table 2. TB13081 was initially identified as heterozygous segregating family. One heterozygous plant was selfed and homozygous progenies (both wild type or mutant) were identified by Sanger Sequencing and further selfed to produce seed for phenotypic evaluation.

Genetic mapping of short root mutant TM5992

For genetic mapping of short root mutant TM5992, seeds were immersed in a 0.5% (v/v) sodium hypochlorite solution for 5 minutes, rinsed with demineralized water and incubated in the dark at 28°C for 24 hours. Germinated seeds were placed between two sheets of 50 x 25 cm of filter paper (Carta filtro Labor, Gruppo Cordenons SpA, Milan, Italy) soaked in demineralized water, rolled, positioned vertically in a 5-litres plastic beaker with 1 litre of demineralized water and grown for ten days at 24°C with a 16-hour photoperiod. Bulked Segregant Analysis (BSA) (Michelmore *et al.*, 1991) was carried out using 7 days old F2 plants derived from the cross TM5992 x Barke (a 2-row barley cv). For bulks preparation, 15 wild types (bulk +/+) and 15 short root (bulk -/-) individuals were chosen. DNA from a leaf of each selected plant was extracted with a commercial kit (Macheray-Nagel Nucleospin Plant II) and bulked together in equal amounts in two (+/+ and -/-) bulks, reaching a final concentration of 50 ng/ul. The two DNA bulks along with eight short-root single-plant DNA samples and eight wild-type single-plant DNA samples were genotyped using the 9k Illumina Infinium iSelect barley SNP array (Comadran *et al.*, 2012). SNPs signal was analysed with the GenomeStudio software (Illumina, San Diego, Inc.) calculating the delta theta score as the squared difference between the theta values (Hyten *et al.*, 2008) of the two bulks.

Exome capture and sequencing

DNA samples from TM5992 was subjected to exome capture (Mascher *et al.*, 2013*b*) and Next Generation Shotgun sequencing with Illumina HiSeq2000 PE100, at IPK, Gatersleben, Germany. Mutation mapping was carried out following a consolidated pipeline (Mascher *et al.*, 2014). Reads were aligned to the reference genome sequence of barley cultivar Morex (Mascher *et al.*, 2017) by means of the BWA-MEM algorithm v.0.7.4 (Li and Durbin, 2009). Sorting was performed with Novosort (Novocraft Technologies SDN BHD) and read mapping statistics were obtained with Samtools (Li *et al.*, 2009; Li, 2011). Only reads uniquely mapped to the reference sequence were kept for downstream analysis. Variant calling was performed via Samtools mpileup, considering as filtering criteria a minimum call quality of Phred score >=40 and a minimum coverage of 10x. At each variant position, mutant allele frequencies were calculated as the number of reads supporting the mutant allele on the total number of reads (DV/DP in the Variant Call Format file), with a custom AWK script (Mascher *et al.*, 2014). A variant was considered private to a certain mutant when it showed a mutant allele

frequency not lower than 0.9. In order to remove Morex intra-cultivar standing variation, we called the mutant-identified SNPs in a barley diversity panel (267 accessions, (Russell *et al.*, 2016) and focused on the panel target region (i.e. regions showing a minimum coverage of 10x in 95% of the accessions). We further considered only variants showing a maximum mutant allele frequency of 0.1 across the panel samples. To focus on the region previously targeted by the SNP array based BSA described above, the resulting SNP dataset was merged to the POPSEQ map (Mascher *et al.*, 2013*a*) to retrieve the POPSEQ positions of the sequenced BACs. Called mutations were intersected with the annotation of the barley cv Morex reference (Mascher *et al.*, 2017) and SNP effects were predicted with SNPEff (Cingolani *et al.*, 2012).

Non-destructive X-Ray microCT root phenotyping of barley PIN1a mutants

Morex and pin1a mutant alleles harboring lines TM5141 and TM5992 (n=6 independent replicates) were pre-germinated in petri dishes for 1 day at 21°C in dark. Equally germinated seedlings (seed lengths were compared visually to assess equal germination) were transferred to PVC columns (8cm diameter, 15 cm height) filled with well water sandy-loam soil and grown until 9 DAG. Each column was scanned using a Phoenix v|tome|x M ® CT scanner (GE Measurement & Control Solutions, Wunstorf, Germany) at the Hounsfield Facility (University of Nottingham, Sutton Bonington Campus, UK.), using a voltage and current of 180 kV and 180 µA respectively also at a voxel size resolution of 55 µm, with the specimen stage rotating through 360 degrees at a rotation step increment of 0.166 degrees over a period of approximately 75 minutes, so a total of 2160 projection images were obtained by averaging 4 frames with an exposure of 250 ms each, at every rotation step. A 0.1mm Copper filters was applied for the scans in front of the exit window of the X-ray tube. Scans were reconstructed into 16-bit grayscale 3D volumes using DatosRec software (GE Sensing and Inspection Technologies, Wunstorf, Germany). Reconstructed image stacks were segmented and root traits where quantified using RooTrak (Mairhofer *et al.*, 2012).

Barley root kinetics and root tip imaging

Root length data of Barley cv. Morex, TM-5992, TM-5141, Barke, TB_WT and TB13081 were tracked daily for 3-5 days to assess the root growth kinetics. Only roots touching the agar surface were considered for the analysis. From the same roots, root tip samples were

sectioned at 1.5 cm from the root mature zone (mid root region) and an adapted protocol from (Kurihara *et al.*, 2015; Ursache *et al.*, 2018) was used to prepare root tips for confocal imaging. Samples were fixed in PFA for 1.5 hours on vacuum and then were left on CLEARSEE solution for 7 days before the staining with Yellow direct 96 dye on vacuum for 1.5 hours. Cell counting from epidermal, cortical and central metaxylem tissues were performed using image stacks which have been imported in FIJI (ImageJ) and then aligned in order to have an on-focus image of the whole root apical meristem (RAM) which includes cells from columella to the first visible root hair.

Barley and *Brachypodium distachyon* PIN1a mutants root cross sectioning

An adapted protocol from (Atkinson and Wells, 2017) was used for root cross sectioning and confocal imaging. Root sections of approximately 1.5cm were taken from the root mature zone (mid root region) and fixed in 4.5% agarose blocks. Blocks where then sliced (Slice height = 100 μm, Frequency = 50 Hz, Amplitude = 1mm) and for barley, the samples were stained either using calcofluor white for 30”-1’ before confocal imaging or a combination of Calcofluor White (Sigma 18909-100ML-F) and Basic Fuchsin to stain lignin (Ursache *et al.*, 2018). For this latter method, the agarose slices obtained from the vibratome were then stained with a 50% mixture of Calcofluor White and Basic Fuchsin (0.2%) for 5 minutes, washed 2 times in ClearSee every 30 minutes and then left clearing for 2 days in a fresh ClearSee solution. Images were collected using confocal microscope Leica-SP5 by exciting root cross sections with UV laser at 405nm for calcofluor white and 543nm for basic Fuchsin. For *Brachypodium distachyon* cross sectioning, plants were dipped in water for 30 minutes-1hour before collecting the samples and fixing them in agarose blocks. This avoids to roots to get hyper oxidated which causes cell-wall to degrade and turn brown in colour, compromising the staining and the imaging. Samples were then stained as above using Calcofluor White for 30”-1’ and imaged using confocal microscope Leica SP5.

NPA treatment

Germinated seedlings were transferred to 1% agar plates supplemented with DMSO and DMSO with 100nM, 1μM, 10μM, 20 μM and 50μM NPA for barley and grown from 3 up to 11-days old seedlings. For *Brachypodium distachyon*, DMSO with 1μM NPA for *Brachypodium distachyon* was applied to ½ MS agar plates at the condition listed in the previous section.

Root growth images were taken and then sections of 1.5 cm were harvested from the mature root zone (mid root region) and cross sectioning were performed as described in the section above.

Results

A novel barley short root mutant exhibits defects in root cell number, size and patterning

Root mutant line *TM5992* identified in the barley TILLMore TILLING population exhibited a short root defect (Fig. 4.2a). The mutant line *TM5992* was phenotypically characterized using 2D and 3D root phenotyping methods. A growth pouch-based method (19) validated the short root defect and non-invasive imaging using X-ray microCT (20) demonstrated that the barley mutant line also exhibited a short root when grown in soil (Figure 4.2a-b, S.Fig. 4.1). To reveal the cellular basis of the *TM5992* root defect, growth rates of mutant versus Morex lines were initially monitored. Root growth analysis over the first 5 days after germination identified much slower growth for *TM5992* in the first two days compared to the accelerated growth behaviour observed in wildtype Morex. Over the next three days, the growth rate slowed in both genotypes relative to the first two days. Nevertheless, *TM5992* exhibited less than half the growth rate of Morex (Fig. 4.2c).

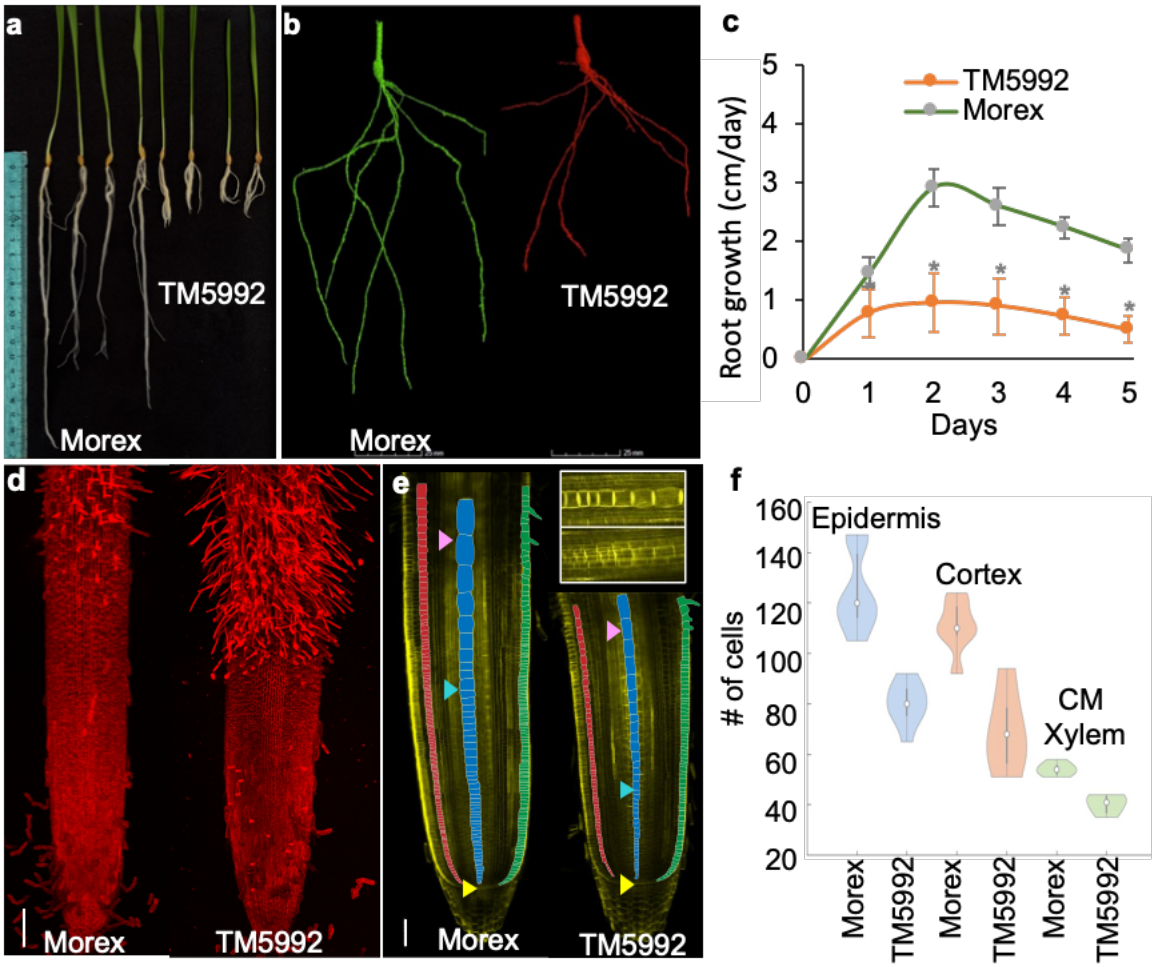


Fig. 4.2. Barley TILLING mutant line TM5992 shows short root phenotype with root growth and development defects.

Representative images showing root growth of TM5992 and Morex (wild-type) in (a) paper rolls for 9 days (b) sandy loam soil filled columns for 10 days, imaged using X-ray microCT, scale bar = 25mm. Data quantification in S.Fig. 4.1) Line graph showing root growth rate over 5 days post germination on 1% Agar plates. Mean and standard deviations from 3 biological replicates, >7 seedlings per replicate. *indicates significance (P-value < 0.01, *T-test*). d) Representative maximum projection confocal images of 7-day old root tips stained with PI showing differences in root hair differentiation zones and root hair density. Scale bar = 200µm. e) Representative confocal image of longitudinal sections of 7-day old root tips stained with Direct Yellow 96 stain showing difference in root growth zones and defects in vascular patterning. Scale bar = 100µm. Red, blue and green filled cells mark epidermis, cortex and central metaxylem (CM Xylem) tissues, respectively, which were used to quantify number of cells between quiescent centre (yellow arrow) and first visible root hair (purple arrow;

differentiation zone). Turquoise arrow marks the first elongating metaxylem cell (highlighting elongation zone). The white bordered inset box indicates the irregularities in the central metaxylem tissue (brighter stained cells) of TM5992 (bottom) compared to Morex (top). f) Violin plot showing distribution of number of cells in root epidermis, cortex and xylem tissues. >8 seedlings per genotype used.

Next, we investigated whether these root growth differences were due to altered sizes of apical meristem and/or elongation zones where cells divide and expand, respectively. Root zone measurements were performed by generating maximum surface projection images of 7-day old root tips stained with propidium Iodide then imaged using a confocal microscope. This approach revealed TM5992 roots had shorter apical meristem and elongation zones compared to wild type, causing the root hair differentiation zone in the mutant to appear closer to the root apex (Figure 4.2d).

To determine whether cells in root tissues exhibit size and number defects, 7-day old root tips were cleared using ClearSee and stained with yellow direct 96 (Fig. 4.2e). Barley root cell numbers and lengths in cortical, epidermal and central metaxylem tissues were visualized and measured from the stem cell initials at the root tip to the first differentiated root hair (Fig. 2f). This revealed that the number and length of cells in the meristem and elongation growth zones were strikingly different in TM5992 compared to Morex. We also noted an increased root hair density and vascular patterning irregularities in the mutant line compared to Morex (Fig. 2e). These analyses suggested that TM5992 exhibited several root anatomical developmental defects. In contrast, no growth defects were detected in mutant shoot tissues. Taken together, our results indicated that the short root phenotype of TM5992 is due to a slower root growth rate and developmental defects.

The short root phenotype is caused by a recessive mutation in the *HvPIN1a* gene

To pinpoint the underlying genetic basis of the short root phenotype in TM5992, we tested its inheritance by crossing TM5992 with the 2-row barley cv Proctor. F_1 plants exhibited a wild type phenotype, whereas evaluation of 91 F_2 plants for root length revealed segregation for either short or wild-type roots (example given in Fig. 3a). Numbers and rate of phenotypic classes fitted a Mendelian pattern (72:19 wild-type:short root plants, P = n.s. χ^2 test 3:1).

These results revealed that the root phenotype segregating in the cross TM5992 × Proctor was controlled by a single locus, with a wild dominant allele from cv Proctor and a mutated recessive allele from TM5992.

A SNP-based bulk segregant analysis (BSA) was performed to genetically map TM5992 using the F_2 population. BSA results indicated that the mutated locus mapped on chromosome 7 (Fig. 3b), in a large pericentromeric region spanning c. 200 Mb between markers *SCRI_RS_150016* and *BOPA1_4850-969* (38.8 - 68.4 cM based on the barley POPSEQ reference map)(Beier *et al.*, 2017). In order to pinpoint the mutation, we performed exome sequencing of TM5992 and mapped reads on the Morex reference genome. A total 27 missense variants were revealed to be in the coding sequences genome-wide. All mutations were G>A transitions, as expected based on NaN_3 chemical treatment (Talamè *et al.*, 2008). However, within the chromosome 7 region highlighted by BSA only three coding genes were found to carry mutations in TM5992 compared to Morex. These genes were *HORVU7Hr1G029650* at 47.78 cM, annotated as SEUSS transcriptional co-repressor, *HORVU7Hr1G038520* at 64.36, annotated as Nuclear Migration protein and *HORVU7Hr1G038700* at 64.75 cM, annotated as auxin efflux carrier family protein (*HvPin1a*).

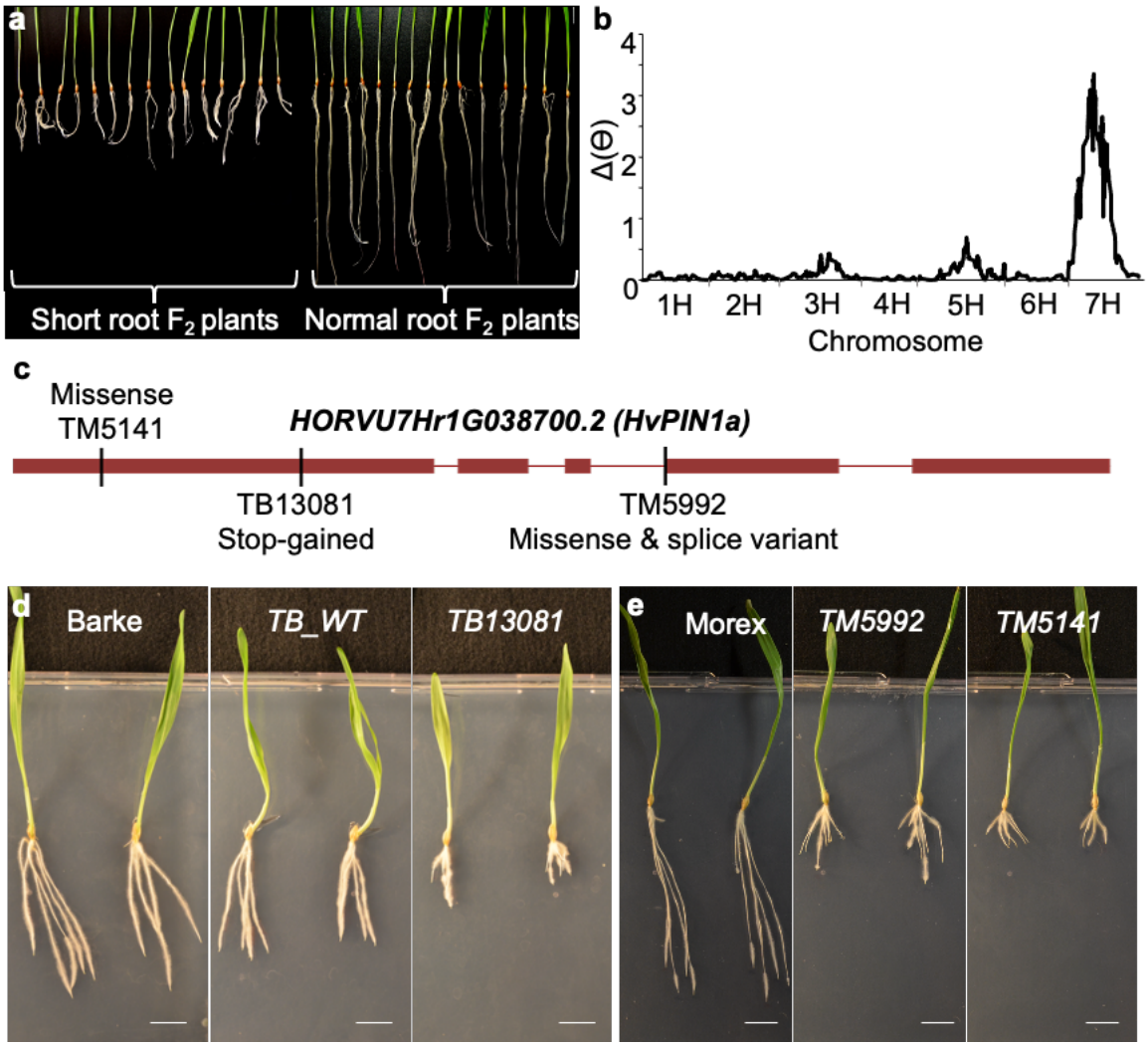


Fig. 4.3. Mutation in HvPIN1a causes short root phenotype and developmental defects.

a) F2 plants from the cross TM5992 x barley cultivar Proctor utilized in bulked DNA samples for SNP-based bulk-segregant-analysis (BSA). b) Genome-wide plot of unbalanced allelic frequency from SNP-based BSA. ΔTheta parameter represents the difference in allele frequency for each tested SNP. c) A representation of *HvPIN1a* (gene model *HORVU7Hr1G038700.2*) with position of TM5992 and additional mutant alleles identified from TILLMore (TM5141) and Barke (TB13081) TILLING collections. showing short root phenotypes (d,e). TB_WT is a Barke TILLING background containing all mutations except *HvPIN1a*. Growth rate data quantification in Fig. 4.4.

To validate which mutation in these 3 candidate genes conferred the short root defect, we characterized independent alleles isolated from a different mutant population (background cv. Barke) (Gottwald *et al.*, 2009) and identified one line, TB13081 which was heterozygous

for a premature stop codon mutation in the first exon of *HvPin1a* (Fig. 4.3c). Seedlings homozygous for the premature stop codon mutation showed a clear short root phenotype (Fig. 4.3d). A third *HvPin1a* mutant allele was subsequently found within the TILLMore population. Line TM5141 contains a mis-sense mutation within the first exon and showed an even stronger short root phenotype compared to TM5992 (Fig. 4.3c-e). Root growth rate and root development analyses showed very similar results to the line TM5992 (Fig. 4.3-4). Taken together, these results provide conclusive evidence that *HvPIN1a* is responsible for the short root phenotype observed in TM5992, TM5141 and TB13081.

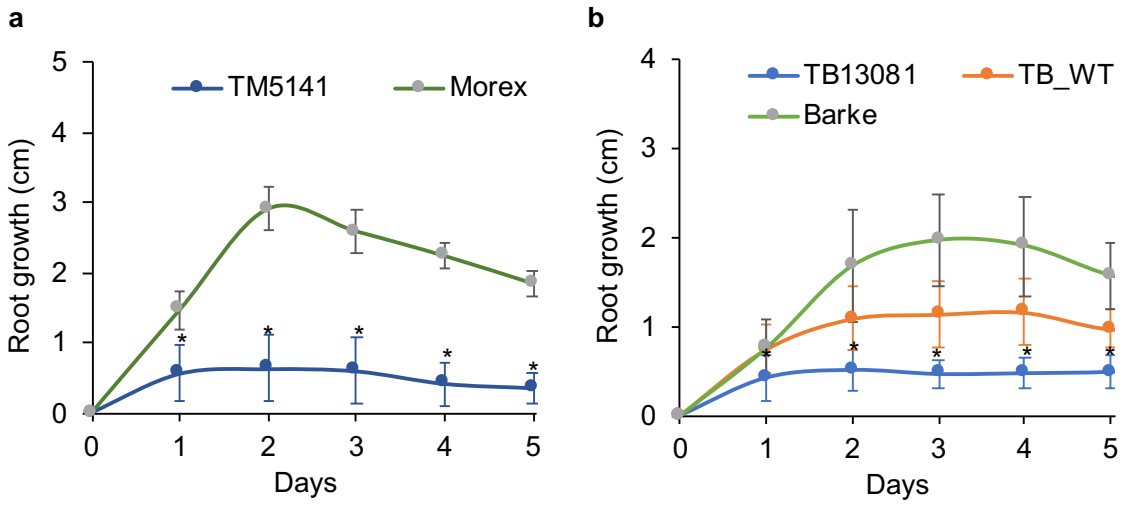


Fig. 4.4. HvPIN1a allelic mutant lines TM5141 and TB13081 exhibit similar root growth rate as line TM5992.

a) Line graph showing root growth rate of Morex and TM5141 (second *Hvpin1a* mutant allele from Morex TILLING population) (b) Line graph showing root growth rate of Barke, TB_WT (Barke TILLING background with functional *HvPIN1a*) and TB13081 (third *Hvpin1a* mutant allele from Barke TILLING population) over 5 days post germination on 1% Agar plates. Both plots showing mean and standard deviations from at-least 2 biological replicates and included minimum 7 seedlings per replicate. *indicates significance (P-value < 0.01, *T-test*) between respective timepoints of Morex vs TM5141 and Barke vs TB13081.

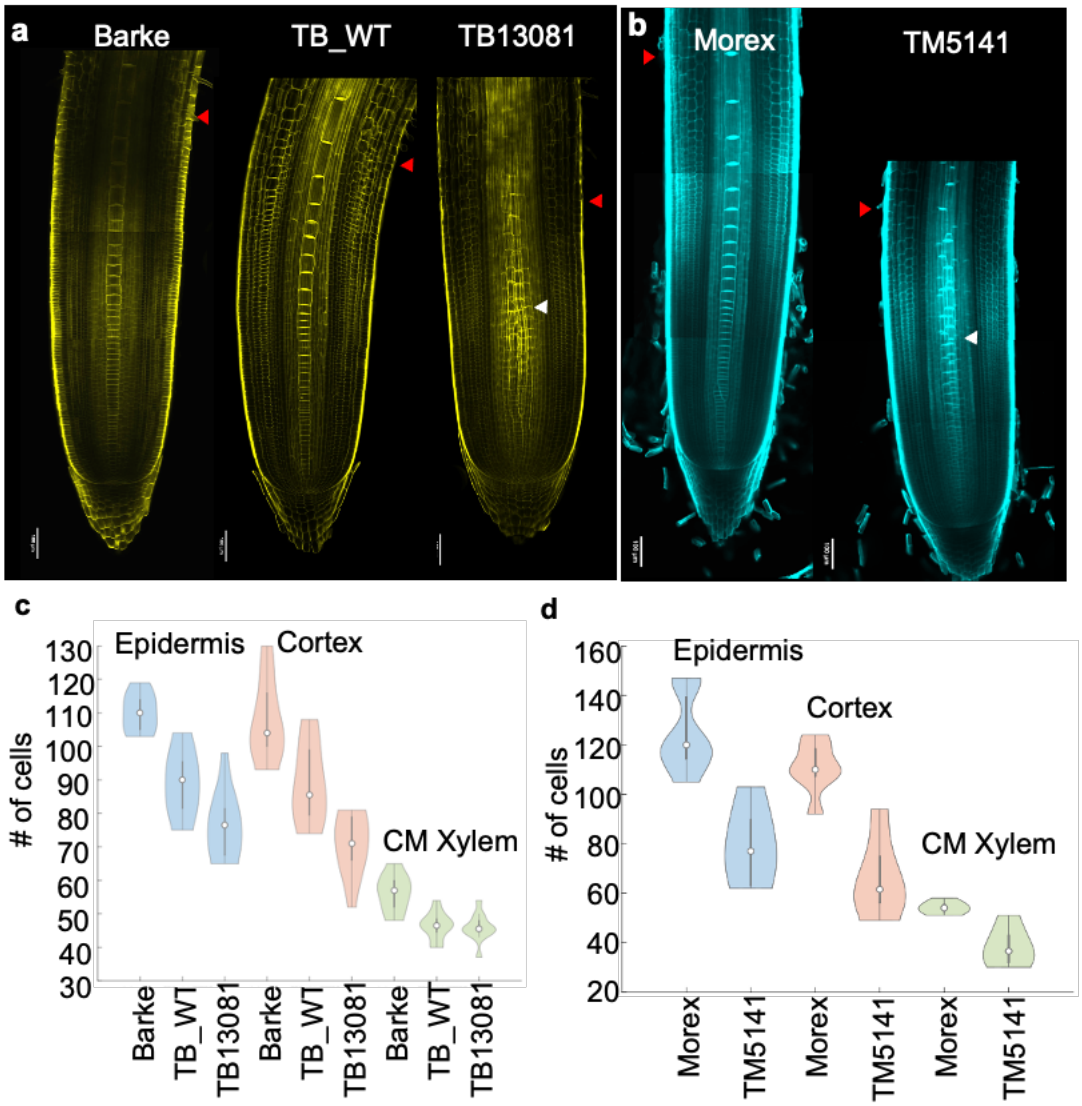


Fig. 4.5. HvPIN1a allelic mutant lines TM5141 and TB13081 exhibit similar root developmental defects as line TM5992.

Representative confocal image of longitudinal sections of (a) Barke, TB_WT and TB13081 root tips stained with yellow direct 96 and (b) Morex and TM5992 root tips stained with Calcofluor showing difference in first visible root hair (red) and visible defects in vascular patterning (white). Seedlings were vertically grown for 7 days on 1% w/v Agar plates. N > 2 in-dependant biological replicates and n > 5 seedlings per replicate were analysed. Scale bar = 100µm. (c-d) Violin plots showing distribution of number of cells in root epidermis, cortex and xylem tissues between quiescent centre and first visible root hair in TB13081 compared to Barke and TB_WT (c) and TM5141 compared to Morex (d). Measurements were obtained from a clearly visible one cell file per tissue type. >8 seedlings were used for each genotype.

***HvPIN1a* is essential for vascular patterning in barley roots**

Longitudinal sections of all 3 *Hvpin1a* mutant alleles revealed striking irregularities in the root vasculature compared to their respective wild type backgrounds (Fig. 4.5, S.Fig.4.2). To investigate this further, we studied cross-sections of 4 day old roots from mutant alleles and their wild type controls (Fig. 4.6a-c, Fig. 4.7). Remarkably, all mutant alleles showed enlarged cells in the First Parenchymatic Stele cells Layer (FPSL) surrounding the central metaxylem and thus significantly reduced number of cells from 12±3 to 18±2 in in that cell layer compared to their wild types (Fig. 4.6-7). As a likely effect of this cell layer enlargement, the root stele diameter in all mutant alleles was significantly bigger than their wildtypes (mean >13% in TM5992 and TM5141 compared to Morex and >20% bigger in TB13081 compared to Barke and TB_WT) (Fig. 4.6-7). Ectopic proliferation of protoxylem cells was also observed such that each xylem pole often contained multiple protoxylem cell files (Fig. 4.6 a-c).

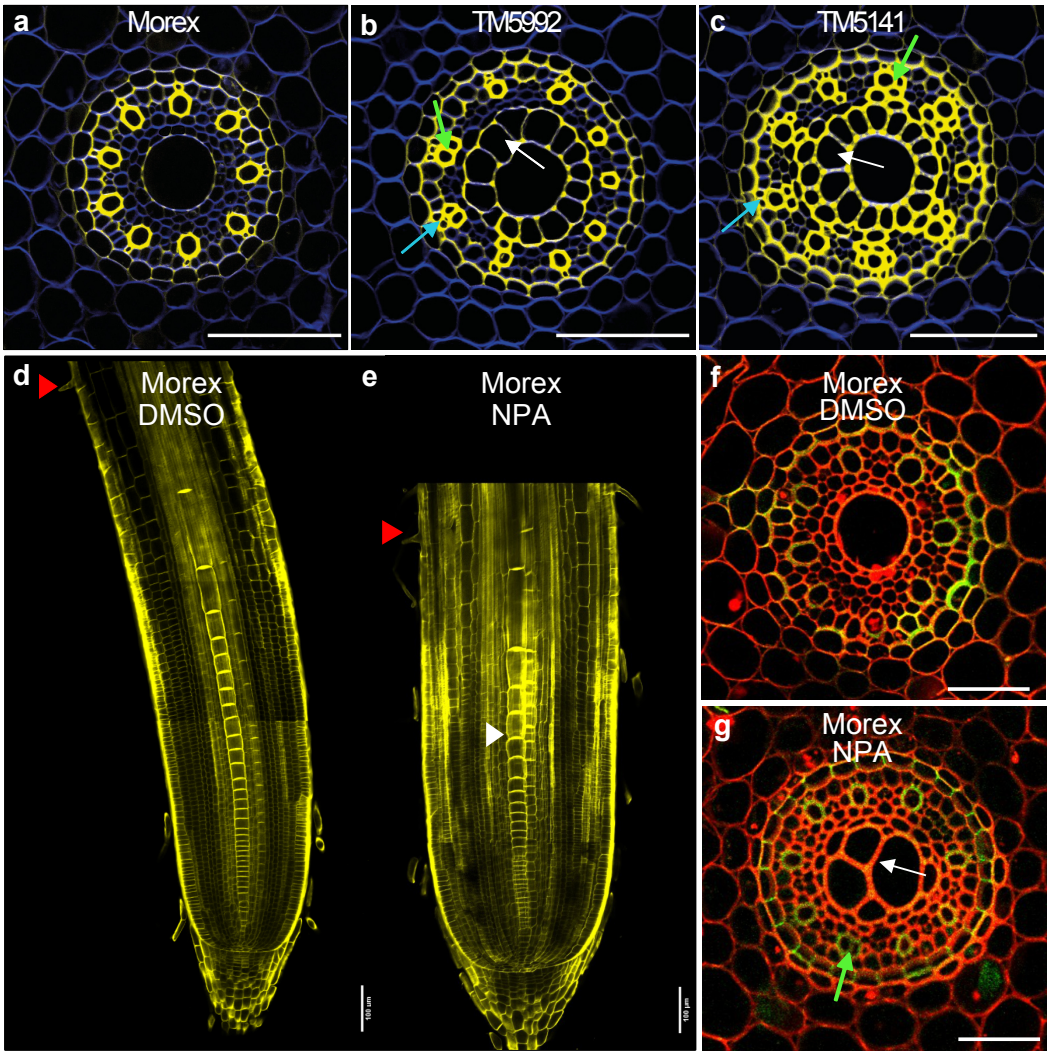


Fig. 4.6. Hvpin1a mutant alleles shows root vascular defects that can be mimicked by blocking PIN activity in Morex by NPA treatment.

(a-c) Representative images showing root cross-section of Morex, TM5992 and TM5141. Seedlings were vertically grown for 4 days on 1% agar and the mid regions (~3-4 cm from the root apex) of the seminal root were cross-sectioned using a vibratome, stained with Calcofluor White and Basic Fuchsin (see methodology). Blue, green and white arrows indicate irregularities in protoxylem, peripheral metaxylem vessels and first parenchymatic cell layer around the central metaxylem respectively. Scale bar = 100 µm. N > 3 independent biological replicates and n > 5 seedlings per replicate. (d-g) Representative images showing direct yellow 96 stained longitudinal sections (d-e) and propidium iodide (PI) stained root cross-sections (f-g) of 12 days old seedlings of Morex, grown in DMSO (control) and 50 µM NPA dissolved in DMSO. Scale bar = 100 µm (d-e) and 50 µm (f-g). Red arrow-head (d-e) indicates the first visible root hair and white arrow-head shows visible defects in vascular patterning. Green and white arrows in (g) show irregularities in peripheral metaxylem vessels and first parenchymatic cell layer around the central metaxylem. N = 2 independent biological replicates and n > 5 seedlings were analysed per replicate.

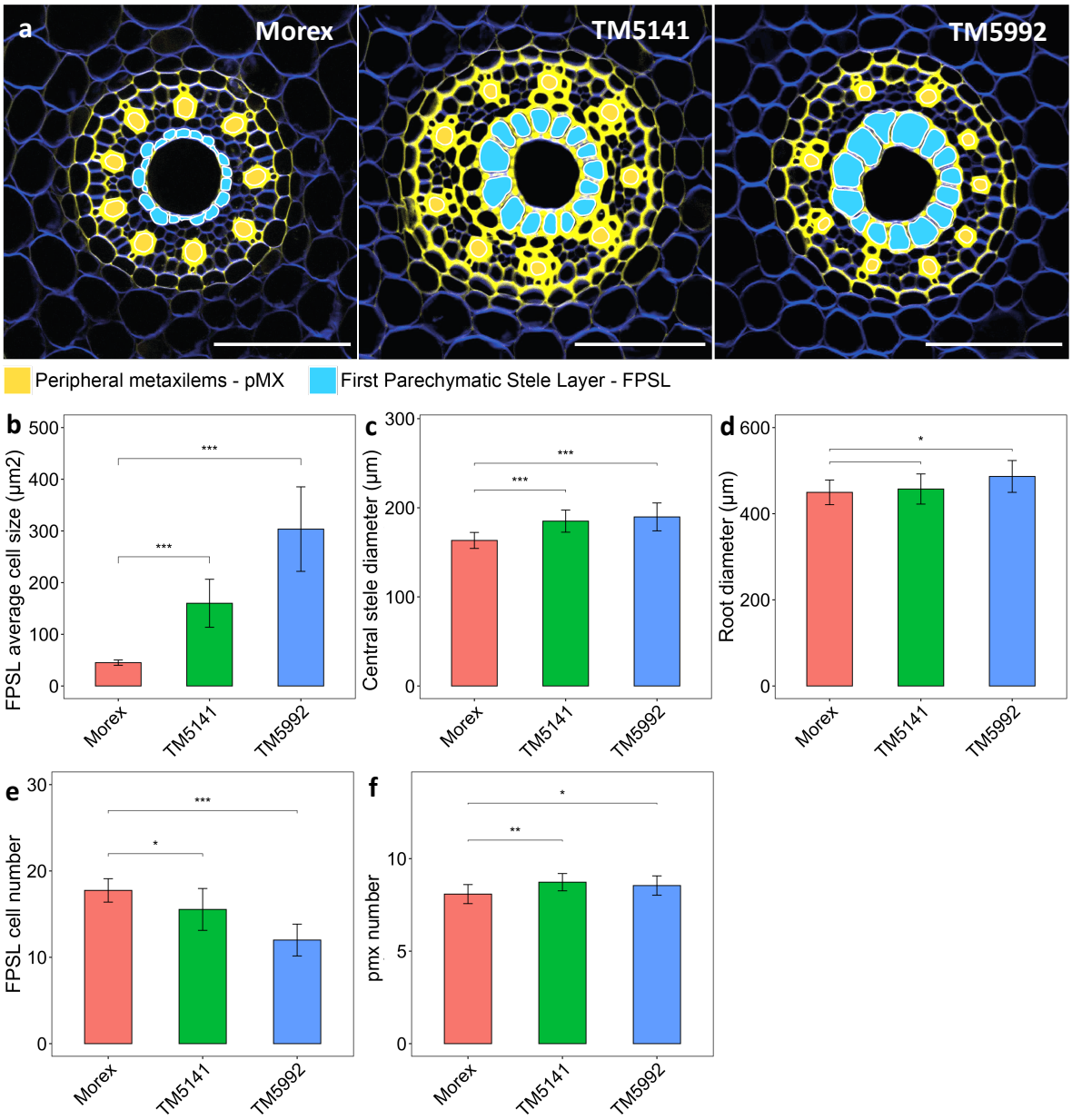


Fig. 4.7. Phenotypic anatomical data collected from mid seminal root cross sections of barley seedlings of the genotypes Morex, TM5141, and TM5992.

a) Representative images from of mid seminal root cross section of Morex, TM5141, and TM5992 stained with calcofluor white (blue) and Basic Fuchsin (yellow). Scale bar = 100µM (b,c,d,e,f) Data of FPSL cell size (b), stele diameter (c), root diameter (d), FPSL cell number (e) and the number of pMX (f). Images were collected and processed from n biological replicates = 11-12 and using ImageJ. Statistical differences between Morex and mutants was tested using t.test using R studio (rstatix package) with p significance values *<0.05, **<0.01, ***<0.001. FPSL = First Parenchymatic Stele Layer, pmx = Peripheral metaxylem

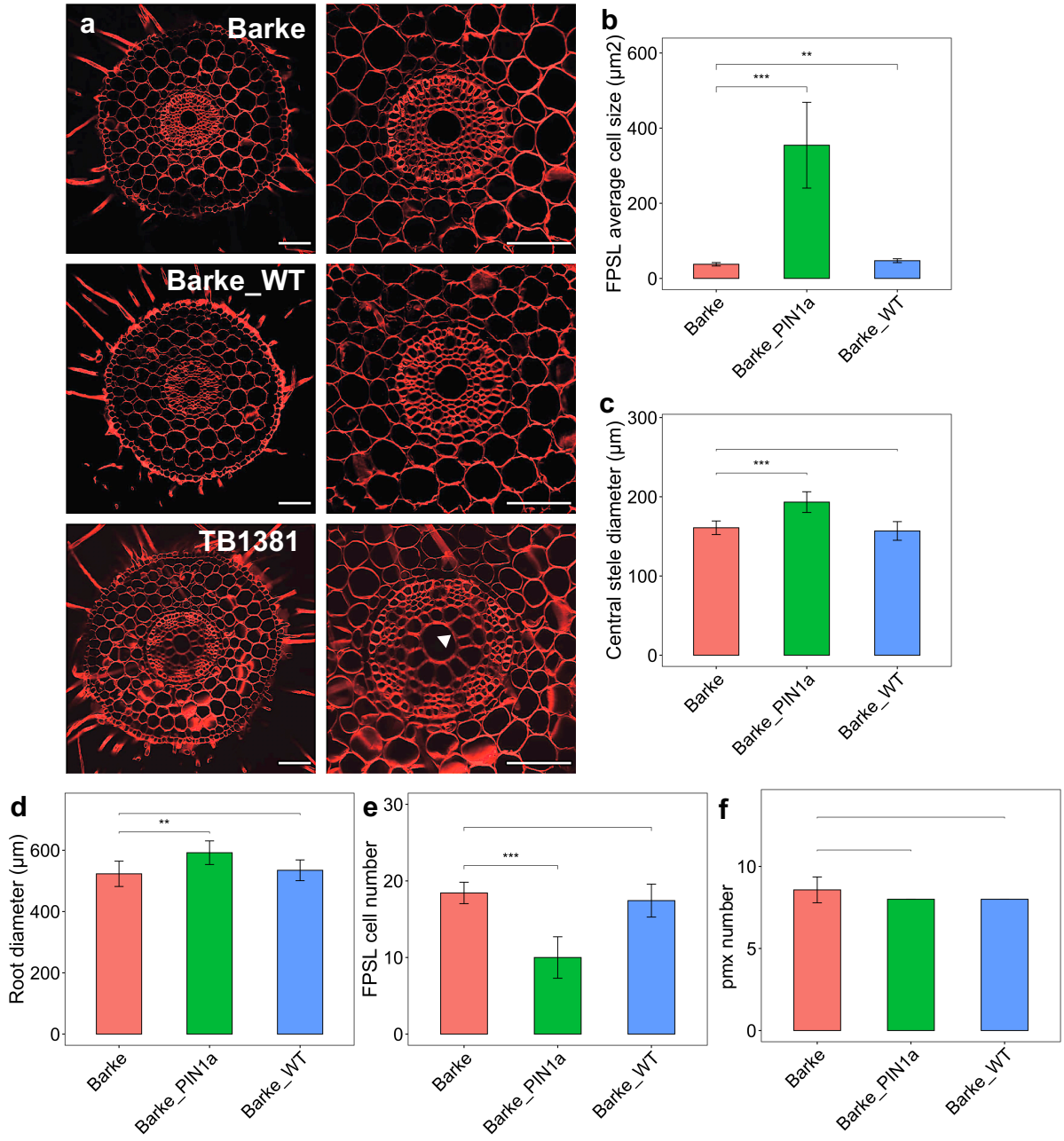


Fig. 4.8. Phenotypic anatomical data collected from mid seminal root cross sections of barley seedlings of the genotypes Barke, Barke_WT, and TB1381 (Barke_PIN1a) exhibits similar root anatomical defects as line TM5992 and TM5141.

a) Representative images from of mid seminal root cross section of WT and *PIN1A* mutant TB1381 in Barke background. Scale bar = 100µM. (b,c,d,e,f) Data of FPSL cell size (b), stele diameter (c), root diameter (d), FPSL cell number (e) and the number of pMX (f) from n biological replicates=5 and n roots >7 using ImageJ. Statistical differences between Morex and

mutants was tested using t.test using R studio (rstatix package) with p significance values *<0.05, **<0.01, ***<0.001. FPSL = First Parenchymatic Stele Layer, pMX = Peripheral mataxylem

Basic Fuchsin staining of root-cross sections of TM5992 and TM5141 revealed a stronger signal in the central metaxylem, its surrounding first parenchymatic cell layer and in the neighbouring cells of peripheral metaxylem and protoxylem cells, indicating greater lignin deposition and possibly ectopic divisions in these tissue types. Overall, these results indicated that *HvPIN1a* was important for patterning of root vascular tissues.

To independently validate the importance of polar auxin transport (PAT) in controlling the root vascular patterning trait in barley, we employed the PAT inhibitor NPA to block PIN mediated hormone transport in barley roots and study its impact on root growth and anatomy. The root growth of Morex was severely affected when transferred to 1% agar supplemented with high concentration of NPA, especially 20μM and 50μM, phenocopying the short root behaviour observed in *Hvpin1a* mutant alleles (Fig. 4.5d-g, Fig. 4.9). Similarly, root longitudinal and cross-section analysis showed similar developmental and anatomical defects observed in mutants (Fig. 4.5d-g, Fig. 4.9). These results demonstrated that the short root and vascular developmental defects observed in *HvPIN1a* mutant lines can be phenocopied in wild type barley by blocking PIN activity using NPA.

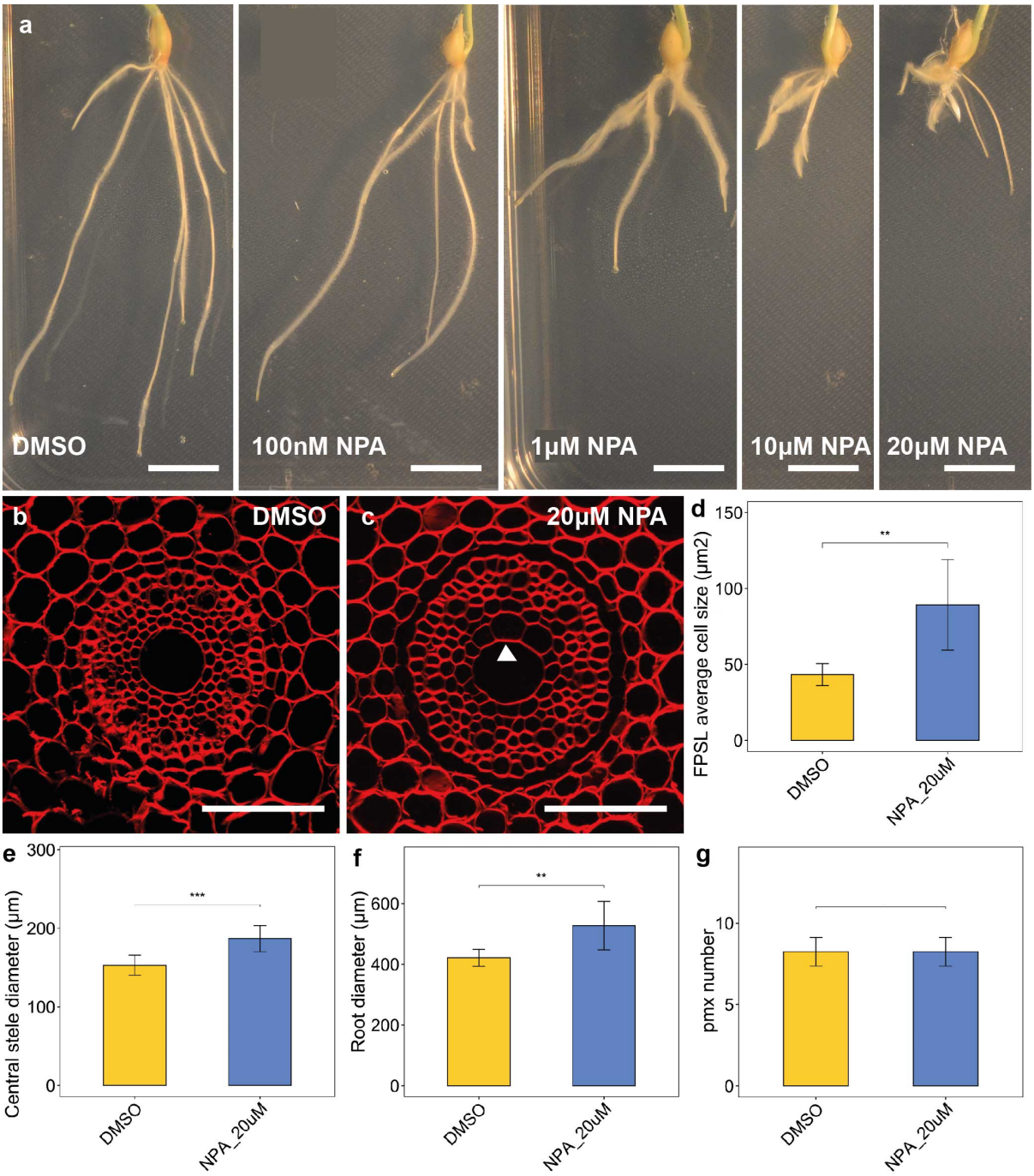


Fig. 4.9. Short root phenotype in HvPIN1a mutant alleles can be mimicked in barley wild type roots using NPA treatment.

a) Representative images showing root growth of 3 DAG (post germination) old seedlings of Morex grown on 1% Agar supplemented with DMSO (control) treated with increasing concentration of 100nM, 1µM, 10µM and 20µM NPA dissolved in DMSO. Scale bar = 10mm. b,c) Representative images from of mid seminal root cross section of Morex root seedlings grown in DMSO (Mock) and 20µM NPA. Scale bar = 100µm. (d,e,f,g) Data from such treatment of FPSL cell size (d), stele diameter (e), root diameter (f) and the number of pMX (g). Images

were collected and processed from n biological replicates = 8 using ImageJ. Statistical differences between DMSO and NPA 20µM treated seedlings was tested using t.test using R studio (rstatix package) with p significance values *<0.05, **<0.01, ***<0.001 FPSL = First Parenchymatic Stele Layer, pmx = Peripheral metaxylem

***PIN1a* plays a conserved role regulating root vascular patterning in other cereals**

HvPIN1a belongs to a clade of 3 *PIN1*-related genes in the barley genome (Fig. 4.1). Phylogenetic analysis reveals that Barley PIN1 members exhibit a high degree of conservation with *Brachypodium distachyon* PIN1 family members (Fig. 4.1). We initially investigated whether the function of *HvPIN1a* in root vascular patterning was conserved in *Brachypodium distachyon* by characterising root anatomy of a recently described *Bdpin1a* mutant line. Root cross-section analysis revealed *Bdpin1a* roots had similar defects as *Hvpin1a* mutants such as irregular CM xylem, larger and thicker FPSL cells with an increased central stele and root diameter. (Fig. 4.10i-k, Fig. 4.11). These defects were also mimicked by NPA treatment to wildtype (*Brachypodium distachyon* accession 21.3) Bd21.3 roots (Fig. 4.12). Hence, *BdPIN1a* and *HvPIN1a* appear to play orthologous developmental functions.

As the PIN1a and PIN1b duplication in grasses is conserved and SoPIN1 and PIN1 clades appear to mediate distinct functions, we wondered whether any functional redundancy exists between PIN1a and PIN1b in controlling root vascular patterning. As no material was available to investigate the role of *HvPIN1b* in root vascular patterning, we were able to characterise root anatomy in a recently described *Bdpin1b* mutant line. However, we did not observe any patterning defects in *Bdpin1b* mutants (Fig. 4.10-11). Although we cannot conclude that PIN1b necessarily behaves the same way in *Brachypodium distachyon* and barley, our results indicated that, whilst PIN1b may function redundantly with PIN1a to control vascular patterning, PIN1a plays a master regulatory role, and this is likely to be conserved across cereal species.

We noted that the *Bdpin1a* and *Hvpin1a* patterning defects are mainly associated with protoxylem, central and peripheral metaxylem. To explore whether PIN1 clade members are specifically expressed in root vascular cell types, we examined GFP-based reporters of *Brachypodium distachyon* PIN1a and PIN1b (and SoPIN1) for differences in their expression

domains. Analysis of PIN1 reporters revealed both BdPIN1a and BdPIN1b are expressed in root vasculature tissues specifically in protoxylem and metaxylem (central and peripheral), while SoPIN1 is mainly expressed in the peripheral metaxylem vessels (Fig. 4.10c-e). The overlapping spatial expression patterns revealed for PIN1a and PIN1b suggest they could function redundantly to regulate vascular patterning. Nevertheless, genetic evidence demonstrates that PIN1a plays a more critical regulatory role patterning vascular tissues in cereal roots.

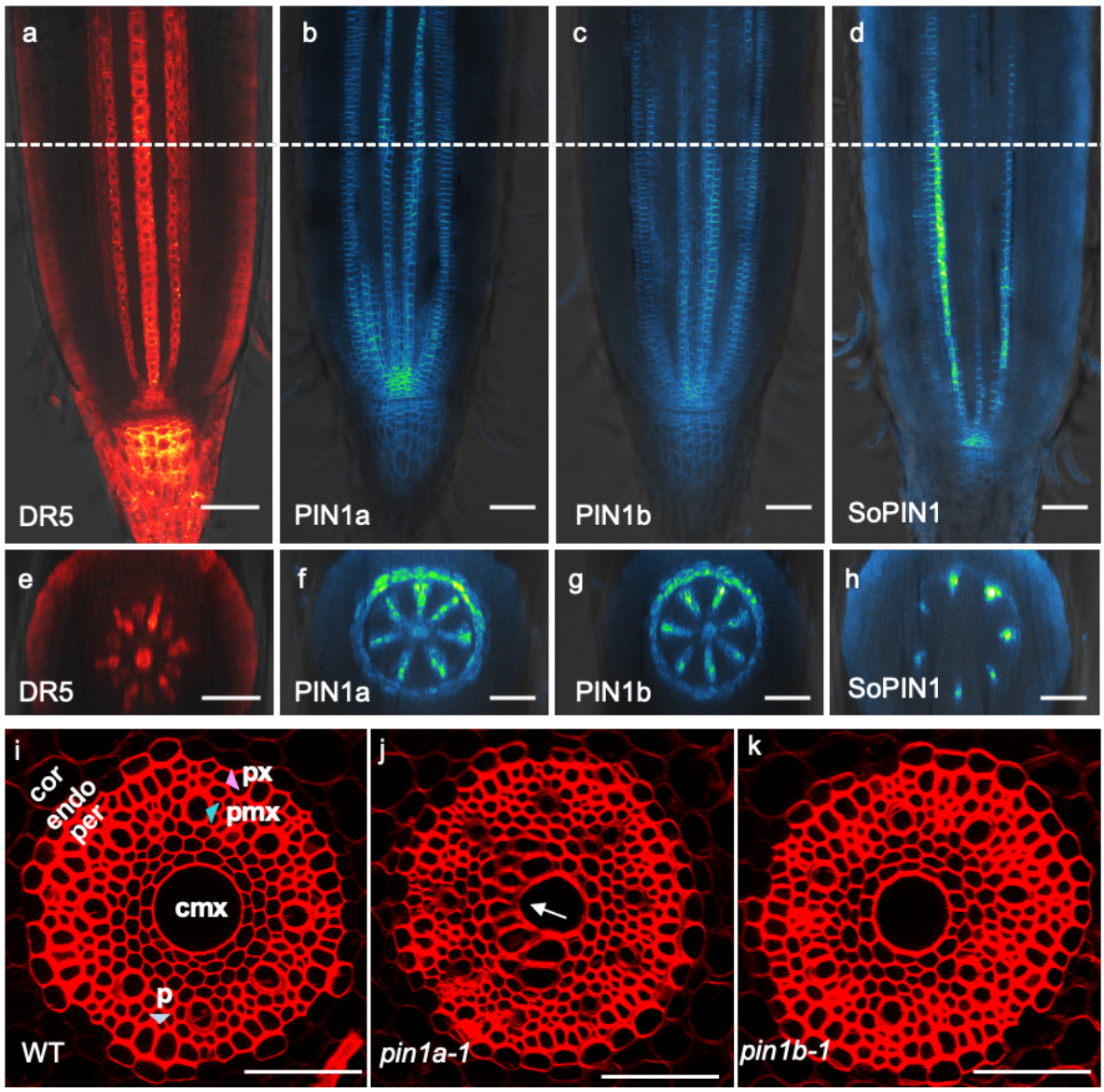


Fig. 4.10. The role of PIN1a in root vascular patterning is conserved in cereal model *Brachypodium distachyon*.

Representative confocal images showing *Brachypodium distachyon* roots expressing (a) auxin response reporter DR5, (b-d) auxin efflux carrier reporters PIN1a, PIN1b and SoPIN1 reporters. Scale bar = 100 µm. (e-h) represents orthogonal views of (a-d) showing YZ axis (cross-sections) in root meristem at position marked by the white dotted line. Scale bar = 100 µm. (i-k) Representative confocal images of propidium iodide stained root cross sections of *Brachypodium distachyon* accession 21.3 (WT), *pin1a* and *pin1-b* mutants. Seedlings were vertically grown for 7 days on 1% Agar and mid regions (~2-3 cm from the root apex) of the main root were cross-sectioned and imaged using confocal. N > 3 in-dependant biological replicates and n > 5 seedlings per replicate were analysed. Scale bar = 50µm. Cor – Cortex;

endo – endodermis, per – pericycle; p – phloem poles (light blue arrow); px – protoxylem (purple arrow); pmx – peripheral metaxylem (cyan arrow) and cmx – central metaxylem.

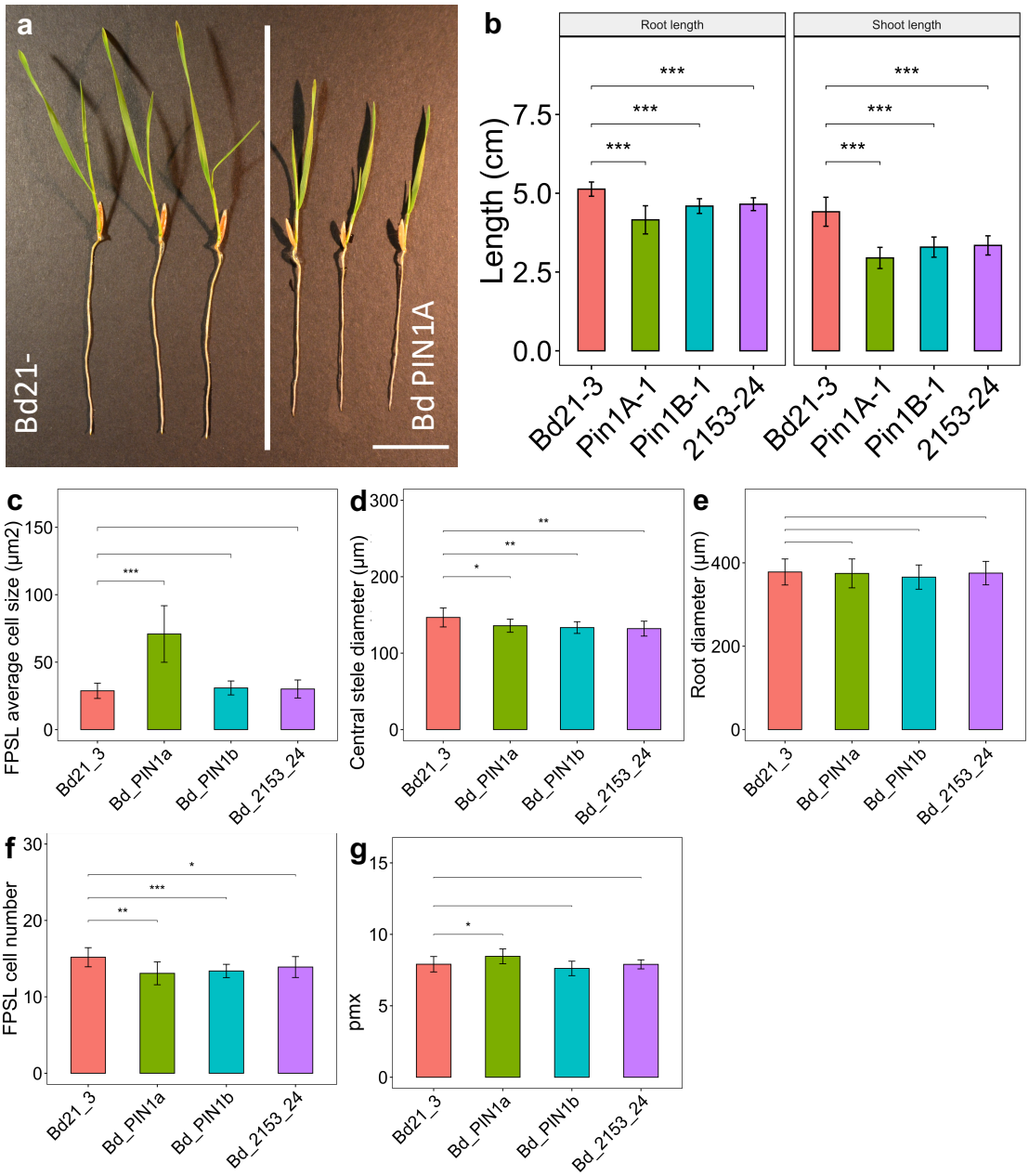


Fig. 4.11. Architectural and anatomical data collected from mid primary root cross sections of *Brachypodium distachyon* seedlings of genotypes Bd21-3(WT), BdPIN1A-1, BdPIN1b-1 and 2153-24.

(a) Representative images of 7DAG *Brachypodium distachyon* seedlings grown in ½ MS media. (c) Data of root and shoot length of 7DAG *Brachypodium distachyon* seedlings n>13. (c,d,e,f,g) Data of FPSL cell size (c), stele diameter (d), root diameter (e), FPSL cell number (f) and the number pMX (g) from n roots > 10 using ImageJ. All the statistical differences between Morex

and mutants was tested using t.test using R studio (rstatix package) with p significance values *<0.05, **<0.01, ***<0.001. FPSL = First Parenchymatic Stele Layer, pmx = peripheral metaxylem

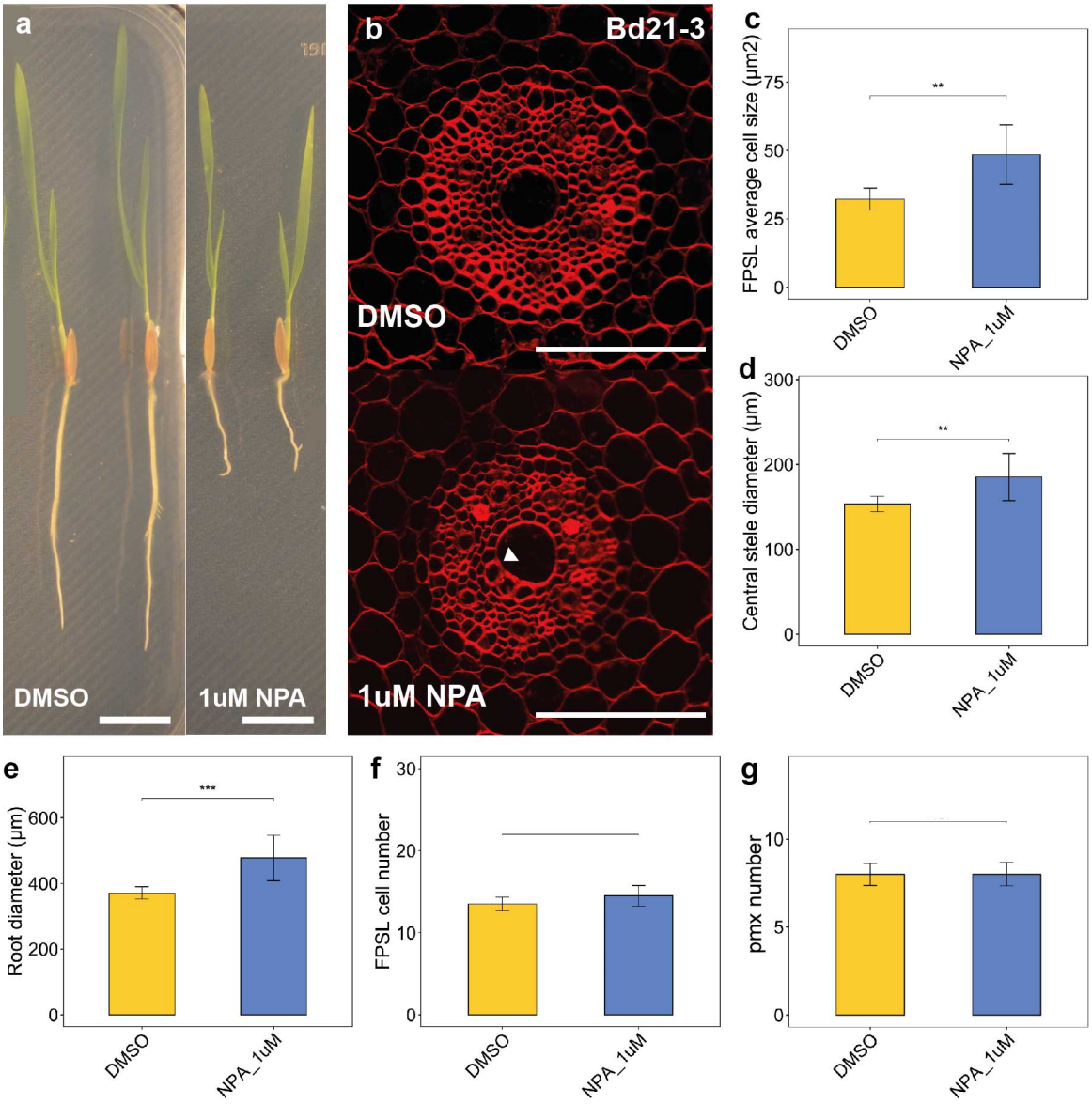


Fig. 4.12. Short root phenotype in HvPIN1a mutant alleles can be mimicked in *Brachypodium distachyon* wild type roots using NPA treatment.

a) Representative images showing root growth of 3 DAG (post germination) old seedlings of Morex grown on 1% Agar supplemented with DMSO (control) treated with increasing concentration of 100nM, 1µM, 10µM and 20µM NPA dissolved in DMSO. Scale bar = 10mm. b,c) Representative images from of mid seminal root cross section of 3DAG Morex root seedlings grown in DMSO (Mock) and 20µM NPA. Scale bar = 100µm. (d,e,f,g) Data from such

treatment of FPSL cell size (d), stele diameter (e), root diameter (f) and the number of pMX (g). Images were collected and processed from n biological replicates = 8 using ImageJ. Statistical differences between DMSO and NPA 20µM treated seedlings was tested using t.test using R studio (rstatix package) with p significance values *<0.05, **<0.01, ***<0.001 FPSL = First Parenchymatic Stele Layer, pmx = Peripheral Meta-Xylem

Discussion

AtPIN1 and BdPIN1 have previously been shown to play key roles patterning leaf vascular tissues (Gälweiler *et al.*, 1998; Scarpella *et al.*, 2006; O'Connor *et al.*, 2014). In the eudicot model Arabidopsis*,* PIN1 is a key regulator of polar auxin transport and is expressed in differentiating cell lineages of developing root vascular tissues including xylem precursors i.e. protoxylem and metaxylem (Omelyanchuk *et al.*, 2016). While in the cereal model *Brachypodium distachyon*, PIN1 is functionally diversified and has two duplicate PIN1 members PIN1a and PIN1b and a single gene in a sister clade, SoPIN1. Collectively these three proteins recapitulate expression domains and polarization behaviours observed for AtPIN1 alone in Arabidopsis (O'Connor *et al.*, 2014, 2017). Hence, AtPIN1 and the cereal PIN1 clade members are all root expressed, and AtPIN1 mutants have either ectopic or failed protoxylem differentiation (Bishopp *et al.*, 2011).

This work reports the characterization a barley mutation in the *HvPIN1a* auxin efflux carrier gene which causes a short root phenotype with slower root growth rate and reduced meristem size in different barley backgrounds (Fig. 4.2-4). Closer examination of the *hvpin1a* mutant's root anatomy revealed a striking vascular patterning defect. Characterization of a mutant line disrupting the orthologous *BdPIN1a* gene in *Brachypodium distachyon* revealed a comparable root vascular patterning defect. Similar root vascular patterning defects larger and thicker cells around CM xylem vessels, named as First Parechymatic Stele Layer (FPSL), an ectopic increased number of protoxylems and a wider stele and root diameter. These results suggests that PIN1a plays a key role regulating root vascular patterning in cereals. Moreover, we show that when treated with high concentration of NPA, both barley and *Brachypodium distachyon* wild type seedlings mimic similar root anatomical defects with the respective PIN1a mutants in those species.

Puzzlingly, BdPIN1a and its closely related homologue BdPIN1b exhibit overlapping expression patterns in *Brachypodium distachyon* root vascular cell types. Using DR5 and *BdPIN1a, BdPIN1b and SoPIN1* revealed that such gene expression accumulates surrounding the areas where auxin accumulates in the vasculature tissues. Specifically, BdPIN1a and BdPIN1b expression is localised in the central metaxylem and peripheral metaxylems (as well as the endodermis), while SoPIN1 expression is localised in only the peripheral metaxylem region. Interestingly, we only observed a vasculature patterning defect in *bdpin1a* but not *bdpin1b* mutant roots. This observation contrasts results in *bdpin1b* leaves which reveals BdPIN1b plays a more important vascular patterning role in this organ (O'Connor *et al.*, 2014, 2017). Accordingly, a moderate root length reduction was observed in *bdpin1b* compared *bdpin1a* mutants where a more evident reduction was observed in the shoot length in these mutants when compared to WT (Fig. 4.11b). Our mutant studies suggest that members of the *PIN1* clade in cereals are undergoing a process of sub-functionalization comparable to what happens in *Brachypodium distachyon* during shoot organogenesis. However, in contrast to what happens in the shoot, we hypothesise that BdPIN1a and BdPIN1b synergically regulate auxin flux in the vasculature, rather than being in between vasculature and epidermal tissues, where BdPIN1a plays a prevalent role.

In addition, our study clearly demonstrates that also in other cereals such as barley, conserved members of the PIN1 clade, such as PIN1a, play a key role regulating root growth vascular patterning in roots. However, the crosstalk between different PIN1 members process still remain unclear due to the current unavailability of PIN1b and SoPIN1 mutants/reporters and the current challenges in developing stable DII/DR5 auxin reporters (Kirschner *et al.*, 2018). Moreover, experiments to assess if such anatomical changes in HvPIN1a mutants causes a defect in auxin accumulation, hormonal profiling will be performed in the future.

Physiological relevance of PIN1a in crops was proved in maize plants on root architectural traits (Li *et al.*, 2019). Overexpressing ZmPIN1*a* caused the accumulation of auxin in roots forming a deeper root system which results a more stress resilient plants with an increased yield under drought and phosphate starvation. In parallel, in this study we show a key role of PIN1 to control root vasculature patterning in an anatomical level, in particular regarding central metaxylem organization which is also a key regulator of water transport. Further

perspective will be directed to investigate physiological impact of the observed vasculature for water uptake in order to provide more insight for developing stress resilient crops.

Chapter 5

Discussion & Perspectives

Exploiting the knowledge gained about the molecular mechanisms regulating deeper rooting in crops represents one of the most promising approaches in plant biology to help offset carbon emissions, whilst also serving to improve food security in increasingly challenging climate conditions. To date, the majority of research studies have focused on identifying root traits which control deeper roots with increased root length densities at depth. These studies mainly fall into two categories: focused on either **anatomical traits** that enable roots to grow 'deeper' as they are 'cheaper' to build due to their reduced carbon costs such as enhanced programmed cell death in cortical tissues (CCS,CCFN,TCA and RCA); and **architectural traits** such as angle that enable roots to grow 'deeper' as they are 'steeper' (Lynch, 2007). Field studies have demonstrated crops with steeper root angle or a reduced total cortical area can explore deeper soil layers more efficiently, while maintain yield in drought stressed environments (Lynch, 2019). Nevertheless, despite the increased interest in this approach, few studies go beyond an anatomical or architectural scale of understanding to pinpoint the key genes and mechanisms that control these traits. To address this issue, my thesis describes how advanced phenomic approaches combined with forward genetic screens, genome wide association and natural variation have been used to pinpoint novel candidate genes that control root anatomical and architectural traits, followed by functional validation studies exploiting reverse genetic techniques such as CRISPR/Cas9-based gene editing to pinpoint several key regulatory genes. This molecular scale information promises to accelerate efforts by breeders to select deeper rooting crop varieties using DNA marker (rather than time consuming phenomics) based approaches.

Exploiting advanced phenomics and genomics to pinpoint root anatomical regulatory genes

Root anatomical traits represent an under-appreciated and under-utilised scale at which to select novel deeper rooting crop varieties with improved field performance, climate resilience and carbon offset potential (Lynch, 2019). Whilst accumulating evidence over the past decade highlights to the importance of root anatomical traits, analysing crops and pinpointing the

genes that control traits at this physical scale has proved challenging to date. The creation of an integrated phenomic and genomic 'DEEPGENES' pipeline as part of the ARPA-E DEEPER project has greatly accelerated efforts to overcome these previous challenges. The DEEPGENES pipeline features high throughput anatomical scale sectioning and imaging of field grown roots using laser ablation tomography (LAT) from a maize diversity collection; bespoke software to capture anatomical scale traits from LAT root images; and a genome wide association based gene discovery approach. This thesis has exploited these rich maize datasets to characterise several promising candidate genes controlling root cortical anatomical traits. The exploitation of closely related genetic models - *Brachypodium distachyon* and rice – was critical to accelerate efforts to functionally validate roles of genes and hormone signals during root cortical developmental programmes. *For example,* CRISPR-cas9 based studies in *Brachypodium distachyon* identified that the orthologue *BdQKY* represents a promising gene regulating total root cortical area (Chapter 2). Similarly, the rice mutant *eil1* was instrumental for demonstrating a key role for ethylene response during RCA formation (Chapter 2).

Despite the clear potential of the DEEPGENES pipeline to study anatomical traits, major bottlenecks remain in its throughput. *For example,* by implementing new image analysis techniques such as Artificial Intelligence (AI) and neural networking models, it will be possible in the near future to characterise anatomical features of 2D and 3D root sections generated using LAT in an automated fashion, greatly boosting the throughput of the DEEPGENES pipeline. More generally, new AI approaches combined with Laser Ablation Technology (LAT) promise to revolutionise the selection of many other anatomical scale traits in crop shoot and seed tissues, in addition to roots.

Exploiting forward genetics to pinpoint novel root angle regulatory genes in crops

Root angle represents a widely targeted trait to select novel deeper rooting crop varieties with improved climate resilience and carbon offset potential (Uga et al, 2012; Lynch, 2019). In contrast to root anatomical traits, screening crops grown in the field for root angle variation is relatively straight forward (ref). High throughput screens to score seedling stage root angle traits in crops have also been developed (ref). These developments which, when combined with the recent availability of sequenced genomes in crops such as barley, have catalysed

efforts to perform forward genetic (i.e mutant-based) screens in these species. In this thesis, I described how the use of barley mutant resources based on the TILLMore TILLING population, combined with BSA and NGS technologies, proved to be a highly effective method for identifying a novel gene regulating root angle in barley (Talamè *et al.*, 2008; Salvi *et al.*, 2014). Using this approach, I was able to characterise a novel Tubby-like F-box gene in barley called *Enhancing Gravitropism 1* (*HvEGT1*). Mutations in *HvEGT1* caused roots to exhibit an enhanced gravitropism response, resulting in a much steeper root angle (for all root classes). Interestingly, this mutant phenotype was phenocopied in tetraploid (durum) wheat when both orthologous gene copies were mutated. However, mutants in one of the closest orthologous genes in diploid Arabidopsis (AtTLP2) didn't exhibit changes in gravity response, suggesting that EGT1-mediated regulation of root angle may be cereal (or monocot) specific. However, a more detailed reverse genetic analysis in Arabidopsis and other plant species, characterising mutants in other gene family members, would be necessary to validate this last hypothesis. Another mutant called *Enhancing Gravitropism 2* (*HvEGT2*) has recently been described in barley which also exhibits a much steeper root angle (Kirschner et al, 2021). HvEGT2 encodes a sterol binding domain containing protein which exhibits homology to a gene previously reported to control shoot gravitropism in a dicot tree species (Kirschner et al, 2021). Hence, unlike *HvEGT1*, *HvEGT2* function appears to be conserved between dicots and monocot species, mediating an organ angle regulatory mechanism operating in both root and shoot tissues. The observation that the *EGT1* mutant root angle phenotype had not been identified in plant models like Arabidopsis, but was instead identified in crops, illustrates the potential of conducting forward genetic screens directly in crops in order to identify mutations in novel genes with desirable traits.

Hvegt1 and *Hvegt2* are distinct from earlier reported gravitropic mutations like *aux1* in that when these genes are mutated they enhance (rather than disrupt) root gravitropic responses. In addition, neither mutation appears to disrupt auxin response (based on hormone sensitive root growth and bending, plus transcript profiling to reveal differentially expressed genes in the mutant versus wildtype), a hormone which is central to 'classical' positive gravitropic responses in roots. Instead, RNA-seq profiling of wildtype versus mutant root tip tissues revealed changes in cell-wall related genes. Moreover, *in situ* hybridisation studies reveals *HvEGT1* is expressed specifically in the central stele tissues in the elongation-division zone,

which is distinct from root cap and epidermal tissues identified to be critical for auxin-dependent root gravitropic curvature (Swarup et al, 2005).

I hypothesise a model featuring *HvEGT1* regulating cell-wall stiffening in the central stele tissues (Fig. 5.1a-b), where differences in stiffness between inner and outer root tissues will determine the rate of gravitropic curvature. To validate this, requires use of biomechanical assays such as Atomic Force Microscopy (AFM) for measuring the stiffness of fresh biological material (Fig. 5.1c) (Pattem *et al.*, 2018; Hendow *et al.*, 2020). Based on the applied force, material indentation and shape of the probe, it is possible to assess mechanical properties, in this case as stiffness (pN/nm) (Butt *et al.*, 2005; Pattem *et al.*, 2018). Probing 50μm longitudinal sections from wild-type barley root tips for their tissue stiffness using AFM (Fig. 5.1d) recently revealed outer root tissues are significantly stiffer than inner tissues (Fig. 5.1e). After optimisation, additional work was performed to determine whether differences in the stiffness of the outer versus inner tissues is *EGT1*-dependent and is showed in Fig.5.2. Results indicate the outer elongating tissues in the root tip to be less stiff in TM194 compared to WT allowing the gravitropic machinery to bend the root more rapidly. Hence, this provide a simple mechanism where *EGT1* regulates a novel mechanism distinct from earlier reported studies that featured a gravity-induced lateral auxin gradient targeting outer root tissues in the elongation zone, triggering differential root bending. Such a mechanical mechanism could provide the basis for a novel anti-gravitropic offset system, which functions to counteract the action of the gravitropic response pathway in outer root tissues and (collectively) determine the angle an organ grows.

In addition to promising to provide fundamental new insight into organ angle regulation, genetic studies described in chapter 3 of this thesis have revealed that allelic variation at the *EGT1* locus influences root angle in a barley diversity collection. This important observation opens up the possibility to exploit natural or induced allelic variation in *EGT1* in barley (and potentially other cereal crops) to select deeper rooting crop varieties with improved climate resilience and carbon offset potential.

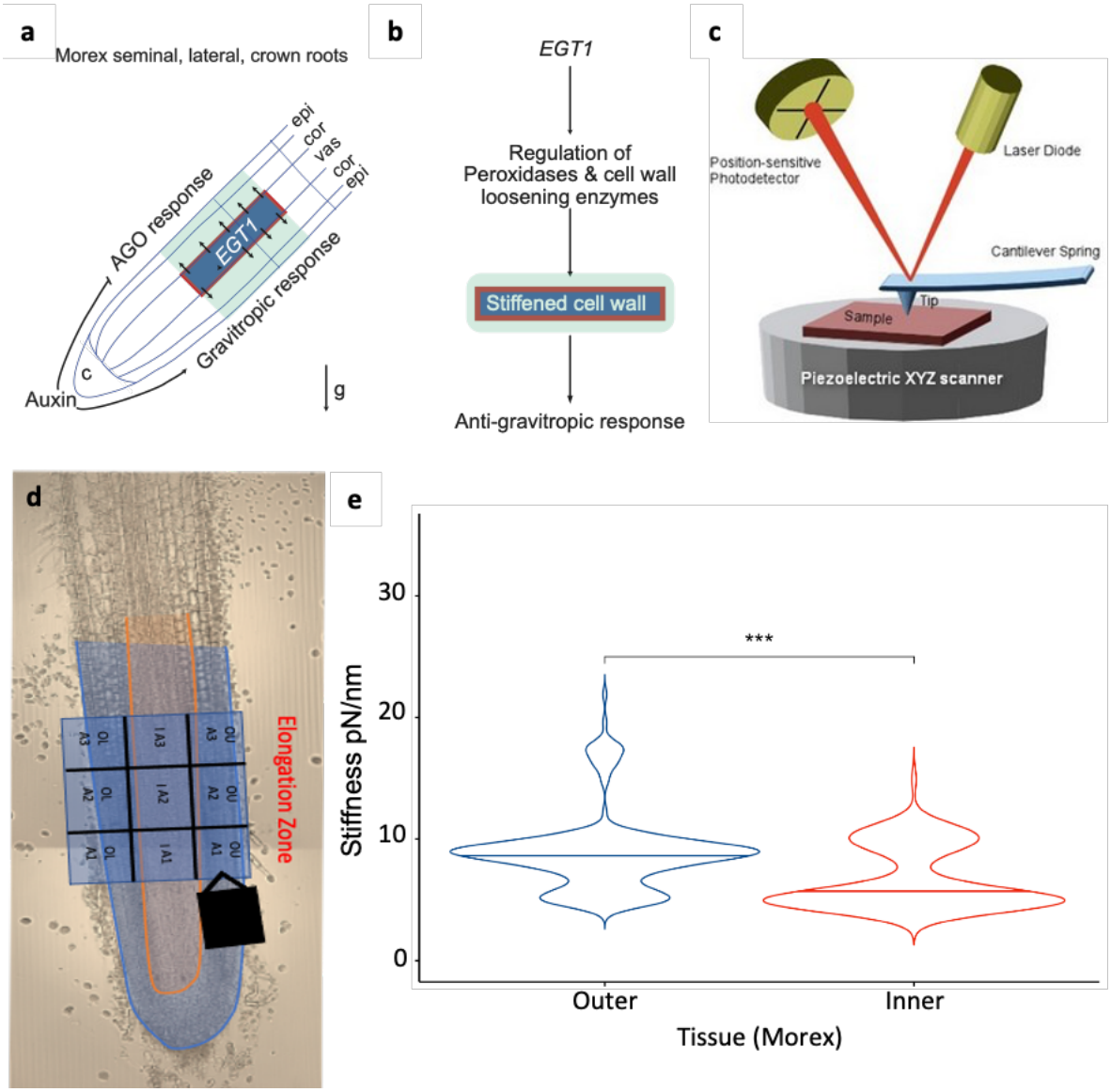


Fig. 5.1. Atomic Force Microscope (AFM) to investigate stiffness properties in root tissues. a-b) Hypothesised gravitropism mechanism regulated by HvEG1 where mutation in this gene de-regulates cell-wall stiffening in the inner tissues then blocking the Anti Gravitropic Offset machinery and enhancing gravitropic response. c) Schematic of the Atomic Force Microscope (AFM) components. The biological sample is mounted on a piezoelectric scanner while a probe and a set of laser and detectors measures stiffness force on a nanoscale level (UniBerkeley; Pattem *et al.*, 2018). d) Representative Morex root RAM longitudinal section slice of 50μm and probing methodology applied to test different areas within the elongation-division zone. Inner and outer tissues where initially divided in 3 different areas to test the robustness of the method. e) Difference in stiffness (pN/nm) between all the outer and inner tissues areas. *** indicates significant p value < 0.001 using Wilcoxon test.

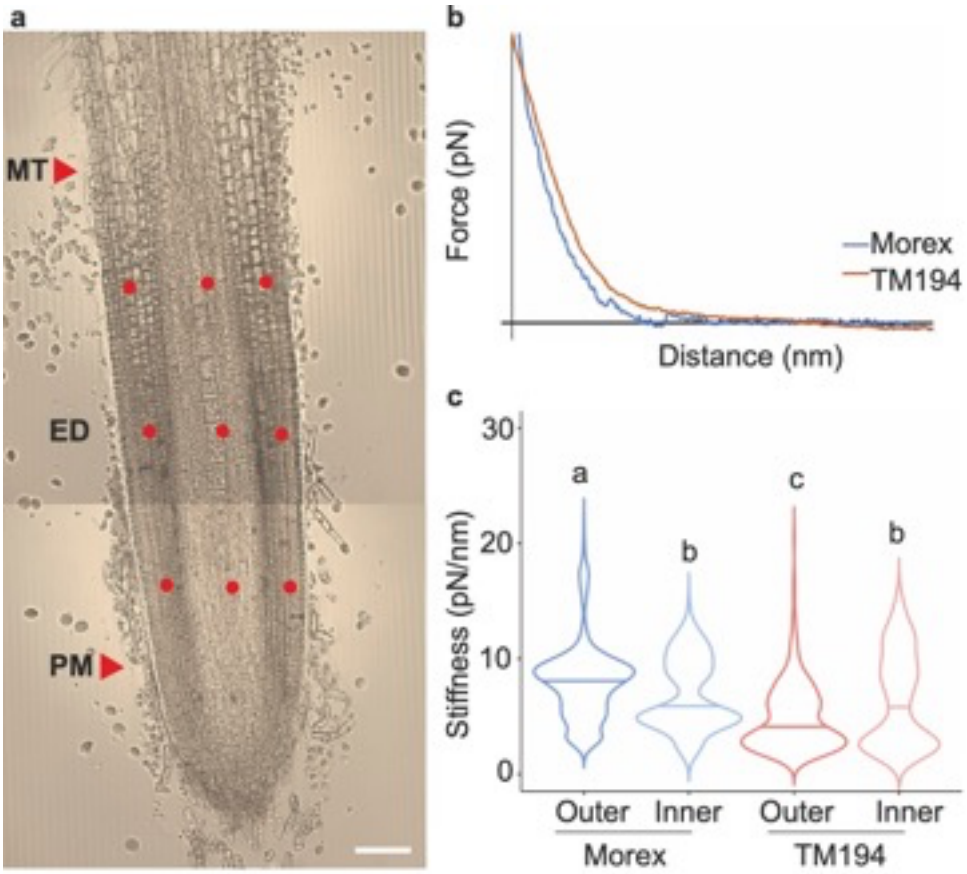


Fig. 5. 2 AFM nanomechanical force spectroscopy of tissues within the elongation zone of the root meristem in Morex and TM194

a) Example of a 50 µm longitudinal section of Morex (MT – maturation zone, ED – elongation/division zone and PM – proximal meristem). Red dots show approximate locations of AFM force spectroscopy tests. Indentations were performed in the observable centre of root meristem cells on each section generating a total of 100 < n < 360 force curves for each biological replicate. b) Example showing typical force-distance curves measured on Morex and TM194 sections. The slope of the indentation part of the curve was used for determining apparent stiffness (pN/nm). c) Summary of force spectroscopy results showing the stiffness values of the inner and outer areas of the tissue. The pooled data from each area was analysed using a non-parametric Wilcoxon test for significant differences between sample type and area ($p < 0.001$).

References

Abas L, Benjamins R, Malenica N, Paciorek T, Wišniewska J, Moulinier–Anzola JC, Sieberer T, Friml J, Luschnig C. 2006. Intracellular trafficking and proteolysis of the Arabidopsis auxin-efflux facilitator PIN2 are involved in root gravitropism. Nature cell biology **8**, 249–256.

Adamowski M, Friml J. 2015. PIN-dependent auxin transport: action, regulation, and evolution. The Plant Cell **27**, 20–32.

Alahmad S, El Hassouni K, Bassi FM, Dinglasan E, Youssef C, Quarry G, Aksoy A, Mazzucotelli E, Juhász A, Able JA. 2019. A major root architecture QTL responding to water limitation in durum wheat. Frontiers in plant science **10**, 436.

Anders S, Huber W. 2010. Differential expression analysis for sequence count data. Genome Biology **11**, R106.

Anders S, Pyl PT, Huber W. 2015. HTSeq—a Python framework to work with high-throughput sequencing data. Bioinformatics **31**, 166–169.

Atkinson JA, Wells DM. 2017. An Updated Protocol for High Throughput Plant Tissue Sectioning. Frontiers in Plant Science **8**, 1–8.

Band LR, Wells DM, Larrieu A, *et al.* 2012. Root gravitropism is regulated by a transient lateral auxin gradient controlled by a tipping-point mechanism. Proceedings of the National Academy of Sciences of the United States of America **109**, 4668–4673.

Beier S, Himmelbach A, Colmsee C, Zhang X-Q, Barrero RA, Zhang Q, Li L, Bayer M, Bolser D, Taudien S. 2017. Construction of a map-based reference genome sequence for barley, Hordeum vulgare L. Scientific Data **4**, 1–24.

Van Bel M, Diels T, Vancaester E, Kreft L, Botzki A, Van de Peer Y, Coppens F, Vandepoele K. 2018. PLAZA 4.0: an integrative resource for functional, evolutionary and comparative plant genomics. Nucleic acids research **46**, D1190–D1196.

Benfey PN, Bennett M, Schiefelbein J. 2010. Getting to the root of plant biology: impact of the Arabidopsis genome sequence on root research. The Plant journal : for cell and molecular biology **61**, 992–1000.

Benková E, Hejátko J. 2009. Hormone interactions at the root apical meristem. Plant Molecular Biology **69**, 383–396.

Benková E, Michniewicz M, Sauer M, Teichmann T, Seifertová D, Jürgens G, Friml J. 2003.

Local, efflux-dependent auxin gradients as a common module for plant organ formation. Cell **115**, 591–602.

Bennett MJ, Marchant A, Green HG, May ST. 1996*a*. Arabidopsis AUX1 gene: a permease-like regulator of root gravitropism. Science **273**, 948.

Bennett MJ, Marchant A, Green HG, May ST, Ward SP, Millner PA, Walker AR, Schulz B, Feldmann KA. 1996*b*. Arabidopsis AUX1 gene: A permease-like regulator of root gravitropism. Science **273**, 948–950.

Bensen RJ, Johal GS, Crane VC, Tossberg JT, Schnable PS, Meeley RB, Briggs SP. 1995. Cloning and characterization of the maize An1 gene. The Plant Cell **7**, 75–84.

Berezin C, Glaser F, Rosenberg J, Paz I, Pupko T, Fariselli P, Casadio R, Ben-Tal N. 2004. ConSeq: the identification of functionally and structurally important residues in protein sequences. Bioinformatics **20**, 1322–1324.

Billou I, Xu J, Wildwater M, Willemsen V, Paponov I, Frimi J, Heldstra R, Aida M, Palme K, Scheres B. 2005. The PIN auxin efflux facilitator network controls growth and patterning in Arabidopsis roots. Nature **433**, 39–44.

Bilsborough GD, Runions A, Barkoulas M, Jenkins HW, Hasson A, Galinha C, Laufs P, Hay A, Prusinkiewicz P, Tsiantis M. 2011. Model for the regulation of Arabidopsis thaliana leaf margin development. Proceedings of the National Academy of Sciences **108**, 3424–3429.

Bishopp A, Help H, El-Showk S, Weijers D, Scheres B, Friml J, Benková E, Mähönen AP, Helariutta Y. 2011. A mutually inhibitory interaction between auxin and cytokinin specifies vascular pattern in roots. Current Biology **21**, 917–926.

Boggon TJ, Shan W-S, Santagata S, Myers SC, Shapiro L. 1999. Implication of tubby proteins as transcription factors by structure-based functional analysis. Science **286**, 2119–2125.

Boonsirichai K, Sedbrook JC, Chen R, Gilroy S, Masson PH. 2003. ALTERED RESPONSE TO GRAVITY is a peripheral membrane protein that modulates gravity-induced cytoplasmic alkalinization and lateral auxin transport in plant statocytes. The Plant Cell **15**, 2612–2625.

Bovina R, Rosignoli S, Milner SG, Tuberosa R, Salvi S. 2020. A collection of root architecture mutants in barley (Hordeum vulgare L.) (Unpublished).

Bovina R, Talamè V, Ferri M, Tuberosa R, Chmielewska B, Szarejko I, Sanguineti MC. 2011. Identification of root morphology mutants in barley. Plant Genetic Resources: Characterisation and Utilisation **9**, 357–360.

Bragg N. J, Anderton A, Nieu R, Vogel JP. 2014. Agrobacterium protocols: Third edition.

Agrobacterium Protocols: Third Edition **1**, 1–368.

Bragg JN, Wu J, Gordon SP, Guttman ME, Thilmony R, Lazo GR, Gu YQ, Vogel JP. 2012. Generation and Characterization of the Western Regional Research Center Brachypodium T-DNA Insertional Mutant Collection. PLOS ONE **7**, e41916.

von Braun SS, Schleiff E. 2008. The chloroplast outer membrane protein CHUP1 interacts with actin and profilin. Planta **227**, 1151–1159.

Brown RH, Singh J, Singh S, Dahleen LS, Lemaux PG, Stein N, Mascher M, Bregitzer P. 2015. Behavior of a modified Dissociation element in barley: a tool for genetic studies and for breeding transgenic barley. Molecular Breeding **35**, 1–15.

Brunoud G, Wells DM, Oliva M, *et al.* 2012. A novel sensor to map auxin response and distribution at high spatio-temporal resolution. Nature **482**, 103–106.

Brutnell TP, Bennetzen JL, Vogel JP. 2015. *Brachypodium distachyon* and *Setaria viridis* : Model Genetic Systems for the Grasses. Annual Review of Plant Biology **66**, 465–485.

Burghardt LT, Young ND, Tiffin P. 2017. A Guide to Genome-Wide Association Mapping in Plants. Current Protocols in Plant Biology **2**, 22–38.

Burton RA, Gidley MJ, Fincher GB. 2010. Heterogeneity in the chemistry, structure and function of plant cell walls. Nature chemical biology **6**, 724–732.

Bustos-Korts D, Dawson IK, Russell J, *et al.* 2019. Exome sequences and multi-environment field trials elucidate the genetic basis of adaptation in barley. Plant Journal **99**, 1172–1191.

Butt H-J, Cappella B, Kappl M. 2005. Force measurements with the atomic force microscope: Technique, interpretation and applications. Surface science reports **59**, 1–152.

Cermak T, Curtin SJ, Gil-Humanes J, *et al.* 2017. A multi-purpose toolkit to enable advanced genome engineering in plants. The Plant Cell, tpc.00922.2016.

Char SN, Neelakandan AK, Nahampun H, *et al.* 2017. An Agrobacterium-delivered CRISPR/Cas9 system for high-frequency targeted mutagenesis in maize. Plant Biotechnology Journal **15**, 257–268.

Chimungu JG, Brown KM, Lynch JP. 2014. Reduced Root Cortical Cell File Number Improves Drought Tolerance in Maize. Plant Physiology **166**, 1943–1955.

Chmielewska B, Janiak A, Karcz J, Guzy-Wrobelska J, Forster BP, Nawrot M, Rusek A, Smyda P, Kedziorski P, Maluszynski M. 2014. Morphological, genetic and molecular characteristics of barley root hair mutants. Journal of applied genetics **55**, 433–447.

Chochois V, Voge JP, Rebetzke GJ, Watt M. 2015. Variation in adult plant phenotypes and

partitioning among seed and stem-borne roots across Brachypodium distachyon accessions to exploit in breeding cereals for well-watered and drought environments. Plant Physiology **168**, 953–967.

Cholodny N. 1927. Wuchshormone and Tropismen bei den Pflanzen. Biol Zentralbl **47**, 604–629.

Cingolani P, Platts A, Wang LL, Coon M, Nguyen T, Wang L, Land SJ, Lu X, Ruden DM. 2012. A program for annotating and predicting the effects of single nucleotide polymorphisms, SnpEff. Fly **6**, 80–92.

Clement M, Snell Q, Walker P, Posada D, Crandall K. 2002. TCS: estimating gene genealogies. Parallel and Distributed Processing Symposium, International. IEEE Computer Society, 184.

Comadran J, Kilian B, Russell J, *et al.* 2012. Natural variation in a homolog of Antirrhinum CENTRORADIALIS contributed to spring growth habit and environmental adaptation in cultivated barley. Nature Genetics **44**, 1388–1392.

Concordet J-P, Haeussler M. 2018. CRISPOR: intuitive guide selection for CRISPR/Cas9 genome editing experiments and screens. Nucleic Acids Research **46**, W242–W245.

Darwin C, Darwin F. 1880. Sensitiveness of plants to light: it's transmitted effect. The power of movement in plants.

Deacon JW, Drew MC, Darling A. 1986. Progressive cortical senescence and formation of lysigenous gas space (aerenchyma) distinguished by nuclear staining in adventitious roots of Zea mays. Annals of Botany **58**, 719–727.

Deltcheva E, Chylinski K, Sharma CM, Gonzales K, Yanjie C, Zaid A. P, Maria R. E, Jorg V, Charpentier E. 2011. CRISPR RNA maturation by trans-encoded small RNA and host factor RNase III. Nature. **471**, 602–607.

DIGBY J, FIRN RD. 1995. The gravitropic set-point angle (GSA): the identification of an important developmentally controlled variable governing plant architecture. Plant, Cell & Environment **18**, 1434–1440.

Dinneny JR, Mace D, Ohler U, Benfey PN. 2007. Dominant Expression Patterns. Cell, 801–806.

Dolan L, Janmaat K, Willemsen V, Linstead P, Poethig S, Roberts K, Scheres B. 1993. Cellular organisation of the Arabidopsis thaliana root. Development **119**, 71–84.

Draper J, Mur L a. J, Jenkins G, Ghosh-Biswas GC, Bablak P, Hasterok R, Routledge APM. 2001. Brachypodium distachyon. A New Model System for Functional Genomics in Grasses1. Plant physiology **127**, 1539–1555.

Duhamel du Monceau HL. 1758. La physique des arbres, ou il est traite de l'anatomie des plantes et de l'economie vegetale, pour servir d'introduction au traite complet des bois et des forSts; avec une dissertation sur l'utilite des methodes de botanique.

Edgar RC. 2004. MUSCLE: a multiple sequence alignment method with reduced time and space complexity. BMC bioinformatics **5**, 1–19.

Fagerstedt K V. 2010. Programmed Cell Death and Aerenchyma Formation Under Hypoxia. , 99–118.

FAO. 2019. FAOSTAT Statistics Database. 2019.

Feldman L. 1994. The Maize Root. In: Freeling M,, In: Walbot V, eds. The Maize Handbook. New York, NY: Springer New York, 29–37.

Francoz E, Ranocha P, Nguyen-Kim H, Jamet E, Burlat V, Dunand C. 2015. Roles of cell wall peroxidases in plant development. Phytochemistry **112**, 15–21.

Friml J, Wisniewska J, Benkova E, Mendgen K, Palme K. 2002. Lateral relocation of auxin efflux regulator PIN3 mediates tropism in ArabidopsisFriml, Jiří; Wiśniewska, Justyna; Benková, Eva; Mendgen, Kur Lateral relocation of auxin efflux regulator PIN3 mediates tropism in Arabidopsis. Letters to Nature **415**, 1–4.

Fulton L, Batoux M, Vaddepalli P, Yadav RK, Busch W, Andersen SU, Jeong S, Lohmann JU, Schneitz K. 2009. DETORQUEO, QUIRKY, and ZERZAUST represent novel components involved in organ development mediated by the receptor-like kinase STRUBBELIG in Arabidopsis thaliana. PLoS Genetics **5**.

Gagne JM, Downes BP, Shiu S-H, Durski AM, Vierstra RD. 2002. The F-box subunit of the SCF E3 complex is encoded by a diverse superfamily of genes in Arabidopsis. Proceedings of the national academy of sciences **99**, 11519–11524.

Gahoonia TS, Nielsen NE, Joshi PA, Jahoor A. 2001. A root hairless barley mutant for elucidating genetic of root hairs and phosphorus uptake. Plant and Soil **235**, 211–219.

Gälweiler L, Guan C, Müller A, Wisman E, Mendgen K, Yephremov A, Palme K. 1998. Regulation of polar auxin transport by AtPIN1 in Arabidopsis vascular tissue. Science **282**, 2226–2230.

Gasparis S, Kała M, Przyborowski M, Łyznik LA, Orczyk W, Nadolska-Orczyk A. 2018. A simple and efficient CRISPR/Cas9 platform for induction of single and multiple, heritable mutations in barley (Hordeum vulgare L.). Plant Methods **14**, 1–14.

Gasparis S, Przyborowski M, Kała M, Nadolska-Orczyk A. 2019. Knockout of the HvCKX1 or

HvCKX3 gene in barley (Hordeum vulgare L.) by RNA-Guided Cas9 Nuclease affects the regulation of cytokinin metabolism and root morphology. Cells **8**, 782.

Ghosh S, Watson A, Gonzalez-Navarro OE, *et al.* 2018. Speed breeding in growth chambers and glasshouses for crop breeding and model plant research. Nature Protocols **13**, 2944–2963.

Gottwald S, Bauer P, Komatsuda T, Lundqvist U, Stein N. 2009. TILLING in the two-rowed barley cultivar 'Barke' reveals preferred sites of functional diversity in the gene HvHox1. BMC Research Notes **2**, 258.

Gray WM, Kepinski S, Rouse D, Leyser O, Estelle M. 2001. Auxin regulates SCFTIR1-dependent degradation of AUX/IAA proteins. Nature **414**, 271–276.

Guenot B, Bayer E, Kierzkowski D, Smith RS, Mandel T, Žádníková P, Benková E, Kuhlemeier C. 2012. PIN1-Independent Leaf Initiation in Arabidopsis . Plant Physiology **159**, 1501–1510.

Guyomarc'h S, Léran S, Auzon-Cape M, Perrine-Walker F, Lucas M, Laplaze L. 2012. Early development and gravitropic response of lateral roots in Arabidopsis thaliana. Philosophical Transactions of the Royal Society B: Biological Sciences **367**, 1509–1516.

Hansey CN, Johnson JM, Sekhon RS, Kaeppler SM, de Leon N. 2011. Genetic diversity of a maize association population with restricted phenology. Crop Science **51**, 704–715.

Hart JW. 1990. *Plant tropisms: and other growth movements*. Springer Science & Business Media.

Hay A, Barkoulas M, Tsiantis M. 2006. ASYMMETRIC LEAVES1 and auxin activities converge to repress BREVIPEDICELLUS expression and promote leaf development in Arabidopsis.

Hendow EK, Moazen M, Iacoviello F, Bozec L, Pellet-Many C, Day RM. 2020. Microporous Biodegradable Films Promote Therapeutic Angiogenesis. Advanced Healthcare Materials **9**, 2000806.

Ho MD, Rosas JC, Brown KM, Lynch JP. 2005. Root architectural tradeoffs for water and phosphorus acquisition. Functional Plant Biology **32**, 737–748.

Hochholdinger F. 2009*a*. The Maize Root System: Morphology, Anatomy, and Genetics. In: Bennetzen JL,, In: Hake SC, eds. Handbook of Maize: Its Biology. New York, NY: Springer New York, 145–160.

Hochholdinger F. 2009*b*. The Maize Root System: Morphology, Anatomy, and Genetics. In: Bennetzen JL,, In: Hake SC, eds. Handbook of Maize: Its Biology. New York, NY: Springer New York, 145–160.

Hochholdinger F, Zimmermann R. 2008. Conserved and diverse mechanisms in root development. Current Opinion in Plant Biology **11**, 70–74.

Hoppe DC, McCully ME, Wenzel CL. 1986. The nodal roots of Zea: their development in relation to structural features of the stem. Canadian Journal of Botany **64**, 2524–2537.

Hsia MM, O'Malley R, Cartwright A, *et al.* 2017. Sequencing and functional validation of the JGI Brachypodium distachyon T-DNA collection. The Plant Journal **91**, 361–370.

Hu Z, Qi X, Zhang M, Chen X, Nakazono M. 2016. Roles of Phytohormones in Morphological and Anatomical Responses of Plants to Flooding Stress BT - Plant Hormones under Challenging Environmental Factors. In: Ahammed GJ,, In: Yu J-Q, eds. Dordrecht: Springer Netherlands, 117–132.

Huang X. 2019. Achieving sustainable cultivation of barley. , 457–470.

Huang G, Liang W, Sturrock CJ, *et al.* 2018. Rice actin binding protein RMD controls crown root angle in response to external phosphate. Nature Communications **9**, 1–9.

Hyten DL, Song Q, Choi I-Y, Yoon M-S, Specht JE, Matukumalli LK, Nelson RL, Shoemaker RC, Young ND, Cregan PB. 2008. High-throughput genotyping with the GoldenGate assay in the complex genome of soybean. Theoretical and Applied Genetics **116**, 945–952.

IPCC. 2014. Part A: Global and Sectoral Aspects. (Contribution of Working Group II to the Fifth Assessment Report of the Intergovernmental Panel on Climate Change). Climate Change 2014: Impacts, Adaptation, and Vulnerability., 1132.

Jackson VG. 1922. Anatomical structure of the roots of barley. Annals of Botany **os**-**36**, 21–40.

Jaganathan D, Ramasamy K, Sellamuthu G, Jayabalan S, Venkataraman G. 2018. CRISPR for Crop Improvement: An Update Review. Frontiers in Plant Science **9**, 1–17.

Jia Z, Liu Y, Gruber BD, Neumann K, Kilian B, Graner A, Von Wirén N. 2019. Genetic dissection of root system architectural traits in spring barley. Frontiers in plant science **10**, 400.

Jiao Z, Du H, Chen S, Huang W, Ge L. 2021. LAZY Gene Family in Plant Gravitropism. Frontiers in Plant Science **11**, 1–12.

Jinek M, Chylinski K, Fonfara I, Hauer M, Doudna JA, Charpentier E. 2012. A Programmable Dual-RNA – Guided. **337**, 816–822.

Jones T, Lowe K, Hoerster G, Anand A, Wu E, Wang N, Arling M, Lenderts B, Gordon-Kamm W. 2019. Maize transformation using the morphogenic genes Baby Boom and Wuschel2. Transgenic Plants. Springer, 81–93.

Jouhet J, Gray JC. 2009. Interaction of actin and the chloroplast protein import apparatus. Journal of Biological Chemistry **284**, 19132–19141.

Kawamoto N, Kanbe Y, Nakamura M, Mori A. 2020. Required for " Anti-Gravitropic " Phenotypes of lzy. Plants **1**.

Kelley LA, Mezulis S, Yates CM, Wass MN, Sternberg MJE. 2015. The Phyre2 web portal for protein modeling, prediction and analysis. Nature protocols **10**, 845–858.

Kile BT, Schulman BA, Alexander WS, Nicola NA, Martin HME, Hilton DJ. 2002. The SOCS box: a tale of destruction and degradation. Trends in biochemical sciences **27**, 235–241.

Kim D, Paggi JM, Park C, Bennett C, Salzberg SL. 2019. Graph-based genome alignment and genotyping with HISAT2 and HISAT-genotype. Nature biotechnology **37**, 907–915.

Kirschner GK, Stahl Y, Imani J, von Korff M, Simon R. 2018. Fluorescent reporter lines for auxin and cytokinin signalling in barley (Hordeum vulgare). PLoS ONE **13**, 1–25.

Kirschner GK, Stahl Y, Von Korff M, Simon R. 2017. Unique and conserved features of the barley root meristem. Frontiers in Plant Science **8**.

Kitomi Y, Hanzawa E, Kuya N, Inoue H, Hara N, Kawai S, Kanno N, Endo M, Sugimoto K, Yamazaki T. 2020. Root angle modifications by the DRO1 homolog improve rice yields in saline paddy fields. Proceedings of the National Academy of Sciences **117**, 21242–21250.

Klein SP, Schneider HM, Perkins AC, Brown KM, Lynch JP. 2020. Multiple Integrated Root Phenotypes Are Associated with Improved Drought Tolerance. Plant Physiology **183**, 1011 LP – 1025.

Kleine-Vehn J, Ding Z, Jones AR, Tasaka M, Morita MT, Friml J. 2010. Gravity-induced PIN transcytosis for polarization of auxin fluxes in gravity-sensing root cells. Proceedings of the National Academy of Sciences of the United States of America **107**, 22344–22349.

Knight TA. 1806. V. On the direction of the radicle and germen during the vegetation of seeds. By Thomas Andrew knight, Esq. FRS In a letter to the right Hon. Sir Joseph banks, KBPR S. Philosophical Transactions of the Royal Society of London, 99–108.

Kolkman JM, Conrad LJ, Farmer PR, Hardeman K, Ahern KR, Lewis PE, Sawers RJH, Lebejko S, Chomet P, Brutnell TP. 2005. Distribution of Activator (Ac) throughout the maize genome for use in regional mutagenesis. Genetics **169**, 981–995.

Konings H, de Wolf A. 1984. Promotion and inhibition by plant growth regulators of aerenchyma formation in seedling roots of Zea mays. Physiologia Plantarum **60**, 309–314.

Kozlova L, Petrova A, Ananchenko B, Gorshkova T. 2019. Assessment of Primary Cell Wall

Nanomechanical Properties in Internal Cells of Non-Fixed Maize Roots. Plants **8**.

Krasileva K V, Vasquez-Gross HA, Howell T, *et al.* 2017. Uncovering hidden variation in polyploid wheat. Proceedings of the National Academy of Sciences **114**, E913 LP-E921.

Kumar S, Stecher G, Li M, Knyaz C, Tamura K. 2018. MEGA X: molecular evolutionary genetics analysis across computing platforms. Molecular biology and evolution **35**, 1547–1549.

Kumlehn J. 2016. Embryogenesis and plant regeneration from isolated wheat zygotes. In Vitro Embryogenesis in Higher Plants. Springer, 503–514.

Kurihara D, Mizuta Y, Sato Y, Higashiyama T. 2015. ClearSee: a rapid optical clearing reagent for whole-plant fluorescence imaging. Development **142**, 4168–4179.

Lai C-P, Lee C-L, Chen P-H, Wu S-H, Yang C-C, Shaw J-F. 2004. Molecular analyses of the Arabidopsis TUBBY-like protein gene family. Plant Physiology **134**, 1586–1597.

Lawrenson T, Harwood WA. 2019. Creating targeted gene knockouts in barley using CRISPR/Cas9. Barley. Springer, 217–232.

Leyser O. 1999. Plant hormones: Ins and outs of auxin transport. Current Biology **9**, R8.

Li H. 2011. A statistical framework for SNP calling, mutation discovery, association mapping and population genetical parameter estimation from sequencing data. Bioinformatics **27**, 2987–2993.

Li H, Durbin R. 2009. Fast and accurate short read alignment with Burrows–Wheeler transform. Bioinformatics **25**, 1754–1760.

Li H, Handsaker B, Wysoker A, Fennell T, Ruan J, Homer N, Marth G, Abecasis G, Durbin R, Subgroup 1000 Genome Project Data Processing. 2009. The Sequence Alignment/Map format and SAMtools. Bioinformatics **25**, 2078–2079.

Li Z, Li P, Zhang J. 2019. Expression analysis of PIN-formed auxin efflux transporter genes in maize. Plant Signaling & Behavior **14**, 1632689.

Li Y, Segal G, Wang Q, Dooner HK. 2013. Gene tagging with engineered Ds elements in maize. Plant Transposable Elements. Springer, 83–99.

Liu X, Huang M, Fan B, Buckler ES, Zhang Z. 2016. Iterative Usage of Fixed and Random Effect Models for Powerful and Efficient Genome-Wide Association Studies. PLOS Genetics **12**, e1005767.

Liu HJ, Jian L, Xu J, *et al.* 2020. High-throughput CRISPR/Cas9 mutagenesis streamlines trait gene identification in maize. Plant Cell **32**, 1397–1413.

Lynch JP. 1995. Root Architecture and Plant Productivity. Plant Physiology **109**, 7–13.

Lynch JP. 2013. Steep, cheap and deep: an ideotype to optimize water and N acquisition by maize root systems. Annals of Botany **112**, 347–357.

Lynch JP. 2015. Root phenes that reduce the metabolic costs of soil exploration: Opportunities for 21st century agriculture. Plant, Cell and Environment **38**, 1775–1784.

Lynch JP. 2019. Root phenotypes for improved nutrient capture: an underexploited opportunity for global agriculture. New Phytologist.

Mace ES, Singh V, Van Oosterom EJ, Hammer GL, Hunt CH, Jordan DR. 2012. QTL for nodal root angle in sorghum (Sorghum bicolor L. Moench) co-locate with QTL for traits associated with drought adaptation. Theoretical and Applied Genetics **124**, 97–109.

Maddison DR, Swofford DL, Maddison WP. 1997. NEXUS: an extensible file format for systematic information. Systematic biology **46**, 590–621.

Mairhofer S, Zappala S, Tracy SR, Sturrock C, Bennett M, Mooney SJ, Pridmore T. 2012. RooTrak: Automated Recovery of Three-Dimensional Plant Root Architecture in Soil from X-Ray Microcomputed Tomography Images Using Visual Tracking. Plant Physiology **158**, 561–569.

Mascher M, Gundlach H, Himmelbach A, *et al.* 2017. A chromosome conformation capture ordered sequence of the barley genome. Nature **544**, 427–433.

Mascher M, Jost M, Kuon J-E, Himmelbach A, Aßfalg A, Beier S, Scholz U, Graner A, Stein N. 2014. Mapping-by-sequencing accelerates forward genetics in barley. Genome Biology **15**, R78.

Mascher M, Muehlbauer GJ, Rokhsar DS, *et al.* 2013*a*. Anchoring and ordering NGS contig assemblies by population sequencing (POPSEQ). The Plant Journal **76**, 718–727.

Mascher M, Richmond TA, Gerhardt DJ, *et al.* 2013*b*. Barley whole exome capture: a tool for genomic research in the genus Hordeum and beyond. The Plant Journal **76**, 494–505.

May BP, Liu H, Vollbrecht E, Senior L, Rabinowicz PD, Roh D, Pan X, Stein L, Freeling M, Alexander D. 2003. Maize-targeted mutagenesis: a knockout resource for maize. Proceedings of the National Academy of Sciences **100**, 11541–11546.

Mayer KFX, Waugh R, Langridge P, *et al.* 2012. A physical, genetic and functional sequence assembly of the barley genome. Nature **491**, 711–716.

McCallum CM, Comai L, Greene EA, Henikoff S. 2000. Targeted screening for induced mutations. Nature biotechnology **18**, 455–457.

McCarty DR, Mark Settles A, Suzuki M, *et al.* 2005*a*. Steady-state transposon mutagenesis in

inbred maize. Plant Journal **44**, 52–61.

McCarty DR, Mark Settles A, Suzuki M, Tan BC, Latshaw S, Porch T, Robin K, Baier J, Avigne W, Lai J. 2005*b*. Steady-state transposon mutagenesis in inbred maize. The Plant Journal **44**, 52–61.

McCarty DR, Meeley RB. 2009. Transposon resources for forward and reverse genetics in maize. Handbook of Maize. Springer, 561–584.

McCaw ME, Wallace JG, Albert PS, Buckler ES, Birchler JA. 2016. Fast-flowering mini-maize: Seed to seed in 60 days. Genetics **204**, 35–42.

McCully ME, Canny MJ. 1988. Pathways and processes of water and nutrient movement in roots. Plant and Soil **111**, 159–170.

Miao J, Guo D, Zhang J, Huang Q, Qin G, Zhang X, Wan J, Gu H, Qu LJ. 2013. Targeted mutagenesis in rice using CRISPR-Cas system. Cell Research **23**, 1233–1236.

Michelmore RW, Paran I, Kesseli R V. 1991. Identification of markers linked to disease-resistance genes by bulked segregant analysis: a rapid method to detect markers in specific genomic regions by using segregating populations. Proceedings of the National Academy of Sciences **88**, 9828 LP – 9832.

Morita MT, Tasaka M. 2004. Gravity sensing and signaling. Current opinion in plant biology **7**, 712–718.

Mühlenbock P, Plaszczyca M, Plaszczyca M, Mellerowicz E, Karpinski S. 2007. Lysigenous aerenchyma formation in Arabidopsis is controlled by LESION SIMULATING DISEASE1. Plant Cell **19**, 3819–3830.

Myers AB, Firn RD, Digby J. 1994. Gravitropic sign reversal-a fundamental feature of the gravitropic perception or response mechanisms in some plant organs. Journal of Experimental Botany **45**, 77–83.

Nagel KA, Putz A, Gilmer F, Heinz K, Fischbach A, Pfeifer J, Faget M, Blossfeld S, Ernst M, Dimaki C. 2012. GROWSCREEN-Rhizo is a novel phenotyping robot enabling simultaneous measurements of root and shoot growth for plants grown in soil-filled rhizotrons. Functional Plant Biology **39**, 891–904.

Nice LM, Steffenson BJ, Brown-Guedira GL, Akhunov ED, Liu C, Kono TJY, Morrell PL, Blake TK, Horsley RD, Smith KP. 2016. Development and genetic characterization of an advanced backcross-nested association mapping (AB-NAM) population of wild× cultivated barley. Genetics **203**, 1453–1467.

O'Connor DL, Leyser O, Hsia MM, Vogel JP, Ticchiarelli F, Elton S. 2017. Cross-species functional diversity within the PIN auxin efflux protein family. eLife **6**, 1–29.

O'Connor DL, Runions A, Sluis A, Bragg J, Vogel JP, Prusinkiewicz P, Hake S. 2014. A division in PIN-mediated auxin patterning during organ initiation in grasses. PLoS Computational Biology **10**, e1003447.

Omelyanchuk NA, Kovrizhnykh V V, Oshchepkova EA, Pasternak T, Palme K, Mironova V V. 2016. A detailed expression map of the PIN1 auxin transporter in Arabidopsis thaliana root. BMC plant biology **16**, 1–12.

Opitz N, Marcon C, Paschold A, Malik WA, Lithio A, Brandt R, Piepho HP, Nettleton D, Hochholdinger F. 2016. Extensive tissue-specific transcriptomic plasticity in maize primary roots upon water deficit. Journal of Experimental Botany **67**, 1095–1107.

Ottenschläger I, Wolff P, Wolverton C, Bhalerao RP, Sandberg G, Ishikawa H, Evans M, Palme K. 2003. Gravity-regulated differential auxin transport from columella to lateral root cap cells. Proceedings of the National Academy of Sciences **100**, 2987–2991.

Oyiga BC, Palczak J, Wojciechowski T, Lynch JP, Naz AA, Léon J, Ballvora A. 2020. Genetic components of root architecture and anatomy adjustments to water-deficit stress in spring barley. Plant Cell and Environment **43**, 692–711.

Paradis E. 2010. pegas: an R package for population genetics with an integrated–modular approach. Bioinformatics **26**, 419–420.

Pattem J, Davrandi M, Aguayo S, Allan E, Spratt D, Bozec L. 2018. A Multi-scale Biophysical Approach to Develop Structure-Property Relationships in Oral Biofilms. Scientific Reports **8**, 1–10.

Petrášek J, Mravec J, Bouchard R, Blakeslee JJ, Abas M, Seifertová D, Wiśniewska J, Tadele Z, Kubeš M, Čovanová M. 2006. PIN proteins perform a rate-limiting function in cellular auxin efflux. Science **312**, 914–918.

Portwood II JL, Woodhouse MR, Cannon EK, *et al.* 2019. MaizeGDB 2018: the maize multi-genome genetics and genomics database. Nucleic Acids Research **47**, D1146–D1154.

Price MN, Dehal PS, Arkin AP. 2009. FastTree: computing large minimum evolution trees with profiles instead of a distance matrix. Molecular biology and evolution **26**, 1641–1650.

Raggi S, Ferrarini A, Delledonne M, Dunand C, Ranocha P, De Lorenzo G, Cervone F, Ferrari S. 2015. The Arabidopsis class III peroxidase AtPRX71 negatively regulates growth under physiological conditions and in response to cell wall damage. Plant physiology **169**, 2513–

2525.

Raizada MN. 2003. RescueMu protocols for maize functional genomics. Plant Functional Genomics. Springer, 37–58.

Ramireddy E, Hosseini SA, Eggert K, Gillandt S, Gnad H, von Wirén N, Schmülling T. 2018. Root Engineering in Barley: Increasing Cytokinin Degradation Produces a Larger Root System, Mineral Enrichment in the Shoot and Improved Drought Tolerance. Plant physiology **177**, 1078–1095.

Raudvere U, Kolberg L, Kuzmin I, Arak T, Adler P, Peterson H, Vilo J. 2019. g:Profiler: a web server for functional enrichment analysis and conversions of gene lists (2019 update). Nucleic Acids Research **47**, W191–W198.

Rebouillat J, Dievart A, Verdeil JL, Escoute J, Giese G, Breitler JC, Gantet P, Espeout S, Guiderdoni E, Périn C. 2009. Molecular genetics of rice root development. Rice **2**, 15–34.

Reinhardt D, Pesce E-R, Stieger P, Mandel T, Baltensperger K, Bennett M, Traas J, Friml J, Kuhlemeier C. 2003. Regulation of phyllotaxis by polar auxin transport. Nature **426**, 255–260.

Reitz MU, Bissue JK, Zocher K, Attard A, Hückelhoven R, Becker K, Imani J, Eichmann R, Schäfer P. 2012. The subcellular localization of tubby-like proteins and participation in stress signaling and root colonization by the mutualist Piriformospora indica. Plant Physiology **160**, 349–364.

Roberts A, Pimentel H, Trapnell C, Pachter L. 2011. Identification of novel transcripts in annotated genomes using RNA-Seq. Bioinformatics **27**, 2325–2329.

Robinson H, Hickey L, Richard C, Mace E, Kelly A, Borrell A, Franckowiak J, Fox G. 2016. Genomic regions influencing seminal root traits in barley. The plant genome **9**, plantgenome2015-03.

Robinson JT, Thorvaldsdóttir H, Winckler W, Guttman M, Lander ES, Getz G, Mesirov JP. 2011. Integrative genomics viewer. Nature biotechnology **29**, 24–26.

Rosquete MR, Von Wangenheim D, Marhavý P, Barbez E, Stelzer EHK, Benková E, Maizel A, Kleine-Vehn J. 2013. An auxin transport mechanism restricts positive orthogravitropism in lateral roots. Current biology **23**, 817–822.

Roychoudhry S, Del Bianco M, Kieffer M, Kepinski S. 2013. Auxin controls gravitropic setpoint angle in higher plant lateral branches. Current Biology **23**, 1497–1504.

Roychoudhry S, Kepinski S. 2015. Shoot and root branch growth angle control-the wonderfulness of lateralness. Current Opinion in Plant Biology **23**, 124–131.

Roychoudhry S, Kieffer M, Del Bianco M, Liao CY, Weijers D, Kepinski S. 2017. The developmental and environmental regulation of gravitropic setpoint angle in Arabidopsis and bean. Scientific Reports **7**, 1–12.

RStudio Team. 2020. RStudio: Integrated Development for R. RStudio, PBC, Boston, MA.

Di Ruocco G, Di Mambro R, Dello Ioio R. 2018. Building the differences: a case for the ground tissue patterning in plants. Proceedings of the Royal Society B: Biological Sciences **285**, 20181746.

Russell J, Mascher M, Dawson IK, *et al.* 2016. Exome sequencing of geographically diverse barley landraces and wild relatives gives insights into environmental adaptation. Nature Genetics **48**, 1024–1030.

Salvi S, Druka A, Milner SG, Gruszka D. 2014. Biotechnological Approaches to Barley Improvement. **69**, 287–310.

Santagata S, Boggon TJ, Baird CL, Gomez CA, Zhao J, Shan WS, Myszka DG, Shapiro L. 2001. G-protein signaling through tubby proteins. Science **292**, 2041–2050.

Sato EM, Hijazi H, Bennett MJ, Vissenberg K, Swarup R. 2015. New insights into root gravitropic signalling. Journal of Experimental Botany **66**, 2155–2165.

Sato Y, Takehisa H, Kamatsuki K, Minami H, Namiki N, Ikawa H, Ohyanagi H, Sugimoto K, Antonio BA, Nagamura Y. 2013. RiceXPro Version 3.0: Expanding the informatics resource for rice transcriptome. Nucleic Acids Research **41**, 1206–1213.

Scarpella E, Marcos D, Friml J, Berleth T. 2006. Control of leaf vascular patterning by polar auxin transport. Genes & development **20**, 1015–1027.

Schindelin J, Arganda-Carreras I, Frise E, Kaynig V, Longair M, Pietzsch T, Preibisch S, Rueden C, Saalfeld S, Schmid B. 2012. Fiji: an open-source platform for biological-image analysis. Nature methods **9**, 676–682.

Schneider HM, Klein SP, Hanlon MT, Kaeppler S, Brown KM, Lynch JP. 2020*a*. Genetic control of root anatomical plasticity in maize. The Plant Genome **13**, e20003.

Schneider HM, Klein SP, Hanlon MT, Nord EA, Kaeppler S, Brown KM, Warry A, Bhosale R, Lynch JP, Dodd I. 2020*b*. Genetic control of root architectural plasticity in maize. Journal of Experimental Botany **71**, 3185–3197.

Schneider HM, Lor VSN, Hanlon MT, *et al.* 2021*a*. Root angle in maize influences nitrogen capture and is regulated by calcineurin B-like protein (CBL)-interacting serine/threonine-protein kinase 15 (ZmCIPK15). Plant, Cell & Environment **n/a**.

Schneider HM, Strock CF, Hanlon MT, Vanhees DJ, Perkins AC, Ajmera IB, Sidhu JS, Mooney SJ, Brown KM, Lynch JP. 2021*b*. Multiseriate cortical sclerenchyma enhance root penetration in compacted soils. Proceedings of the National Academy of Sciences of the United States of America **118**, 1–11.

Schneider HM, Wojciechowski T, Postma JA, Brown KM, Lücke A, Zeisler V, Schreiber L, Lynch JP. 2017. Root cortical senescence decreases root respiration, nutrient content and radial water and nutrient transport in barley. Plant Cell and Environment **40**, 1392–1408.

Schneider HM, Wojciechowski T, Postma JA, Brown KM, Lynch JP. 2018. Ethylene modulates root cortical senescence in barley. Annals of botany **122**, 95–105.

Schoonenberg VAC, Cole MA, Yao Q, Macias-Treviño C, Sher F, Schupp PG, Canver MC, Maeda T, Pinello L, Bauer DE. 2018. CRISPRO: identification of functional protein coding sequences based on genome editing dense mutagenesis. Genome Biology **19**, 169.

Schreiber M, Barakate A, Uzrek N, Macaulay M, Sourdille A, Morris J, Hedley PE, Ramsay L, Waugh R. 2019. A highly mutagenised barley (cv. Golden Promise) TILLING population coupled with strategies for screening-by-sequencing. Plant methods **15**, 1–14.

Sekhon RS, Lin H, Childs KL, Hansey CN, Robin Buell C, De Leon N, Kaeppler SM. 2011. Genome-wide atlas of transcription during maize development. Plant Journal **66**, 553–563.

Shiono K, Yamada S. 2014. Waterlogging tolerance and capacity for oxygen transport in Brachypodium distachyon (Bd21). Plant Root **8**, 5–12.

De Smet S, Cuypers A, Vangronsveld J, Remans T. 2015. Gene Networks Involved in Hormonal Control of Root Development in Arabidopsis thaliana: A Framework for Studying Its Disturbance by Metal Stress. International Journal of Molecular Sciences **16**, 19195.

Smith S, De Smet I. 2012. Root system architecture: insights from Arabidopsis and cereal crops. Philosophical transactions of the Royal Society of London. Series B, Biological sciences **367**, 1441–1452.

Stelpflug SC, Sekhon RS, Vaillancourt B, Hirsch CN, Buell CR, de Leon N, Kaeppler SM. 2016. An expanded maize gene expression atlas based on RNA sequencing and its use to explore root development. Plant Genome **9**.

Strock CF, Schneider HM, Galindo-Castañeda T, *et al.* 2019. Laser ablation tomography for visualization of root colonization by edaphic organisms. Journal of Experimental Botany.

Supek F, Bošnjak M, Škunca N, Šmuc T. 2011. REVIGO summarizes and visualizes long lists of gene ontology terms. PloS one **6**, e21800–e21800.

Swarup R, Kramer EM, Perry P, Knox K, Leyser HMO, Haseloff J, Beemster GTS, Bhalerao R, Bennett MJ. 2005. Root gravitropism requires lateral root cap and epidermal cells for transport and response to a mobile auxin signal. Nature Cell Biology **7**, 1057–1065.

Swarup R, Péret B. 2012. AUX/LAX family of auxin influx carriers-An overview. Frontiers in Plant Science **3**, 1–11.

Tai H, Lu X, Opitz N, Marcon C, Paschold A, Lithio A, Nettleton D, Hochholdinger F. 2016. Transcriptomic and anatomical complexity of primary, seminal, and crown roots highlight root type-specific functional diversity in maize (Zea mays L.). Journal of Experimental Botany **67**, 1123–1135.

Takehisa H, Sato Y, Igarashi M, *et al.* 2012. Genome-wide transcriptome dissection of the rice root system: implications for developmental and physiological functions. The Plant Journal **69**, 126–140.

Talamè V, Bovina R, Sanguineti MC, Tuberosa R, Lundqvist U, Salvi S. 2008. TILLMore, a resource for the discovery of chemically induced mutants in barley. Plant Biotechnology Journal **6**, 477–485.

Trachsel S, Kaeppler SM, Brown KM, Lynch JP. 2011. Shovelomics : high throughput phenotyping of maize (Zea mays L .) root architecture in the field. , 75–87.

Trachsel S, Kaeppler SM, Brown KM, Lynch JP. 2013. Maize root growth angles become steeper under low N conditions. Field Crops Research **140**, 18–31.

Trehin C, Schrempp S, Morel P, Berne-Dedieu A, Faure J-E, Thierry A-M, Chauvet A, Negrutiu I. 2013. QUIRKY interacts with STRUBBELIG and PAL OF QUIRKY to regulate cell growth anisotropy during Arabidopsis gynoecium development. Development **140**, 4807–4817.

Tucker MR, Lou H, Aubert MK, Wilkinson LG, Little A, Houston K, Pinto SC, Shirley NJ. 2018. Exploring the role of cell wall-related genes and polysaccharides during plant development. Plants **7**, 42.

Uga Y, Sugimoto K, Ogawa S, *et al.* 2013. Control of root system architecture by DEEPER ROOTING 1 increases rice yield under drought conditions. Nature Genetics **45**, 1097–1102.

UniBerkeley. AFM - Atomic Force Microscope Description Manual. , 1–55.

Ursache R, Andersen TG, Marhavý P, Geldner N. 2018. A protocol for combining fluorescent proteins with histological stains for diverse cell wall components. The Plant Journal **93**, 399–412.

Vissenberg K, Oyama M, Osato Y, Yokoyama R, Verbelen J-P, Nishitani K. 2005. Differential

Expression of AtXTH17, AtXTH18, AtXTH19 and AtXTH20 Genes in Arabidopsis Roots. Physiological Roles in Specification in Cell Wall Construction. Plant and Cell Physiology **46**, 192–200.

Vogel J, Hill ÆT. 2008. High-efficiency Agrobacterium -mediated transformation of Brachypodium distachyon inbred line Bd21-3. , 471–478.

Waidmann S, Ruiz Rosquete M, Schöller M, *et al.* 2019. Cytokinin functions as an asymmetric and anti-gravitropic signal in lateral roots. Nature Communications **10**.

Wang L, Guo M, Li Y, Ruan W, Mo X, Wu Z, Sturrock CJ, Yu H, Lu C, Peng J. 2018. LARGE ROOT ANGLE1, encoding OsPIN2, is involved in root system architecture in rice. Journal of Experimental Botany **69**, 385–397.

Wang M, Xu Z, Ahmed RI, Wang Y, Hu R, Zhou G, Kong Y. 2019*a*. Tubby-like protein 2 regulates homogalacturonan biosynthesis in Arabidopsis seed coat mucilage. Plant molecular biology **99**, 421–436.

Wang T, Zhang H, Zhu H. 2019*b*. CRISPR technology is revolutionizing the improvement of tomato and other fruit crops. Horticulture Research **6**, 77.

Watson A, Ghosh S, Williams MJ, *et al.* 2018. Speed breeding is a powerful tool to accelerate crop research and breeding. Nature Plants **4**, 23–29.

Watt M, Schneebeli K, Dong P, Wilson IW. 2009. The shoot and root growth of Brachypodium and its potential as a model for wheat and other cereal crops. Functional Plant Biology **36**, 960–969.

Went F. 1926. On growth-accelerating substances in the coleoptile of Avena sativa. Proc Kon Akad Wetensch Amsterdam.10–19.

Winter D, Vinegar B, Nahal H, Ammar R, Wilson G V, Provart NJ. 2007. An "Electronic Fluorescent Pictograph" Browser for Exploring and Analyzing Large-Scale Biological Data Sets. PLOS ONE **2**, e718.

Wisniewska J. 2006. Polar PIN Localization Directs Auxin Flow in Plants. Science **312**, 883–883.

Wu S, Xie Y, Zhang J, Ren Y, Zhang X, Wang J, Guo X, Wu F, Sheng P, Wang J. 2015. VLN2 regulates plant architecture by affecting microfilament dynamics and polar auxin transport in rice. The Plant Cell **27**, 2829–2845.

Xi W, Gong X, Yang Q, Yu H, Liou Y-C. 2016. Pin1At regulates PIN1 polar localization and root gravitropism. Nature communications **7**, 1–10.

Xie K, Yang Y. 2013. RNA-Guided Genome Editing in Plants Using a CRISPR–Cas System. Molecular Plant **6**, 1975–1983.

Xing H-L, Dong L, Wang Z-P, Zhang H-Y, Han C-Y, Liu B, Wang X-C, Chen Q-J. 2014. A CRISPR/Cas9 toolkit for multiplex genome editing in plants. BMC Plant Biology **14**, 327.

Yang C, Ma B, He S-J, Xiong Q, Duan K-X, Yin C-C, Chen H, Lu X, Chen S-Y, Zhang J-S. 2015. MAOHUZI6/ETHYLENE INSENSITIVE3-LIKE1 and ETHYLENE INSENSITIVE3-LIKE2 Regulate Ethylene Response of Roots and Coleoptiles and Negatively Affect Salt Tolerance in Rice . Plant Physiology **169**, 148–165.

Yoder TL, Zheng HQ, Todd P, Staehelin LA. 2001. Amyloplast sedimentation dynamics in maize columella cells support a new model for the gravity-sensing apparatus of roots. Plant Physiology **125**, 1045–1060.

Yoshida S, Hasegawa S. 1982. The rice root system: its development and function. Drought resistance in crops with emphasis on rice **10**, 97–134.

Zeng J, Dong Z, Wu H, Tian Z, Zhao Z. 2017. Redox regulation of plant stem cell fate. The EMBO journal **36**, 2844–2855.

Zhang Y, Xiao G, Wang X, Zhang X, Friml J. 2019. Evolution of fast root gravitropism in seed plants. Nature Communications **10**, 4–13.

Zhao D, Ferguson AA, Jiang N. 2016. What makes up plant genomes: The vanishing line between transposable elements and genes. Biochimica et Biophysica Acta (BBA) - Gene Regulatory Mechanisms **1859**, 366–380.

List of abbreviations

CCC = Cortical Cell Count

CCFN = Cortical Cell File number

TCA = Total Cortical Area

RCA = Root Cortical Aerenchyma

GWAS = Genomic Wide Association Studies

BSA = Bulk Segregant Analysis

NGS = Next-generation sequencing

DMSO = Dimethyl sulfoxide

NPA = Naphthylphthalamic acid

NAA = 1-Naphthaleneacetic acid

2,4D = 2,4-Dichloropheroxyacetic acid

RAM = Root Apical Meristem

MT = Maturation Zone

ED = Elongation-Division Zone

PM = Proximal Meristem

QC = Quiescent centre

CM = Columella

cor = Cortex

endo = endodermis

per = pericycle

p = phloem poles

px = protoxylem

pmx = peripheral metaxylem

cmx = central metaxylem

FPSL = First Parenchymatic Stele layer

AFM = atomic force microscope

LAT = Laser Ablation Tomography

Papers arising from this thesis

Riccardo Fusi, **Serena Rosignoli**, **Haoyu Lou**, Giuseppe Sangiorgi, Riccardo Bovina, Aditi N. Borkar, Cristian Forestan, Sara G. Milner, Jayne L. Davis, Gwendolyn K. Kirschner, Alberto Tassinari, Bipin K. Pandey, Larry M. York, Brian S. Atkinson, Craig J. Sturrock, Sacha J. Mooney, Frank Hochholdinger, Matthew R. Tucker, Axel Himmelbach, Nils Stein, Martin Mascher, Kerstin Nagel, James Simmonds, Cristobal Uauy, Roberto Tuberosa, Jonathan P. Lynch, Malcolm Bennett, Rahul Bhosale & Silvio Salvi. **Root angle is controlled by *EGT1* in cereal crops employing a novel anti-gravitropic mechanism.** (Under review)

Riccardo Fusi, **Serena Rosignoli**, Sara Giulia Milner, Riccardo Bovina, Cristovão De Jesus Vieira Teixeira, Haoyu Lou, Brian S. Atkinson, Larry M. York, Craig J. Sturrock, Nils Stein, Martin Mascher, Roberto Tuberosa, Anthony Bishopp, Devin O'Connor, Malcolm J. Bennett, Rahul Bhosale and Silvio Salvi. **The auxin efflux carrier PIN1a regulates vascular patterning in cereal roots.** (Ready for submission)

Supplementary information

							Maize		
Gene Name	**Brachypodium orthologue**	**Rice orthologue**	**Trait**	**Bd CRISPR**	**Zm CRISPR**	**Os CRISPR**	**Translational reporter**	**Transcriptional reporter**	**Gene Overexpression**
ZmHAL3	BdHAL3		CCC	X*	X*		X**		
ZmFERONIA	BdFERONIA		CCC	✓	-		X**	X**	
ZmHIF1-a		OsHIF1-a	RCA		X*	X	X**		
ZmCLAVATA3			CCFN		X*			X**	
ZmQKY	BdQKY		TCA	✓	X*			X**	
ZmACCSynthase			CCFN		X*				X**
ZmEPFL6			TCA		X*			X**	

S.Tab. 2.1. Summary of genes and corresponding genetic resource we attempted to develop to characterise Deepgenes.

Check marks indicate resources successfully developed such as CRISPR lines in BdFERONIA and BdQKY. X indicate we were not able to regenerate plants from tissue culture transformation. X* indicate we were able to regenerate CRISPR lines from tissue culture, however we couldn't spot positive edited plants through Sanger sequencing. X** Gene specific sequences have been synthesized then entry and destination vectors have been prepared in-silico for Golden Gate transformation, however molecular cloning still need to be performed

gRNA_id	5'-3' gRNA sequence	primer orientatation	5'-3' primer sequence	Tm	Amplicon
QKY_89	CTGGTGCCCAAGGACGGTCT	fw	GATCGCTTTCCCATTCACCC	58	385
		rw	AGAACTGGGAGCCGTAGATG		
QKY_371	GCAGGCTTCGTTTCTCGAGC	fw	GCCGCTTCAACCCTTCCG	58	346
		rw	GGAGGCTGAAACTGTGGC		
FER_107	GGCCACGTTGCCCTAAATTG	fw	CCCAAATCCCACCAAGCAAA	59	352
		rw	GGACTGTGGAGGGAAGTGAA		
FER_152	GATAATGGTCGGACTTGGGA	fw	same as FER_107		
		rw			

S.Tab. 2.2. gRNAs, primers and PCR conditions use to generate and sequence DeepGenes *Brachypodium distachyon* CRISPR events.

Primers were designed using Primer3 and optimised using NET Primers for secondary structure stability. PCR was performed using Phusion-HF polymerase optimised from standard settings. Tm = melting temperature, fw = primer forward, rw = primer reverse

Gene name	gRNA number	5'-3' gRNA sequence	n T0 events
CLAVATA3	gRNA_1	CGGTAACAAGGTAATACGGG	8
	gRNA_2	CAGGAGCGTGACGACCACGC	
ACCsynt	gRNA_1	GCCAATGGCGATCGTCGAGT	2
	gRNA_2	AGGAGGCCGTAGTCCGAGTG	
BHLH60	gRNA_1	CGGCAATGCTAGGTCGACGG	0
	gRNA_2	CCAAAACGGTCACCTCAGGG	
HIF1-a	gRNA_1	GACATCTGCCGCAAACTCGT	8
	gRNA_2	TGAGATCCCCGTAGAACACA	
EPFL6	gRNA_1	CTCGATGAACAGATTCCGGC	3
	gRNA_2	AGGAGATGGTTTACACCGGA	
HAL3	gRNA_1	CTATCAACGAAGTGCAAGGA	7
	gRNA_2	TGAAGATGCCGCTCCGTGAA	
QKY	gRNA_1	CACTGCGGGCTCAGGTCTCG	4
	gRNA_2	GAGACGGCGCATAGTAATCC	

S.Tab. 2.3. gRNAs and PCR conditions use to generate and sequence DeepGenes Maize CRISPR events.

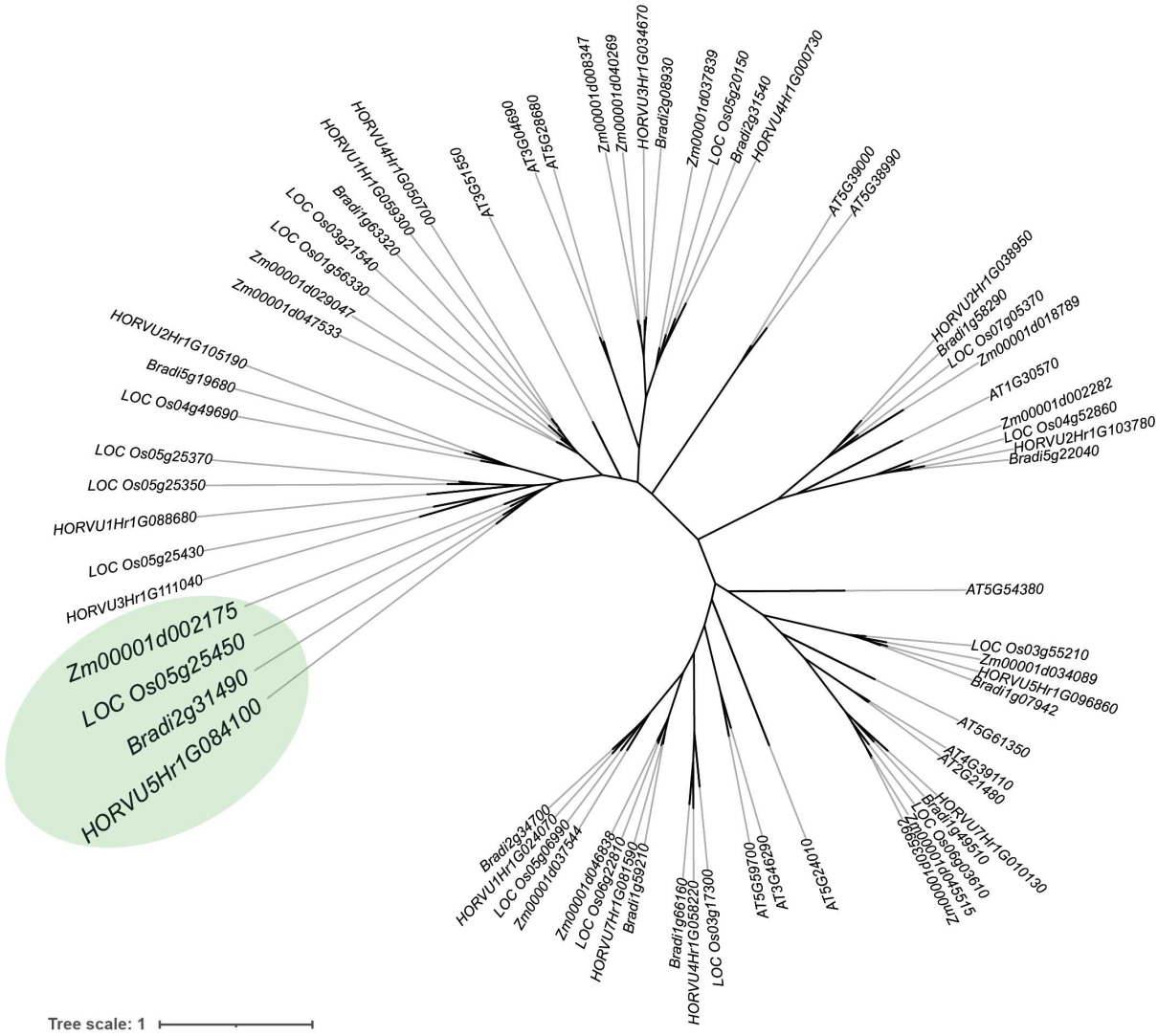
Gene	gRNA number	Primer_name	Primer sequence	Tm	Amplicon
ZmCLAVATA3	1 and 2	ZmCLV3_1/2_F	ACCTCCACTTGATCCACCAC	58	417
	1 and 2	ZmCLV3_1/2_R	ACCGACAGTGTCTTGTTTCG		
ZmHAL3	1	ZmHAL3_1_F	TCAGAGCCAGTACAAGAGAGT	58	306
		ZmHAL3_1_R	TGGAGCGATCACCATAACGT		
	2	ZmHAL3_2_F	ATGCGACAACCTCTTGACCT	58	445
		ZmHAL3_2_R	GTGACAACAGCCTTTCCCC		
ZmACCsynthase	1	ACS_1_F	TAGCCAGTCACCACCAAAGT	58	271
		ACS_1_R	CTCATACCCATCGTCGTGCT		
	2	ACS_2_F1	CTTGGCGTCGCACATGATG	58	279
		ACS_2_R1	TGTCGCAAAGCAACCGTAC		
ZmAEPFL6	1	EPFL6_1_F	AGTAGTAGATGCAGAGCCGC	58	387
		EPFL6_1_R	AACAACCCAACGCCAAACAT		
	2	EPFL6_2_F	CCCTGAGCGACCATACCATA	58	357
		EPFL6_2_R	GCATGTAGAGCTGGTTCCG		
ZmHIF1a	1	HIF1_1_F	TGTGCGGAGAGGGAGAATG	58	581
		HIF1_1_R	CGACGGTTGAAGTGAAATGC		
	2	ZmHIF1_2_F	TATGAGGCGTCGGGTTGAAA	58	377
		ZmHIF1_2_R	CTCCCTTGAACTAGCTGGCT		
ZmQKY	1	ZmQKY_1_F	GTCGCCTTCTCGCATTCTTT	58	418
		ZmQKY_1_R	AGAACTGGGAGCCGTAGATG		
	2	ZmQKY_2_F	CACCCACCGATGATGATGC	58	545
		ZmQKY_2_R	CTGATGGCGAACACCTGGT		

S.Tab. 2.4. List of primers used for screening by genotyping of the maize Deepgenes CRISPR lines. List of primers used for screening by genotyping of the maize Deepgenes CRISPR lines.

Species	UNIPROT_ID	Domain	%Id	%Cov	e-val
Z.mays	A0A1D6DXI0	Malectin_like	100%	100%	0
Z.mays	A0A1D6DXI0	Tyrosine_kinase	100%	100%	0
O.Sativa	A0A0P0WKX1	Malectin_like	74.86%	100%	0
O.Sativa	A0A0P0WKX1	Tyrosine_kinase	88.93%	99%	0
H.vulgare	F2DER3	Malectin_like	68.82%	100%	0
H.vulgare	F2DER3	Tyrosine_kinase	87.82%	99%	0
Arabidopsis thaliana	Q9SCZ4	Malectin_like	51.74%	100%	8.00E-133
Arabidopsis thaliana	Q9SCZ4	Tyrosine_kinase	78.75%	100%	2.00E-167
Brachypodium distachyon	I1HKP3	Malectin_like	71.62%	100%	0
Brachypodium distachyon	I1HKP3	Tyrosine_kinase	88.93%	99%	0

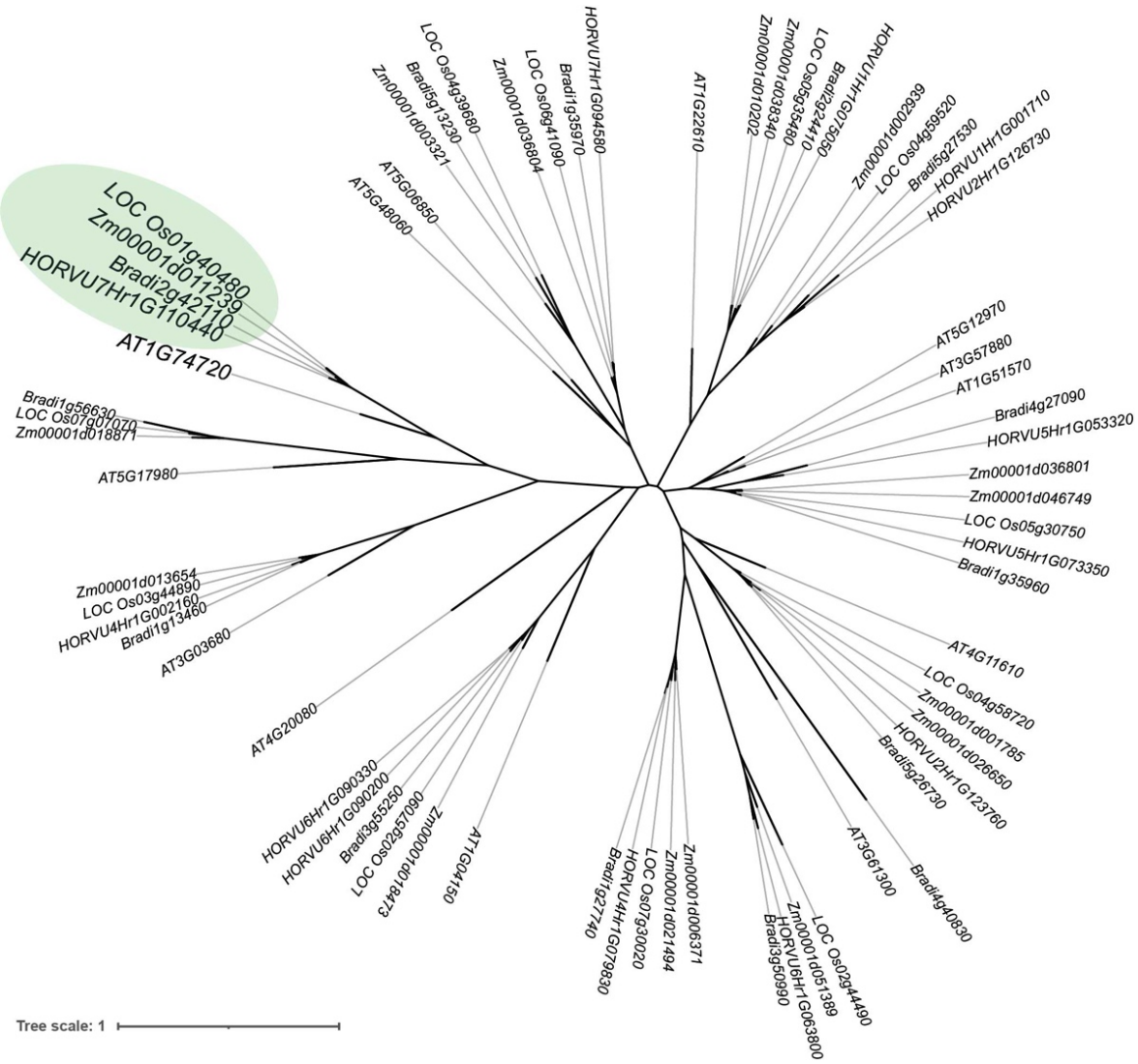
S.Tab. 2.5. Summary table of protein domain conservation analysis of main monocots and Arabidopsis orthologues of ZmFERONIA.

Protein domain structure of *ZmFERONIA* (*Zm00001d002175)* and the orthologous genes from monocot species such as barley (Hordeum Vulgare), rice (Oryza Sativa spp. Japonica) and *Brachypodium distachyon* as well as the monocot model Arabidopsis (Arabidopsis thaliana) was analysed in the Uniprot and the PFam database. Protein sequences of both the malectin_like and tyrosin-kynase for each orthologues were then aligned using ZmFERONIA as query using NCBI-blast. For each, it was then generated the percentage of protein identity (%id), coverage and the resulted e-value (e-value)



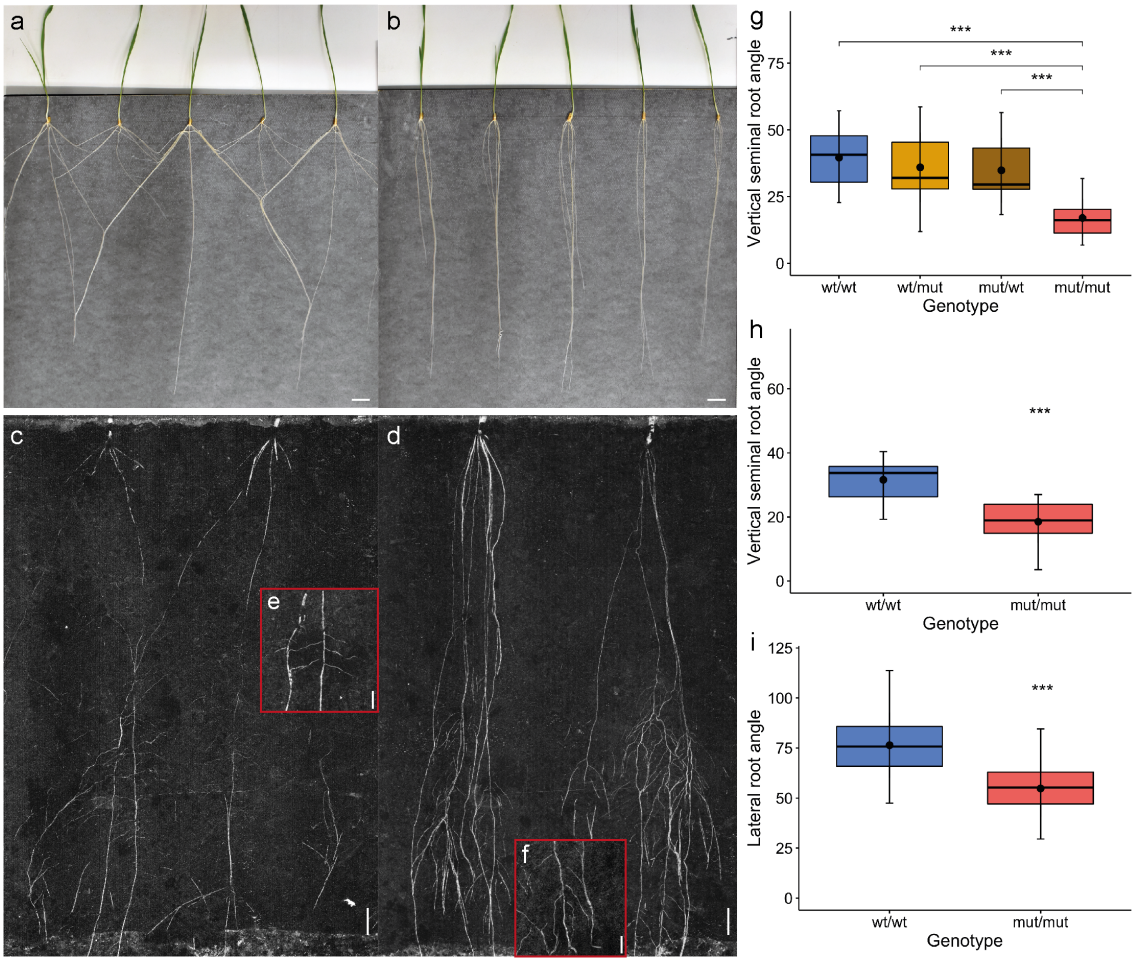
S.Fig. 2.1. Phylogenetic analysis of Malectin-like tyrosine kinases sequences in maize, barley, rice, *Brachypodium distachyon* and Arabidopsis.

ZmFERONIA (Zm00001d002175) was used as a seed gene to select orthologous genes (>40 identity percentage, bitscore >500) from key monocot species such as barley (Hordeum Vulgare), rice (Oryza Sativa spp. Japonica), maize (Zea Mays B73) and *Brachypodium distachyon* and Arabidopsis (Arabidopsis thaliana) using interactive phylogenetic module of Monocots Plaza 4.5 (Van Bel et al., 2017). Protein sequences were aligned using MUSCLE and tree was constructed using FastTree algorithm. Generated Newick file was imported into iTOL to create an unrooted tree. Green colour highlights the distinct clade formed by *ZmFEORNIA* with 1 ortologue each from barley, rice and *Brachypodium distachyon*. Tree scale = 1 indicates 100% of aminoacidic substitution occurred between two aminoacidic sequences. Confidence between clades was calculated using bootstrap method (>100 interactions)



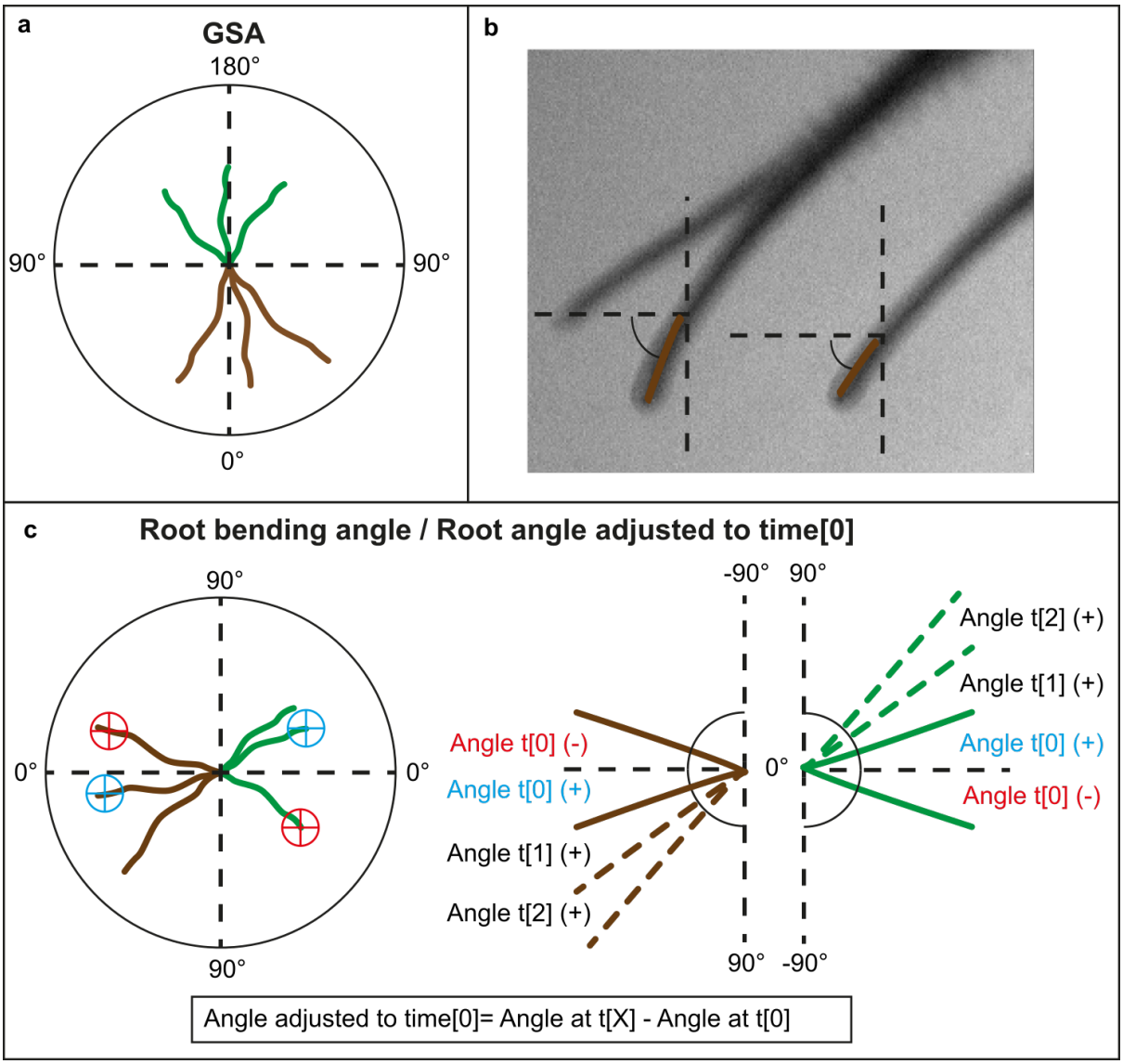
S.Fig. 2.2. Phylogenetic analysis of C2 C-terminus-phosphoribosyltransferases sequences in maize, barley, rice, *Brachypodium distachyon* and Arabidopsis.

ZmQKY (Zm00001d011230) was used as a seed gene to select orthologous genes (>40 identity percentage, bitscore >500) from key monocot species such as barley (Hordeum Vulgare), rice (Oryza Sativa spp. Japonica), maize (Zea Mays B73) and *Brachypodium distachyon* using interactive phylogenetic module of Monocots Plaza 4.5 (Van Bel et al., 2017). Protein sequences were aligned using MUSCLE and tree was constructed using FastTree algorithm. Generated Newick file was imported into iTOL to create an unrooted tree. Green colour highlights the distinct clade formed by *ZmQKY* with 1 orthologue each from barley, rice and *Brachypodium distachyon*. Tree scale = 1 indicates 100% of aminoacidic substitution occurred between two aminoacidic sequences. Confidence between clades was calculated using bootstrap method (>100 interactions).



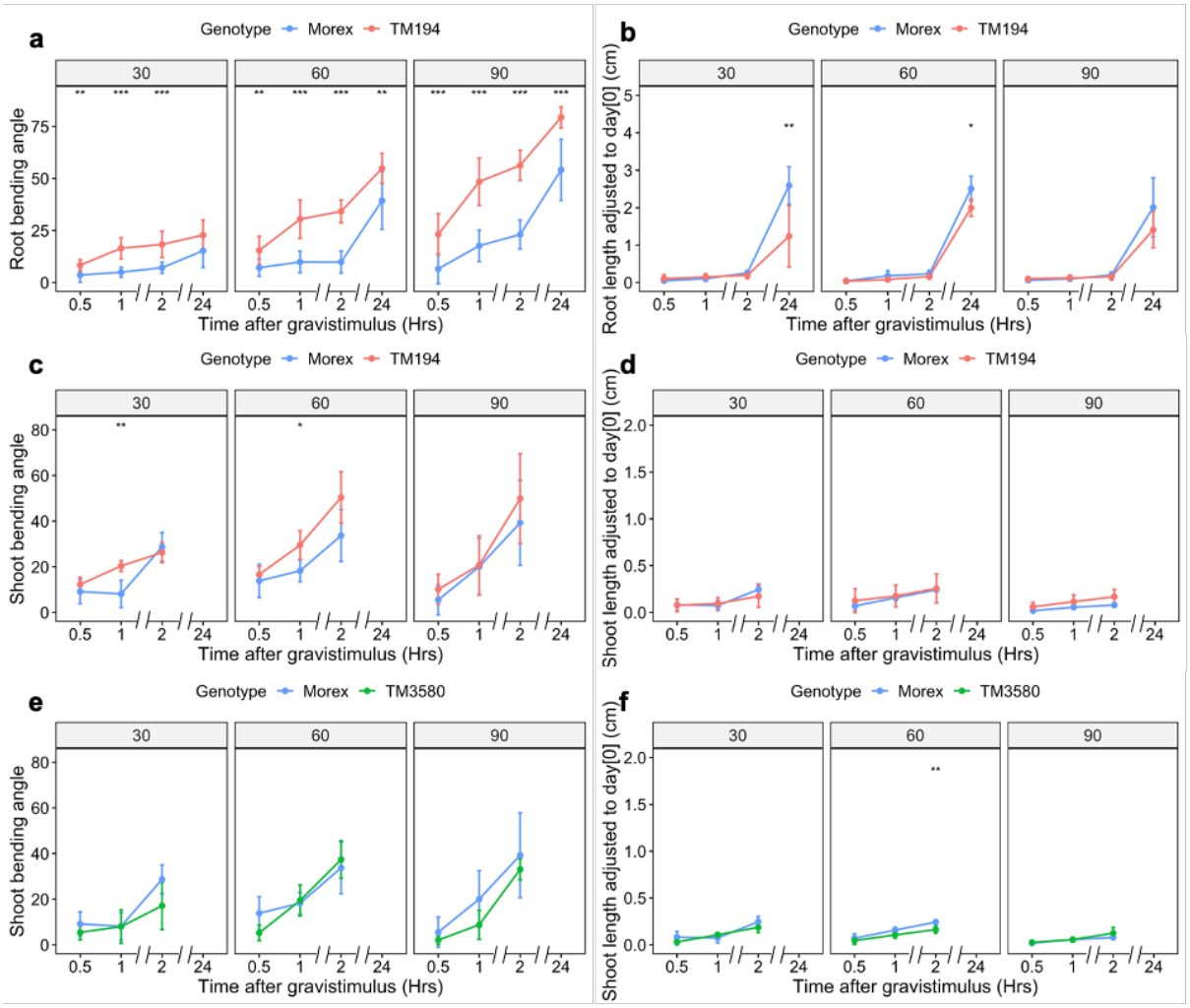
S.Fig. 3.1. *TdEGT1* loci also control root growth angle in wheat.

a-b) Representative images showing root growth angle 8-days old a, wildtype *TdEGT1* (wtA/wtB) and (b) homozygous cross of *Tdegt1* mutant (mutA/mutB) grown in semi-hydroponic condition. Scale bar = 2 cm. c-d, Representative images of 20-days old. c) wtA/wtB and (d) mutA/mutB mutant grown in soil rhizotrons. Scale bar = 2 cm. (e-f) Representative magnified images of lateral roots from (c-d) respectively. Scale bar = 1 cm. g, Quantification of seminal root angle from 8-days old wtA/wtB, wtA/mutB, mutA/wtB and mutA/mutB grown in semi-hydroponic condition. h) Quantification of seminal root angle from 12-days old wtA/wtB and mutA/mutB grown in soil rhizotrons. i) Quantification of lateral root angle (from seminal roots) of 20-days old wtA/wtB and mutA/mutB grown in soil rhizotrons. *** shows statistically significant difference between wild types at one or both homologs (wtA/wtB, mutA/wtB and wtA/mutB) versus double mutants (mutA/mutB), assessed using Welch's t-test, $p<0.001$, n=12-28 seminal roots and 86-91 lateral roots.



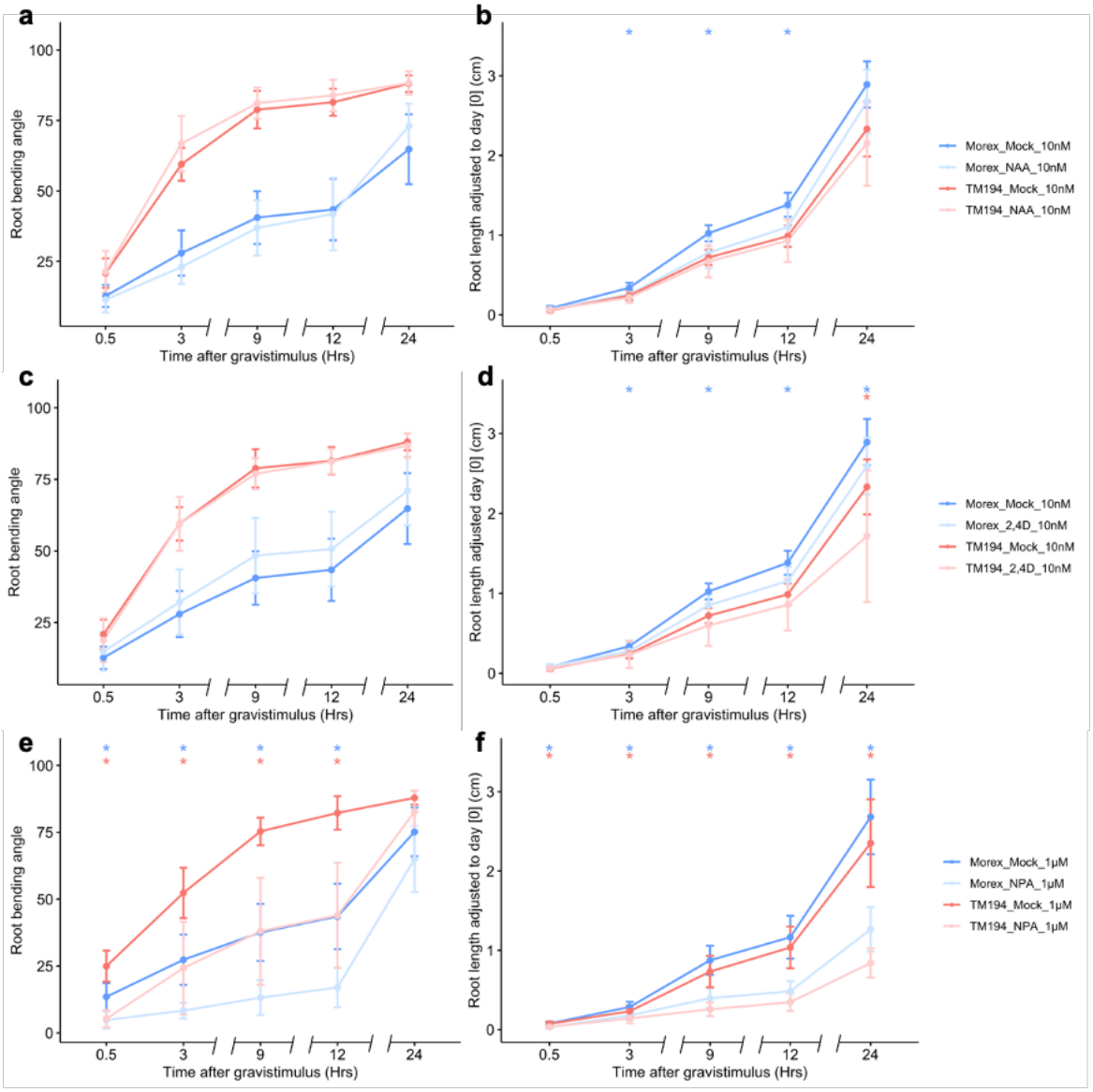
S.Fig. 3. 2. Methodology to measure root bending angle (Root angle adjusted to time [0]) using FIJI.

a) Canonical quantification to measure the Growth Setpoint Angle (GSA). b) Examples from root tips images after 24h 90° rotation was imposed and using the line tool in FIJI to quantify the root bending angle. For consistent measurements, lines were always drawn toward the right-hand side in FIJI. c) Schematic of rotation and quantification using the acquired angle data from FIJI. For consistency, only roots (and shoot) with an Angle at [0] within a range of ± 15°° were chosen for the analysis. Root length adjusted to day [0] was used using the same formula.



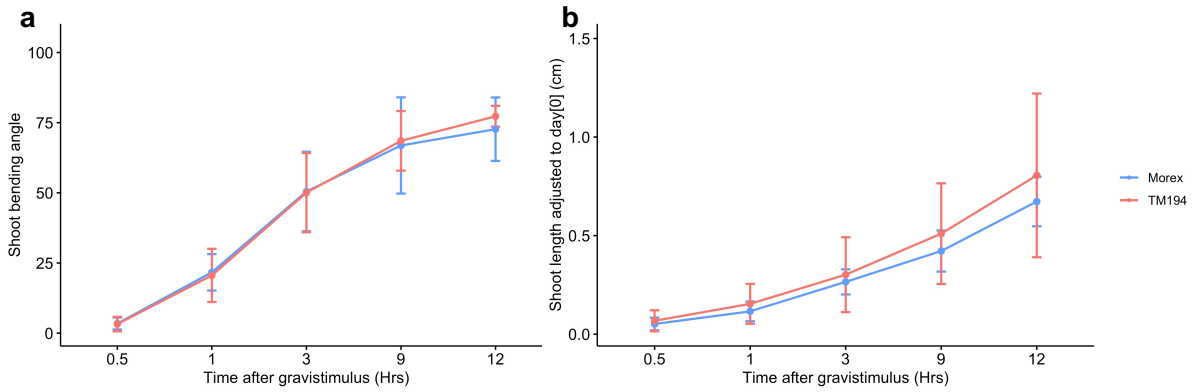
S.Fig. 3. 3. Additional quantification of root and shoot bending angle and root length from the root bending response assay on Morex, TM194 and TM3580.

a,c,e) Measurement of dynamic change in root (a) and shoot (c,e) tip bending angle with increasing titling angle gravistimulations (from 30° to 60° to 90°) at 0.5, 1, 2 and 24 hours after 90° tilting gravistimulus in Morex TM194 and TM3580. b,d,f) Root and shoot length measurements of the growth increment adjusted to day [0] for each timepoint considered (0.5,1,2 and 24) hours). Last 12hours were performed in light so gravitropic and phototropic effect were considered during this timepoints. * represents statistically significant difference, between treated and mock samples from respective genotype, assessed using Welch's T-Test at $p<0.05$ in n=2-6 biological replicates.



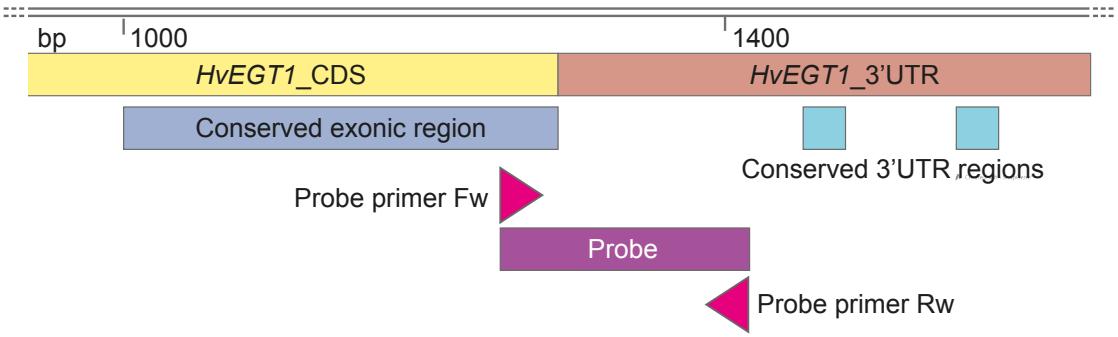
S.Fig. 3. 4. Auxin root bending sensitivity bioassay.

Quantification of the response in root bending angle (a,c,e) and root length (b,d,f) in Morex and TM194 at 0.5,3,9,12 and 24 hours after 90° gravistimulus during exogenous application of 10nM 1-Naphthaleneacetic acid (NAA) (a,b) , 10nm 2,4-Dichlorophenoxyacetic acid (2,4D) (c,d) and 1µM auxin transport inhibitor 1-N-Napthylphthalamic acid (NPA) (e,f). Last 12hours were performed in light so gravitropic and phototropic effect were considered during this timepoints. * represents statistically significant difference, between treated and mock samples from respective genotype, assessed using Welch's T-Test at $p<0.05$ in n=5-6 biological replicates.



S.Fig. 3.5. Shoot bending response assay revealed no significant differences between Morex and TM194.

Quantification of the response in root bending angle (a) and root length(b) in Morex and TM194 at 0.5,3,9 and 12 hours after 90° gravistimulus from DMSO control mock plates. * represents statistically significant difference, between treated and mock samples from respective genotype, assessed using Welch's T-Test at $p<0.05$ in n=5-6 biological replicates, 2 plates per treatment.

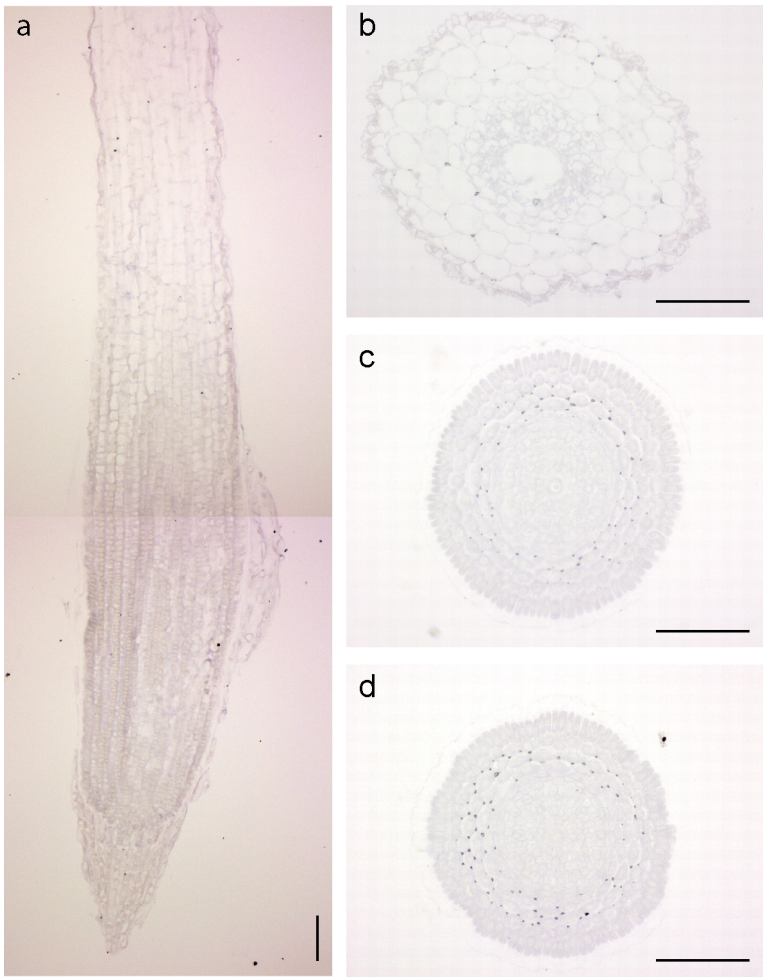


S.Fig. 3. 6. Schematic of probe design for EGT1 RNA in situ hybridisation experiment.

The complete coding sequence and 3'UTR sequence of *HvEGT1* (HORVU6Hr1G068970) were obtained to design probes. The three conserved regions were annotated as shown in the diagram, including one at the end of coding sequence (998-1284bp), and two in the 3'UTR region (1428-1438bp and 1529-1539bp). The primers were designed to frame partial coding sequence and partial 3'UTR and avoided conserved sequence to increase the specificity of probe recognition. To syntheses the antisense and sense probes, an adaptor sequence (T7 promoter, TAATACGACTCACTATAGGG) was added to the reverse and forward primer, respectively. The probe used in this study is 156bp.

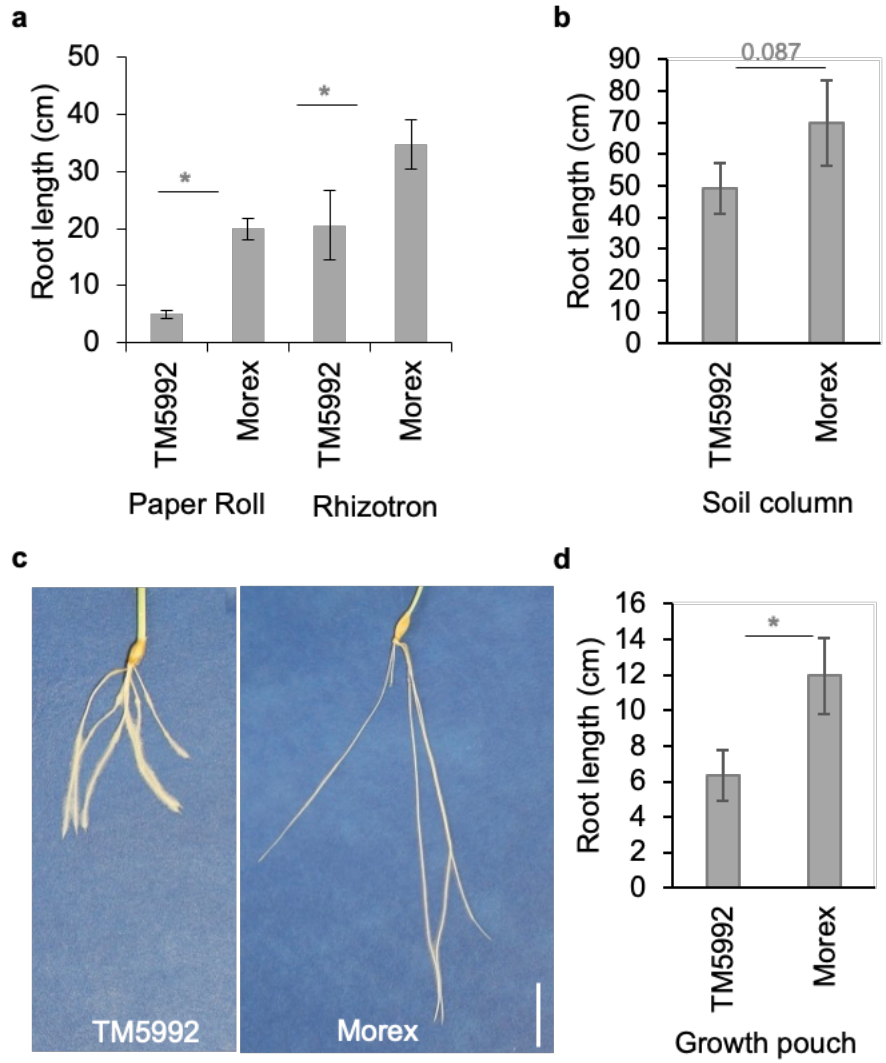
Probe Sequence (156bp):

CTAGCTTCGACACCAAACCGGCCTGCGAATGACCGAAGAAGGCGGCGTTAACCGGGCCAGCCAGCT
TGAGACATTACCTGCCCCTTGGATGGTGTAAATTCTGATATCTTTGCTTCAATTCTCGGACGCTGCCC
CTGGGGAGATGGATGGTAGGTG



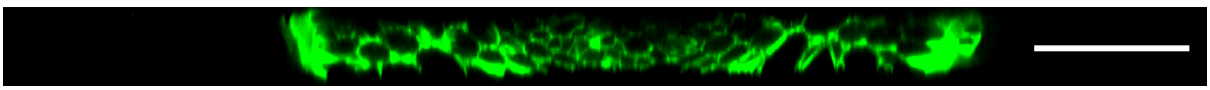
S.Fig. 3. 7. In Situ Hybridisation (ISH) on root tips of Morex with HvEgt1 sense probe.

a) ISH on longitudinal section of root tip of Morex. b-d) ISH on cross-sections of Morex in ED (b), higher PM (c) and lower PM (d). (scale bar=100µm).



S.Fig. 4.1. Measured root growth parameters of TM5992 and Morex.

Average root lengths of Morex and TM5992 grown in (**a**) paper roll and rhizotron for 9 days and (**b**) soil columns for 10 days. (**c**) Representative image showing root architecture of Morex and TM5992 grown in growth pouch system for 7 days. Scale bar = 2cm (**d**) Average root lengths measured for (**c**). For all experiments, mean and standard deviations from 3 biological replicates, > 7 seedlings per replicate. * Indicates significance (P-value < 0.01, T-test).



S.Fig. 4.2. Orthogonal Z-stack view of a longitudinal section in Morex.

Longitudinal root tip section of Morex showing the different tissue types and the visible inner vasculature in the middle of the section which helped identifying the central focus for the tip characterisation of all the *HvPINa* mutants. Scale bar=100µM

Supplementary Datasets

Reserved DOI: 10.17639/nott.7172

Dataset S1. Exome sequencing results of TM194 and TM3580 compared against Morex highlighting (red) mutations within HORVU6Hr1G068970 (HvEGT1), encoding Tubby-Like F-box domain protein.

Dataset S2. Differentially expressed genes between comparisons of TM194 vs Morex, TM3580 vs Morex and TM194 vs TM3580. Genes with Benjamini Hochberg controlled FDR < 0.05, FC +/- 1.5 and FPKM >1 were assigned as differentially expressed.

Dataset S3. gProfiler GO enrichment analysis of selected 988 genes that are differentially expressed in Hvegt1 mutant alleles compared to Morex. Green filled section indicates biological processes (BP) used for further analysis.

Dataset S4. List of genes enriched in cell wall organisation and biogenesis and hydrogen peroxide metabolic processes. Orthologous genes in Arabidopsis and rice were identified using Plaza 4.5 comparative genomics database and only BHIF (Best-Hits-and-Inparalogs(BHI)family) evidence was retained.